Decoding Individual Contralateral and Ipsilateral Finger Movements from Electrocorticographic Signals Recorded over the Human Sensorimotor Cortex of a Single Hemisphere

Thesis submitted in partial fulfillment of
the requirements to obtain the degree of

Master of Science
in
Interaction Technology

Submitted by Fabian Benjamin Dijkstra

Under the supervision of

UMC Utrecht
Brain Center Rudolf Magnus

Dr. Mariana Branco

UNIVERSITY OF TWENTE.

Dr. Mannes Poel
Dr. Nattapong Thammasan
Prof. Dr. Dirk Heylen

Faculty of Electrical Engineering, Mathematics and Computer Science

University of Twente
Enschede, the Netherlands

April 3, 2020

Abstract

The field of Brain Computer Interface (BCI) research has seen tremendous growth in the last years. This research handles an endeavor towards improvement of specifically Sensorimotor Rhythm BCIs based on Electrocorticographic measurements (ECoG) by investigating the possibility to decode individual finger movements from both the hand contralateral to the implanted ECoG electrode grid as well as the hand ipsilateral to the implanted grid. Although the hemispherical organization of the limbs is largely contralateral, cortical activation during ipsilateral hand movement has been reported in literature. The possibility to decode both ipsilateral and contralateral finger movements from a single hemisphere could increase the available degrees of freedom for device control without the necessity of placing electrode grids on both hemispheres, which is unfavorable given the tremendous impact of the surgery associated with implantation. This research included four participants with intractable epilepsy who underwent placement of HD ECoG grids over the hand knob of the SMC of a single hemisphere. The participants performed individual finger movement of the thumb, index and little finger of the hand contralateral and ipsilateral to the implanted ECoG grid. A synchronous (cue-based) experiment showed that individual movement of contralateral and ipsilateral fingers along with trials of rest can be decoded with a performance significantly above chance level ($p<0.05$) for all participants with an accuracy of 79.22 ± 6.30 (Mean $\pm$ SD) across participants. In this synchronous experiment, only ipsilateral finger movement showed confusion with rest (i.e. false positive detections). In addition to this synchronous experiment, an asynchronous experiment (non cue-based) was approximated such that it closely resembled a real-life BCI use case. In this experiment, the occurrence of false positive detections of especially ipsilateral finger movements was grossly exacerbated, which has strong implications for the eventual usability of individual ipsilateral finger movement as a BCI control signal. This research is, to the best of the author's personal knowledge, the first research to investigate the possibility to decode both contralateral and ipsilateral individual finger movements from ECoG signals recorded over the Sensorimotor Cortex (SMC) of a single hemisphere. Future research should focus on a much more elaborate asynchronous evaluation and eventually experiments with end users should be performed to determine the full extent to which both contralateral and ipsilateral (attempted) finger movements can be used as a viable control signal in BCIs.

Keywords: Electrocorticography, ECoG, Unimanual, Finger, Movement, Contralateral, Ipsilateral, Decoding, Classification, Machine Learning, Brain Computer Interface, BCI, Synchronous, Asynchronous

Acknowledgments

A large number of people have uniquely contributed to my development as a student and have helped me towards the final aptitude test as an academic, of which the fulfillment of thesis is the final step.

I would firstly like to thank all the members of my graduation committee. Your empathy, constant encouragement and patience along with your expertise on diverse fields have allowed me to greatly improve the quality of my work on all aspects and have helped me to develop myself into a more confident young academic. Thank you for providing me with the opportunity to perform my research at the BCI group of the University Medical Center Utrecht (UMCU) and allowing me to explore a topic of my interest in a unique and very exciting way. Mannes, thank you for teaching me so much about Brain Computer Interfacing, Data Science and Machine Learning. Your enthusiasm and unique way of teaching made all your courses highly interesting and fun and I am glad to have joined that many. Mariana, thank you for taking me under your wing during my time at the UMCU. I really enjoyed your teaching, our weekly contact and our many interesting conversations. It has been a pleasure to be part of the UMCU BCI Group consisting of so many kind and smart people who strive to help each other forward. Dirk, thank you for always being so sympathetic and enabling during my studies. When I needed it the most, you always made sure that there were new possibilities. You did this not just for me, but for every student, which I think is very special. Thank you Natty, for taking on the role as supervisor on such a short notice. I am glad we were eventually able to meet each other via Skype due to the quarantine surrounding the Corona virus and have an enjoyable conversation prior to my graduation.

I would also thank those who did not have a direct impact on this thesis, but have greatly contributed to my personal development. Thank you, Alma Schaafstal, Erik Faber and Thea de Kluijver for taking on a mentor role towards me during my studies and providing me with an empathetic ear and advice on all aspects of my study and (student) life. Your door has always been open for me and for that, I am profoundly grateful.

Additionally, I would like to express my gratitude towards the Creative Technology and Interaction Technology community. It has been and it will remain a pleasure to be part of such a unique close knit group of individuals with such an open and positive attitude towards each other.

Naturally, I would like to thank my family and friends for always being there for me. To my girlfriend, Kim, thank you for once more taking me in your home and for providing me with your unlimited love, support, encouragement and comfort every day.

Without all of you I would not have been able to deliver this thesis.

The happiest and most successful people do not necessarily have the best of everything, they simply make the best of everything they have.

- Unknown

Table of Contents

List of Acronyms

BCI	Brain Computer Interface
LIS	Locked in Syndrome
ALS	Amyotrophic Lateral Sclerosis
EEG	Electroencephalography
ECoG	Electrocorticography
MEG	Magnetoencephalography
fMRI	functional Magnetic Resonance Imaging
BOLD	Blood Oxygen Level Dependent
SMC	Sensorimotor Cortex
SMRs	Sensorimotor Rhythms
LFB	Low Frequency Band
HFB	High Frequency Band
PrCG	Precentral Gyrus
PCG	Postcentral Gyrus
CS	Central Sulcus
S1	Primary Somatosensory Cortex
M1	Primary Motor Cortex
SFS	Superior Frontal Sulcus
UMCU	University Medical Center Utrecht
UNP	Utrecht Neuroprosthesis
HD	High Density
COMs	Centers of Mass
pRF	population Receptive Field
CAR	Common Average Referencing
SAM	Synthetic Aperture Magnetometry
LMP	Local Motor Potential
SCP	Slow Cortical Potential
CSP	Common Spatial Patterns
PCA	Principal Component Analysis
PC	Principal Component
ICA	Independent Component Analysis
SIDWT	Shift Invariant Discrete Wavelet Transform
AM	Auto-regressive Model
EMD	Empirical Mode Decomposition
LDA	Linear Discriminant Analysis
RLDA	Regularized Linear Discriminant Analysis
GLM	Generalized Linear Model

SVM	Support Vector Machine
PTC	Pattern Template Correlation
CSSD	Common Spatial Subspace Composition
DSLVQ	Distinction Sensitive Learning Vector Quantization
NB	Naive Bayes
LMD	Mahalanobis Distance Classifier
QMD	Quadratic Mahalanobis Distance Classifier
BSC	Bayesian Classifier
MLP	Multi Layer Perceptron
PNN	Probabilistic Neural Network
HMM	Hidden Markov Model
kNN	k-Nearest Neighbours
MLR	Multi-linear Regression
DT	Decision Tree
PLS	Partial Least-squares Regression
WSC	Wiener Cascade Decoder
RNN	Recurrent Neural Network
LR	Linear Regression
PR	Pace Regression
SNDS	Switched Non-parametric Dynamic System
AF	Adaptive Filtering
CRF	Conditional Random Fields
LSTM	Long Short-term Memory
SLR	Sparse Linear Regression
PCs	Principal Components
ANN	Artificial Neural Network
OVA	One Versus All
OVO	One Versus One
DSP	Discriminative Spatial Patterns
IC	Intentional Control
NC	No Control
FP	False Positive
FN	False Negative
CT	Computerized Tomography
prCS	Precentral Sulcus
pCS	Postcentral Sulcus
DFT	Discrete Fourier Transform
t-SNE	t-Distributed Stochastic Neighbour Embedding
ECOC	Error Correcting Output Codes
LOOCV	Leave One Out Cross Validation
eb-TPR	event-based True Positive Rate
sb-FRP	sample-based False Positive Rate
DC	Direct Current

1 Introduction

An illustrative definition of a Brain Computer Interface (BCI) has been provided by Graimann and colleagues by referring to an excerpt from the science fiction series Star Trek (Graimann et al., 2009). The character Captain Pike was struck by severe radiation which left him paralyzed. The dialog between the characters Piper and Mendez describe the situation of Pike:

> PIPER: We're forced to consider every possibility, sir. We can be certain Captain Pike cannot have sent a message. In his condition he's under observation every minute of every day.
>
> MENDEZ: And totally unable to move, Jim. His wheelchair is constructed to respond to his brain waves. Oh, he can turn it, move it forwards, or backwards slightly.
>
> PIPER: With the flashing light, he can say yes or no.
>
> MENDEZ: But that's it, Jim. That's as much as that poor devil can do. His mind is as active as yours and mine, but it's trapped inside a useless vegetating body. He's kept alive mechanically, a battery-driven heart.
>
> Original Airdate: 17 Nov 1966

For Pike, the only way to control his wheelchair and communicate with the outside world is via a computer that can read his brains' signals (hereafter referred to as cortical signals) and convert those signals to commands which control his wheelchair and communication device. Graimann states that such a device would indeed be perfect for a science fiction movie but hardly imaginable in real life (Graimann et al., 2009).

To date, almost 50 years after the airing of that Star Trek episode, a large number of BCIs have been developed that use physiological measures of brain activity to facilitate an alternative manner of communication for those individuals who can no longer use their muscles to communicate through speech or movement (Wolpaw et al., 2002) (Birbaumer, 2006). Such a disability can be found in individuals with Locked in Syndrome (LIS). Individuals with LIS lose, in varying gradation, control over primary muscles of the body leaving them unable to move or speak. The causes for LIS are diverse, including but not limited to brainstem stroke or Amyotrophic Lateral Sclerosis (ALS) (Kübler et al., 2005). In extreme cases, these individuals have no way of communicating their desires to the outside world and are thus "locked" in their own body (Bauer et al., 1979). For individuals with LIS, quality of life has been strongly correlated with the ability to communicate (Rousseau et al., 2015) (Pels et al., 2017) and for this reason, this particular group of individuals may benefit strongly from such a BCI.

1.1 Structure of a Brain Computer Interface

Currently, a wide variety of BCIs exist but in essence, their structure can often be reduced to five fundamental components namely: signal acquisition, preprocessing, feature extraction, decoding and feedback (Wolpaw et al., 2002) (See Figure 1.1).

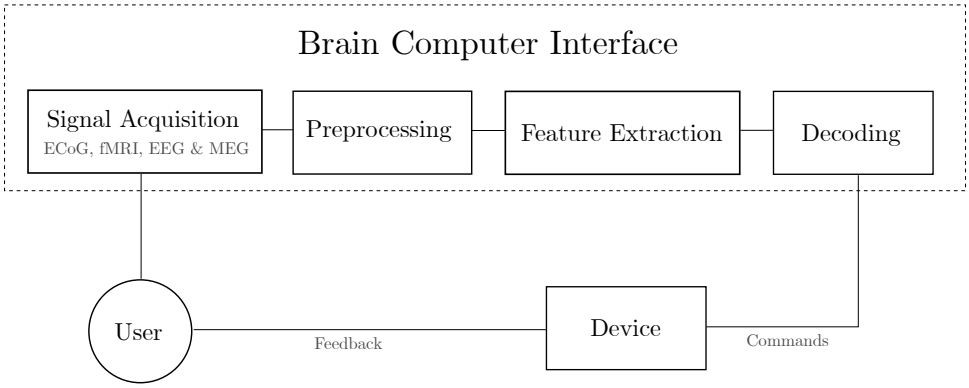

Figure 1.1: *Simplified architecture of the incorporation of a BCI system in a control loop consisting of the signal acquisition, preprocessing, feature extraction, decoding and feedback stages. (figure recreated from (Wolpaw et al., 2002).)*

The signal acquisition encompasses the recording of the brain signals. For this, several techniques exist for the recording of cortical signals including but not limited to Electroencephalography (EEG), Electrocorticography (ECoG), Magnetoencephalography (MEG) and functional Magnetic Resonance Imaging (fMRI) which can subsequently be divided into invasive and noninvasive recording methods (Wolpaw et al., 2002) (see Box 1). Images of the recording techniques are depicted in Figure 1.2.

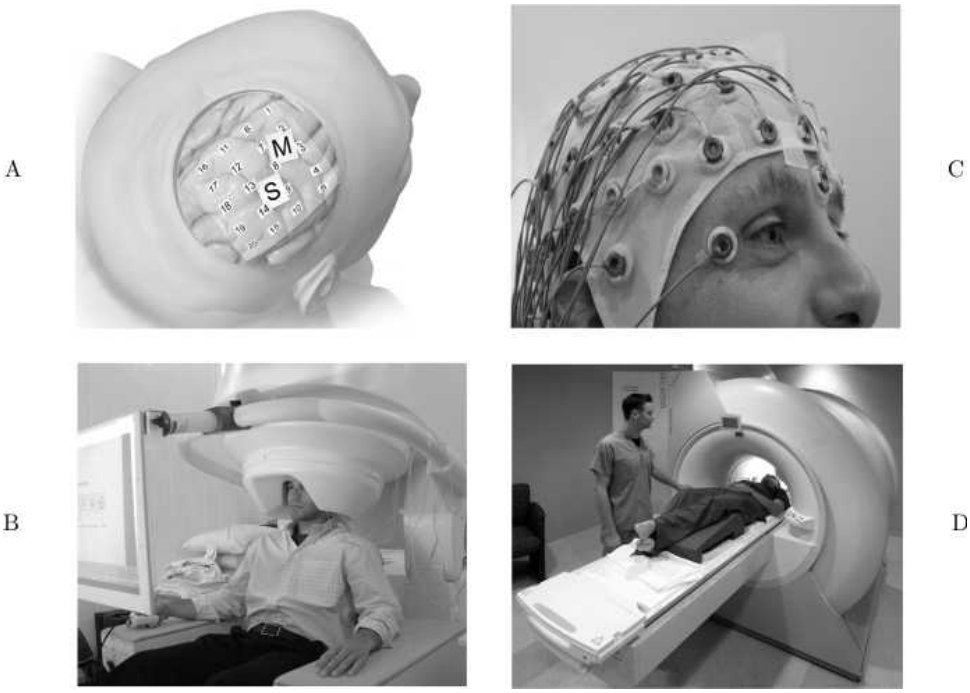

Figure 1.2: *Image A depicts an ECoG electrode grid placed on the cortical surface (Blaus, 2014). Image B depicts an MEG machine (Bodison, 2017). Image C depicts EEG electrodes on the scalp (Hamzelou, 2016). Image D depicts an fMRI machine (Wang, 2018).*

These techniques all have their own advantages and disadvantages: Noninvasive techniques record through the bone, tissue, muscle and skin that cover the cortical surface which impacts the signal to be measured in several ways. The bodily matter causes attenuation of cortical signals, resulting in a decreased measurement amplitude in noninvasive techniques as opposed to invasive techniques (Schalk, 2010). Additionally, for EEG and MEG, the influence of bodily matter on the signal causes a reduced recording bandwidth as opposed to ECoG (Schalk, 2010). Furthermore, the bodily matter causes scattering of recorded signals and increases the distance between the recording electrodes and the brain. These two factors strongly reduce the spatial resolution of EEG and MEG with respect to ECoG (Hämäläinen et al., 1993) (Hill et al., 2012). FMRI however is able to reach a spatial resolution similar to that of ECoG (Siero et al., 2014). The temporal resolution of fMRI is much lower as opposed to EEG, MEG and ECoG, which is due to the fact that fMRI measures a correlate of activity (BOLD signal) that manifests itself only seconds after activity (Kim et al., 1997). During MEG, EEG and fMRI scanning, the participant must remain completely still as to prevent movement artifacts in the measured data (Kim et al., 1997), something which is not an issue in ECoG recordings. In terms of portability, MEG and fMRI recording devices are large and heavy and are therefore not portable. EEG and ECoG allow for more portable setups, allowing for home use or eventually, in the case of ECoG, full implantation (Vansteensel et al., 2016b). One distinct disadvantage of invasive techniques is that rejection and encapsulation of the electrodes may occur as a defense mechanism of the human body to foreign objects. This phenomenon can decrease both the feasibility and safety of longer-term implementation as well as influence the signal quality negatively (Schendel et al., 2014). Even though the invasive recording techniques are associated with a high impact and risk due to surgical procedures, they have been applied in a wide variety of BCI applications. This holds for BCI users with LIS, for whom the potential of an invasive technique for use in a BCI can outweigh the associated risk and impact of the required surgery.

Box 1: Recording Techniques

Noninvasive: Non-invasive techniques record activity either directly from the scalp of the subject, as in EEG, or surrounding the head of the subject, as in fMRI and MEG. Noninvasive recording techniques do not require surgery for the installation of recording electrodes:

- **EEG**: applies electrodes on the scalp (skin) of the head to measure cortical electrical activity (Henry, 2006).
- **MEG**: records the weak orthogonal magnetic field resulting from electrical currents flowing through neurons (Hämäläinen et al, 1993).
- **fMRI**: uses a strong magnetic field to measure a correlate of cortical activity, namely the metabolic response referred to as the Blood Oxygen Level Dependent (BOLD) response. Active neurons produce an increase in oxygen-rich blood flow in surrounding tissue, and this metabolic change can be measured by fMRI (Logothetis et al, 2001).

Invasive: In medical terms, an invasive procedure requires entering or penetrating the body, through the skin, tissue or bone. This means surgery is required during which the scalp is temporarily removed in order to place the recording electrodes on top of the cortical surface, as with ECoG:

- **ECoG**: involves recording electrical activity directly with electrodes placed directly onto the cortical surface (Hill et al., 2012).

Following acquisition, the raw data is preprocessed in order to remove artifacts, noise

and other irrelevant signal components. After the preprocessing stage, the feature extraction is performed. This process entails the transformation of the raw signal into a meaningful and useful representation from which the user's intent can be inferred. In the decoding step, a computerized method bases a classification or regression decision on these informative features and outputs a discrete or a continuous control signal that represents the intent of the user and is used to control an auxiliary device, such as a wheelchair (Tanaka et al., 2005) or spelling computer (Kübler et al., 2009). The control signal is additionally presented to the user via feedback (Cincotti et al., 2007). Feedback additionally serves a key role during stages of training for BCI usage. With the aid of feedback, the user can adapt his or her actions depending on whether the outcome was desired or not in order to improve the usability of the BCI (Nijboer et al., 2008).

1.2 The Sensorimotor Cortex & the Sensorimotor Rhythms

The cortical signals that are being measured can originate from various cortical areas. There is however one specific cortical area which has been exploited by many BCIs, namely the Sensorimotor Cortex (SMC) (Yuan and He, 2014) (Figure 1.3). An area of the SMC of particular interest for at least ECoG BCI usage is the hand knob; the area on the SMC that is mainly responsible for coordinating and performing hand and finger movements (Yousry et al., 1997).

The SMC has several distinct properties that make it attractive for BCI use. The first distinct property of the SMC is that it presents an ordered representation of all the limbs of the human body across the cortical surface; this mapping is referred to as the *somatotopic mapping* (Figure 1.3B). The second distinct property of the SMC is the modulation of cortical activity patterns during movement as well as during attempted movement and imagined movement (Box 2) (Yuan and He, 2014). These patterns, when considered in the frequency domain, are referred to as Sensorimotor Rhythms (SMRs) and can be divided into several bands; namely the delta (δ) (0-4Hz), theta (θ) (4-7), alpha (α) (7-15), beta (β) (15-30), and gamma (γ) (>30 Hz) bands (Jochumsen et al., 2017). Although, the exact definitions of the upper and lower frequencies of these bands vary largely in literature. The modulation of the SMRs during movement manifest itself in decreases of spectral power in the α and β frequency bands (hereafter referred to as the Low Frequency Band (LFB)) as well as an increase in the γ frequency band (hereafter referred to as the High Frequency Band (HFB)) (Miller et al., 2007) (Figure 1.3C). Lastly, the third property of the SMC is the contralateral hemispheric organization. In this context, a contralateral organization denotes the crossing of cortical pathways from the SMC to the muscles of the hands and fingers (Figure 1.3D). As such, the SMC of the left hemisphere is mainly involved in coordinating movement of the right hand and similarly, the SMC of the right hemisphere is mainly involved in coordinating movement of the left hand.

Box 2: Imagined Movement

Imagined Movement: Also known as motor imagery, denotes the mental rehearsal of physical movement. It has been shown that imagined movement produces largely identical SMR modulations as actual performed movement. Alternatively, imagining the kinesthetic experience of movement can result in an identical effect (Lotze et al., 2000).

To make the use of the words contralateral and ipsilateral clearer, the definitions will be defined here per modality. For EEG, MEG and fMRI the words ipsilateral and con-

tralateral will be defined with respect to the hemisphere and corresponding arm, since EEG, MEG and fMRI can consider both hemispheres during the movement of one or both arms, the usage of contralateral and ipsilateral may become confusing. Contralateral/Ipsilateral activity will refer to activity in the hemisphere contralateral/ipsilateral to the moving hand, regardless of whether the left or right hand was moved. In cases were only one hand was used (in a unimanual task), this will be mentioned. In ECoG studies, the electrode grid is often placed on a single hemisphere and therefore, contralateral activity is defined as activity resulting from movement of the arm contralateral to the electrode grid and ipsilateral activity is defined as activity resulting from movement of the arm ipsilateral to the electrode grid.

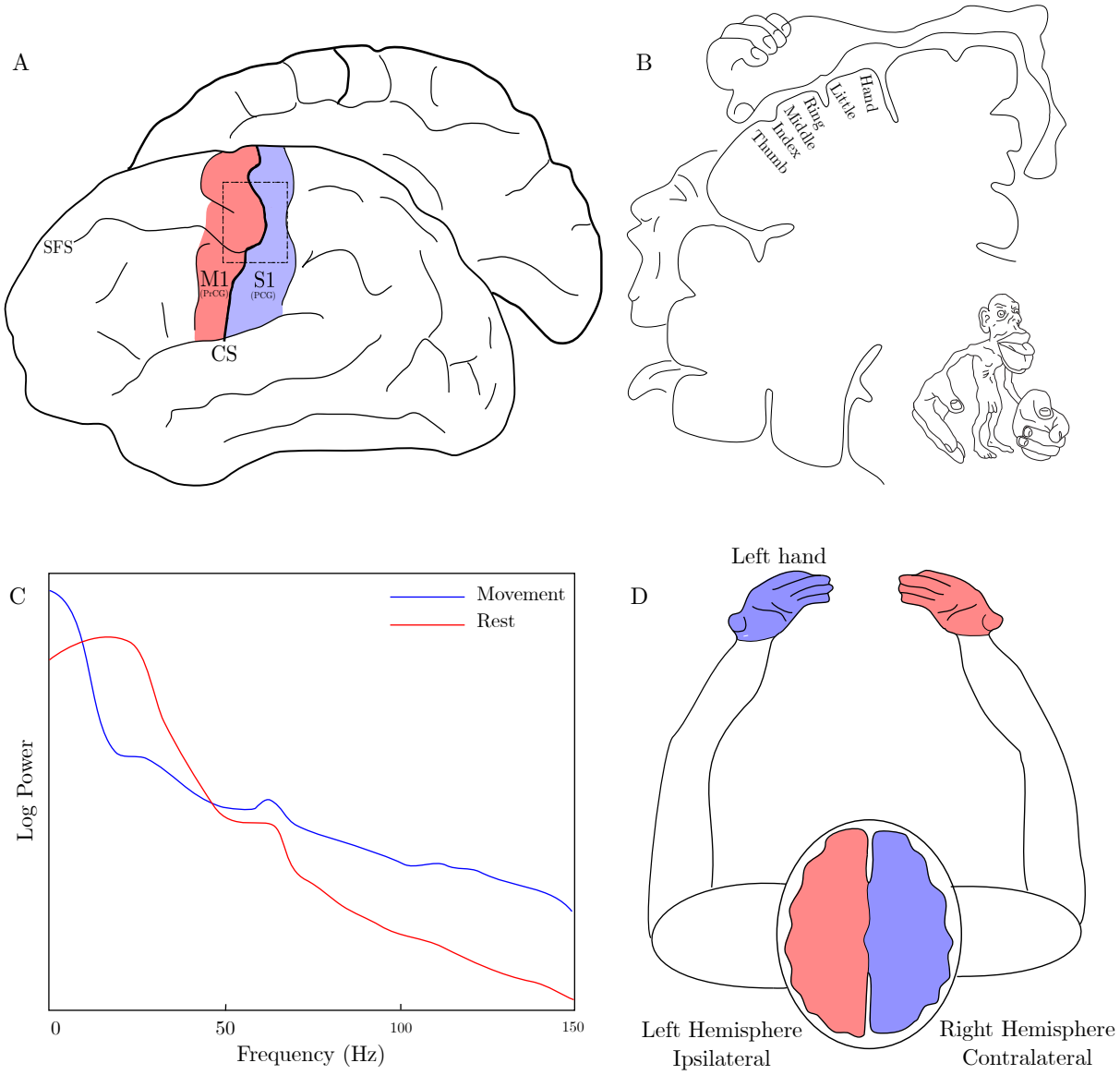

Figure 1.3: *The SMC and its three distinct properties. A) The SMC consists of the Precentral Gyrus (PrCG) and Postcentral Gyrus (PCG), which are separated by the Central Sulcus (CS). The Primary Somatosensory Cortex (S1) - denoted in this figure in blue - is located on the PCG and is believed to be mainly responsible for the processing of sensory information (Martuzzi et al., 2014). The Primary Motor Cortex (M1) - denoted in this figure in light blue - is located on the PrCG and is believed to be mainly responsible for the planning and execution of movement (Zang et al., 2003). The hand knob, which can be found with aid of the Superior Frontal Sulcus (SFS) constitutes a particularly large area of the SMC and is pictured inside the dashed rectangle. Image created from images of (Purves et al., 2011).*

B) An important characteristic of the SMC is the orderly arrangement of the limb representations on both the cortical areas S1 and M1 of the SMC, which is referred to as the somatotopic organization. This image provides a coronal view of M1 and shows the hand representation over the hand knob. These mappings have been determined by stimulation studies by Penfield and Boldrey (Penfield and Boldrey, 1937). It was observed that the cortical areas for the hands and face are relatively much larger than cortical areas associated with other limbs. This disproportional representation of these areas was made visual with the aid of the human homunculus ("little man") depicted in the dashed rectangle. Image created from images of (Purves et al., 2011). C) Changes in SMRs during movement compared to rest. During movement, attempted movement or imagined movement, a decrease in power in the LFB can be observed with an additional an increase in power in the HFB (and occasionally theta band (Yanagisawa et al., 2011)). The x-axis denotes the frequency in Hertz and the y-axis denotes the logarithmic power. Since the illustration solely shows the relative increases and decreases, the y-axis has no scale and units. This figure has been constructed from results from (Miller et al., 2007). D) The contralateral hemispheric organization. The SMC of the contralateral (opposing side) right hemisphere is mainly responsible for the control of the left hand. Here, the left hemisphere is referred to as the hemisphere ipsilateral (same side) to the left hand. Image created from images of (Purves et al., 2011).

1.3 Research Motivation & Problem Statement

The concept of the somatotopic mapping of limbs on the cortical surface as well as distinct modulations of the SMRs during (imagined) movement form the fundamentals on which sensorimotor based BCIs are developed that can distinguish the movement of different limbs based on the spectral and spatial aspects of cortical activity measured with ECoG. In such a way, the (imagined) movements of distinct limbs can be coupled to various control commands. Given the fact that movement, attempted movement and imagined movement result in similar SMR modulations, such SMR based BCIs can also be used by individuals with LIS who no longer have control over their muscles but are able to modulate their SMRs (Ang et al., 2011).

This notion has been recently explored by the University Medical Center Utrecht (UMCU) Brain Center in a BCI referred to as the Utrecht Neuroprosthesis (UNP) which has been implanted and tested on two individuals with LIS in order to restore their communication abilities (Vansteensel et al., 2016a). The current UNP system uses an ECoG electrode grid implantation over the hand knob to obtain a stable and pronounced signal for control which allows these individuals to perform a computer mouse click by mentally performing certain actions or tasks. Motivated by the progress made in four years of implementation, the ultimate goal of the UNP project is to develop a BCI that is 100% accurate and 100% reliable.

Even though the current system has proven to be reliable, it still suffers from two limitations. Firstly, the current version of the UNP system uses a bipolar measurement technique with a relatively low spatial resolution, where signal is recorded from only 2 electrodes at once in a pairwise fashion. Secondly, the number of degrees of freedom available for control in the current project is limited to one, namely the aforementioned mouse click.

Several strategies for the improvement of the current version of the UNP can be considered. The measurement resolution can be improved by making use of larger High Density (HD) electrode grids (Wang et al., 2016). The increased number of electrodes and reduced inter-electrode spacing of such HD electrode grids can significantly increase the measurement area and -resolution compared to the first iteration of the UNP system. This means that a larger cortical area can be measured at a finer level of detail. The usage of electrode grids with an increased resolution may enable to discern more detailed differences between cortical activity patterns associated with ipsilateral and contralateral finger movements (Jiang et al., 2018), subsequently improving the decoding results (Hermiz et al., 2018). To increase the degrees of freedom for device control, one can consider using not only the SMR modulations resulting from movement performed by the hand contralateral to the hemisphere on which the ECoG electrode grid is implanted, but also the SMR modulations resulting from movement performed by the hand ipsilateral to the hemisphere on which the electrode grid is implanted. Although the hemispherical organization is largely contralateral, cortical activity in a single hemisphere during ipsilateral hand movement has been reported in literature (Fujiwara et al., 2017), (Verstynen et al., 2005), (Bundy et al., 2018). The possibility to decode both contralateral and ipsilateral finger movements from a single hemisphere additionally alleviates the necessity of placing electrode grids on both hemispheres, which is unfavorable given the tremendous impact of the surgery associated with implantation.

There are several unknowns surrounding these possible improvement strategies that need to be further researched. Firstly, it is currently unknown whether contralateral and ipsilateral finger movement can be accurately classified from the SMC of a single hemisphere.

Secondly, it is unknown whether the HD electrode grids allow for classification of these finger movements from a small area of the SMC of a single hemisphere. Hence, the problem statement that reflects the resulting knowledge requirement can be formulated as follows:

It is unknown to what extent contralateral and ipsilateral individual finger movements can both be classified from the same small area of SMC of a single hemisphere.

The rationale behind the desire to perform classification from a small area - with an arbitrary location and with an arbitrary size in cm2 - of SMC follows from the philosophy of the UNP which aims at simplicity and minimal invasiveness of a BCI. The rationale behind classifying both contralateral and ipsilateral finger movements to increase the degrees of freedom stems from a more universal desire for BCI use which may in addition to the UMCU, benefit the BCI community as a whole.

This research will firstly use the problem statement as a guide to determine the scope of an initial literature review. Afterwards, the insights gained from this literature review will be used to formulate novel research questions that the remainder this research will address with the aid of several experiments. In this way, this research will partially fulfill the knowledge requirement of the UMCU and will provide novel insights for the field of (academic) BCI research.

2 Literature Review

Based on the problem statement defined in the previous section, this literature review will shed light on the underlying physiological principles, preprocessing methods, features and decoding methodologies that enable the classification of both contralateral and ipsilateral finger movements from a single hemisphere. Additionally, this literature review will address and discuss the technical implications for the development of BCIs that decode both contralateral and ipsilateral movements from a single hemisphere and additionally identify gaps in knowledge and literature on this topic.

2.1 Literature Outline

This literature review will commence with Section 2.3, which will address finger somatotopy in light of both contralateral and ipsilateral finger and hand movements. In Section 2.4, the underlying physiological phenomena of both contralateral and ipsilateral finger movements will be discussed. These physiological phenomena will be handled separately in terms of spatial, temporal and spectral aspects. This division allows for an ordered overview of physiological phenomena which translates well to the three feature domains (the spatial, temporal and spectral domains) that are used in decoding processes. For ECoG, EEG and MEG, the spatial and temporal aspects are tightly coupled to the spectral aspects; the spatial and temporal aspects are different for each frequency band and therefore, the spatial and temporal aspects cannot be considered outside the spectral context and will consequently be handled within the section on spectral aspects. One exception to this layout can be made for studies using fMRI. The usage of this technique does not involve any spectral aspects but will be handled in this same section nevertheless. Section 2.5 will present the state of the art on the decoding of hand and finger movements in general and will discuss how the physiological aspects divided in the three aspects are used in the decoding process. Section 2.6 will be devoted to the classification of both contralateral and ipsilateral hand and finger movement, which is the subject that is most relevant to the problem statement of this literature review. With this structure, all relevant aspects around the classification of contralateral and ipsilateral hand and finger movements are handled: from the underlying physiological principles to the translation of these principles into features and back to the elaboration on physiological principles with aid of classification outcomes.

2.2 Literature Selection

The databases that were used for this literature review were Scopus, Embase, PubMed, Google Scholar and BioRxiv. Pubmed, Embase and BioRxiv are oriented towards the medical domain, while Scopus and Google Scholar do not have a specific focus domain. Cochrane was not considered for this literature review, because it focuses more on clinical healthcare and reviews of treatments. Several inclusion and exclusion criteria were defined which will be handed during the initial assessment of an article based on its title, abstract, methodology and results. These criteria are listed below. A more detailed description of

the formulation of the inclusion criteria is included in Appendix B.

- **Date**: Articles on physiological process were included regardless of the publication date. Only decoding papers more recent than 2000 were included.
- **Participants**: Only studies with human participants were included.
- **Methodology**: Only studies that recorded hand and finger movement were included, additionally, studies with imagined movement were excluded. Studies with attempted movement were however included.
- **Language**: Only articles written in English were included.
- **Literature types**: Literature from peer-reviewed (Scopus, Embase, Pubmed, Google Scholar) and non-peer reviewed sources (BioRxiv) were included.
- **Modalities**: Articles using ECoG, fMRI, EEG and MEG were included. Studies that combine two or more of these modalities were also included.

The keywords that are relevant for finding literature within the scope of this research were extracted from the problem statement in Section 1.3 and the inclusion- and exclusion criteria mentioned in the sections above. The search keywords that will be used are listed in (Table 2.1). These search keywords were combined with logical operators (AND, OR, NOT) to form search queries.

Concept	**Keywords and Search Terms**
Imaging modality	*Functional magnetic resonance imaging, fMRI, MRI, ECoG, electrocorticography, electroencephalography, EEG, iEEG, intracranial, EEG, magnetoencephalography, MEG*
Cortical areas	*Primary somatosensory cortex, sensory cortex, primary motor cortex, motor cortex, sensorimotor cortex, SMC, M1, S1, cortical areas, precentral gyrus, postcentral gyrus*
Decoding and Classification	*Encoding, decoding, mapping, somatotopy, somatotopic, mapped, classification, representation*
Movement	*Finger, hand, gesture, unimanual, movement*
Laterality	*contralateral, ipsilateral*
Participant type	*Human*
Study type	*Comparing*

Table 2.1: *Keywords and search terms for the literature search summarized per concept*

In order to restrict the number of results, the queries are created such that they return not more than 100 results per database were included. The reader can refer to Appendix C for the combination of keywords with the Boolean operators and Appendix D for an overview of constructed queries and search results that were obtained and included.

The search process yielded 1830 articles. This number also included articles that were found prior to the systematic search from for example literature recommendations by colleagues, related articles or references inside these articles. After removing duplicates, 1618 unique articles were retained. At first, articles handling pathology were removed. After that, the relevance of the articles was judged based on the title. The relevance was

determined by evaluating which articles focused on the SMC and are related to the decoding or physiological aspects of either contralateral hand or finger movement, ipsilateral hand or finger movement or both contralateral and ipsilateral hand or finger movement. After this process, 386 of the 1618 articles were retained. Afterwards, the relevance of this subset of articles was judged on the abstract, after which 202 of the 386 articles were retained. The relevance was determined in an analogous manner as above, but the abstract was used to assess the research on the "Participants", "Modality" and "Methodology" criteria so that studies with recorded or attempted movement using fMRI, ECoG, EEG or MEG in human participants were included. After this process, 202 of the 386 articles were retained. These articles have been assigned to several categories and sorted per modality. The resulting overview is listed in Table 2.2.

Topic	**ECoG**	**fMRI**	**EEG**	**MEG**	**Total**
Somatotopy	1	36	0	0	37
Ipsilateral or contralateral hand or finger movement	46	17	19	8	90
Ipsilateral and contralateral hand or finger movement	11	15	14	4	44
Preprocessing and decoding	12	1	5	0	18
Physiological background	0	10	1	2	13
Total	70	79	39	14	202

Table 2.2: *The division of literature in five distinct categories and sorted per modality*

2.3 Somatotopy of the Fingers on the SMC

Much of the knowledge on somatotopy is attributed to a study dating back to 1937 by Penfield and Boldrey (Penfield and Boldrey, 1937). The work by Penfield and colleagues made use of electrical cortical stimulation of the M1 and S1 areas upon which the authors observed whether movement of the participant's limbs occurred during stimulation of M1, or whether the participant reported a sensory related sensation upon stimulation, such as a tingling sensation, during stimulation of S1. The article by Penfield and his colleagues has been used widely in literature as an argument for the existence of a clear somatotopic map, without any mention of the complex context of the research itself. Even Penfield and his colleague have warned against a too simplistic interpretation of their work (Kaufman, 1950). Therefore, to no surprise, the classical interpretation of a fine grained, segregated and homogenic map of the distinct body parts cannot always be reproduced in more recent studies, in particular in M1.

More recent studies have successfully reproduced the finger specific somatotopic map in S1. In contrast to using electrical cortical stimulation, these studies elicit cortical activity in S1 through tactile input, by means of applying touches, brush strokes or vibrations onto the fingers of the participants. Using fMRI, a lateral to medial finger somatotopy in S1 can be established by using either calculations of Centers of Mass (COMs) for voxel groups associated with fingers or assigning a voxel to the finger for which it was most activated (Sanchez Panchuelo et al., 2018), (Pfannmöller et al., 2016), (Besle et al., 2014), (Martuzzi et al., 2014), (Stringer et al., 2011), (Weibull et al., 2008), (Overduin and Servos, 2004), (Blankenburg et al., 2003). Albeit, the somatotopies showed overlapping finger representations (Sanchez Panchuelo et al., 2018), (Besle et al., 2014), (Overduin and Servos, 2004), (Meier et al., 2008) and large inter-participant differences (Martuzzi

et al., 2014), (Stringer et al., 2011), (Weibull et al., 2008).

2.3.1 Finger Somatotopy During Movement

Within the context of this literature review, somatotopy studies involving movement rather than tactile input are more relevant and will provide results that are more representative for movement research (Kolasinski et al., 2016). Although the finger somatotopy in S1 has been reproduced by means of tactical input, no studies were found that have reproduced the finger somatotopy in S1 during finger movement. Several studies have however researched finger somatotopy in M1 during movement and discrepancy over the existence of a clear finger somatotopy exits between these studies. Several studies report a rather limited ordered somatotopy with overlap (Olman et al., 2012a), (Beisteiner et al., 2004), (Dechent and Frahm, 2003) while other studies report a clearer somatotopy (Lotze et al., 2000), (Zang et al., 2003) however still with significant overlap and high inter-participant variability.

One explanation for the broad spatial overlap of finger somatotopy in M1 is extensively brought up; movement requires collaboration of multiple muscles and therefore, the larger and more separated cortical activation seen during movements is the result of multiple muscle groups being called upon in an orchestrated manner (Beisteiner et al., 2004), (Dechent and Frahm, 2003), (Sanes and Donoghue, 2002), (Meier et al., 2008), (Sanes and Schieber, 2001). In addition, different movement tasks can result different cortical activation patterns depending on the type and complexity of movement (Lotze et al., 2000) as well as the order of movements. For example, individual finger movements reportedly produce more overlapping activation patterns than movements of two fingers simultaneously (Dechent and Frahm, 2003). Additionally, a random finger tapping task may produce differently arranged cortical activation patterns than a sequential finger tapping task (Olman et al., 2012a). The authors of this paper argue that the differences between sequential and random tapping tasks may be attributed to movement anticipation and preparation. Furthermore, it is often difficult during a motor task move solely the intended finger and minimize movement of adjacent fingers (Ejaz et al., 2015), (Li et al., 2016). This movement of non-cued fingers has been linked to coincide with patterns of daily use (Kolasinski et al., 2016). This theory closely follows the notion of finger enslavement (Yu et al., 2009), in which movement of non-cued fingers was observed during force deficit in one finger in tasks that require high force production. These notions serve as an argument for the desire of a standardized movement task across different studies to enable the production of more reproducible somatotopic maps in M1 in movement (Beisteiner et al., 2004).

At this point, the need to investigate the finger somatotopy in S1 and M1 during movement still exists. Only two studies have researched finger somatotopy in both S1 and M1, which enable a comparison between S1 and M1.

At first, Hlustik performed an fMRI study with two different movement tasks for thumb and little finger, and index, middle and ring finger respectively (Hlustik, 2001). The thumb and little finger were moved by simple flexion and extension, while the index, middle and ring finger where moved sequentially by pressing on a keypad. Notably, M1 and S1 were defined with the aid of the central, precentral and postcentral sulci. The study design included (COM) calculations for each participant, where each voxel was weighted by its correlation coefficient with a certain finger so that voxels which contained more active tissue were assigned a larger weight. The results were compared at group level, of which an interpretation is depicted in Figure 2.1. Their study shows presence of somatotopy in S1 and M1 when considering the average COMs of the participants. By hand, it can be

measured that the finger representations of M1 and S1 span an area of roughly 2.5x4.5 mm and 4x4.5 mm (x,y; lateral-medial x anterior-posterior), respectively. The authors showed that centroid of the thumb representation in S1 was located more laterally than the respective thumb centroid of M1. Moreover, each finger movement was not segregated into discrete areas, but showed overlap, in accordance with the studies outlined in the previous sections. The authors presented as main finding that somatotopy exists for both M1 and S1, but that the somatotopy observed in S1 is more discrete and segregated in contrast to the integrated and overlapping somatotopy in M1. The authors explain their spatial variability in COMs by the variable size and topography of the cortices of individual participants, which the authors did not compensate for using a standard coordinate system or universal cortical model. Unfortunately, this study presents the results only on group level and not on particpant level. The authors do state that the somatotopy obtained by group results was clearer than the variable individual finger somatotopy, but do not present any results to prove this statement.

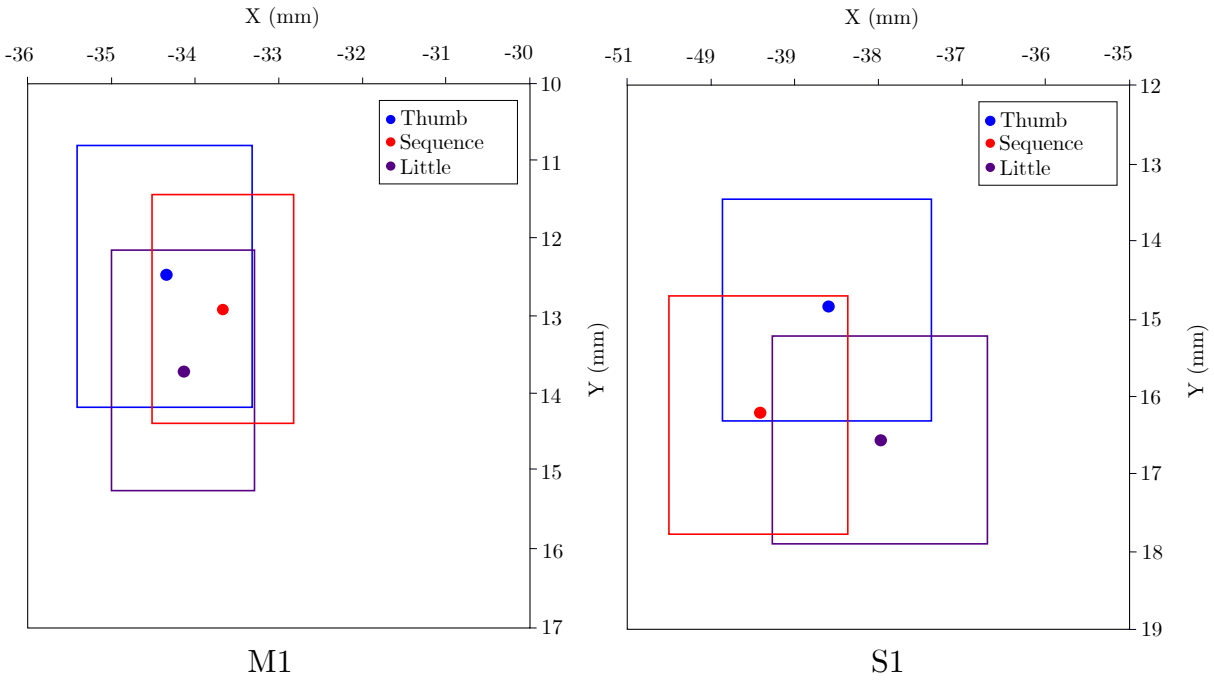

Figure 2.1: *Group average of COM calculations for each of the fingers during the two different movement types for M1 on the left-hand side (A) and S1 on the right-hand side (B) constructed from the results of (Hlustik, 2001). The images are depicted in the axial (x,y) (lateral-medial, anterior-posterior) plane. The x-axes denotes the x coordinate in mm and the y-axes denote the y coordinate in mm. Note that the coordinates on the axis differ between (A) and (B), but the proportions are equal. The thumb and little finger movements are shown, together with the results of sequential finger movements of the index, middle and ring finger.*

Secondly, study by Schellekens and colleagues have presented their findings using a different method by considering Gaussian population Receptive Field (pRF) models (Schellekens et al., 2018). The authors of this paper used a finger flexion and extension task to consider both the somatotopic differences between S1 and M1 (including the central sulcus) as well as the somatotopic differences between finger flexion and extension in both areas. The method in which the center of the Gaussian pRFs associated mostly with each finger was visualized, resulted in a gradient that shows distinct somatotopic organization in M1 and S1 (in S1 only during finger flexion) where each cortical area responds to movement of a preferred digits but also, albeit to a lesser extent, to other fingers. The authors also observed a medial to lateral layout from thumb to little finger for both M1 and S1. Interestingly, upon visual inspection of the results, it can be inferred

that the somatotopy computed for S1 was located more laterally than the somatotopy for M1, which is in accordance for the thumb centroid placing between M1 and S1 in the study by Hulstik (Hlustik, 2001). In addition to the definition of Gaussian pRF centers, the spread of the Gaussian pRFs was used as a measure for the finger specificity, where a larger spread dictated less finger specificity of a neuronal population. The largest pRF spread was observed in M1, which the authors interpret as the notion that sensory information processing in S1 occurs in a more specific, less segregated level than the processing of movement activity in M1. These results seem to be in line with the previous study handled in this section. The article by Schellekens and colleagues unfortunately do not report any quantifiable differences in terms of measurements (in mm or cm) that can support or oppose the findings of the Hlustik and colleagues.

2.3.2 Finger Somatotopy During Contralateral and Ipsilateral Movement

The findings presented up till now have portrayed an image of the finger somatotopy in the SMC resulting from contralateral movement. However, a limited number of studies have examined the differences between the finger somatotopies in the SMC resulting from contralateral and ipsilateral finger movements. Interestingly enough, Hlustik (Hlustik, 2001) observed additional cortical activity in the ipsilateral hemisphere in both S1 and M1 in some participants. However, this cortical activity could not resolve a structured somatotopy in the ipsilateral hemisphere, due to the activation not being statistically significant for all participants. In total, two studies were found that research contralateral and ipsilateral finger somatotopy.

Alkhadi and colleagues published a study researching the somatotopy in M1 of a single hemisphere during ipsilateral finger movements, using the same data that was used in a previous study investigating the somatotopy of contralateral movement in a single hemisphere ((Alkadhi et al., 2000); (Alkadhi et al., 2002)). Both research papers investigated a larger scale somatotopy between finger, hand and other body parts. The research used a brisk finger task, during which all fingers of the right hand were simultaneously opened and closed once. Using again a COM approach, a large scale somatotopy was reported for the contralateral hemisphere and significant activity was reported for all runs of the finger task. For the ipsilateral hemisphere, significant cortical activation was only reported during less than half of the finger task runs, in which it was always smaller in comparison with activation in the contralateral hemisphere. However, a high-level somatotopy for the ipsilateral hemisphere could be constructed from data obtained over 2 imaging sessions. The authors of the articles did not provide a one on one comparison between the layout of the somatotopies observed in the two hemispheres, but the authors did use the same Talairach coordinate system and scale for the presentation of the results of both contralateral and ipsilateral somatotopies. The finger somatotopies during contralateral and ipsilateral movement can therefore be visualized by manually overlaying the COMs of both contralateral and ipsilateral runs (Figure 2.2). The COMs were calculated from all voxels that crossed the significance threshold and were uniformly weighed in the calculation.

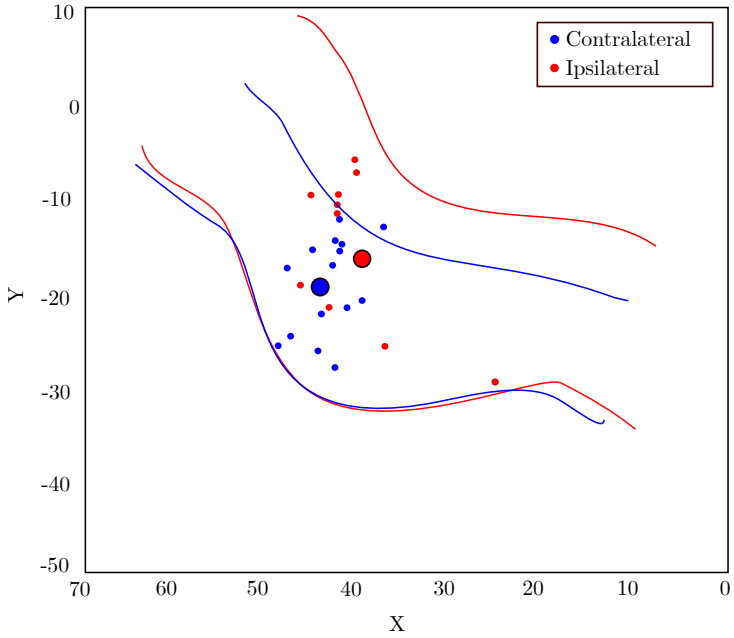

Figure 2.2: *Two dimensional plots of the COMs of the statistically significant runs from all participants observed in M1 of the contralateral and ipsilateral hemisphere constructed by overlaying the results of both papers by Alkhadi et al. ((Alkadhi et al., 2000); (Alkadhi et al., 2002)). The figure gives an axial view and the axes denote the y and x coordinates in Talairach space. Negative y coordinates denote the posterior brain. The x coordinates denote medial (0) to lateral (70). In blue, the borders of the contralateral M1 and the COMs of finger task runs of all participants are given. In red, the approximated borders of the ipsilateral M1 and the COMs of finger task runs of all participants are given. The contralateral results have been mirrored over the vertical axis to match the orientation of the ipsilateral results. The dots with the black outline indicates the mean COMs of the separate COMs of each of the runs for the ipsilateral and contralateral hemisphere respectively. Note that for contralateral hemisphere, more dots are depicted because more runs reached statistically significant activation in contrast to the ipsilateral hemisphere. For the contralateral hemisphere the COMs of 24 runs are depicted, and for the ipsilateral hemisphere, the COMs of 11 runs are depicted. Any COMs from the different tasks recorded in this study have been omitted in this figure.*

A different study conducted by Stippich and colleagues also investigated the contralateral and ipsilateral larger scale somatotopy in M1 between fingers and other body parts (Stippich et al., 2007). The area under consideration did extent the central sulcus onto S1 but no activity related to finger movement was observed there. The authors used a finger opposition task with all digits towards the thumb, with both the left and right hand. In their findings, ipsilateral cortical activation was present during more than 90% of runs for the finger task, although the cortical activation levels were lower than those for contralateral cortical activity. The results of their study presented both individual runs of all participants and COM calculations for the runs of all participants (Figure 2.3). The authors noted that the Euclidean coordinates of the COMs of the ipsilateral activation were shifted anteriorly for both hemispheres, which is in line with the results from Alkadhi and colleagues ((Alkadhi et al., 2000); (Alkadhi et al., 2002)), who also report the COM for the contralateral finger movements to be further posterior in addition to being located more lateral. The authors did not discuss the varying number of contralateral and ipsilateral task runs for both the ipsilateral and contralateral runs. Again, the COMs of contralateral and ipsilateral runs have been constructed from a different number of datapoints between the contralateral and ipsilateral runs, in this study, there were more ipsilateral data points. The COM and the lower boundary of the contralateral activity are shifted slightly more posterior in the left hemisphere than in the right hemisphere

and in addition, the contralateral COMs are narrower in a medial to lateral.

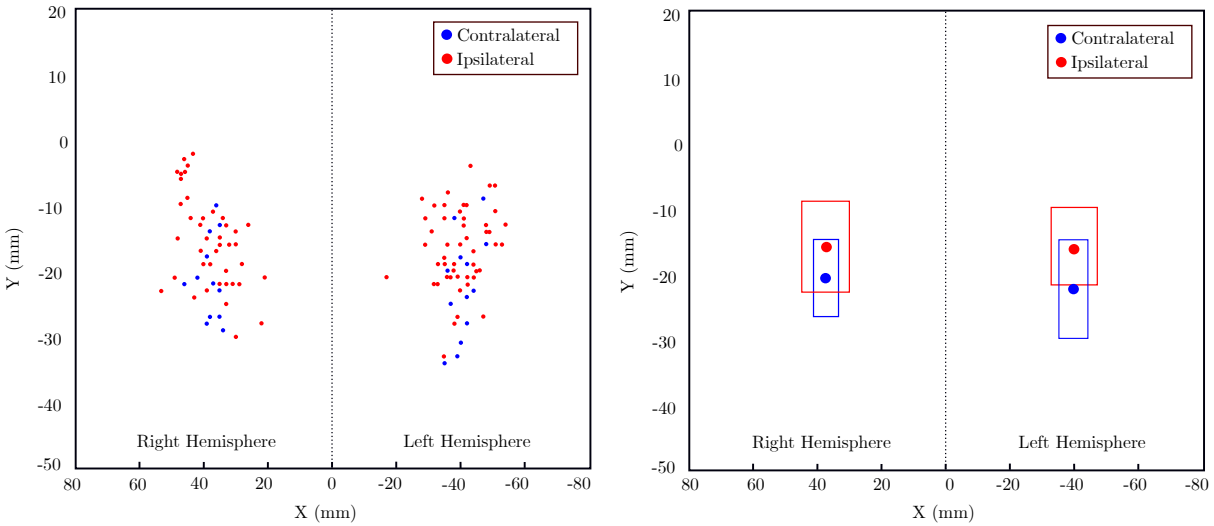

Figure 2.3: *Two dimensional plots, recreated from the results by Stippich and colleagues (Stippich et al., 2007), of both the individual runs (left hand figure) and the COMs of these runs (right hand figure) observed in M1. The figure gives an axial view and the axes denote the y and x coordinates in tens of millimeters in Euclidean space. Negative x coordinates denote the left hemisphere and positive x coordinates denote the right hemisphere. The x coordinates denote medial (0) to lateral (80/-80). Negative y coordinates denote the posterior brain. The blue dots represent the individual contralateral runs and the red dots represent the individual ipsilateral runs, for both hemispheres. The COMs are depicted in blue for contralateral runs and in red for ipsilateral runs. No exact information on the number of runs for the right and left hand was available. Any information from individual runs or COMs from the different tasks recorded in this study have been omitted in this figure.*

In conclusion, more recent studies were in some cases able to reproduce the somatotopic maps of M1 and S1 depending on the visualization methodology and task paradigm that was used. The studies that used a movement paradigm task showed overlapping finger representations, where the somatotopy in S1 seems more segregated and distinct relative to M1. Two studies present an overlap in contralateral and ipsilateral finger representations and that the ipsilateral finger representations are located more anteriorly than contralateral movement, but this was researched only in M1.

2.4 Spatial, Temporal and Spectral Aspects of Contralateral and Ipsilateral Movement

Neuronal signals can be characterized into three separate aspects; namely the spatial (with respect to magnitude of the signal), temporal and spectral aspects. For ECoG, EEG and MEG, the spatial and temporal aspects are tightly coupled to the spectral aspects, as these vary per frequency band. On the other hand, fMRI signals do not have a spectral or temporal representation, thus only the spatial aspects related to these studies are discussed in this section.

2.4.1 Spatial Aspects

Findings from fMRI Studies

Various fMRI studies have reported different outcomes on the presence of ipsilateral cortical activity. Contralateral cortical activity was reported in all participants in all studies, whereas ipsilateral activity was found in either all participants (Horenstein et al., 2009) or only a subset of participants (Ehrsson et al., 2000), Hanakawa et al. (2005), (Singh et al., 1998), (Cramer et al., 1999), (Kim et al., 1993), (Nirkko et al., 2001). Several studies reported less pronounced ipsilateral activity in comparison with contralateral activity (Hanakawa et al., 2005), (Singh et al., 1998), (Baraldi et al., 1999), (Diedrichsen et al., 2013), (Kim et al., 1993) while some studies even reported ipsilateral deactivation (Kobayashi et al., 2003), (Wu et al., 2008).

It appears that the occurrence and degree of ipsilateral activity depends on several aspects. First, several studies report that the task complexity influences the magnitude of ipsilateral cortical activity in the SMC. Three studies compared the degree of ipsilateral cortical activation during a simple and more complex tasks: Ehrsson and colleagues compared a simple power grip to a more complex precision grip (Ehrsson et al., 2000), Verstynen and colleagues compared simple finger tapping to more complex multi-finger chord tapping (Verstynen et al., 2005) and Huo and colleagues compared a simple hand squeeze to a more complex finger opposition task (Huo et al., 2010). All three studies found increased levels of ipsilateral cortical activity during the complex task in comparison with the ipsilateral cortical activity levels observed during the simple tasks. Although the two tasks in the study by Verstynen and colleagues involved a different number of fingers, a control experiment performed by the authors did not show a linear increase of ipsilateral activity with the number of fingers used. In the three studies, the contralateral cortical activity did not change significantly during the increasing task complexities, underlining the theory of a supportive role of ipsilateral activity during complex and precise movement.

Secondly, the handedness of participants influences the magnitude of ipsilateral cortical activity. In M1 of ten right-handed participants, movement of the non-dominant left hand resulted in contralateral activity in all participants and ipsilateral activity in half of the participants whereas dominant right hand movement resulted in contralateral activity, but not in ipsilateral activity (Kobayashi et al., 2003). A similar phenomena has been observed by Singh and colleagues over the whole SMC during a finger opposition task (Singh et al., 1998). Conversely, Wu and colleagues performed a study in M1 of both left and right-handed participants and observed no change in ipsilateral activity levels during movement of the dominant hand but instead observed significant ipsilateral deactivation during movement of fingers of the non-dominant hand in all participants (Wu et al., 2008). A study performed by Kim and colleagues observed that for an ambidextrous participant, ipsilateral activation was more pronounced during both non-dominant and dominant hand movement than for the right-handed participants, with a factor of ten (Kim et al., 1993). Verstynen and colleagues additionally found that left-handed participants recruited the left hemisphere more during movements than right-handed participants (Verstynen et al., 2005). However, the topic of hand dominance is far from being understood, thus this report should be cautiously interpreted.

Two studies have further compared the spatial distribution of contralateral and ipsilateral activity (Verstynen et al., 2005), (Horenstein et al., 2009). Verstynen and colleagues visualized the spatial distribution of contralateral and ipsilateral peak activation from a finger tapping task in the axial plane of M1 (Figure 2.4).

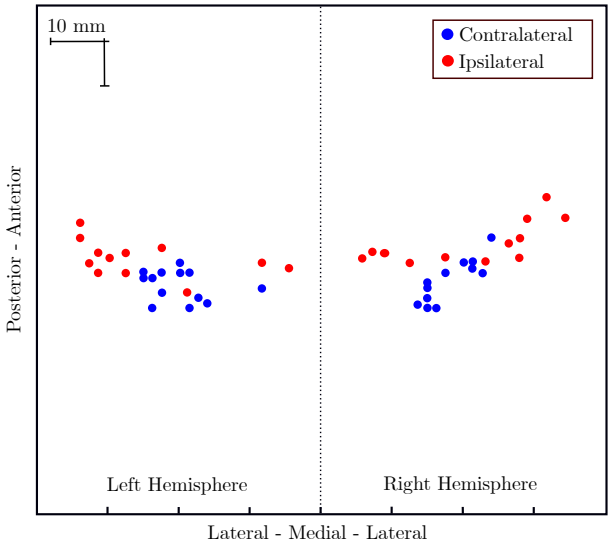

A

Figure 2.4: *Two dimensional plot of the COMs of peak activation from runs of all participants during the two complex finger movements observed in M1 in both hemispheres. The figure gives an axial view where the x axis denotes a lateral to medial to lateral progression over both hemispheres and the y axis denotes the posterior to anterior progression. The peak activation locations for contralateral and ipsilateral activity have been denoted in blue and red respectively. This image has been constructed with the results from the paper by Verstynen et al. (Verstynen et al., 2005)*

Additionally, Horenstein and colleagues visualized the voxel coordinates for contralateral and ipsilateral movements in M1 during a finger tapping task in the axial plane for two participants (Figure 2.5).

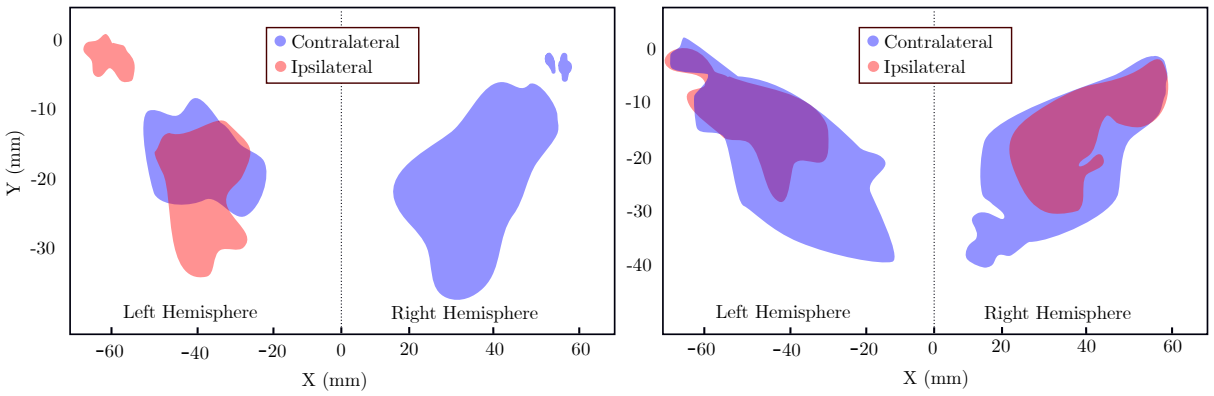

Figure 2.5: *Two-dimensional plot of the activated voxel coordinates of M1 of both hemispheres in participant P2 (left hand figure) and P4 (right hand figure) respectively. The figure gives an axial view where the x axis denotes a lateral to medial (0) to lateral (60/-60) progression over both hemispheres and the y axis denotes the posterior to anterior progression where negative y coordinates denote posterior. Note that the y-axis of the results from participant P4 (right hand figure) has a different range. The activated voxel coordinates for contralateral and ipsilateral activity have been denoted in blue and red respectively. Participant P2 (left hand figure) showed no ipsilateral activity in the right hemisphere. This image has been constructed with the results from the paper by Horenstein et al. (Horenstein et al., 2009)*

In both studies, the analyses were limited to M1 and/or pre-motor areas and results for S1 were not presented. Furthermore, both studies report that the ipsilateral activity sites

were shifted laterally, and anteriorly with respect to the contralateral activity sites in a single hemisphere. The anterior shift of ipsilateral activity is in accordance with the literature handled in the somatotopy section, although a lateral shift was not reported by Stippich and colleagues (Stippich et al., 2007) (Figure 2.3) and a contrasting medial shift was seen after overlaying the results of Alkadhi and colleagues ((Alkadhi et al., 2000); (Alkadhi et al., 2002)) (Figure 2.2). However, significant spatial overlap between contralateral and ipsilateral activity was reported in all five studies. Horenstein and colleagues have additionally calculated that the spatial overlap in M1 was greater than 70% in the right hemisphere of nine out of ten participants (Participant P2 showed no ipsilateral activation in the right hemisphere (Figure 2.5)) and in the left hemisphere for eight out of eleven participants (Horenstein et al., 2009).

Findings From EEG, ECoG and MEG Studies

The differences in magnitude between contralateral and ipsilateral cortical activity have been similarly researched in EEG, ECoG and MEG studies. In an unimanual hand movement EEG study, Formaggio and colleagues observed a spectral decrease in the LFB during contralateral movements in all participants (Formaggio et al., 2008). In seven out of nine participants, a less pronounced spectral decrease in the LFB was observed during ipsilateral movements. This observation of a less pronounced spectral decrease in the LFB were acknowledged by the findings of an EEG study by Gerloff and colleagues (Gerloff et al., 2000) and those of a MEG study by Muthuraman and colleagues (Muthuraman et al., 2012). Notably, Muthuraman and colleagues found that the spectral decreases in the LFB during ipsilateral movement were more pronounced during left hand movements than during right hand movements, indicating a similar hemispheric asymmetry as was observed in the fMRI studies. In ECoG studies, the spectral decreases in the LFB during both contralateral and ipsilateral movement were visible (Zanos et al., 2009) (Jin et al., 2016) although a pronounced difference as in the EEG and MEG studies was more difficult to observe. This may be caused by the choice of electrode referencing methods; all ECoG studies used Common Average Referencing (CAR) while Gerloff et al. and Muthuraman et al. used a mastoid reference electrode and Formaggio et al. used Fz as reference electrode. The ECoG studies additionally described the spectral modulation patterns in the HFB, where an increase in spectral power during ipsilateral movements was either absent (Wisneski et al., 2008) or smaller in comparison with contralateral movement(Zanos et al., 2009), (Jin et al., 2016).

The more focal spatial distribution of HFB modulations in contrast to the more broad spatial distribution of LFB modulations resulting from contralateral movements has been reported widely in literature (Crone, 1998) (Miller et al., 2009). When observing the spatial aspects of the various frequency bands with EEG and MEG, it is useful to use source localization methods given the limited spatial resolution of these techniques (Dalal et al., 2008). The same observations of more spatially focal HFB modulations in comparison with the spatially broad LFB modulations resulting from contralateral movement have been observed in an EEG study that utilized the sLORETA localization method (Kuo et al., 2014) and a MEG study that made use of the Synthetic Aperture Magnetometry (SAM) beamformer localization method (Huo et al., 2010). A later study by Jin et al. observed the spatial differences between modulations resulting from both contralateral and ipsilateral hand gestures (Jin et al., 2016). The spatial extent of HFB modulations resulting from contralateral movements was larger (i.e. spanning more electrodes) than that of ipsilateral movements, but the modulations took place over similar electrodes, implying that HFB modulations resulting from ipsilateral movements are more focal than those resulting from contralateral movements, but still overlap to a large degree. This finding is in line with the earlier findings from the fMRI studies. The only contrasting finding was

reported by Wisneski and colleagues who observed that the ipsilateral hand movements produced more notable modulations in the LFB than for than in the HFB during a hand movement task in six participants (Wisneski et al., 2008). The authors do report that the spectral modulations in the HFB resulting from contralateral and ipsilateral movement show overlap in a third of the electrodes. The authors observed that the electrodes over which spectral modulations resulting from contralateral movement were observed, lay mostly over the SMC. In contrast, electrodes over which spectral modulations resulting from ipsilateral movement were observed, did not lay over the SMC but lay either over pre-motor areas or cortical areas that have no direct relation to movement. The discrepancy in results between the other studies and this study could not be explained with the information presented in this study. Something that may have contributed to the contrasting results is the fact that the electrode grids that were used in this study were large 64 channel electrode grids located over various (non-motor) areas and were in some cases placed bilaterally. Therefore, the results obtained in this study may not be representative of the results obtained in the studies that had mainly grid coverage over the SMC.

A recent study by Scherer and colleagues focused on a single patient with an atypical electrode grid arrangement (Scherer et al., 2009). The standard clinical electrode grid of this participant was interleaved with several smaller electrodes, which reduced the effective inter-electrode distance to 0.7mm and increased the measurement resolution. Two different movement tasks were performed by the participant; one movement task that included movement of all the fingers on one hand (whole hand movement) and the other task consisted of individual finger movement. The authors reported a spatially broad modulation of the LFB and more focal modulation of the HFB in electrodes covering the SMC, for both tasks. The electrodes that showed modulations in the HFB during contralateral movement were similar to those that showed modulations in the HFB during ipsilateral movements. However, again the HFB modulations for ipsilateral movements were more spatially focal. The spatial distributions of LFB modulations were highly similar between whole hand and individual finger movements and the spatial extent of the LFB modulations was thus large for both whole hand and individual finger movements. However, the spatial extent of the modulations in the HFB was larger for whole hand movement than for individual finger movement. The group additionally reported that the HFB modulations took place over a smaller number of electrodes for ipsilateral finger movements in comparison with contralateral finger movements, but that these electrodes did overlap. More interestingly, the authors found that even though the HFB modulations took place over the same electrodes for contralateral and ipsilateral tasks, the electrodes that recorded the highest activity for contralateral finger movements were different from electrodes which recorded the highest activity during ipsilateral finger movement. The authors of the current paper attribute the discovery of these finer grained differences between cortical activity resulting from ipsilateral and contralateral finger movements to the increased measurement resolution of the electrode grid. The authors further argue that the use of higher density electrode grid enabled them to capture non-redundant patterns of HFB modulations and that the exact small differences in finger representations might not be discernible with clinical electrode grids. Although this finding is interesting, the study included only a single participant and the results of this participant were not compared to results of a participants with a standard clinical electrode grid in the same study.

2.4.2 Temporal Aspects

So far, the spatial and spectral aspects have been considered from a rather stationary point of view. Movements are highly dynamic and require the collaboration of multiple

muscles and cortical areas during various stages of movement, so that changes of in cortical activity patterns over time are expected. Only the findings from EEG, MEG and ECoG studies on this matter will be presented here; temporal aspects in fMRI studies will not be discussed here due to the limited temporal resolution of this technique. While multiple studies have examined the temporal aspects of LFB modulations of only contralateral hand and finger movement (Yong et al., 2004), (Quandt et al., 2012), (Huo et al., 2010), (Talakoub et al., 2017), (Erbil and Ungan, 2007), (Pfurtscheller et al., 1996), only a small number of studies could be found that handle the timing differences between LFB modulations resulting from both contralateral and ipsilateral movements. Bai and colleagues (Bai et al., 2007) observed hemispheric asymmetry and hand dominance related timing differences in an EEG study. During left hand movements, the decrease in spectral power in the LFB was observed as early as almost 2000ms prior to movement onset distributed over both the contralateral and the ipsilateral hemisphere. From 640ms after movement onset, the decrease in spectral power in the LFB decreased on both hemispheres but showed a prolonged suppression only over the ipsilateral left hemisphere at around 1200ms after movement onset. During right hand movements, the decrease in spectral power in the LFB was most notable over the contralateral left hemisphere from 1400ms to 380ms prior to movement onset. This early appearance of LFB modulations in the contralateral hemisphere have additionally been described in other studies (Yong et al., 2004), (Quandt et al., 2012), (Rau et al., 2003). Bai and colleagues observed the decrease in spectral power in the LFB over the ipsilateral hemisphere rather late in comparison to the contralateral hemisphere, only at 130ms prior to movement onset for both hands. No further evidence of the later occurrence of ipsilateral LFB modulations before movement could be found. During movement, Bai and colleagues observed prolonged suppression of spectral power in the LFB over both hemispheres. This prolonged suppression has been similarly observed by studies researching the contralateral hemisphere (Huo et al., 2010), (Erbil and Ungan, 2007). Bai and colleagues additionally observed that a decrease in spectral power sustained longer during ipsilateral movement than during contralateral movement, of which further proof was not found in other studies. The study by Bai and colleagues demonstrates that a notion of hemispheric asymmetry, which was also observed in the spatial aspects in the chapter above, may also be present in the temporal aspects. However, the proof to support any statements surrounding this theory is too scarce. Such detailed results have additionally not been reproduced in ECoG studies that were included in this literature selection. However, the studies by Wisneski and Leuthardt (Wisneski et al., 2008), (Leuthardt et al., 2009) both show that decreases in spectral power in the LFB as a result of ipsilateral movement occur on average 160ms earlier than the decreases in spectral power in the LFB resulting from contralateral movement. This observation makes the authors of both studies argue that the hemisphere ipsilateral to hand or finger movement may be involved in the planning of motor action, however this claim cannot be supported sufficiently with the results from these studies alone.

No articles could be found on the differences in timing of HFB modulations between contralateral and ipsilateral movement. What is known from studies handling contralateral movement is that in contrast to LFB modulations, the HFB modulations have been shown to be highly time locked to movement (Talakoub et al., 2017), (Huo et al., 2010), (Erbil and Ungan, 2007) which makes the modulations in the HFB an effective marker of movement onset and termination. Given this fact, one might argue that a comparison of these modulations between contralateral and ipsilateral movement may be performed. However, as has been mentioned, no such study has been found. Only one ECoG study has examined the temporal aspects of HFB signals, but only between M1 and S1 during contralateral movement (Sun et al., 2015). The authors of this study showed that the occurrence of spectral power increases in the HFB located in S1 preceded those of M1 by 136ms. These results were found in five participants included in the study. Although

interesting, no reproduction of this result has been found in the literature selection.

As a last remark, there is one temporal aspect that has been found that deserves some attention, albeit for contralateral movement only. In addition to considering signals in the frequency domain, as has been done in previous sections, one can consider these signals from the temporal domain. When comparing signals in the time domain, the informative (although difficult to interpret) phase information can be retained (Quandt et al., 2012). Such a temporal representation of cortical signals has found its applications in both ECoG and EEG where these time series signals are referred to as the Local Motor Potential (LMP) and the Slow Cortical Potential (SCP) respectively (Salyers et al., 2018). The LMP can be obtained by low pass filtering (<10 Hz) cortical recording time series (Acharya et al., 2010) and the authors of this study have shown that the LMP strongly correlates with the time course of finger movement. Unfortunately, no study so far has attempted to compare LMP signals between ipsilateral and contralateral hand or finger movement.

In conclusion, several fMRI studies have shown that ipsilateral cortical activity (in comparison to contralateral cortical activity) was less pronounced (in magnitude) and depends on both handedness and task complexity. Additionally, several authors found a large spatial overlap between contralateral and ipsilateral cortical activity, where some studies report an anterior shift of ipsilateral cortical activity. EEG, MEG and ECoG studies have similarly shown that spectral modulations in both the LFB and HFB manifested with a smaller magnitude for ipsilateral movement in comparison with contralateral movement. It was shown that the LFB spectral modulations were less spatially focal than HFB modulations and that spectral modulations in the HFB resulting from both contralateral and ipsilateral movement show a large spatial overlap, but that HFB modulations resulting from ipsilateral movements were more spatially focused (i.e. occurring over less electrodes). Such a spatial difference between contralateral and ipsilateral fingers could not be observed for the LFB. The temporal patterns of modulations in the LFB have been researched and it appears that the differences of the LFB modulation patterns in both hemispheres are related to handedness. For the HFB, timing has been researched in ECoG studies in which the onset of spectral modulations appeared earlier during ipsilateral movements with respect to contralateral movements. Additionally, the time series signal referred to as the LMP has been introduced in this section.

2.5 State of the Art on Decoding Hand and Finger Movement

So far, the physiological principles surrounding cortical activity related to contralateral and ipsilateral movement have been covered. These sections have provided a segregated view of the spatial, temporal and spectral aspects surrounding cortical activity resulting from movement. However, in practice these aspects are in dynamic interplay, often in multiple dimensions, and are related to complicated mechanisms of the brain of which many have not yet been unraveled. Decoding of cortical signals is only possible with an informative representation of these complex processes in the form of (combinations of) features in the temporal, spatial or spectral domain. This chapter will therefore be devoted to the state of the art on decoding hand and finger movement in general. This section will summarize, on a high abstraction level, the main insights that are related to decoding of only ipsilateral or contralateral hand or finger movement. A later section will be devoted to decoding of both contralateral and ipsilateral movement.

2.5.1 Insights from Decoding Attempts of Hand and Finger Movement

Before delving into the details of the decoding, a distinction must be made between to different decoding strategies that were commonly found in literature: classification and regression. Classification refers to the division of movement into discrete classes or states, such as movement or no movement, or movement of an index finger versus movement of a thumb. In classification, movement is modeled as having a direct relationship with cortical activity and these models often discard the temporal evolution of movement parameters (Wang, 2011), an aspect that is important in regression problems. In regression, the movement is represented as a continuous variable and is decoded as such (Xie et al., 2018). The temporal information is of substantial importance in regression tasks; the cortical and physical movement aspects at one point in time are dependent on those of previous time and influence those that follow. Regression studies that were found in this literature selection handle mostly kinetic and kinematic aspects, such as the position of the finger or arm movements over time (trajectory) or the acceleration of a limb. Although regression methods in movement studies mostly attempt to model temporal evolution of movement and cortical activity, they can be used for classification.

Whether a classification method or a regression method is more suitable depends highly on the eventual application. A form of continuous control obtained with regression might provide more degrees of freedom, but for some BCI applications, having several discrete classes is enough and may provide more simplicity to the user. In this literature review, the focus mainly lies on the classification of individual finger movement, and to a lesser extent on the classification of hand movements or regression of both hand and finger movements.

A broad overview of features, classifiers, regressors and corresponding decoding accuracies that were found in this literature selection are presented in Table 2.3. One should be cautious with directly interpreting and comparing decoding accuracies; the accuracies have been obtained from different datasets and using different features. Additionally, only the lower and upper bound of the performances are listed. However, the accuracies can aid in model and feature selection in a later stage. Additionally, this table can be used to infer general statements about features, classifiers and regressors.

Author	**Modality**	**Task**	**Features**	**Classifier**	**Performance**
Classification					
(Jiang et al., 2018)	ECoG	Grasp	CSP	LDA	93.6–97.4%
(Fifer et al., 2011)	ECoG	Grasp	(8–14), (16–30), (30–50) (70–100), (100–150) Hz + LMP	GLM	0.79<r<0.81
(Waldert et al., 2007)	EEG & MEG	Grasp	LMP	RLDA	54-57%
(Li et al., 2017)	ECoG	Gestures	(4–8) (8–12), (70–135) Hz	SVM	55-90%
(Yanagisawa et al., 2011)	ECoG	Gestures	(2-8), (25-40), (80-150) Hz	SVM	25-60%

Continued on next page

Table 2.3 – continued from previous page

Author	Modality	Task	Features	Classifier	Performance
(Bleichner et al., 2016)	ECoG	Gestures	(4–8), (8–14), (15–30), (65–95), (70–125) Hz + LMP	PTC	30-100%
(Chestek et al., 2013)	ECoG	Gestures	(66–114) Hz	NB	55-96%
(Branco et al., 2017)	ECoG	Gestures	(70–125) Hz	PTC	59-100%
(Hotson et al., 2016)	ECoG	Individual Finger Movement	(72-110) Hz	LDA	76.0-96.5%
(Xiao & Ding, 2013)	EEG	Individual Finger Movement	(8–12), (13–30) Hz	SVM	35-45%
(Bai et al., 2007)	EEG	Individual Finger Movement	PCA, ICA, CSP, DWT	LMD, QMD, BSC, MLP, PNN, SVM	53-63%
(Xiao & Ding, 2015)	EEG	Individual Finger Movement	(0-70) Hz, PCA	SVM	55-99%
(Shenoy et al., 2007)	ECoG	Individual Finger Movement	(11-40), (71-100) Hz	SVM	30 - 91%
(Wissel et al., 2013)	ECoG	Individual Finger Movement	(11-30), (60-300) Hz	HMM, SVM	37-100%
(Liao et al., 2014)	EEG	Individual Finger Movement	(0-200) Hz, PCA	SVM	45-92%
(Onaran et al.,2011)	ECoG	Individual Finger Movement	CSP	SVM	18-85%
(Elgharabawy & Wahed, 2012)	ECoG	Individual Finger Movement	SIDWT + Gram Schmidt	SVM	r=0.82
(Samiee et al., 2010)	ECoG	Individual Finger Movement	(1-60), (60-100), (100-200) Hz, AM, DWT	LDA, SVM, kNN	15-55%
Regression					
(Talakoub et al., 2017)	ECoG	Hand Reaching	(1–4), (8–12), (13–30), (> 30) Hz + LMP	MLR	0.80<r<0.95
(Bundy et al., 2016)	ECoG	Reaching	(4–8), (8–12), (12–24), (24–34), (34–55), (65–95), (130–175) Hz + LMP	PLS	0.22<r<0.80
(Waldert et al., 2008)	MEG	Reaching	(<7), (10-30), (62-87) Hz	RLDA	35–78%

Continued on next page

Table 2.3 – continued from previous page

Author	Modality	Task	Features	Classifier	Performance
(Acharya et al., 2010)	ECoG	Grasp	LMP	GLM	0.51<r<0.91
(Flint et al, 2017)	ECoG	Grasp	(0–4), (7-20), (70-115), (130-200), (200-300) Hz + LMP	WSC	0.2<r<0.6
(Pan et al., 2018)	ECoG	Gestures	-	RNN	43-90%
(Flamary & Rakotomamonjy, 2012)	ECoG	Individual Finger Movement	AR	LR	r=0.42
(Kubánek et al., 2009)	ECoG	Individual Finger Movement	(8–12), (18–24), (75–115), (125–15), (159–175) Hz + LMP	PR	40-100%
(Liang & Bougrain, 2012)	ECoG	Individual Finger Movement	(1–60, (60–100), (100-300), (300-600) Hz	LR	0.21<r<0.48
(Wang, 2011)	ECoG	Individual Finger Movement	(8-12), (18-24), (75-115), (125-159), (159-175) Hz + LMP	PR, SNDS	0.64<r<0.86
(Hazrati & Hofmann, 2012)	ECoG	Individual Finger Movement	EMD	AF	r=0.55
(Saa et al, 2016)	ECoG	Individual Finger Movement	(70-170) Hz	CRF	62–65%
(Saa et al., 2018)	ECoG	Individual Finger Movement	(0.5-40), (70-170) Hz	LDA, MLR	0.55<r<0.78
(Elango et al., 2017)	ECoG	Individual Finger Movement	-	LDA, HMM, LSTM	53 - 82 %
(Chen et al., 2014)	ECoG	Individual Finger Movement	(1-60), (60-100), (100-300), (300-6000) Hz + LMP	LWR	0.40<r<0.70
(Marjaninejad et al., 2017)	ECoG	Individual Finger Movement	(1-60), (60-100), (100-200) Hz	MLP, LDA	0.40<r<0.69
(Nakanishi et al., 2014)	ECoG	Single Finger Movement	(0–4), (4–8), (8–14), (14–20), (20–30), (30–60), (60–90), (90–120), (120–150) Hz	SLR	0.86<r<0.97
(Xie et al., 2018)	ECoG	Single Finger Movement	-	RNN	0.32<r<0.79

Continued on next page

Table 2.3 – continued from previous page

Author	Modality	Task	Features	Classifier	Performance

Table 2.3: *Overview of articles that handle decoding of hand and finger movement, sorted by whether the research includes regression or classification and whether these research focused on decoding of hand movement or finger movement. For each study, the features, classifiers and the obtained lower and upper bound for accuracy in percent, or the correlation value (r) is listed. The abbreviations for the Features are formulated as follows, in order of appearance; Common Spatial Patterns (CSP), Principal Component Analysis (PCA), Independent Component Analysis (ICA), Shift Invariant Discrete Wavelet Transform (SIDWT), Auto-regressive Model (AM), Empirical Mode Decomposition (EMD). The abbreviations for the classification or regression models are formulated as follows, in order of appearance; Linear Discriminant Analysis (LDA), Regularized Linear Discriminant Analysis (RLDA), Generalized Linear Model (GLM), Support Vector Machine (SVM), Pattern Template Correlation (PTC), Naive Bayes (NB), Mahalanobis Distance Classifier (LMD), Quadratic Mahalanobis Distance Classifier (QMD), Bayesian Classifier (BSC), Multi Layer Perceptron (MLP), Probabilistic Neural Network (PNN), Hidden Markov Model (HMM), k-Nearest Neighbours (kNN), Multi-linear Regression (MLR), Partial Least-squares Regression (PLS), Wiener Cascade Decoder (WSC), Recurrent Neural Network (RNN), Linear Regression (LR), Pace Regression (PR), Switched Non-parametric Dynamic System (SNDS), Adaptive Filtering (AF), Conditional Random Fields (CRF), Long Short-term Memory (LSTM) Sparse Linear Regression (SLR).*

The findings from Table 2.3 will be discussed in the same order as that of a decoding methodology, starting with features and ending with actual classification or regression. From Table 2.3 it appears that a large number of studies, either focused on regression or classification, make use of frequency domain features. It is therefore interesting to elaborate on how the various frequency bands relate to movement, which can be done by means of classification and regression results.

Several studies handling the classification or regression of hand or finger movement have already selected one particular frequency band or component of interest. From the articles included here, these are either the HFB or LMP. In hand movement studies, the HFB shows good classification of gestures (e.g. (Chestek et al., 2013), (Branco et al., 2017)). The LMP shows to be able to hold information regarding brisk hand movements and has been successfully applied for both classification (Waldert et al., 2007) and regression tasks (Acharya et al., 2010). For studies handling finger movement, the HFB shows to be informative in both regression (Delgado Saa et al., 2016) and classification problems (Hotson et al., 2016), (Liao et al., 2014). Notably, for all studies that involved individual finger movement, the LMP was not found to be the only feature that was used.

The studies that have researched - in a methodological way - the contribution of each frequency band on the decoding accuracy can provide insight into the informativeness of one frequency band in comparison to the other frequency bands. From these studies, it could be inferred that the HFB is more informative for decoding brisk hand movement than the LFB in classification (Fifer et al., 2011) and more informative than both the LFB as well as the LMP (Li et al., 2017) (Bleichner et al., 2016) in classification. For decoding individual finger movement, the same observations can be made; the HFB showed better discriminative power for fine movement than the LFB in classification (Onaran et al., 2011), (Wissel et al., 2013), (Hotson et al., 2016) and regression studies (Liang and Bougrain, 2012). Again, the LMP was not mentioned as the most informative feature in any of the studies involving individual finger movement.

Bundy and Yanagisawa (Bundy et al., 2016), (Yanagisawa et al., 2011) demonstrated

that during hand and finger movement, the number of electrodes showing significant activity in the HFB was smaller than the number of electrodes showing significant activity in the LFB meaning that the lower frequencies have a more diffuse spatial representation and that the higher frequencies show a more focal spatial representation, which is in accordance with the spatial acuity of the LFB and HFB bands discussed in the section 2.4.1. The notion that the HFB has a different spatial distribution than the LFB or LMPs had led to the hypothesis that these phenomena are governed by different underlying neuronal mechanisms and further spatial discrepancies between the frequency bands made Bundy and colleagues (Bundy et al., 2016) hypothesize that the brain represents finger movement in different abstraction levels; i.e. a difference between the coarse aspects (such as distinction between movement or rest) and the finer aspects related to finger movement, such as the exact amount of finger flexion.

Interestingly, such a hypothesis was paralleled by the results of Flint and colleagues (Flint et al., 2017). The authors of this paper have used PCA to reduce the high dimensional (22 dimensions) data coming from a Cyberglove data recording glove that tracked the exact positions of the joints from the hand that was being moved. The first Principal Component (PC) was attributed to the large and brisk hand grasping motions, while the second and third PCs were attributed to the finer and smaller finger movements during the grasp task. The authors found that the first PC in this brisk hand movement was highly correlated with the activity in the LFB. However, the authors also found that the second and third PCs, containing the more detailed information about precise joint angles, were mostly correlated with the HFB, instead of the LFB. This contributed to the hypothesis that finer movements may be encoded in higher frequency signals and thus that different gradations of detail may be encoded in different frequency bands. A similar finding was observed in the results by Acharya and colleagues (Acharya et al., 2010), who found that the first PC decoded from the cyberglove recordings of hand grasping motions represented the slow opening and closing of the hand. This slow movement was found to be highly correlated with the low frequency LMP. Similarly, Onaran and colleagues (Onaran et al., 2011) observed that the LFB alone did not yield high classification accuracy for a finger movement task and argued that these frequency bands may only have relation to a general cognitive state of movement. Bundy and colleagues (Bundy et al., 2016) later applied this insight in practice and were able to increase classification accuracy with a two stage hierarchical approach in which the authors used the LFB to first coarsely differentiate rest from movement, after which the finer movement kinematics were decoded with the information from the HFB and the LMP.

These results show that hand or finger movements are not solely represented in one specific frequency band of cortical signals. Several studies have demonstrated that combining information from the LFB with either the LMP or information from the HFB led to higher decoding accuracies for classification (Chestek et al., 2013), (Bleichner et al., 2016), (Li et al., 2017) and regression (Talakoub et al., 2017), (Bundy et al., 2016) of brisk hand and finger movements (Kubánek et al., 2009), (Shenoy et al., 2007). Additionally, selection of narrower sub-bands in the larger frequency bands (that were sometimes rather coarsely defined by some authors as can be observed from Table E.1) may yield better decoding results (Scherer et al., 2009) and it is therefore perhaps useful to define multiple narrower frequency band that may give information about more specific narrow band activities that govern movement.

Although these results give no final conclusion on which frequency bands are best for decoding movements in all participants, the results of this analysis show that different frequency components may be related to unique aspects of movement and that especially the higher frequencies show the spatial acuity necessary for successfully decoding fine

movements such as those of individual fingers. These findings also show that the cortical processes governing hand and finger movement are inherently complex and are represented in varying degrees in the frequency spectrum and recording channels without a clear structure, which makes optimal decoding a challenging task.

For that reason, it is no surprise that much research has been done into feature selection, channel selection and classification schemes that provide the best decoding results. In some cases, especially in studies of a more exploratory nature, the features and channels may be manually selected a priori. Afterwards, the classification results can be analyzed to determine what channels or features were most informative. However, this process can be time consuming and the results may be difficult to interpret. Additionally, selecting one broad set of frequencies for all participants may lead to discarding of narrow band participant-specific activity, consequently leading to sub-optimal decoding results that may not generalize well across participants.

From a machine learning point of view, the trade-off often lies on the transparency of the results versus a black box approach that determines a (locally) optimal set of features and channels for each participant resulting in a possibly more uniform decoding performance. This notion is especially important given the high dimensionality (substantial number of frequency bands and channels) and the often low number of trials found in especially ECoG studies. It is therefore not surprising that many authors have applied automated methods to optimize the selection of representative and informative features of the various aspects of cortical activity. There is a vast number of well validated filtering and signal decomposition techniques available for feature extraction and feature selection. For now, these will not be covered in much detail, given that most provide no comparison with respect to alternative options, but rather show that these can achieve good performance. Examples of techniques include Independent Component Analysis (ICA) (Bai et al., 2007), Common Spatial Patterns (CSP) (Onaran et al., 2011), (Jiang et al., 2018). Shift Invariant Wavelet Decomposition Trees (SIDWT) (Elghrabawy and Wahed, 2012) with Gram Schmidt feature selection (Samiee et al., 2010), (Elgharabawy and Wahed, 2017), Auto-regressive Coefficients (AR) (Flamary and Rakotomamonjy, 2012) Empirical Mode Decomposition (EMD) (Hazrati and Hofmann, 2012) or combinations of spatial and spectral filtering methods (Saa et al., 2018).

Apart from spatial, spectral or temporal filtering and feature subset selection, these techniques also have the important function of dimensionality reduction. The importance of dimensionality reduction here can be illustrated with a dimensionality reduction technique that was found in this collection of literature. The technique concerns a type of spectral PCA, which has been designed by Miller and colleagues (Miller et al., 2009). The authors hypothesized that the increases in spectral power in the HFB are part of a broadband phenomenon that is visible over the whole frequency spectrum. By applying PCA on the cortical data (in the frequency domain) from individual finger flexion task the authors obtained so called Principal Spectral Components (PSCs). The authors observed that this decomposition resulted in several PCs, of which the third spectral component reflected changes in spectral power in the θ and α range, the second PSC reflected changes in spectral power in the β range and the first PSC reflected changes in spectral power over the whole power spectrum ranging from 0 to 200 Hz, which was the limit of the bandwidth that the authors have selected (Figure 2.6).

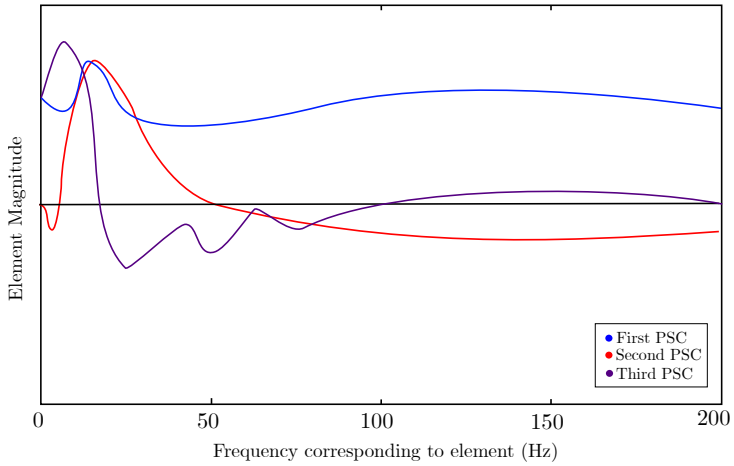

Figure 2.6: *The resulting elements of the Principle Spectral Component Analysis. The first PSC corresponds to the broadband phenomena of which the samples are higher than zero over the whole bandwidth. The second PSC corresponds to the β band. The third PSC is depicted in green and represents the θ and α bands. This figure was taken from the paper by (Miller et al., 2009).*

Miller and colleagues hypothesize that the increase in spectral power in the HFB is part of this broadband spectral activity taking place over the whole power spectrum. This phenomenon denoted by the first PSC was found consistently in all participants and varied in magnitude over electrode locations. Surprisingly, the authors found that the relative magnitude of the first PSC related to a certain finger was different at neighboring channels and showed indirectly, that the first PSC showed similar spatial specificity as the normally used HFB.

Xiao and Ding (Xiao and Ding, 2015) later hypothesized that this well defined broadband spectrum could also be detected in noninvasive methods and have applied this technique in decoding of individual finger movements in EEG. The authors showed that the first PSC was able to decode individual finger movement better than the second PSC, third PSC or LFB separately for all participants except two. Notably, when classifying with only the LFB features, the confusion matrix showed that all fingers were classified as being the thumb, while for classification of the PSCs separately, much better results were obtained. Liao and colleagues (Liao et al., 2014) have similarly applied this spectral PCA technique on EEG data (128 channels) from an individual finger movement task, but additionally provide a comparison of this technique with ECoG data from a similar finger movement task. The authors showed that the first PSC representing the broadband phenomena from the EEG data was able to classify individual finger movements better than the LFB or HFB separately in all participants. The authors show the results of the classification using the first PSC from the ECoG data in comparison and it shows that the differences in accuracy between EEG and ECoG decoding differ from 10 to 20 percent. However, given that the results were obtained from different datasets and recording techniques, a direct comparison may be questionable. However, as an indication for baseline results from ECoG studies, it is remarkable to see that both EEG studies, with limited bandwidth and resolution, are able to classify individual fingers with the use of this methodology, something which was not possible with using only the modulations of the LFB and HFB as features.

This shows that the use of dimensionality reduction as a means of feature subset selection can improve classification and increase the noise robustness of a decoding process. However, the curse of high dimensionality and data scarcity is not only reflected in the feature selection stages. The results of classification are not solely attributable to the features, but also to the classifiers or regressors. And naturally, low quality features can-

not be compensated for with complex classifiers and vice versa. From Table 2.3 it can be qualitatively observed that a vast number of articles have applied lightweight sparse or linear classification or regression models. Although it is unlikely that brain works in a linear fashion, there is some discussion as to whether the high dimensionality of data combined with the small number of trials allows for successful application of nonlinear classifiers. On the one hand, nonlinear classifiers can capture the nonlinear nature of cortical recordings but may on the other hand may be prone to overfitting on high dimensional data if no generalization can be found with the limited amount of training data. As an example, Marjaninejad and colleagues (Marjaninejad et al., 2017) have compared a linear classifier (LDA) with a non-linear classifier (MLP). The authors extracted features from three broad frequency bands from 1 to 200 Hz and fed this as a feature vector in both decoding models. The authors observed that the classification accuracy between the linear and nonlinear model did not differ to a considerable extent. The authors used this observation as an argument for the fact that although the physiological processes resulting in the energy in the frequency bands stem from nonlinear processes, they can be approximated well with a linear classifier. Of note, the MLP used in their research only contained a single layer. However, the authors observed that upon increasing the number of layers of the MLP and thus increasing its ability to capture non-linearity, the decoding accuracy degraded because of overfitting. It is to be noted that the classification was performed after a strong reduction of the dimensionality of the feature vector.

For the studies that do not apply sophisticated dimensionality reduction techniques (for example when using a more exploratory research approach), the use of sparse and linear models appears to be suitable option. Focusing for now only on classification of individual finger movement, it can be stated from Table E.1 that the SVM is used rather often. While most authors do not give an explicit explanation for the choice of an SVM, Wissel and colleagues (Wissel et al., 2013) have mentioned that the SVM can be considered as the gold standard within BCI applications thanks to its robustness, ability to handle nonlinear relationships and ability to problems that come with small datasets with high dimensional data (Wang et al., 2010). A study by Shenoy and colleagues (Shenoy et al., 2007), demonstrate the ability of a sparse SVM with a L1 regularization norm to continuously perform well under an increase of the number of channels in the feature vector. The sparseness of the classifier indicates that most weights are zero, which the authors interpret as a form of dimensionality or feature reduction. A similar dimensionality reduction is observed in pace regression (Wang and Witten, 1999), which is used by several studies in Table 2.3.

In general, the linear and simplistic models (or in some cases template matching approaches e.g. (Branco et al., 2017), (Bleichner et al., 2016)) for both classification and regression that are used in the studies in Table E.1 provide the ability to decode with little training data and more importantly, the ability to interpret the results, which is often needed in studies that use classification as a means to explain underlying neurological principles. The use of deep learning and Artificial Neural Network (ANN) models apparent from this table is not ignored, but the models that are observed in these studies remain rather shallow; Xie and colleagues (Xie et al., 2018) have used a 4 layer RNN and both Saa and colleagues (Saa et al., 2018) and Marjaninejad and colleagues (Marjaninejad et al., 2017) have used a single layer MLP. It must be mentioned that there is definitely no consensus on whether nonlinear models are substantially better than linear models and vice versa (Wang, 2011). However, the implications of limited data and high dimensionality are clearly visible in preprocessing, feature selection and classification stages.

2.5.2 Classification Schemes and Results on Finger Movement Classification

Since this literature review focuses on the classification of individual fingers, it is sensible to provide more detail into the results of studies that have handled classification of individual finger movements. For such a multi-class classification problem, generally a One versus All (OVA) or One versus One (OVO) scheme was used. Although they both provide valid options, there has been one report that the OVA scheme suffered from class imbalance (Shenoy et al., 2007). Much of the studies unfortunately do not report what exact classification scheme has been used, and those who do report this, have used an OVO scheme (Samiee et al., 2010), (Onaran et al., 2011), (Liao et al., 2014), (Xiao and Ding, 2015). However, regardless of the scheme or classifier that was used, there was a large similarity between studies for the individual finger classification results. Generally, the thumb was decoded with higher accuracy than other fingers (Elgharabawy and Wahed, 2017), (Onaran et al., 2011), (Liao et al., 2014), (Hotson et al., 2016), (Xiao and Ding, 2013), (Xiao and Ding, 2015), (Shenoy et al., 2007), (Elghrabawy and Wahed, 2012). Some mixed results were reported for the other fingers. For the little finger, in some cases it was well classified (Elgharabawy and Wahed, 2017), (Liao et al., 2014), (Xiao and Ding, 2013), (Xiao and Ding, 2015), (Elghrabawy and Wahed, 2012) and in other cases, there was considerable misclassification between the little finger, the ring finger and the middle finger or index finger (Onaran et al., 2011), (Hotson et al., 2016), (Liang and Bougrain, 2012). For the studies considered, there was considerable confusion between the middle three fingers. Anatomically, this could be explained by the fact that the tendons of the index, middle, ring and little finger are coupled to the same flexor, namely the flexor digitorum profundus. The thumb is hereby the only finger that is not coupled to the same flexor, which is a likely explanation for the fact that it is less often confused with other fingers (Elghrabawy and Wahed, 2012). Additionally, the movement of non cued fingers has been linked to coincide with patterns of daily use (Kolasinski et al., 2016). Whether the higher classification accuracies of the thumb could be attributed to the larger cortical representation of this finger on the (Olman et al., 2012a), (Overduin and Servos, 2004) remains unknown.

2.5.3 Applying Pragmatic Anatomical Constraints to Improve Decoding

Literature has demonstrated another particular way of increasing the decoding results of methodologies. One way that was found is to incorporate certain anatomical constraints into the decoding scheme. An example is provided by Wang and colleagues (Wang, 2011), who included a constrained graph model in the decoding process. This graph model contained transitions based on the three states a finger can be in; namely extension, flexion or rest. Each state is associated with particular movement patterns described by kinematic parameters such as speed and acceleration, of which there is little in resting state and more in movement states. Also, there is a finite set of transitions between the states, so that transitions are not truly random. The inclusion of these constraints have shown to provide a better fit than pace regression that had been used as a comparison. Chen et al. (Chen et al., 2014) have applied a similar approach by approaching movement not solely as a pure regression problem, but as having what the authors refer to as the binary property of being either in motion or in a resting state. The authors incorporate this knowledge into their logistic weighted regression algorithm and show improvement over pace regression and linear regression which the authors use as comparison. A slightly different approach was suggested by Bundy et al., (Bundy et al., 2016) in a study into asynchronous decoding of movement. The authors hypothesized that the cortical activity recorded during rest would be different from that during movement and therefore constructed a hierarchi-

cal regression model that first determined whether there was movement or not and after that was established, applied regression of kinematic parameters, improving on their own model.

There are, however, some possible downsides to these approaches. At first, these constraints have often been tailored specifically for each task implying that the constraints possibly only generalize across that task or participant (Xie et al., 2018). Secondly, some constraints that are designed may not include all possible patterns of for example finger flexion or usage (Wang, 2011). These two factors can limit how well these models may generalize with different data (Elango et al., 2017).

In conclusion, different movement types were encoded differently in various frequency bands, where the LFB contained most information around brisk movements and the HFB showed to be informative in decoding fine movements. However, it has been demonstrated that different frequency components may be informative in combination with several frequency components, so that there is no definite answer on what frequency band encodes what aspect of movement. In addition, the most informative frequency bands were participant-specific. Due to the high data dimensionality and often low number of trials, much attention is paid to dimensionality reduction, feature selection and classifier selection. In some cases, this poses a tradeoff in sacrificing transparency of the obtained results. In terms of individual finger decoding, it has been shown that the thumb is generally well decoded, while the other fingers are often confused, possibly due to the fact that these are connected to the same flexor. The additional inclusion of prior knowledge of finger movements in the form of pragmatic constraints may improve the decoding process.

2.6 Classification of Contralateral and Ipsilateral Hand and Finger Movement

The previous section provided an overview of the state of the art of decoding hand and finger movements in general. This section focuses particularly on decoding both contralateral and ipsilateral hand and finger movement. Table 2.4 gives an overview of the articles that decode of only ipsilateral, contralateral or both ipsilateral and contralateral movement of either the whole hand or the individual fingers (Appendix E provides the actual references that have been used to construct this table).

Laterality and Limb	**ECoG**	**fMRI**	**EEG**	**MEG**	**Total**
Contralateral Hand	10	1	3	1	15
Contralateral Finger	24	0	4	0	28
Ipsilateral Hand	0	0	0	0	0
Ipsilateral Finger	1	0	0	0	1
Contralateral and Ipsilateral Hand	2	0	1	0	3
Contralateral and Ipsilateral Finger	1	1	2	1	5
Total	39	2	10	2	

Table 2.4: *Overview of literature handling decoding of hand and finger movements sorted per category and per measurement modality*

It should be noted that this table has been made from the viewpoint of contralateral and ipsilateral hand movements, relative to a single hemisphere. Such a viewpoint holds for ECoG studies. However, as has become clear from other sections in this review, the other

imaging techniques (EEG, MEG and fMRI) can observe the complete cortical surface and give insight to both hemispheres at the same time. However, for the interpretation of this table, the division was made by analyzing whether the classification was performed for a single hand or both hands, and which hemisphere(s) had been used for decoding.

The number of articles that focus only on decoding ipsilateral finger movement with ECoG is strikingly small, only a single article was included in this literature selection that equipped ECoG. Unfortunately, the authors of this article have made a note that the results were not reproducible. Therefore, this article will not be handled. Similarly, a very small number of articles is available that handle the classification of both contralateral and ipsilateral hand or finger movement, which is the most important topic in light of this literature review. Notably, only a single article focuses on the classification of both contralateral and ipsilateral finger movements. This chapter begins with handling the methods that allow to investigate both hemispheres at the same time, being EEG, MEG and fMRI. After those methods, the focus will be shifted to ECoG.

2.6.1 Findings from fMRI, EEG and MEG

Diedrichsen and colleagues (Diedrichsen et al., 2013) performed classification of both contralateral and ipsilateral individual finger movements in fMRI. The authors used a searchlight based approach using two classifiers for each hand. The classification of ipsilateral movements was most successful in regions that showed a decrease in cortical activity in comparison with the rest condition. The areas that contributed highly to the classification of ipsilateral finger movements overlapped to a great extent with the areas that contributed to the correct classification of contralateral movements in both M1 and S1 (Figure 2.7).

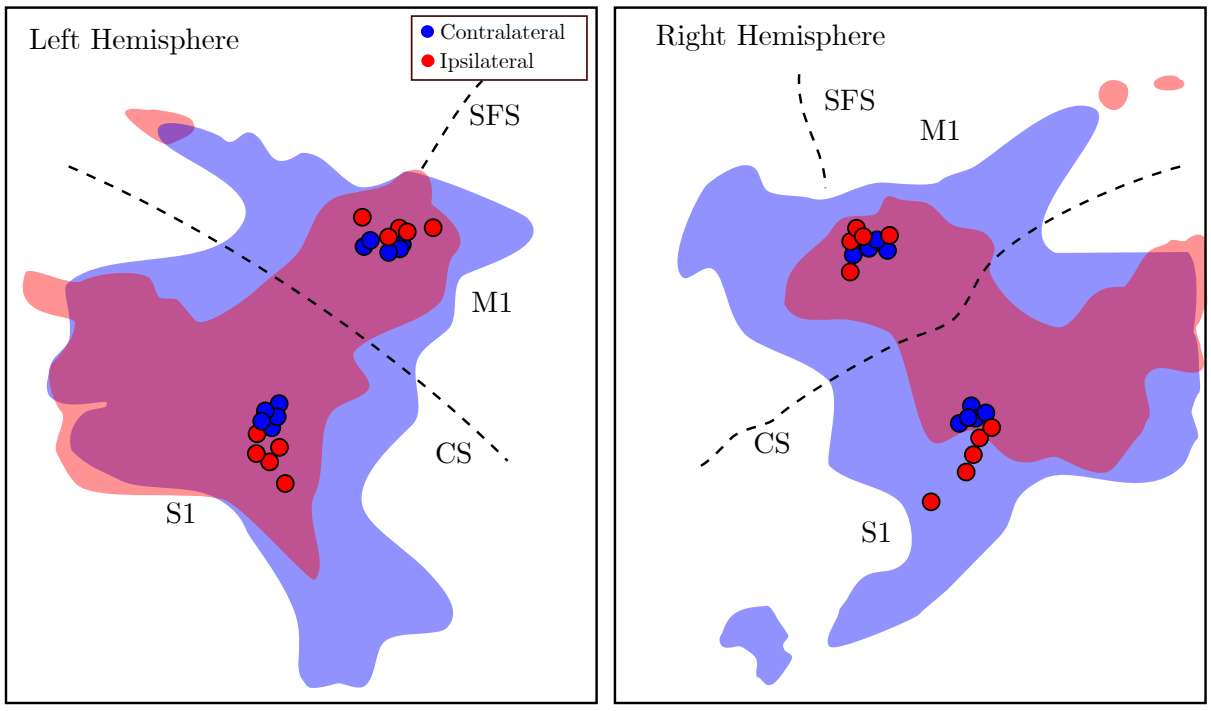

Figure 2.7: *The overlap in regions in which classification accuracy was larger than 32%. The circles and denote the COMs of classification accuracy for the individual participants in both M1 and S1. The central sulcus is denoted with CS and the superior frontal sulcus is denoted with SFS. This figure was taken from the paper by (Diedrichsen et al., 2013)*

As seen from Figure 2.7, the COMs for ipsilateral classification accuracy in S1 seem to be shifted anteriorly, which is an observation that has not been reproduced in other

studies. In other studies, such an anterior shift was only observed in M1 (Alkadhi et al., 2000), (Alkadhi et al., 2002), (Stippich et al., 2007) (Figure 2.3), (Verstynen et al., 2005), (Horenstein et al., 2009) (Figure 2.5). Such a shift in M1 has not been reported in this study by Diedrichsen and colleagues (Diedrichsen et al., 2013). The authors report that the voxels that showed cortical activity in a single hemisphere during movement of a finger contralateral to that hemisphere also showed activation during movement of the identical finger on the hand ipsilateral to that hemisphere, although ipsilateral activity in those voxels was less pronounced. This is in accordance with the spatial aspects discussed in section 2.4. Additionally, the classification accuracies for ipsilateral finger movements were lower than for contralateral finger classification, an effect that was slightly more apparent in S1 than in M1. Unfortunately, the authors do not present the classification results of individual fingers and do not discuss or observe any difference in classification between hemispheres.

Cho and colleagues (Cho et al., 2004) have discriminated left and right finger index movement with the use of EEG. The authors used the spectral power decreases in the LFB (parameters obtained by an auto-regressive model) as features. The classification was performed over the channels C3, Cz and C4, corresponding to the SMC. Their approach using a simple neural network yielded good discrimination accuracy, albeit the accuracies obtained for the left hand were higher than for the right hand in most participants, which were all right handed. This indicates that the hemispheric symmetry observed in earlier chapters, might impact classification performance. Liao and colleagues (Liao et al., 2007) used the so called Movement Related Potentials (MRPs), which are similar to LMPs, in addition to spectral modulations in the LFB as features. The authors found that the MRPs at the electrodes contralateral to the movement produced a more rapid decrease in signal amplitude in comparison with electrodes ipsilateral to the side of movement. The authors additionally found that the modulation of the LFB was more pronounced for right index finger movement than for left index finger movement and that these modulations were more pronounced at contralateral electrode sites. These effects were used as the features for classification by means of Discriminative Spatial Patterns (DSP) and CSP using electrodes C3 and C4. This method provided reliable results, although the authors do not present results related to difference in finger classification accuracy.

Pires and colleagues performed the same index finger movement task and classified left and right finger movements based on the Bereitschaftspotential (BP) and modulations in the LFB, which were obtained with EEG (Pires et al., 2007). After removing much of the trials due to artefacts, the authors obtained a high accuracy by using these features in combination with Common Spatial Subspace Composition (CSSD) on electrodes around C3 and C4. In a MEG study, Kauhanen and colleagues observed that the post movement β rebound was more pronounced over contralateral electrodes than over ipsilateral electrodes and have consequently used this phenomenon as a classification feature, yielding good results (Kauhanen et al., 2006). Classification accuracy improved by increasing the number of channels around the SMC, which is in line with the theory that the LFB modulation patterns are spatially widespread phenomenon in which information from a larger spatial region can increase classification.

Both EEG and MEG are able to classify left and right hand or finger movement with low frequency features. The reduced spatial resolution of these techniques did not per se limit the effectiveness of classification. However, these articles only studied classification between 1 finger of both hands, making the classification task more focused on separating left- and right-hand movement, rather than separating individual fingers from both hands. The large advantage of the three techniques (fMRI, EEG and MEG) is that these allow to use both hemispheres for the classification of movement from both hands. All

these studies make use of observed differences observed between the electrodes over the left and right hemispheres in a bipolar measurement.

2.6.2 Findings from ECoG

Such an approach is not possible with ECoG, given that the electrode grid is normally placed over a single hemisphere. ECoG studies therefore require a different decoding approach. As an example, Fujiwara and colleagues have hypothesized that ipsilateral hand movement is decoded in the same was as contralateral hand movement (Fujiwara et al., 2017). To test this hypothesis, the authors used a cross-decoding methodology where one classifier was trained with data from ipsilateral movement and tested this classifier on data of contralateral movement and vice versa, a methodology that has seen application in a similar setting but then for brisk arm movements in a study by Bundy and colleagues (Bundy et al., 2018). The authors of this paper have used spectral domain features from both the LFB and HFB. In addition, the authors included the LMP. The classification was performed with a SVM with L1 regularization to prune off irrelevant features. Decoding accuracies were lower for ipsilateral movements than for contralateral movements. For all participants, the best results were obtained when using features from the HFB recorded from both M1 and S1, although the selection of an optimal subset of features from the HFB differed for each participant. If their hypothesis of a similar neural pattern between contralateral and ipsilateral movement is true, their classifiers should generalize well on data of movement from either hand. The authors found that when using the HFB obtained from M1, the classifiers generalized in both directions (trained with ipsilateral data and tested on contralateral data and vice versa) for all participants. The LMP from M1 was able to generalize in one direction (trained with ipsilateral data and tested on contralateral data). A similar result was found for the HFB features obtained from S1. A spatial analysis revealed that the spatial patterns of HFB modulations in M1 were more focal than those of the LFB. Additionally, the authors showed that the HFB modulations resulting from both contralateral and ipsilateral movement show high spatial similarity, although the magnitude of ipsilateral activity was lower. Their results indicate that identical neural patterns exist for both contralateral and ipsilateral hand movements in the HFB obtained from M1.

Jin and colleagues researched the decodability of the gestures used in the rock paper and scissors game, performed with the contralateral and ipsilateral hand (Jin et al., 2016). Notable differences in the magnitude and spatial distribution of the spectral changes in the HFB between the three gestures were found. The authros do however not report the quantitative differences between the spectral changes in the HFB resulting from contralateral and ipsilateral movements. After classification with a SVM using features from the HFB, the authors inferred that the increase in spectral power in the HFB was larger during contralateral movement than during ipsilateral movement. By comparing the single channel decoding performance, the number and distribution of informative channels seemed similar between contralateral and ipsilateral movements, but no quantitative analysis was performed. The decoding accuracies were slightly lower for ipsilateral movement than for contralateral movements.

Following these two articles, only one article was found that was in line with the problem statement; namely the classification of contralateral and ipsilateral individual finger movement. Scherer and colleagues have applied a clustering approach referred to as Distinction Sensitive Learning Vector Quantization (DSLVQ) which allows for feature subset selection by assigning lower weights to features that contribute less to the decoding accuracy and assigning higher weights to features that were more relevant to increasing the decoding accuracy (Scherer et al., 2009). The authors performed research on two

participants of which one was implanted with a clinical electrode grid with 1cm spacing and the other with a similar grid, but interleaved with smaller electrodes, increasing the electrode spacing to 0.7cm. The authors composed 4 binary classification schemes that required classification of different fingers from the same hand (contralateral thumb versus contralateral index and ipsilateral thumb versus ipsilateral index) as well as classification of identical fingers from the different hands (contralateral thumb versus ipsilateral thumb and contralateral index versus ipsilateral index). The accuracies were computed for 9 time lags ranging from 0 to 4 seconds in steps of 0.5 seconds. The authors present that the classification yielded good results using the combined information from both the LFB as well as the HFB, of which the results are displayed in Table 2.5.

Participant	**Classification**	**Channel**	**Accuracy**
1	Contra thumb vs. Contra index	41	81.7% (+/- 7.3)
	Ipsi thumb vs. Ipsi ndex	28	66.6% (+/- 7.1)
	Contra thumb vs. Ipsi thumb	50	**94.7**% (+/- 3.3)
	Contra index vs. Ipsi index	20	**98.5**% (+/- 1.5)
2	Contra thumb vs. Contra index	16	79.2% (+/- 6.9)
	Ipsi thumb vs. Ipsi ndex	16	81.3% (+/- 5.3)
	Contra thumb vs. Ipsi thumb	32	**100.0**% (+/- 0.0)
	Contra index vs. Ipsi index	24	**100.0**% (+/- 0.0)

Table 2.5: *Classification results from the DSLVQ classification on the different classification schemes using all features from the LFB and HFB in the study by (Scherer et al., 2009). The results are listed per participant. The channel that is listed denotes the best performing individual channel. Classification accuracies are given as mean classification accuracies and the standard deviation is provided between brackets. The mean and standard deviations are computed from 100 runs of the DSLVQ method for the time lag with the highest accuracy.*

From this study it was no possible to infer which feature combinations and electrode locations were selected by the DSLVQ algorithm, but interestingly the authors observe that the binary classification schemes that involve the separation of finger movements from identical fingers of different hands (classification accuracies in bold in Table 6) are better classified than different fingers from one hand. The authors show for three arbitrary channels, that the amplitudes in the HFB are highly different between ipsilateral and contralateral finger movements but are highly similar for movements of both fingers from one hand. This serves as an explanation for why the classification between fingers on the same hand proves to be less successful than classifying identical fingers from the two opposing hands (for which in some cases perfect classification was reached), it is likely that the classification between contralateral and ipsilateral movement is based on the difference in amplitude of the power spectrum over the relevant electrodes. The authors further explain that the classification results for the participant with the higher resolution electrode grid were better, although this is not directly observable from their results. The authors demonstrate that selecting participant-specific narrow sub-bands from both the LFB and HFB can in some cases improve classification performance in comparison with using features from the complete LFB and HFB. This effect was most apparent for the second participant (with the clinical electrode grid) and to a lesser extent for the first participant (with the higher density electrode grid), but the authors do not discuss this observation in light of the increased measurement resolution. The authors conclude with the remark that the finer differences in spectral and spatial aspects between the fingers from the same hand may be resolved with higher resolution electrode grids.

Summarizing, several studies used both hemispheres for decoding contralateral and ip-

silateral finger movement and therefore made only a binary decision on contralateral or ipsilateral movement. Several more studies focused on classification between contralateral and ipsilateral hand movements from M1 and observed similar spatial patterns for both movement classes with a smaller magnitude for ipsilateral movement. A single article was found that performed classification of contralateral and ipsilateral individual finger movements and showed similar spatial overlap between the movement categories. The results from the studies show that classification decisions between contralateral and ipsilateral movement can be based on the difference in magnitude of cortical activation related to both movement types and to some extent to spatial differences between the movement types. The article however showed that individual contralateral and ipsilateral finger movements can be distinguished with high accuracy between 66.6% and 100%.

2.7 Summary of Literature Findings

The literature handled in this review covered the broad physiological and computational aspects related to discerning hand and finger movements from the SMC, with the underlying goal to provide answers to the problem statement formulated in Section 1.3:

It is unknown to what extent contralateral and ipsilateral individual finger movements can both be classified from the same small area of SMC of a single hemisphere.

Section 2.3 found that studies using a movement paradigm task, showed overlapping finger representations, with a more segregated and distinct somatotopy in S1 than in M1. Two studies showed overlap between contralateral and ipsilateral finger representations and reported that the ipsilateral finger representations are located more anteriorly than contralateral finger representations in M1, however this difference was only reported at the level of all fingers and the exact somatotopic representations of individual contralateral and ipsilateral fingers was not reported in literature.

In Section 2.4, several fMRI studies have shown that ipsilateral cortical activity (in comparison to contralateral cortical activity) was often less pronounced (in magnitude) and depends on both handedness and task complexity. These studies additionally found a large spatial overlap between contralateral and ipsilateral cortical activity, where some studies additionally report an anterior shift of ipsilateral cortical activity. EEG, MEG and ECoG studies have similarly shown that modulations in both LFB and HFB manifested with a smaller magnitude for ipsilateral movement in comparison with contralateral movement. It was shown that the LFB spectral modulations were less spatially focal than HFB modulations and that spectral modulations in the HFB resulting from both contralateral and ipsilateral movement show a large spatial overlap, with ipsilateral modulations being more spatially focused (i.e. occurring over less electrodes). For the HFB, timing has been researched in ECoG studies in which the onset of modulations appeared earlier during ipsilateral movements with respect to contralateral movements.

Section 2.5 presented the state of the art on the decoding of hand and finger movements in general. Due to the high data dimensionality and often low number of trials, much attention is paid to dimensionality reduction, feature selection and classifier selection. From this section it can be concluded that different movement types are encoded differently in various frequency bands, where the LFB contained the most information about brisk movements and the HFB showed to be informative for decoding fine movements. However, different frequency components may be informative in combination with several other frequency components. In terms of individual finger decoding, it has been shown that the thumb is generally well decoded, while the other fingers are often con-

fused possibly due to the fact that these are connected to the same flexor. The additional inclusion of prior knowledge of finger movements in the form of pragmatic constraints may improve the decoding process.

These sections have provided relevant background knowledge on the topic of decoding of hand and finger movements from the SMC, surprisingly revealing a limited number of studies that focused on the classification of both contralateral and ipsilateral movements. Section 2.6 showed that both hemispheres can be used for classifying contralateral and ipsilateral finger movement by making a binary decision on contralateral or ipsilateral movement. Several studies additionally showed that even though ipsilateral cortical activity was less prominent in terms of magnitude and spatial extent and additionally showed spatial shifts, it is possible to classify contralateral and ipsilateral hand and finger movement from the same area in the SMC as a whole or from M1 and S1 separately; all from a single hemisphere. Only a single article could effectively contribute to the knowledge requirement. This article showed that contralateral and ipsilateral individual thumb and index finger movements can be distinguished using ECoG signals recorded over the SMC of a single hemisphere.

2.8 Implications of Literature Findings on the Problem Statement

Given that the article by Scherer and colleagues (Scherer et al., 2009) is the only article that provides insight into the state of the art on classifying individual contralateral and ipsilateral finger movement, a vast amount of knowledge on this topic remains unexplored. Although the results of Scherer and colleagues showed that contralateral and ipsilateral fingers can be accurately distinguished from the SMC of a single hemisphere as a whole, three topics need further investigation: At first, it remains to be investigated whether contralateral and ipsilateral individual finger movements can both be accurately classified from the SMC of a single hemisphere as a whole. Secondly, it should be investigated whether this classification can be performed from a small sub area of the SMC of a single hemisphere and lastly, whether the usage of HD electrode grids allow the recording of cortical activity in finer detail and therefore allows this classification at a small scale.

2.8.1 The Ability to Classify Contralateral and Ipsilateral Individual Finger Movements from the SMC of a Single Hemisphere

The classification of contralateral and ipsilateral finger movements from the same small area of SMC can be related to the findings on finger somatotopy since these provided insights into the spatial arrangement of the individual fingers on the SMC. The existence of any small- or large-scale finger somatotopy does not directly guarantee the ability to accurately classify individual fingers, but it will in this section help interpret the implications of finger representation in classification of fingers on a smaller scale.

It is unknown if the ability to classify individual fingers from an arbitrary area is strictly governed by somatotopy but the literature findings indicate that the ability to do so certainly relies on the spatial arrangement of HFB signals, as these are described by literature as the most informative features for the classification of fine finger movements. The idea of a perfectly separated finger representation can be beneficial for classification of separate fingers but overlapping finger representations allows for the representation of multiple fingers in a single area which may be beneficial for classifying multiple fingers

from the same area, regardless of where that area is located. Several movement studies demonstrated overlapping somatotopic arrangements of the fingers in M1 and S1 in which many neurons are involved in the movement of several fingers with sometimes a preference towards a single finger or no clear preference to any finger at all. This indicates that different fingers can be distinguished from a single area of the SMC, but it is not known whether there exists a lower limit for an area of the SMC from which both contralateral and ipsilateral individual fingers can be accurately classified and whether this limit is governed by the boundaries of the somatotopic representations of fingers. In the case that the ability to classify from a smaller area of SMC is indeed limited by somatotopy, one can expect that every small area of SMC that is chosen will only provide good classification results of adjacent fingers since those provide the largest overlap in that area, in contrast to good classification results for all fingers.

Literature did not provide enough information to hypothesize about an area from which contralateral and ipsilateral fingers can both be accurately decoded. The results of (Hlustik, 2001) showed that the contralateral finger representations of M1 and S1 span an area of roughly 0.1 cm^2 and 0.2 cm^2, Diedrichsen and colleagues were able to classify fingers (combined, not separately) from an area as small as 3.9 cm^2 in M1 (Diedrichsen et al., 2013). The ECoG studies conducted by Jin, Fujiwara and Diedrichsen do not provide the required information to hypothesize about a lower limit on the area from which contralateral and ipsilateral finger movements can be classified (Jin et al., 2016), (Fujiwara et al., 2017), (Diedrichsen et al., 2013), (Scherer et al., 2009). These studies used a clinical 32-channel electrode grid of which only some electrodes (of which no detailed information was provided) covered the SMC and were used for classification. Siero and colleagues were able to coregister fMRI and ECoG (HD electrode grids) with a similar 1.5 mm spatial resolution and found that the finger representations of the contralateral hand could be discerned on a 1 cm^2 area of the SMC (Scherer et al., 2009).

Additionally, it is not yet known whether the finding of a more discrete and segregated somatotopy in S1 in contrast to M1 (Schellekens et al., 2018), (Hlustik, 2001) impacts the ability to discern finger movements on a smaller scale from M1. Although the SMC as a whole and S1 and M1 separately are suitable for decoding hand and finger movement, no consensus has been reached in this literature review on whether M1 or S1 is a more suitable candidate for classification of contralateral and ipsilateral finger movements on a smaller scale.

More importantly, these considerations have not yet been thoroughly explored in light of discerning both contralateral and ipsilateral finger movement. The studies by Alkadhi and Stippich present an overlap in contralateral and ipsilateral finger representations (Alkadhi et al., 2000), (Alkadhi et al., 2002), (Stippich et al., 2007). However, the studies both considered all fingers of the hand at the same time and did not focus on the individual fingers. Therefore, it is not known to what extent the considerations outlined in the paragraphs above hold in light of both contralateral and ipsilateral finger movements.

2.8.2 The Usage of HD Electrode Grids in Classification of Contralateral and Ipsilateral Individual Finger Movements

The classification accuracies in the study of Scherer and colleagues were slightly higher for one participant with an increased resolution electrode grid (Scherer et al., 2009). The authors have therefore advocated for the usage of higher resolution electrode grids to capture non-redundant spatial patterns of spectral modulations as to improve the overall classification results for distinguishing between contralateral and ipsilateral finger move-

ment. However, the small number of participants in this study begs the question whether the higher accuracy for the participant with the increased resolution electrode grid is to be attributed to chance. The authors of this paper were understandably not able to test on statistically significant differences but therefore it remains unknown whether a higher resolution electrode grid provides significant contribution to classification accuracy and whether this effect generalizes across a larger population.

The studies by Jin, Fujiwara and Diedrichsen are also unable to show the influence of an increased measurement resolution, but these studies have shown a lower classification accuracy for ipsilateral movement than for contralateral movement. Therefore, one can speculate that the spatial extent of ipsilateral cortical activity is thusly small that the spatial resolution of the measurement techniques was not large enough to effectively discern ipsilateral activity. This begs the question whether the reported neural pattern similarity between contralateral and ipsilateral hand movements (Fujiwara et al., 2017) is real or was only observed because the measurement resolution that the authors used was not high enough to discern the actual spatial differences but only the differences in magnitude of cortical activity. This thought can be translated to the findings of (Scherer et al., 2009) where the classification decision between contralateral and ipsilateral finger movements was largely based on a difference in magnitude between contralateral and ipsilateral activity, while spatial overlap was visible. When differences in magnitude were not that large, the classification was less accurate, as could be seen from their results on distinguishing fingers from the contralateral hand. It is not clear from the studies of Jin and Fujiwara whether the classification between contralateral and ipsilateral movement is also mostly based on differences in magnitude similar as in the study by Scherer (Scherer et al., 2009), (Jin et al., 2016), (Fujiwara et al., 2017). The study by Diedrichsen did observe differences in magnitude in BOLD level between contralateral and ipsilateral finger movement which may indicate that the classification was based on differences in signal amplitude (Diedrichsen et al., 2013). One can hypothesize that the finer spatial differences obtained by higher resolution measurement techniques can aid the classification of individual finger movements and additionally allow the classification to rely less on only the difference in magnitude and more on that of finer spatial differences between contralateral and ipsilateral finger movements. If the classification decisions depend less on only differences in magnitude, a more accurate classification of both contralateral and ipsilateral fingers may be expected. Additionally, placing a classification decision solely on differences in magnitude may not provide a robust classification mechanism, since other research has shown that the magnitude of cortical activity resulting from ipsilateral movement is strongly dependent on the movement task, its complexity, the amount of force required and the handedness of the participant.

The exact influence of measurement resolution on classification of movement remains unknown for two reasons. At first, Scherer and colleagues do not show what differences existed between the participants with different resolution electrode grids (Scherer et al., 2009). Secondly, a fair comparison between measurement resolutions is difficult to make. There are findings that cortical activity in the HFB resulting from fine finger movements may be more accurately decoded in participants with higher resolution electrode grids in comparison with those participants who did not have high resolution grids (Flint et al., 2017), (Wang et al., 2016) but a fair comparison between participants in such studies cannot be made due to different cortical structure and differing electrode placement. An alternative would be to artificially reduce the resolution of electrode grids by averaging the signal of neighboring electrodes, resulting in an artificial lower spatial resolution as an artificial larger electrode size. The results by Jiang and colleagues have shown that using such a simulated lower resolution electrode grid severely impacted the ability to classify movement from HFB in comparison with the original HD electrode grid while for the

more spatially spread LFB, the classification results did not change significantly (Jiang et al., 2018). The main problem with these methodologies is that there is no ground truth in comparing performances across resolutions and therefore it remains a topic of discussion whether one can directly compare and attribute increased classification results to an increased measurement resolution. In addition, the HD electrode grids have an increased number of recording channels on a certain cortical area which directly increases the number of features that can be used during classification, which can increase classification performance.

Lastly, the HD electrode grids have a smaller electrode size which means that these electrodes record cortical activity from a smaller neuronal population. In the light of somatotopic representations, it is probable that multiple finger digit representations are present among neuronal populations of a certain size (Schellekens et al., 2018) and that a smaller neuronal sample size recorded by the smaller electrodes of the HD electrode grids may to be more finger specific than a larger neuronal sample size.

2.9 Gap in Literature and Research Questions

Due to the scarce amount of literature, no definite clarifications could be provided towards the problem statement posed in Section 1.3. This problem statement was initially posed as a two-fold problem, of which the first aspect focused on whether contralateral and ipsilateral individual finger movement could be classified and the second aspect focused on the area from which this could be performed. Given that literature is scarce on both of these topics, all efforts in this work are focused on researching the first and most fundamental aspect of the problem statement; whether both contralateral and ipsilateral individual finger movements can be accurately detected and classified at all. Therefore, the main research question for this research is formulated as follows:

1. To what extent can contralateral and ipsilateral individual finger movements both be accurately classified from the SMC of a single hemisphere?

Since this research will handle an exploratory research into this topic, the main research question is intentionally broadly formulated and any assumptions or hypotheses surrounding the ability to classify both contralateral and ipsilateral individual fingers are left unspecified. The definition of accurate classification is defined as classification with an overal accuracy of 85%. This lower boundary was determined by the results from the UNP project (Vansteensel et al., 2016a) and denotes an accuracy with which a BCI can be reliably used.

While literature has shown that it is possible to distinguish contralateral and ipsilateral individual finger movements in binary classification schemes (Scherer et al., 2009), a single performance measure for the classification of contralateral and ipsilateral individual finger movement is still lacking. To contribute to this knowledge, contralateral and ipsilateral individual finger movements can be classified in a similar setting as related research; namely in a synchronous setting. In a synchronous (cue paced) BCI, the participant is expected to perform attempted movement of a finger after a visual cue and within a specific time frame. In machine learning terms, these trials can be classified in a supervised manner, where prior information about which finger is moving is present and predetermined and well defined episodes of cortical activity during finger movement can be used for training and testing of the machine learning model. The classification of cued movement in specific trials provides the opportunity to experiment with various machine learning models and preprocessing- and feature selection techniques under laboratory conditions. For this purpose, the following sub research question has been formulated:

1.1 What performance can be attained on the classification of contralateral and ipsilateral individual finger movements in a synchronous setting?

Although synchronous classification provides a good theoretical ground to build on, the problem of accurately decoding contralateral and ipsilateral finger movements must be viewed from a more pragmatical point of view; synchronous classification does not fully resemble the conditions under which SMR based BCIs are used in daily life by participants. A synchronous BCI analyzes cortical signals during predefined time ranges dictated by the cue and the participant can perform attempted finger movement to issue a command during this specific time. The BCI will not process cortical signals that fall outside this time frame which strongly simplifies the design of a BCI but limits the flexibility of use. An asynchronous BCI on the other hand constantly analyses cortical signals and the user can provide commands at his or her own pace, which offers a more flexible and natural way of BCI usage.

The design of such asynchronous BCIs is more complex for two distinct reasons. At first, the exact moment at which attempted movement corresponding to issuing a command (referred to as episodes of Intentional Control (IC)) takes place is not known in asynchronous BCIs as opposed to synchronous BCIs. Secondly, these episodes of attempted movement are alternated by episodes of rest or no attempted finger movement (referred to as episodes of No Control (NC)) in which the user does not issue a command. This means that the BCI must, in addition to correctly classifying different classes of IC relating to different finger movements, be able to accurately detect episodes of IC and distinguish them from episodes of NC.

Although this more challenging task inherently needs to be handled in any asynchronous BCI, it is brought up here for a more specific reason: Literature has shown that contralateral individual finger movement causes well distinguishable cortical patterns in comparison to motor rest. However, cortical activity resulting from ipsilateral finger movements showed less pronounced activity in terms of both spatial extent and magnitude and was reported to be absent in some studies (e.g. (Zanos et al., 2009), (Diedrichsen et al., 2013), (Hanakawa et al., 2005)). This gives rise to the thought that ipsilateral cortical activity might be more difficult to distinguish from motor rest (i.e. not performing finger movement). This can strongly impact the usability of ipsilateral finger movement in an asynchronous BCI, where it can potentially lead to an increased number of False Positive (FP) detections of ipsilateral finger movement. In light of the main research question, it is therefore desirable to research this issue to reflect on the true extent with which contralateral and ipsilateral finger movements can be classified. Therefore, the following research sub research question has been formulated:

1.2 What performance can be attained on the classification of contralateral and ipsilateral individual finger movements in an asynchronous setting?

Following these experiments, the attained performances from sub research questions 1.1 and 1.2 need to be compared and therefore the following sub research question has been formulated:

1.3 Do the attained performances on the classification of contralateral and ipsilateral individual finger movements differ between synchronous and asynchronous settings and what can explain possible differences?

After these sub- research questions have been answered, a complete answer can be given to the main research question. By assessing the classification performance for contralateral and ipsilateral individual finger movements in both a synchronous and an asynchronous setting, one can reflect on the extent to which contralateral and ipsilateral individual finger movements both be accurately classified from the SMC of a single hemisphere. The obtained results can be considered as a continuation of the studies performed by Scherer and colleagues (Scherer et al., 2009), who may have provided an optimistic view of the ability to classify contralateral and ipsilateral finger movement in a realistic BCI setting. The results obtained in this research additionally allow to determine what possibilities and caveats exist for using both contralateral and ipsilateral individual finger movements as control signal for BCIs. These insights can additionally aid the UMCU and the BCI research field towards the development of an online BCI with more degrees of freedom.

3 Methodology

3.1 Overview of Experiments

This section will shortly handle the dataset and the research methodology that was used to answer the sub research questions and consequently the main research question. It will provide an concise overview of the chronological order of experiments, which are explained in more detail in later sections.

3.1.1 Summary of the Dataset

Based on the literature findings, it could be stated that clinical electrode grids may not provide the spatial resolution necessary to optimally discern individual finger representations and it can be hypothesized that HD electrode grids have the ability to resolve fine spatial patterns of cortical activity beyond those that can be measured with clinical electrode grids. Furthermore, the SMC has proven to be a suitable area for discerning individual finger movement. Therefore, this research made use of an existing dataset recorded at the UMCU that included four subjects with intractable epilepsy who underwent surgery to place HD ECoG electrode grids over the hand knob of the SMC. These subjects have performed contralateral and ipsilateral individual movement of the thumb, index and little finger in a randomized event-related task design, which made this dataset suitable for this research.

3.1.2 Preliminary Data Analysis

Prior to classification, more insight into the current dataset was required. For this purpose, a preliminary data analysis was performed to determine to what extent the literature findings regarding the spatial, spectral and temporal aspects of cortical activity resulting from contralateral and ipsilateral finger movements held for this dataset. Additionally, in-depth knowledge of the data aided in the discussion and explanation of obtained classification results.

The preliminary data analysis consisted of thee separate experiments. The first experiment aimed to visualize the signal envelope of power modulations in the α, β and HFB frequency bands. This analysis enabled a comparison of the temporal and amplitudal differences of cortical activity resulting from contralateral and ipsilateral movement. The second experiment of the preliminary data analysis aimed to visualize the spatial extent and distribution of cortical activity in the α, β and HFB frequency bands across the electrodes of the ECoG grids. As a third and last topic for the preliminary analysis, an attempt was made to visualize the high dimensional cortical data resulting from the contralateral and ipsilateral finger movements in the α, β and HFB frequency bands which aided in formulating preliminary hypotheses before classification.

3.1.3 Experiment I: Synchronous Classification

Following the preliminary analysis, the first experiment of this research handled the synchronous classification, which aimed to obtain the results required to answer the first sub research question. Since it was unknown which machine learning models were able to accurately classify contralateral and ipsilateral individual finger movements, several machine learning models were explored in a synchronous setting These models were evaluated in a synchronous setting and the accuracy in percent along with the corresponding confusion matrices (e.g. (Xiao and Ding, 2015), (Bleichner et al., 2014)) were obtained.

After the classification attempts, several smaller side experiments were conducted. Firstly, the contribution and information content of the α, β and HFB frequency bands on the classification process was separately researched. Secondly, related to the limited amount of data that was available, an investigation was set out to determine how the amount of data used in the training of the classifier influenced classification performance of each of the classifiers. Thirdly, due to the fact that the temporal characteristics of cortical activity were not well defined by literature, a separate experiment set out to determine the influence of several temporal aspects on the classification process. The last experiment of this section investigated the distribution of channels across the cortical surface that were important in distinguishing contralateral and ipsilateral finger movements.

3.1.4 Experiment II: Asynchronous Classification

Following the synchronous classification, the second experiment conducted in this research handled the asynchronous classification which aimed to obtain the results required to answer the second sub research question. Although the dataset used in this research was not specifically designed for the verification of an asynchronous BCI, it was possible to approximate conditions similar to those in asynchronous BCIs since the data contained trials of movement of each of the six fingers (here the six different IC states) alternated with trials of rest (here the NC state). The best performing model in the synchronous classification was used to detect and classify IC states and the NC state in this asynchronous setting by letting the classifier predict a class label at every time point of the ECoG data of a run. The predicted class labels at each time point in combination with other parameters were used for the labeling of an IC or NC event in an asynchronous fashion. The performance of the classifier in this asynchronous setting was evaluated by means of a slightly adapted form of the Event-based True Positive rate (EB-TPR) and the Sample-based False Positive Rate (SB-FPR) metrics (Mason and Birch, 2000).

The following sections in this chapter will provide the rationale, methodological details and theory towards all experiments that were performed in this research and were shortly described in the section above. These methodological descriptions will be provided in the same chronological order as the results section, so that the reader can easily browse forward and backward between methodology and results if desired. This organization additionally allows the reader that is more familiar with machine learning, ECoG and BCIs in general to skip several sections if desired.

3.2 Data Acquisition and Processing

3.2.1 Participants

This research included four participants with intractable epilepsy who underwent subdural ECoG grid implantation for the clinical purpose of seizure localization and monitoring. The participants gave written informed consent to place additional subdural HD ECoG

electrode grids over the SMC (including the hand knob) for the purpose of research. The pathological region of epilepsy did not extend to the SMC and the participants all had normal hand function. All procedures described were approved by the Institutional Review Board of the Utrecht University Medical Center and the informed consent was given in accordance with the Declaration of Helsinki (WMA, 2013).

The HD electrode grids (AdTech, Racine, USA) were localized using co-registration between a high resolution post-implantation Computerized Tomography (CT) scan (Philips Tomoscan SR7000, Best, the Netherlands) and a pre-operative T1-weighed anatomical scan on a 3T MRI scanner (Philips 3T Achieva, Best, the Netherlands) using the methodology as described work of Hermes and colleagues (Hermes et al., 2010) and Branco and colleagues (Branco et al., 2018b). The locations of the electrode grids on the cortical surfaces of the participants are depicted in Figure 3.1.

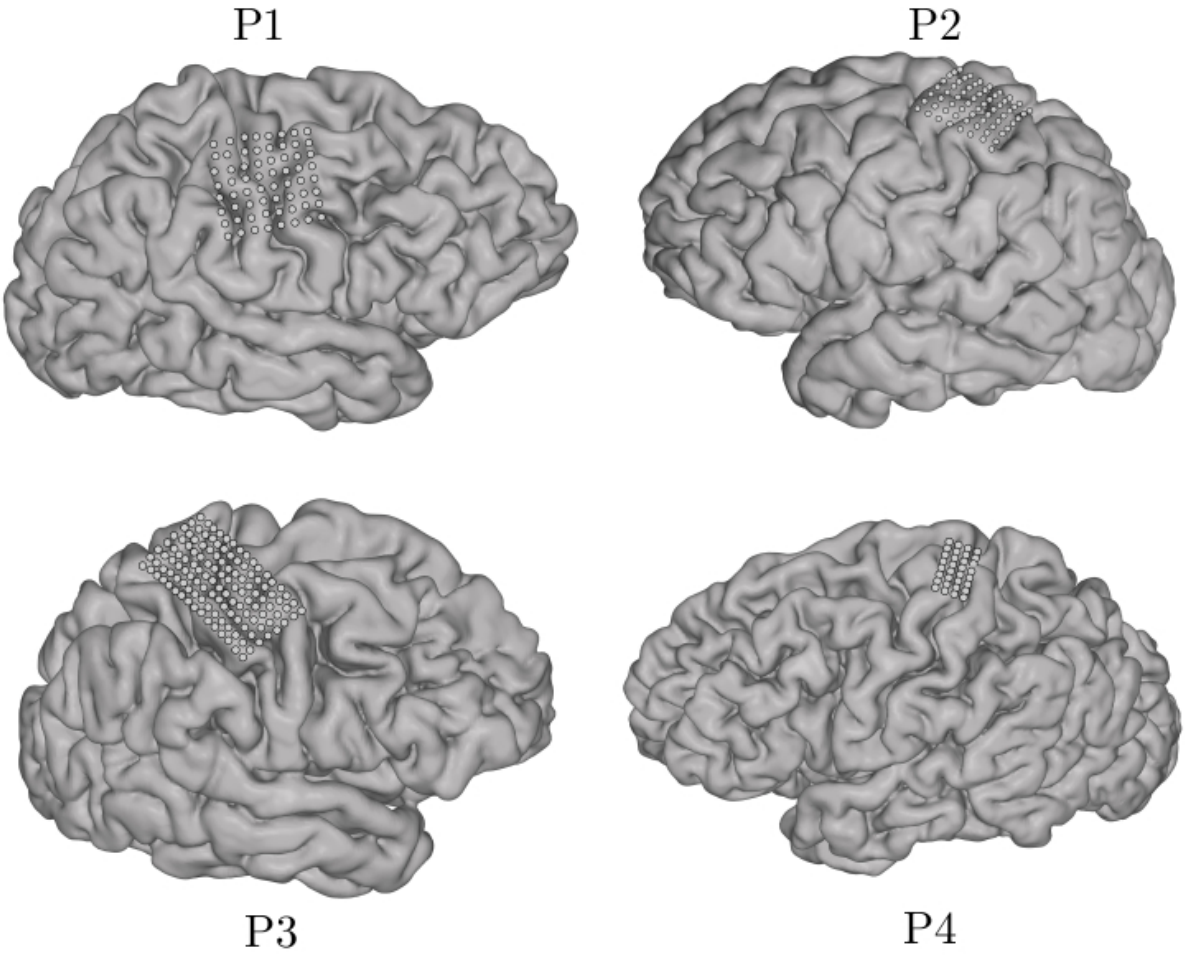

Figure 3.1: *ECoG electrode grid locations on the cortical surface of the four participants included in this research.*

The labeling of electrodes on the cortical surface was performed by means of visual inspection using distinct anatomical landmarks: The electrodes over the CS were defined after which the electrodes anterior to the CS (until the precentral sulcus (prCS)) were labeled as M1 electrodes and those posterior to the CS (until the postcentral sulcus (pCS)) were labeled as S1 electrodes. The resulting electrode layouts are depicted in Figures A.1 through A.3 in Appendix A. Further information about the participants and the implanted electrode grids is summarized in Table 3.1.

Information	Participant P1	Participant P2	Participant P3	Participant P4
Age	34	22	50	42
Gender	Female	Male	Female	Male
Handedness	Right	Right	Left	Right
Implanted Hemisphere	Right	Left	Right	Left
Electrode Layout	8x8	8x8	8x16	8x4
Electrode Diameter	1 mm	1 mm	1 mm	2 mm
Electrode Spacing	4 mm	4 mm	3 mm	3 mm
Covered Area	5.2 cm^2	5.2 cm^2	10.4cm^2	2.5 cm^2
CS Electrodes	10	9	20	11
M1 Electrodes	19	27	18	9
S1 Electrodes	16	18	29	5
Non-SMC Electrodes	19	10	46	6

Table 3.1: *Elaborate information regarding the participants and implanted electrode grids. The handedness of the participants was evaluated by means of the Edinburgh handedness inventory (Oldfield, 1971). The inter-electrode spacing is measured center to center. The number of electrodes over the CS, over S1 and over M1 are listed. The electrodes that are not located over these three areas are marked as non-SMC electrodes. Some electrodes were excluded from all analyses due to noise or other electrode faults.*

3.2.2 Experimental Task

The participants performed a finger movement task which consisted of the flexion and extension of a single finger at a time. Two runs of the task were recorded, one run were the participant performed the task with the fingers on the hand contralateral to the implanted grid and afterwards with the fingers on the hand ipsilateral to the implanted electrode grid. It is to be noted that these runs were performed and recorded on different days for participant P2 and P4. For participants P1 and P3, the runs were recorded on the same day. During the task, the participants were seated in a comfortable position in their bed and focused on a monitor which presented a cue to move either the thumb, index finger or little finger of the specific hand, which constituted one trial. The complete task was constructed following a randomized event-related design with 30 trials per finger.

For participants P1 through P3, one trial of finger movement lasted 1.5 seconds and consisted of one flexion and one extension of the cued finger. Every finger movement trial was succeeded by a trial of rest with a duration of 3.5 seconds, during which no finger movement was allowed. For participant P4, a finger movement trial consisted of one flexion and extension at minimum, but no restriction was placed on the maximal number of flexions and extensions in a trial. For this participant, a finger movement trial had a duration of 4.4 seconds including resting time; no specific trials of rest were included in this participants task. The task designs are graphically represented in Figures 3.2 and 3.3 below.

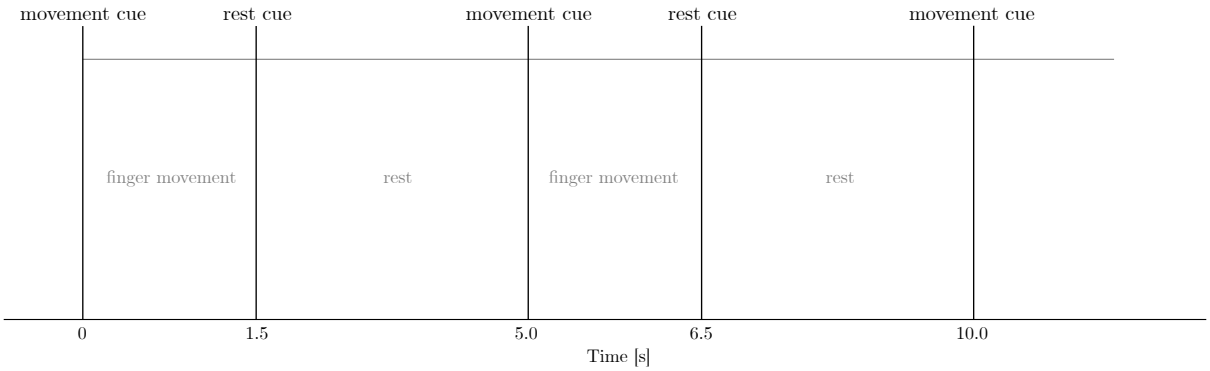

Figure 3.2: *Graphical depiction of the randomized event-related task design of participants P1 through P3. The beginning of each 1.5 second movement trial is marked by a movement cue for a specific finger after which the participants performs one extension and flexion of the cued finger. After each trial of finger movement, a trial of rest is issued by the rest cue, in which the participant performs no movement for the duration of 3.5 seconds.*

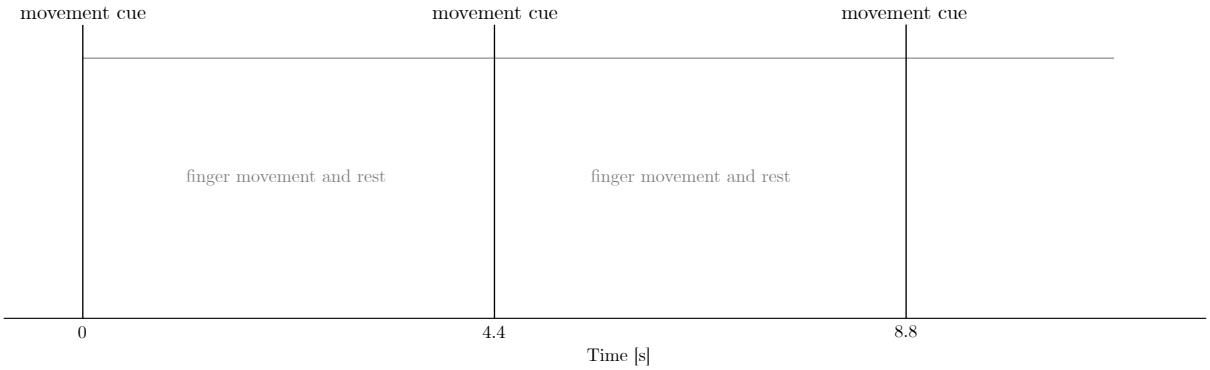

Figure 3.3: *Graphical depiction of the randomized event-related task design of participant P4. The beginning of each 4.4 second movement trial is marked by a movement cue for a specific finger after which this participant performs at least one extension and flexion of the cued finger. Followed by the finger movement, the participant was instructed stay at rest and perform no finger movement.*

3.2.3 ECoG Acquisition and Preprocessing

During each run, the ECoG signals were continuously recorded from the cortical surface. For participants P1 through P3, a 16-bit Blackrock amplifier (Blackrock Microsystems, Salt Lake City, USA) with a sampling rate f_s of 2000 Hz and an internal bandpass filter of 0.3-7500 Hz was used to record the ECoG data. For participant P4, the ECoG signals were recorded with a 22-bit Micromed amplifier (Micromed, Treviso, Italy) with a sampling rate f_s of 512 Hz and an internal band-pass filter of 0.15-134.4 Hz. The recorded ECoG data were processed offline with the `Fieldtrip Toolbox` (Oostenveld et al., 2011) (July 2019) for `MATLAB 2019a`. The subset of noisy and non-functioning electrodes were identified per participant via assessment of signal amplitude (flat electrodes or amplitudal outliers), line noise amplitude and 1/f distribution (Liu et al., 2015). These faulty electrodes are marked in Figures A.1 through A.3. These faulty electrodes were excluded from further analysis, resulting in a subset of functional electrodes (channels) $\mathbf{E}_f$.

All following preprocessing procedures for the ECoG data were applied per run separately. Fistly, the raw voltage ECoG data of each channel $\mathbf{V}_e$ with $e \in \mathbf{E}_f$ were referenced

with the CAR method defined by:

$$\mathbf{V}_{e_{CAR}} = \mathbf{V}_e - \frac{1}{|E_f|} \sum_{e \in \mathbf{E}_f} \left[\frac{1}{N} \sum_{n=1}^{N} \mathbf{V}_e[n] \right] \tag{3.1}$$

Here, N denotes the number of recorded data samples of channel e. Following, a Butterworth band-pass filter was applied to the data of each of the participants. The gain expression at frequency f of this filter is given by $G(f)_{bp}$:

$$G(f)_{bp} = \frac{\frac{f}{f_l}}{\sqrt{[1 + \frac{f_l}{f}]^{2d}[1 + \frac{f}{f_h}]^{2d}}} \tag{3.2}$$

The filter order d was set to three and the lower and upper cutoff frequencies, f_l and f_h, were set to 0.15 and 130 Hz respectively. These cutoff frequency settings reflect the bandwidth limits of the Micromed amplifier used for participant P4. This band-pass filter was applied to the data of all participants to ensure that the same spectral content was retained in the data of all participants regardless of the amplifier bandwidths, which differed between participants P1 through P3 and P4. To remove power line noise, two additional third order Butterworth band-stop filters with gain expression $1 - G(f)_{bp}$ were centered around multiples of the power line frequency (50Hz) with lower and upper cutoff frequencies of [49 51] Hz and [99 101] Hz respectively.

Following, a window function of one second length (based on the average time a participant required to perform a single finger flexion and extension) was centered over each ECoG sample $n \in \mathbf{V}_{CAR}$ of a run. Here, a Hanning window $\mathbf{H}$[n] was used:

$$\mathbf{H}[n] = \begin{cases} \frac{1}{2}\left[1 + \cos\left(\pi\left(\frac{2n}{L} - 1\right)\right)\right] & 0 \leq n \leq \frac{1}{2}L \\ 1 & \frac{1}{2}L < n < 1 - \frac{1}{2}L \\ \frac{1}{2}\left[1 + \cos\left(\pi\left(\left(\frac{2n}{L} - 2\right) + 1\right)\right)\right] & 1 - \frac{1}{2}L \leq n \leq L \end{cases}$$

Here, L denotes the length of the window expressed in the number of datapoints which for a length of one second, corresponds to 2000 datapoints for participants P1 through P3 and 512 datapoints for participant P4. Each one second window of ECoG data $\mathbf{V}_{hann}$ was transformed to the frequency domain by use of the Discrete Fourier Transform (DFT) to obtain $\mathbf{P}_{hann}$, which constituted the collection of normalized $\log_{10}$-transformed frequency bin magnitudes ranging from 6 Hz to 130 Hz in steps of 2 Hz. These frequency bins are described by the set K = {6,8,...,130} :

$$\mathbf{P}_{hann} = \mathcal{F}\{\mathbf{V}_{hann}[k]\} = \log_{10}\left[\frac{1}{N}\left[\sum_{n=0}^{N-1} \mathbf{V}_{hann}[n]\left[\cos(\frac{2\pi}{N}kn - i \cdot \sin(\frac{2\pi}{N}kn)\right]\right]\right] \tag{3.3}$$

Here, k denotes a discrete frequency bins in K for which the spectral magnitudes were obtained. In this case, The resulting spectral data of a window $\mathbf{P}_{hann}$ has dimensionality $\mathbb{R}^{K \times E_f}$. The complete spectral data of a run $\mathbf{P}_{run}$ with in total N samples then has dimensions $\mathbb{R}^{N \times K \times E_f}$.

3.2.4 Dataglove Acquisition and Preprocessing

The finger movements that were performed by the participants during the task were recorded with a five degrees of freedom dataglove (5DT, Irvine, USA) placed only on the hand involved with the task. The dataglove recorded the amount of flexion and extension of all 5 fingers of the hand with a sampling rate of 50 Hz. Two examples of recorded dataglove signals have been depicted in Figure 3.4 below:

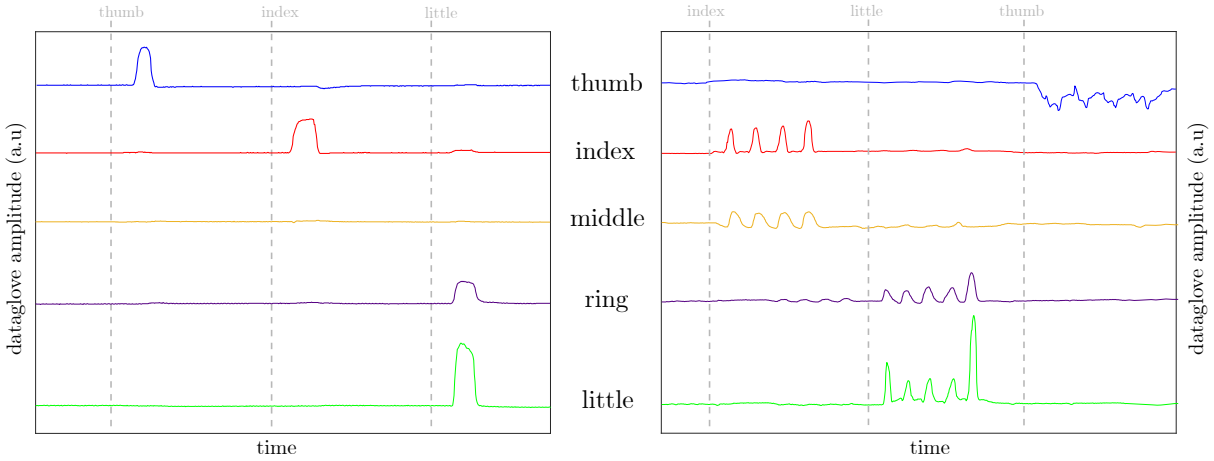

Figure 3.4: *Schematic representation of the recorded movement of each finger by the dataglove. The bumps in the dataglove signals (colored lines) following the movement cues (dashed gray line denoting which finger is cued) demonstrate flexion and extension movements of the cued finger. Rest cues are omitted in this schematic depiction. Participant P1, whose dataglove signals is depicted in the left hand figure, was instructed to flex and extent the cued finger only once, whereas participant P4 (right hand side) was allowed to flex and extent the cued finger multiple times in a trial.*

Following, the task performance of each of the participants was analyzed. For this purpose, a visual inspection of the dataglove signals and the cues (as depicted in Figure 3.4) was performed to determine whether the correct finger was moved in each trial and whether the the finger movement was performed correctly (i.e. no hesitation or correction of movement between fingers). In addition, trials of rest were inspected to ensure that there was actual rest and no residual movement. Trials with faulty task performance were excluded from further analysis. This resulted in the collection of correct trials as depicted in Table 3.2 below.

Finger	**Participant P1**	**Participant P2**	**Participant P3**	**Participant P4**
Contralateral Thumb	30	30	29	30
Contralateral Index	30	30	29	28
Contralateral Little	30	30	30	29
Ipsilateral Thumb	28	29	29	25
Ipsilateral Index	30	29	29	24
Ipsilateral Little	30	30	30	23

Table 3.2: *Number of included trials for each participant and each cued finger of both contralateral and ipsilateral runs.*

Section 2.5.2 of the literature review showed that movement of several fingers can cause conjoined movement of other fingers on that hand due to the fact that all fingers on one hand (with exception of the thumb) are connected to the same flexor digitorum profundus. Therefore, it was important to investigate the extent to which conjoined movement of non-cued fingers took place during movement of the cued finger during a task. Given that each dataglove signals had a significant DC offset and a varying measuring amplitude (hardware related), the separate dataglove signals corresponding to each of the fingers were first z-scored as follows:

$$\mathbf{Z}_v = \frac{\mathbf{D}_v - \overline{\mathbf{D}_v}}{\sigma_{\mathbf{D}_v}} \tag{3.4}$$

Where $\mathbf{Z}_v$ denotes the z-scored dataglove signal for finger v, $\mathbf{D}_v$ denotes the raw dataglove signal for finger v and $\overline{\mathbf{D}_v}$ and $\sigma_{\mathbf{D}_v}$ denote the mean and standard deviation of the raw dataglove signal for finger v.

After z-scoring, the maximum deflection of all fingers during the trials of a cued finger were collected and the amount of conjoined movement was visualized. An example of one of those visualizations is depicted in Figure 3.5. The visualizations of conjoined movement of the other participants are included in Appendix F.

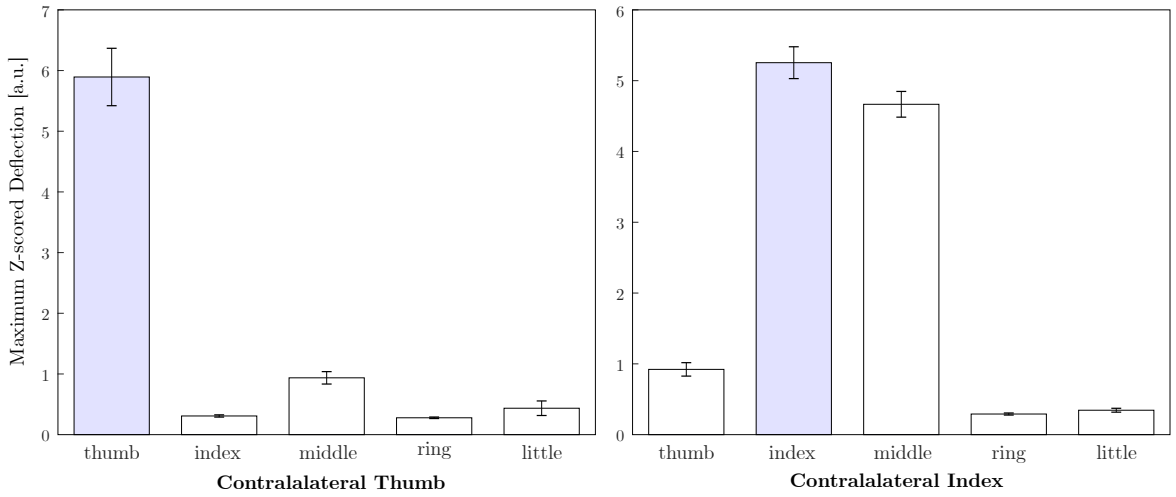

Figure 3.5: *The amount of conjoined movement of non-cued fingers during movement of the cued contralateral thumb (left hand figure) and contralateral index finger (right hand figure) of participant P3. The bar that represents the cued finger is depicted in blue and the non-cued fingers are represented by the white bars. This Figure caption holds for Figures F.1 through F.4 in Appendix F, which show the results for the other participants.*

These figures show that there is little conjoined movement of any of the fingers with the thumb. The index finger shows conjoined movement with the middle finger and the little finger mainly shows conjoined movement with the ring finger. Little conjoined movement occurs between any of the fingers actively employed in the finger movement task that the participants completed (i.e. between the thumb, index finger and little finger).

To quantitatively determine whether the movements of any cued finger was larger than that of non-cued fingers, the maximum deflection amplitudes were subjected to a one-way ANOVA. The resulting p-values of these comparisons are depicted in Table G.1 in Appendix G. The results show that the middle finger moved in conjunction with the index finger and that the ring finger moved in conjunction with the little finger. Additionally, movement of several cued fingers were not significantly larger than that of the non-cued fingers for some participants, but these non-cued fingers did not belong to the set of fingers actively employed during the movement task. Therefore, the participants overall performed well on the task. The only participant that had a decreased task performance was participant P4, who had a somewhat lower number of correct trials during the ipsilateral run (Table 3.2).

The dataglove recordings additionally allowed for determination of the point in time in each trial at which movement onset took place. For this purpose, the dataglove data were first up-sampled using interpolation to match the sampling rate f_s of the ECoG data so that the dataglove data and ECoG data could be aligned. Each value to be interpolated $D_{v,t}$ at position x_t of finger v was calculated using a linear interpolation of the following form:

$$D_{v,t} = \left[\frac{(x_{v,t} - x_{v,t-1})(D_{v,t+1} - D_{v,t-1})}{x_{v,t+1} - x_{v,t-1}} \right] + D_{v,t-1} \tag{3.5}$$

Following, the *start cue* - denoting the time at which the run started - in the ECoG

data was aligned with the *start cue* in the dataglove data so that the ECoG data and the dataglove signals were aligned. Next, the first derivative of the dataglove signal was calculated to obtain the amount of acceleration during movement. The first derivatives of the dataglove signals were approximated as follows:

$$\delta_{\mathbf{Z}_{v,t}} = |(Z_{v,t+1} - Z_{v,t})| \tag{3.6}$$

Where $Z_{v,t}$ represents the datapoint at time t of dataglove signal $\mathbf{Z}_v$ and $\delta_{\mathbf{Z}_{v,t}}$ represents the approximate first derivative of point $Z_{v,t}$. By taking the absolute value of $\delta_{\mathbf{Z}_{v,t}}$, this signal resulted in pronounced peaks during flexion and extension regardless of the envelope of the original dataglove signal, as depicted in Figure 3.6. This signal allowed for more accurate determination of movement (onset) periods than the original dataglove signal.

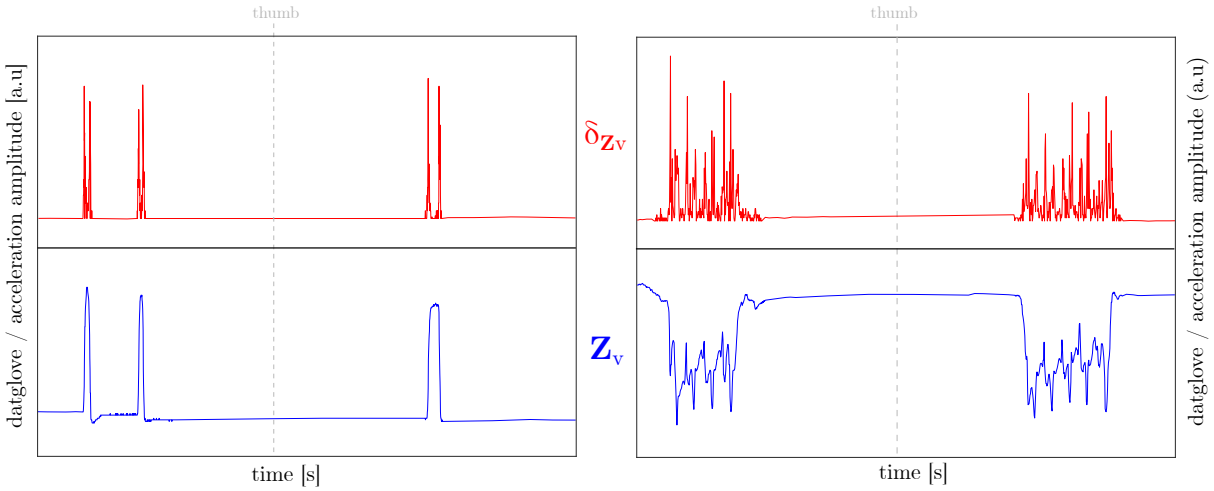

Figure 3.6: *The left hand figure shows signal excerpts for thumb movement performed by participant P1. The right hand figure shows signal excerpts for thumb movement performed by participant P4. The gray dashed lines denote the movement cue, indicating the beginning of a trial in which in thumb movement is desired. In both figures, the datatglove traces for the finger v,* $\mathbf{Z}_v$*, are depicted in blue. The first derivative of* $\mathbf{Z}_v$*, denoted as* $\delta_{\mathbf{Z}_v}$ *is depicted in red.* $\delta_{\mathbf{Z}_v}$ *shows pronounced peaks during movement regardless of whether the orginal dataglove signal denoted by* $\mathbf{Z}_v$ *shows a negative or positive deflection.*

To find the time points at which the finger movements occurred, the first peak of $\delta_{\mathbf{Z}_v}$ in each movement trial of every finger needed to be found. This point denoted the moment at which movement was performed by the participant. This first peak was found by searching for local maxima in $\delta_{\mathbf{Z}_v}$ during each trial. Only the time points corresponding to the first peak in $\delta_{\mathbf{Z}_v}$ in each trial were retained. For this purpose, this research used the `findpeaks` function from the `Signal Processing Toolbox` of `MATLAB 2019a` (MathWorks Inc.). An overview of the complete process is depicted in Figure 3.7.

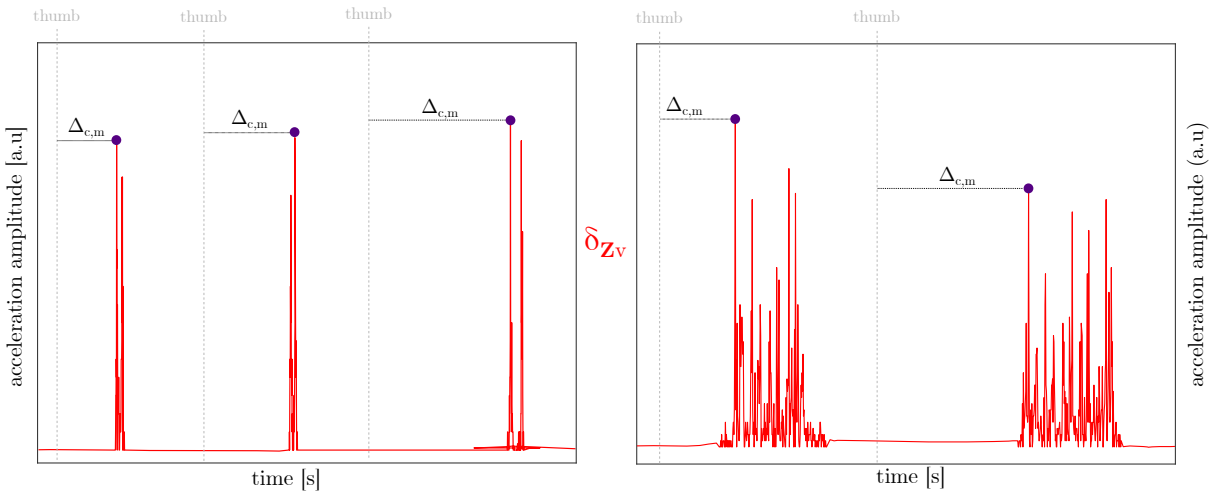

Figure 3.7: *The left hand figure shows dataglove acceleration excerpts for thumb movement performed by participant P1. The right hand figure shows dataglove acceleration excerpts for thumb movement performed by participant P4. The gray dashed lines denote the movement cues. The rest cues are omitted in this figure. The first derivative of* $\mathbf{Z}_v$*, denoted as* $\delta_{\mathbf{Z}_v}$ *is depicted in red. The first peak of* $\delta_{\mathbf{Z}_v}$ *in each trial is indicated by a purple dot. This point denotes the time right after the first finger flexion when the finger is fully flexed and is thus an accurate reflection of the time at which finger movement is taking place. The time between the cue and that first peak is denoted by* $\Delta_{c,m}$*.*

.

The purple dots in Figure 3.7 denoting the time point of the first movement in each trial will be referred to as the *movement markers*. A visual inspection was performed to confirm that indeed the first peak of $\delta_{\mathbf{Z}_v}$ was correctly selected in each trial. The time between the cue and the movement marker $\Delta_{c,m}$, reflecting the position of the movement marker relative to the cue, were stored for each trial. This method of identifying movement could naturally not be used to define similar markers for periods of rest. To define these, a set time value between the rest cue (participants P1 through P3) or the movement cue (participant P4) and an arbitrary time point in a period of rest was defined, such that this arbitrary time point was centered in an interval of rest with a minimal duration of one second, as depicted in Figure 3.8. This set time is referred to as $\Delta_{c,r}$. The one second duration of the selected rest intervals enable the placement of the Hanning windows with a one second length (described in Section 3.2.3) over the intervals so that these particular windows contain only ECoG signal recorded during rest.

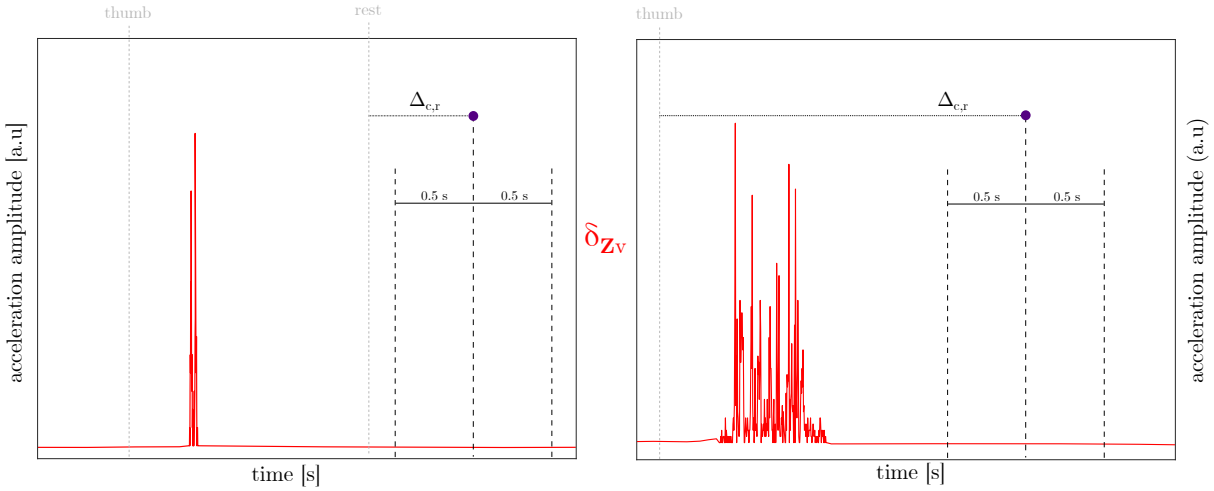

Figure 3.8: *The left hand figure shows dataglove acceleration excerpts for thumb movement and rest performed by participant P1. The right hand figure shows dataglove acceleration excerpts for thumb movement and rest performed by participant P4. The gray dashed lines denote the cues for rest and movement respectively depending on the participant. The first derivative of* $\mathbf{Z}_v$*, denoted as* $\delta_{\mathbf{Z}_v}$ *is depicted in red. The purple dot denotes the arbitrary time point in the rest trial or episode of rest such that it is centered in a period of rest with a minimal duration of one second. The time between the rest cue and this arbitrary time point,* $\Delta_{c,r}$*, is calculated.*

.

The time value $\Delta_{c,r}$ was set at two seconds for participants P1 through P3 and at 3.9 seconds for participant P4. The purple dots in Figure 3.8 are referred to as the *rest markers*. Again, a visual inspection confirmed that the rest markers were indeed surrounded by at least half a second of rest on each side. The number of movement markers and rest markers that were found are summarized in Table 3.3 below:

Finger	**Participant P1**	**Participant P2**	**Participant P3**	**Participant P4**
Contralateral Thumb	30	30	29	30
Contralateral Index	30	30	29	28
Contralateral Little	30	30	30	29
Ipsilateral Thumb	28	29	29	25
Ipsilateral Index	30	29	29	24
Ipsilateral Little	30	30	30	23
Rest	182	182	182	132

Table 3.3: *Overview of the number of found movement markers and rest markers for each participant. The number of rest markers found corresponds to the number of included movement trials listed in Table 3.2. Given that every movement trial is followed by a trial of rest for participants P1 - P3, the number of rest trials constitutes 182 for these participants: each run consists of 30 trials of movement and thus 91 trials of rest. Two runs (contralateral and ipsilateral) were performed which amounts to 182 rest trials and thus 182 rest markers. Finding suitable rest markers for participant P4 was more difficult due to the absence of a clear rest cue. As a result, 60 rest markers had to be discarded resulting in a total of 132 rest markers.*

3.3 Preliminary Data Analysis

3.3.1 Amplitudal Analysis: Visualization of Spectral Modulations

To analyze the envelope of the spectral modulations in each of the α, β and HFB frequency bands, the spectral data of the each of the trials t in the set of trials T_v of a finger v, denoted by $\mathbf{P}_{v,t}$, were aligned on the movement markers similar as in (Talakoub et al., 2014). This process was performed for each participant individually. Following, the spectral data $\mathbf{P}_v$ belonging to finger v, were averaged over all trials to obtain $\mathbf{P}_{v,\overline{T_v}}$:

$$\mathbf{P}_{v,\overline{T_v}} = \frac{1}{|\mathbf{T}_v|} \sum_{t \in \mathbf{T}_v} \mathbf{P}_{v,t} \tag{3.7}$$

The distinct frequency bins k of the spectral data were divided in more narrowly defined frequency bands of [8-12], [16-30] and [60-130] Hz corresponding to the α, β and HFB frequency bands respectively. These frequency ranges are denoted in the set $B = \{\alpha, \beta, \text{HFB}\}$. Following, the averages over the k frequency bins in each frequency band $B \in G$ were taken to obtain $\mathbf{P}_{v,\overline{T_v},\overline{B}}$:

$$\mathbf{P}_{v,\overline{T_v},\overline{B}} = \frac{1}{|\mathbf{B}|} \sum_{b \in \mathbf{B}} \mathbf{P}_{v,b,\overline{T_v}} \tag{3.8}$$

To enable a comparison of the amplitudes of the spectral modulations, the data $\mathbf{P}_{v,\overline{T_v},\overline{B}}$ of all frequency bands and all contralateral and ipsilateral fingers were concatenated to form $\mathbf{P}_{tot}$, and all data $\mathbf{P}_{v,\overline{T_v},\overline{B}}$ were z-scored as follows:

$$\mathbf{Z}_{\mathbf{P}_{v,\overline{T_v},\overline{B}}} = \frac{\mathbf{P}_{v,\overline{T_v},\overline{B}} - \overline{P_{tot}}}{\sigma_{P_{tot}}} \tag{3.9}$$

The data $\mathbf{Z}_{\mathbf{P}_{v,\overline{T_v},\overline{B}}}$ were plotted for each frequency band, channel, finger and participant separately. To enable easy comparison of spectral modulations across fingers, $\mathbf{P}_{v,\overline{T_v},\overline{B}}$ was averaged over channels $\mathbf{E}_f$ to obtain a grand average of spectral modulations:

$$\mathbf{P}_{v,\overline{T_v},\overline{B},\overline{E_f}} = \frac{1}{\mathbf{E_f}} \sum_{e \in \mathbf{E}_f} \mathbf{P}_{v,e,\overline{T_v},\overline{B}} \tag{3.10}$$

Again, the data $\mathbf{P}_{v,\overline{T_v},\overline{B},\overline{E_f}}$ of all frequency bands and all contralateral and ipsilateral fingers were concatenated to form $\mathbf{P}_{tot}$, and all data $\mathbf{P}_{v,\overline{T_v},\overline{B}}$ were z-scored as follows:

$$\mathbf{Z}_{\mathbf{P}_{v,\overline{T_v},\overline{B},\overline{E_f}}} = \frac{\mathbf{P}_{v,\overline{T_v},\overline{B},\overline{E_f}} - \overline{P_{tot}}}{\sigma_{P_{tot}}} \tag{3.11}$$

The data $\mathbf{Z}_{\mathbf{P}_{v,\overline{T_v},\overline{B},\overline{E_f}}}$ were plotted for each frequency band, finger and participant separately.

3.3.2 Spatial Analysis: Channel R^2 Values

The R^2 value of each channel was calculated for the α, β and HFB frequency bands separately. For this purpose, the non z-scored spectral data of each trial separately averaged over the three frequency bands for each specific finger, $\mathbf{P}_{v,t,\overline{B}}$, was used. The average spectral magnitudes of the window centered around the movement marker were extracted, since this point in time showed peak cortical activity, confirmed by the results of Section 3.3.1. For trials of rest, the average spectral magnitudes of the window centered around

the rest marker were taken. Following, the average spectral magnitudes of the trials of both movement and rest were sorted to form the line segment $\mathbf{A}[n]$. This line segment was then overlaid by a Heavidside step function $\mathbf{H}[n]$ as defined below:

$$\mathbf{H}[n] = \begin{cases} 0 & n < 0 \\ \frac{1}{2} & n = 0 \\ 1 & n > 0 \end{cases}$$

The process of forming the line segment $\mathbf{A}[n]$ and the subsequent overlaying with the Heaviside step function $\mathbf{H}[n]$ is depicted in more detail in Figure 3.9 below:

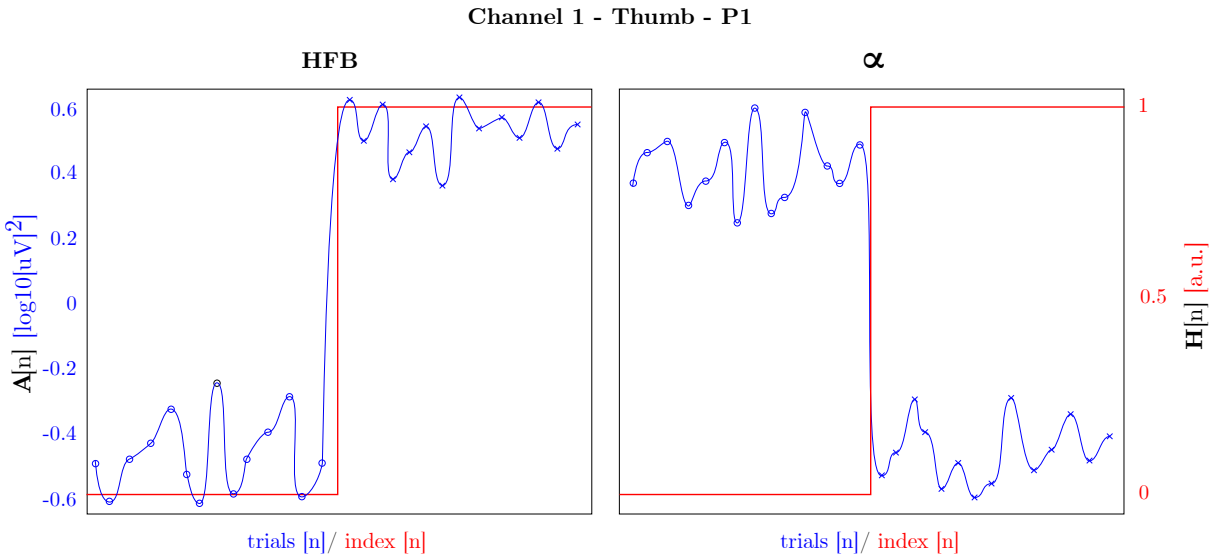

Figure 3.9: *The forming of line segment $A[n]$ and the subsequent overlaying with the Heaviside step function $H[n]$. This figure depicts an example for channel 1 of the electrode grid of participant P1 during contralateral thumb movement. The left hand figure shows the values of the average spectral magnitudes in the HFB as blue crosses, where each cross denotes the average spectral magnitude in the window centered around the movement marker of one trial. The average spectral magnitudes in the HFB during rest are depicted by blue circles where each circle again denotes the average spectral magnitude in the window centered around the rest marker of one trial. The spectral magnitudes during both movement and rest form the line segment A[n], denoted by the blue line. The red line denotes the Heaviside step function $H[n]$. The right hand figure shows the same content, but for the alpha frequency band.*

Following, the correlation coefficient R between $\mathbf{A}[n]$ and $\mathbf{H}[n]$ was calculated as follows:

$$R(\mathbf{A}[n], \mathbf{H}[n]) = \frac{1}{N-1} \sum_{n=1}^{N} \left[\left(\frac{\mathbf{A}[n] - \overline{\mathbf{A}}}{\sigma_{\mathbf{A}}} \right) \left(\frac{\mathbf{H}[n] - \overline{\mathbf{H}}}{\sigma_{\mathbf{H}}} \right) \right] \tag{3.12}$$

More trials were available for rest than there were for movement (Table 3.3) and it was at this point unknown how representative each individual rest trial was. For these reasons, R was calculated between all available trials of movement and a subset of rest trials with an equal amount of trials as were available for movement. This process was repeated until all trials of rest were included in a calculation of R once. The resulting values for R and the corresponding p-values (denoting whether the difference between spectral magnitudes in the specific frequency band between movement and rest were significant) were averaged. This allowed for the most representative calculation of the R^2 values. The obtained averaged correlation value R was squared and the initial sign was retained to obtain the signed $R^2 \in [-1, 1]$ for each electrode during movement of each finger. As can be deduced from Figure 3.9, the R^2 values in the HFB (left hand figure) were mostly large

positive values resembling an increase in spectral power in the HFB during movement. Subsequently, the R^2 values in the α band were mostly negative values, resembling the decrease in spectral power during movement.

The obtained R^2 values were plotted on the cortical surface of the participants to determine the spatial distribution of cortical activity during both contralateral and ipsilateral movement. Only the channels which showed significant ($p<0.05$, Bonferroni corrected for multiple comparisons across channels) cortical activity during movement were plotted on the cortical surface.

3.3.3 Visualization of the Data Space

Several techniques exist for dimensionality reduction and the subsequent visualization of high-dimensional data. In this research, the t-Distributed Stochastic Neighbor Embedding (t-SNE) (Maaten and Hinton, 2008) technique was selected especially for its ability to handle non-linear data structures. This relatively new technique is able to map high-dimensional data to two or three dimensions using the local relations between data points. More specifically, t-SNE technique uses the Euclidean distances between datapoints in the high-dimensional space and uses these to create a probability distribution that describes the relations between the points in high-dimensional space. As an example, t-SNE describes the similarity between datapoints $\mathbf{x}_i$ and $\mathbf{x}_j$ as a conditional probability $p_{j|i}$ under a Gaussian distribution centered at $\mathbf{x}_i$:

$$p_{j|i} = \frac{\exp\left[-||\mathbf{x}_i - \mathbf{x}_j||^2 \cdot (2\sigma_i^2)^{-1}\right]}{\sum_{k \neq i} \left[\exp\left[-||\mathbf{x}_i - \mathbf{x}_j||^2 \cdot (2\sigma_i^2)^{-1}\right]\right]} \tag{3.13}$$

Resulting, datapoints that are similar in the high-dimensional data space show similar probability distributions. Now, for the low dimensional representation of the datapoints $\mathbf{x}_i$ and $\mathbf{x}_j$, noted as $\mathbf{l}_i$ and $\mathbf{l}_j$, a similar distribution $q_{j|i}$ can be defined. For this purpose, a Student's t-distribution with one degree of freedom is used:

$$q_{j|i} = \frac{\exp\left[-||\mathbf{l}_i - \mathbf{l}_j||^2\right]}{\sum_{k \neq i} \exp\left[-||\mathbf{l}_i - \mathbf{l}_k||^2\right]} \tag{3.14}$$

If the low-dimensional mapping has successfully modeled the similarities found in the high-dimensional data space, then the conditional probabilities $p_{j|i}$ and $q_{j|i}$ will be similar. To compute the extent to which these probabilities are indeed similar, the Kullback-Leibner divergence between $p_{j|i}$ and $q_{j|i}$ is computed over all datapoints and used as a cost function F for finding the low dimensional mapping:

$$F = \sum_i \mathrm{KL}(P_i||Q_i) = \sum_i \sum_j p_{j|i} log \frac{p_{j|i}}{q_{j|i}} \tag{3.15}$$

To find a suitable low-dimensional representation $q_{j|i}$, the cost function F is optimized with the gradient descent method. Several caveats surrounding the use of this technique must be addressed. Firstly, because the cost function is non-convex, each run of t-SNE might produce different results. Secondly, the final mapping depends on the selection of a value for σ, for which a hyper-parameter referred to as the *perplexity* needs to be set. Therefore, the results obtained with this technique must be carefully interpreted and were in this research only used during the formulation of several preliminary hypotheses before classification. The `MATLAB 2019a` implementation of t-SNE `tsne` (`Statistics and Machine Learning Toolbox`) was used to reduce the dimensionality of the spectral data of each trial averaged separately over the three frequency bands for each specific finger, $\mathbf{P}_{v,t,\overline{B}}$ and subsequently visualize these data. Again, the average spectral magnitudes of the window centered around the movement marker were extracted. The `perplexity` parameter was set to 30 for all participants.

3.4 Experiment I: Synchronous Classification

Several classifiers were selected for the synchronous evaluation. Firstly, Linear Discriminant Analysis (LDA) and a Support Vector Machine (SVM) were selected given that these have been named as the gold standard in ECoG BCI research (e.g. (Wang et al., 2010), (Wissel et al., 2013)) in literature and have been proven to work with high dimensional data and a small number of training samples. Secondly, a model that had not yet been handled in literature related to this subject was explored, namely a Random Forest (RF), which may be able to handle high dimensional data well (Do et al., 2010). Additionally, a generative statistical model, the Naive Bayes (NB) classifier was explored since it could be argued that the soft decision boundaries and the statistical approach may be suitable to handle noisy ECoG data. The NB classifier assumes independence between features and could therefore be less sensitive to the curse of dimensionality.

3.4.1 Background on Classifiers

Before handling the procedures surrounding the synchronous classification, an introduction of the classifiers is required. For the explanations of the classifiers, a toy data set $\mathbf{D}$ $=\{(\mathbf{x}_1,y_1),...,(\mathbf{x}_n,y_n)\}$ will be considered. This dataset consists of observations $\mathbf{x}_n$ and the corresponding target label y_n which indicates the class to which the observation belongs. Each observation $\mathbf{x}_n$ is described by a set of features f so that $\mathbf{x}_n \triangleq (x_{n_1}, x_{n_2}, ..., x_{n_f})$. This toy dataset contains two classes so that $y_n \in [+1, -1]$. All data is real valued so that $\mathrm{D} \in \mathbb{R}^{|F|+1}$.

3.4.1.1 Linear Discriminant Analysis

The LDA classifier is a linear, probabilistic, inherently multi-class classifier that seeks to find linear discriminant functions that separate data from different classes (Fisher, 1936). The classifier makes use of Baye's rule to compute the posterior probability $P(c|\mathbf{x}_n)$ that an observation $\mathbf{x}_n$ belongs to class c as follows:

$$P(c|\mathbf{x}_n) = \frac{P(\mathbf{x}_n|c)P(c)}{P(\mathbf{x}_n)} \tag{3.16}$$

To compute this posterior probability, LDA assumes that the likelihood $\mathrm{P}(\mathbf{x}_n|\mathrm{c})$ of an observation $\mathbf{x}_n$ belonging to class c is drawn from a multivariate normal distribution $\mathbf{x}_n \sim \mathcal{N}(\mu_n, \mathbf{\Sigma}_n)$ for which the probability density function $f_n(x)$ is defined as:

$$P(\mathbf{x}_n|c) = f_n(x) = \frac{1}{(2\pi)^{f/2}|\mathbf{\Sigma}_c|^{1/2}} \exp\left[-\frac{1}{2}(\mathbf{x}_n - \mu_c)^T \mathbf{\Sigma}_c^{-1}(\mathbf{x}_n - \mu_c)\right] \tag{3.17}$$

It is to be noted that the covariance matrices for all classes are equal. The prior probability of class c, $\mathrm{P}(\mathrm{C})$ is the fraction of training samples belonging to class c out of all training samples N_{tot}, defined as π_c:

$$P(c) = \pi_c = \frac{|\{n : y_n = c\}|}{N_{tot}} \tag{3.18}$$

Given that $P(\mathbf{x}_n)$ does not depend on the class and is equal in the computation of each posterior probability, it can be omitted. Therefore, the posterior probability can be calculated as:

$$P(c|\mathbf{x}_n) = \frac{\pi_c}{(2\pi)^{f/2}|\mathbf{\Sigma}_c|^{1/2}} \exp\left[-\frac{1}{2}(\mathbf{x}_n - \mu_c)^T \mathbf{\Sigma_c^{-1}}(\mathbf{x_n} - \mu_\mathbf{c})\right] \tag{3.19}$$

Rewriting gives the objective function $\delta_c(x)$ to maximize over all classes c defined as follows:

$$\delta_c(x) = \mathbf{w}^T \mathbf{x}_n + b = log(\pi_c) - \frac{1}{2}\mu_k^T \mathbf{\Sigma}^{-1} \mu_c + x^T \mathbf{\Sigma}^{-1} \mu_c \tag{3.20}$$

And as such, a datapoint $\mathbf{x}_n$ will be classified as the class resulting in the highest value for the objective function $\delta_c(x)$:

$$P(c|\mathbf{x}_n) = \hat{y}_n = \underset{c \in C}{\operatorname{argmax}}\, \delta_c(\mathbf{x}_n) \tag{3.21}$$

The decision boundaries (linear discriminants) indicated by the dotted lines in Figure 3.10 are the set of points for which the class probabilities are equally large (i.e. $\delta_{+1} = \delta_{-1}$).

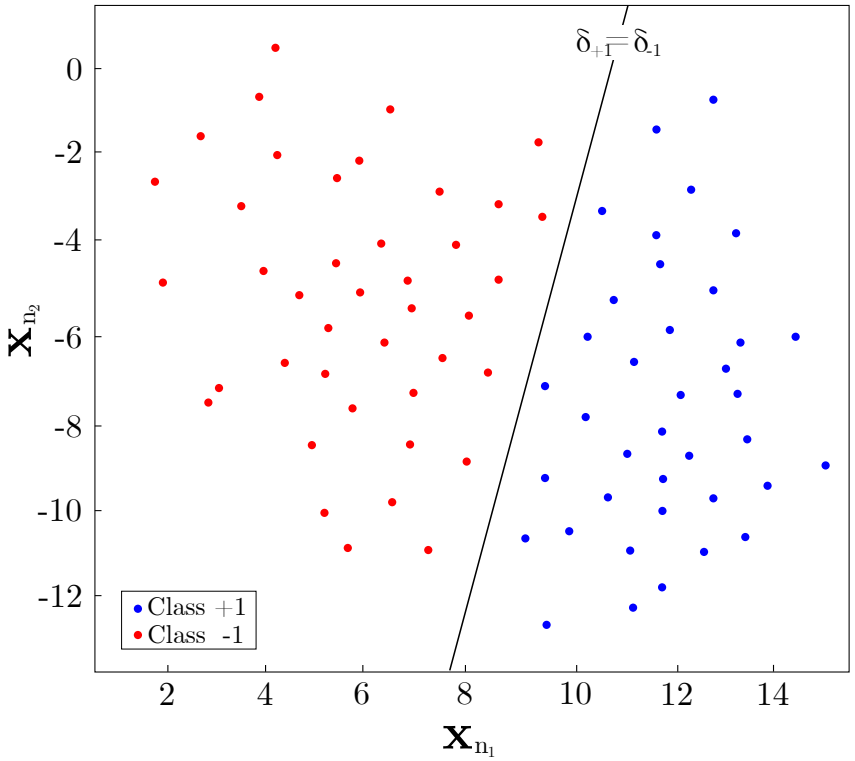

Figure 3.10: *Visualization of the datapoints* $\mathbf{x}_n$ *belonging to classes +1 and -1 in blue and red respectively. The linear discriminant function* $\delta_c(x)$ *is indicated by the black line separating the observations of the two classes classes.*

A drawback of applying the LDA classifier to high-dimensional data is that the covariance matrix $\mathbf{\Sigma}$ may be come singular in the case of a large number of features relative to the number of training observations available for each class. To avoid the covariance matrix from becoming singular, a diagonalization of the covariance matrix can be applied which functions as a form of regularization. The amount of diagonalization of the covariance matrix can be set by the regularization parameter γ as follows:

$$\mathbf{\Sigma} = (1 - \gamma)\mathbf{\Sigma} + \gamma \cdot \text{diag}(\mathbf{\Sigma}) \tag{3.22}$$

If the regularization parameter γ is set to 1, the covariance matrix is completely diagonalized.

The LDA classifier used in this research is the `MATLAB 2019a` implementation of the LDA classifier `fitcdiscr` (`Statistics and Machine Learning Toolbox`). This classifier has two hyper-parameters eligible for optimization, namely the γ (`Gamma` in the `MATLAB`

implementation) regularization parameter and a different regularization parameter that is unique to the `MATLAB` implementation referred to as the *linear coefficient threshold* δ (`Delta` in the `MATLAB` implementation). This parameter can reduce the dimensionality of the feature space by removing features with a weight w in the weight vector $\mathbf{w}$ of the LDA classifier that are lower than the set linear coefficient threshold.

3.4.1.2 Support Vector Machine

The SVM is a binary non-probabilistic linear classifier that aims to find a linear hyperplane that optimally separates observations of different classes (Evgeniou and Pontil, 1999). Given that the SVM is a linear classifier and most real data is not linearly separable, the SVM makes use of a transformation to implicitly map non-linearly separable data to an arbitrary higher dimensional space where the data becomes linearly separable. To perform this operation computationally efficiently, the SVM makes use of a linear kernel function K which computes the inner products between two observations x_i and x_j:

$$K(x_i, x_j) = \langle \phi(x_i), \phi(x_j) \rangle \tag{3.23}$$

Given a binary classification problem with classes +1 and -1, the SVM finds a separating hyperplane so that data points of one class fall to one side of the separating hyperplane and data of the other class falls to the other side of the separating hyperplane while keeping the margin, the distance between the separating hyperplane and the closest observations (the support vectors), as large as possible, as depicted in Figure 3.11.

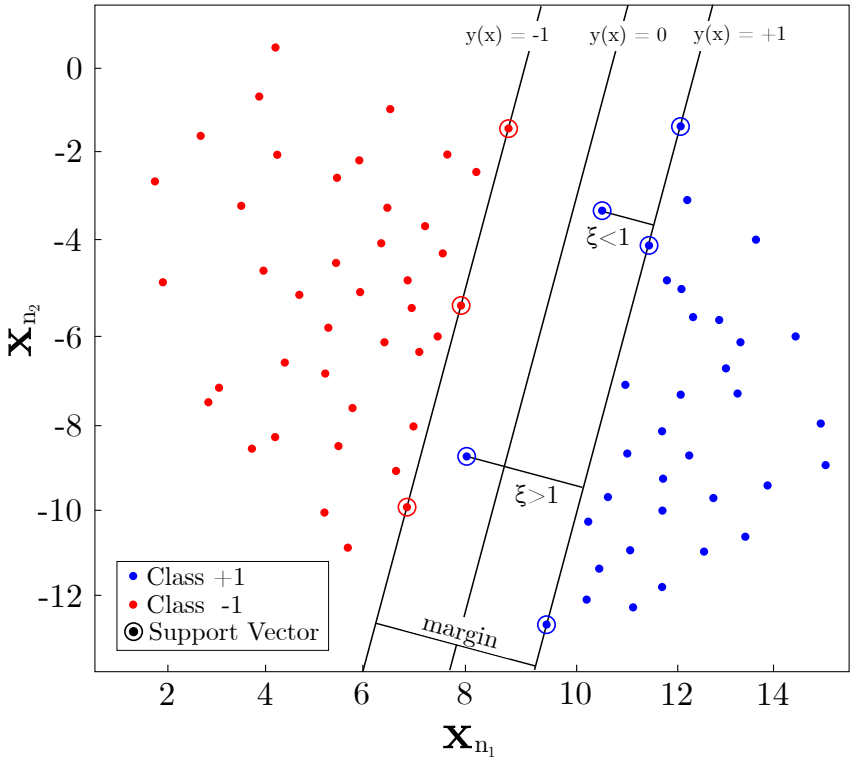

Figure 3.11: *Visualization of the datapoints* $\mathbf{x}_n$ *belonging to classes +1 and -1 in blue and red respectively. The separating hyperplane y(x)=0 is indicated by the black line separating the observations of the two classes classes. The support vectors are indicated by the datapoints surrounded with a circle. The distance between the support vectors between two classes is defined by the margin. The parameter* ξ *denotes the slack parameter.*

This linear separating hyperplane $y(x)$ and the constraints for the correct classification of the observations can be formulated as follows:

$$y(x) = \mathbf{w}^T \phi(\mathbf{x}_n) + b \text{ and } \begin{cases} y(\mathbf{x}_n) \geq 0, & \forall y_n = +1 \\ y(\mathbf{x}_n) \leq 0, & \forall y_n = -1 \end{cases} \tag{3.24}$$

Which can be rewritten as:

$$y_n(\mathbf{w}^T\phi(\mathbf{x}_n) + b) \geq 1 \tag{3.25}$$

If the data is hardly linear separable it may occur that the separating margin becomes very small, leading to the possibility of underfitting and susceptibility to noise. To overcome this, a slack parameter ξ can be introduced which allows a relaxation of the constraints so that most but not all observations are correctly classified. The slack variable can be integrated into the constraint as follows:

$$y_n(\mathbf{w}^T\phi(\mathbf{x}_n) + b) \geq 1 - \xi \tag{3.26}$$

The distance between the support vectors and the separating hyperplane can be found as follows:

$$D_{x,hp} = \frac{|\mathbf{w}^T\mathbf{x}_n + b|}{||\mathbf{w}||} \tag{3.27}$$

The optimal hyperplane can be found by maximizing the distance between the support vectors which can be calculated by minimizing the following equation subject to the relaxed constraint:

$$\text{argmin}\, \frac{1}{2}||\mathbf{x}|| + C\sum_{n}^{N} \xi_n \tag{3.28}$$

$$\text{subject to } y_n(\mathbf{w}^T\phi(\mathbf{x}_n) + b) - 1 + \xi_n \geq 0,\ \xi_n \geq 0 \tag{3.29}$$

This problem forms a quadratic constrained optimization problem that has to be solved. The parameter C regulates the trade-off between the margin width and the number of misclassified observations during training. Setting C to a small value changes the architecture of the SVM classifier from hard-margin to soft margin. A new observation $\mathbf{x}_n$ is accordingly classified in the class +1 or -1 depending on which side of the separating hyperplane it is located.

The SVM classifier used in this research is the `MATLAB 2019a` implementation of the SVM classifier `fitcsvm` (`Statistics and Machine Learning Toolbox`). This classifier has two hyper-parameters that are considered in this research and require optimization, namely the C (`BoxConstraint` in the `MATLAB` implementation) parameter governing the relaxation of the constraint and the kernel scale parameter (`KernelScale` in the `MATLAB` implementation) which governs the scaling of the features of the observations. All data will be standardized before classification with the SVM.

Given that the SVM classifier is a inherently binary classifier, several classifiers must be used to tackle multi-class problems. Literature has discussed OVO and OVA architectures, with the corresponding disadvantages. The possible ambiguity in assigning a class label when an equal number of votes for one class are issued in a majority vote, can be circumvented by making use of Error Correcting Output Codes (ECOC). ECOC make use of binary coding designs (dictating which classes each of the binary learners are trained on) and a corresponding decoding scheme (which determines how the predictions of each of the binary classifiers are aggregated). For example, for a three class problem, a coding design $\mathbf{M}$ could be the following:

$$\mathbf{M} = \begin{matrix} s_1 & s_2 & s_3 \end{matrix} \begin{bmatrix} +1 & +1 & 0 \\ -1 & 0 & 1 \\ 0 & -1 & -1 \end{bmatrix} \begin{matrix} c_1 \\ c_2 \\ c_3 \end{matrix}$$

Here, the three SVM classifiers are denoted by s_1,..,s_3 and the classes are denoted by c_1,..,c_3. To classify the data point $\mathbf{x}_n$, all binary classifiers are evaluated to obtain a

the corresponding bit string. The class label that is assigned to observation $\mathbf{x}_n$ is then calculated as follows:

$$\hat{y}_n = \underset{c}{\operatorname{argmin}} \frac{\sum_{s \in S} [|m_{c,s}| L(m_{c,s}, \hat{p}_s)]}{\sum_{s \in S} |m_{c,s|}} \tag{3.30}$$

Here, $m_{c,s}$ is an element of the coding matrix $\mathbf{M}$ and $\hat{p}_s$ is the predicted label for the positive class of classifier s. $L(\cdot)$ denotes the loss function, for which the binary cross entropy loss function is used:

$$L(m_{c,s}, \hat{p}_s) = m_{c,s} \cdot log(\hat{p}_s) + (1 - m_{c,s}) \cdot log(1 - \hat{p}_s) \tag{3.31}$$

This research uses the `MATLAB 2019a` implementation of ECOC model, named `fitcecoc` (`Statistics and Machine Learning Toolbox`).

3.4.1.3 Naive Bayes

The NB classifier is an inherently multi-class probabilistic classifier which classifies a data sample $\mathbf{x}_n$ to a class based on the maximum posterior probability $P(c|\mathbf{x}_n)$ (Jurafsky and Martin, 2008). Since this probability is often difficult to directly estimate from training data, the NB classifier relies on Bayes Theorem for calculation of this posterior probability:

$$P(c|\mathbf{x}_n) = \frac{P(\mathbf{x}_n|c)P(c)}{p(\mathbf{x}_n)} \tag{3.32}$$

Given that again $P(\mathbf{x}_n)$ is equal in the computation of the posterior probabilities $P(c|\mathbf{x}_n)$ of each class, it can be omitted, so that $P(c|\mathbf{x}_n)$ can be formulated as follows:

$$P(c|\mathbf{x}_n) = P(\mathbf{x}_n|c)P(c) \tag{3.33}$$

Since the likelihood of an observation can be described as the likelihood of each of the features ($\mathbf{x}_n \triangleq x_{n_1}, x_{n_2}, ..., x_{n_f}$), the the posterior probability $P(c|\mathbf{x}_n)$ can be reformulated again:

$$P(c|\mathbf{x}_n) = P(x_{n_1}, x_{n_2}, ..., x_{n_f}|c)P(c) \tag{3.34}$$

However, the likelihood is again difficult to empirically determine. Therefore, the NB classifier makes the naive assumption that each $x_{n_f} \in \mathbf{x}_n$ is independent given the class c, so that the posterior probability $P(c|\mathbf{x}_n)$ can be calculated as follows:

$$P(c|\mathbf{x}_n) = \left[P(x_{n_1}|c) \cdot P(x_{n_2}|c), ..., \cdot P(x_{n_f}|c)\right] P(c) = \left[\prod_{f \in F} P(x_{n_f}|c)\right] P(c) \tag{3.35}$$

The observation $\mathbf{x}_n$ is then assigned to the class for which the largest posterior probability is calculated:

$$\hat{y}(\mathbf{x}_n) = \underset{c \in C}{\operatorname{argmax}} \left[\prod_{f \in F} P(x_{n_f}|c)\right] P(c) \tag{3.36}$$

The decision boundaries of the NB classifier can be visualized and interpreted as a probability distribution over the classes depending on the value of the features, as depicted in Figure 3.12 below:

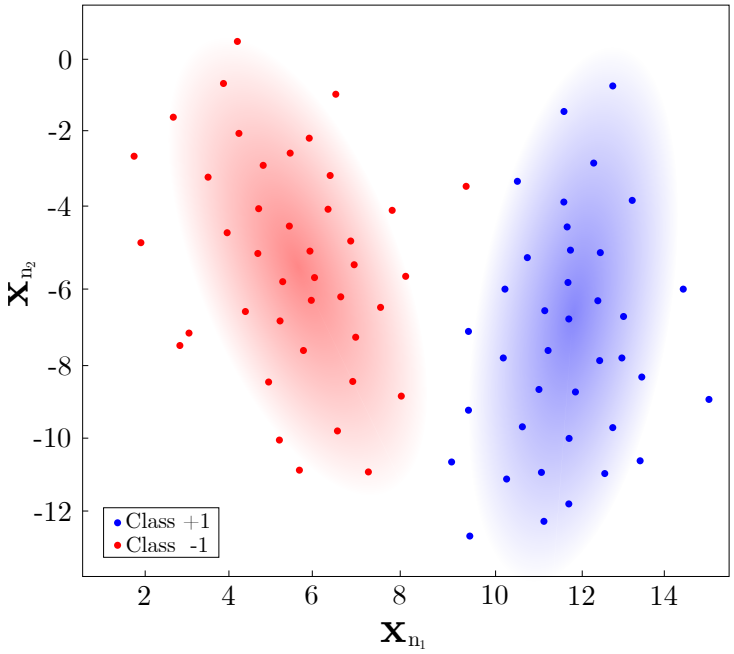

Figure 3.12: *Visualization of the datapoints* $\mathbf{x}_n$ *belonging to classes +1 and -1 in blue and red respectively. The probability distributions over the two classes are indicated by the color gradients.*

Although the independence assumption that the NB classifier makes is often violated in real life cases, the NB classifier has proven to be a useful and simple classifier in many problems. The Naive Bayes classifier used in this research is the `MATLAB 2019a` implementation of the Naive Bayes classifier `fitcnb` (`Statistics and Machine Learning Toolbox`). There are no hyper-parameters that are eligible for optimization.

3.4.1.4 Random Forest

The RF classifier is a tree-structured inherently multi-class classifier that aims to classify observations by means of a collection of Decision Trees (DTs) (Breiman, 2001). A visual representation of a section of such a decision tree is depicted in Figure 3.13 below:

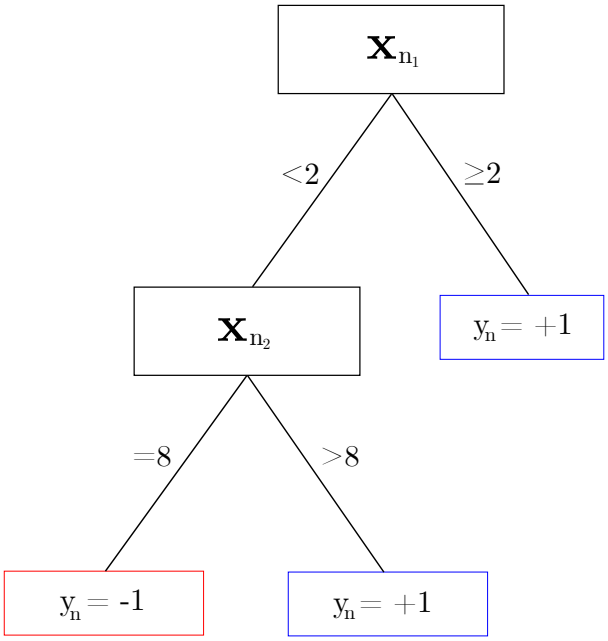

Figure 3.13: *Visualization of the structure of a decision tree. A decision tree aims to build a tree structure from the features of an observation* $\mathbf{x}_m$ *to reach a final decision on the class label of the observation. Such a tree is build up from a starting node at the top of the tree and several child nodes that spring from the starting node (which is then referred to as the parent node). The nodes that contain the targets for the observations are depicted here in red and blue for the -1 and +1 classes respectively and are referred to as leaf nodes.*

The decision tree starts with a root node, which contains all observations of both classes +1 and -1. Next, if the set of observations contains observations of both classes, the decision tree algorithm selects a feature f to partition (or split) the parent node into child nodes based on the value of that feature. Here, the aim is that each child node contains a purer subset of observations. This process of splitting over features is continued until a node is a pure subset containing only observations belonging to one class. Such a node is referred to as a leaf node. By traversing the resulting tree during the classification of a new unknown observation, a class label can eventually be assigned to that observation based on which leaf node the observation falls in.

The best split to be made at each point is dictated by the impurity of the resulting child nodes, where a smaller impurity denotes a better split. A measure used to calculate this impurity is the Gini impurity measure, which calculates the squared sum of the fractions of observations belonging to each class:

$$I_G = \sum_{c \in C} [\frac{|n : y_n = c|}{N_{tot}}]^2 \tag{3.37}$$

To determine the most suitable feature f to split on, a measure is required that compares the Gini impurity of the parent node P with the Gini impurities of the child nodes K after splitting on that feature. For this purpose, the gain criterion Δ can be used:

$$\Delta = I_G P - \sum_{j \in K} \frac{N_{c_j}}{N_{tot}} \tag{3.38}$$

Here, N_{c_j} denotes the number of observations in child node j and N_{tot} denotes the total number of observations in both child nodes.

A problem with applying decision trees to high-dimensional data is that the tree can

become large and complex which increases the risk of overfitting. One way of overcoming this is to combine several of these "weak" decision tree learners and combine them into one stronger ensemble, in that case referred to as a Random Forest (RF). To train multiple weak learners on the data, a method referred to as bagging is used, where t subsets of observations are sampled with replacement from the total set of observations. Following, t weak learners are trained on the t sampled subsets. In addition, at each split of each tree, the RF algorithm selects a random subset of features as candidates for the split. By means of these two methods, the chance of overfitting of the individual decision trees in the ensemble is reduced. The final class label that is assigned to the observation $\mathbf{x}_n$ is based on a majority vote among all of the predicted class labels of each of the decision trees in the random forest.

This research uses the `MATLAB 2019a` implementation of an ensemble method `fitcensemble` (`Statistics and Machine Learning Toolbox`). The ensemble consisted of a collection of template decision trees, for which the `MATLAB 2019a` implementation `templateTree` (`Statistics and Machine Learning Toolbox`) was used. Two hyper-parameters are eligible for optimization, namely the minimum number of observations per leaf (`MinLeafSize` in the `MATLAB` implementation) and the number of trees in the ensemble (`NLearn` in the `MATLAB` implementation).

3.4.2 Baseline Classification

First, this research required a baseline of classification accuracy to compare the accuracy of any further classification attempts throughout this research to. The data that was used for this baseline classification run is described by the dataset $\mathbf{D} = \{(\mathbf{x}_1, y_1), ..., (\mathbf{x}_n, y_n)\}$ The dataset consisted again of observations $\mathbf{x}_n$, where one observation represented one trial of finger movement, and the corresponding target label y_n which idicated the class to which the observation belonged. The features f of each observation were extracted by taking the all individual frequency bin magnitudes of the power data of each trial, $\mathbf{P}_{v,t,k} \in \mathbb{R}^{Ef \times K}$ of the window surrounding the movement marker. This classification constituted a seven-class classification where the classes corresponded to each of the fingers and rest so that $y_n \in \{\text{contrathumb}, \text{contraindex}, \text{contralittle}, \text{ipsithumb}, \text{ipsiindex}, \text{ipsilittle}, \text{rest}\}$. To maintain a balanced distribution of class labels, 30 trials of rest were selected from all available trials of rest of each participant (Table 3.2). The resulting feature vector will from now on be referred to as the baseline feature vector.

Because the performance of the four classifiers was to be compared, care had to be taken that a low initial performance of a classifier was not simply attributable to an erroneous initialization of hyper-parameters. Therefore, a hyper-parameter optimization was first performed which consisted of a grid search over the eligible hyper-parameters of each classifier validated by 10-fold cross validation using all available data. Of note, when the goal is to use the resulting optimized hyper-parameters for model training, the performance evaluation during the hyper-parameter optimization process should be performed on a separate validation set and not on the test set on which the tuned classifier will be employed. Otherwise, the obtained results could be positively biased which in turn may lead to an optimistic view of performance. However, in this research, the focus actually lay on generalization of results across participants. Therefore, not having to perform any hyper-parameter optimization was preferred. The hyper-parameter optimization on all data only served as a quick comparison between (possibly) more optimal settings and the default settings of all classifier hyper-parameters. The ranges and step sizes in which the hyper-parameters were optimized are depicted in Table 3.4 for each classifier separately.

Classifier	**Hyperparameter**	**Range and Step Values**
LDA	`Gamma`	Real Values $\mathbb{R} \in [0,1]$
	`Delta`	Positive Values (log-scaled) $\in [1e^{-6}, 1e^{3}]$
SVM	`BoxConstraint`	Positive Values (log-scaled) $\in [1e^{-3}, 1e^{3}]$
	`KernelScale`	Positive Values (log-scaled) $\in [1e^{-6}, 1e^{3}]$
RF	`NLearn`	Positive Integers (log-scaled) $\in [10,500]$
	`MinLeafSize`	Positive Integers (log-scaled) $\in [1, \max(2, \text{floor}(\texttt{NumObservations} \cdot 0.5))]$

Table 3.4: *Ranges and step sizes for the hyper-parameters values used in the optimization process for each classifier. The parameter* `NumObservations` *of the RF denotes the number of observations* $\mathbf{x}_n$ *in the training data* $\mathbf{D}$.

Given that the dimensionality of the data was high, the covariance matrices of the LDA classifier were diagonalized for all participants, which corresponds to a default value for the `Gamma` hyper-parameter of 1. The NB classifier had no eligible hyper-parameters and therefore no optimization could be performed. The performance after hyper-parameter optimization was compared to the performance obtained by the default `MATLAB 2019a` values for the hyper-parameters. Following, the baseline classification run was performed and validated per participant with Leave One Out Cross Validation (LOOCV) due to the scarcity of data.

3.4.3 Individual Frequency Band Classification

Based on insights from the results of the t-SNE visualizations of the data (Section 3.3.3), it was desirable to further research the contribution of the separate frequency bands on the classification process. Especially the HFB appeared to hold a significant amount of information for the distinction between finger movements. Even though the LFB did not appear to hold important information other than for the distinction between movement and rest, both the LFB and HFB frequency bands were separately classified. This was done for the sake of completeness, but mostly to determine whether an eventual increase in performance was not simply due to the reduction of the dimensionality of the feature vector. At first, the feature vector containing the individual spectral magnitudes of all frequency bins k was reduced to a feature vector containing only the frequency bins in the more narrowly defined frequency bands $B = \{\alpha, \beta, \text{HBF}\}$, for which the feature vector will be denoted by $[\alpha, \beta, \text{HBF}]$. This feature vector was further divided into a feature vector containing only the frequency bins corresponding to the LFB (which will be referred to as the $[\alpha, \beta]$ feature vector) and a feature vector containing only the frequency bins corresponding to the HFB (which will be referred to as the [HFB] feature vector). These feature vectors all showed dimensionality $\mathbb{R}^{Ef \times K}$ where the value of K depended on the selected frequency bands in B.

Additionally, feature vectors were created which contained the average value over the frequency bins k in each frequency band B, which were denoted as $[\alpha, \beta, \text{HBF}]_{\overline{B}} \in \mathbb{R}^{Ef \times 3}$, $[\alpha, \beta]_{\overline{B}} \in \mathbb{R}^{Ef \times 2}$ and $[\text{HBF}]_{\overline{B}} \in \mathbb{R}^{Ef}$ respectively. Since the dimensionality of these averaged feature vectors was much lower than the dimensionality of the original baseline feature vector, the hyper-parameter optimization process was repeated on the $[\alpha, \beta, \text{HBF}]_{\overline{B}}$ feature vector.

Following, all classifications were performed and again validated with LOOCV.The empirical chance level of accuracy was determined by classifying on random data with dimensions equal to that of the corresponding feature vector based on (Combrisson and Jerbi, 2015). The random data were created by randomly sampling numbers from a uniform distribution with upper and lower limits determined by the minimum and maximum value of the corresponding feature vector. The classification process on this random data was repeated as many times as possible (200 times) with LOOCV. The statistical significance of the obtained classification results in this section was determined by the 95th percentile ($p<0.05$) of the accuracy obtained on classification of the random data.

3.4.4 Required Training Data

Up to this point, LOOCV had been the evaluation method of choice since training data was scarce. However, for practical reasons it was sensible to determine how varying the amount of training data used to train the classifiers, influenced classification performance. For this purpose, a different method of cross validation was devised in which one trial per finger was incrementally added to the test set, starting with one trial per finger and continued until twenty trials per finger were included in the test set. This was the maximum amount of trials that could be withheld from the training data before the LDA classifier could no longer be trained for one of the participants due to a resulting singular covariance matrix. At each increment, classification was performed 200 times to increase the likelihood that each trial was included in the classification process at least once, even when only a small number of trials was included in the test set. Additionally, the empirical chance level was again determined at each classification step; especially with a small number of samples the estimation of the classification accuracy may vary strongly, resulting in a wider standard deviation. Therefore, the 95th percentile may shift strongly

and it became necessary to re-estimate the 95th percentile at every size of the test set. This complete process was performed for the baseline, $[\alpha, \beta, \text{HFB}]_{\overline{B}}$ and $[\text{HFB}]_{\overline{B}}$ feature vectors.

3.4.5 Time Lag Classification

Literature has shown that the occurrence of cortical activity does not coincide exactly with the time of movement. Additionally, literature has shown that cortical activity resulting from ipsilateral movement may appear earlier than cortical activity resulting from contralateral movement. This finding was additionally supported by the findings of the amplitudal analysis carried out in Section 3.3.1. Therefore, it was worth investigating how the classification performance was influenced by the selection of features extracted at different time points relative to the movement marker. For this purpose, the feature extraction and classification processes were repeated for several $[\alpha, \beta, \text{HFB}]_{\overline{B}}$ feature vectors that were extracted at various time lags, starting from one second prior to the movement marker until one second after the movement marker in steps of 0.05 seconds. The corresponding empirical chance level of Section 3.4.3 was used as a reference. The time lag classification process was repeated several times; once only with contralateral fingers including rest, once only with ipsilateral fingers including rest and once with both the contralateral and ipsilateral fingers including rest.

3.4.6 Spatial Analysis: Relative Channel Importance

This second spatial analysis was set out in an attempt to determine the cortical areas that were most informative for distinguishing movement of individual contralateral and ipsilateral fingers. For this purpose, the classifier weights were used; the weight w that a classifier assigns to each feature f during training serves as an indicator of the importance of that feature. In the case where one feature is assigned per channel, the weight can subsequently indicate the importance of this channel in distinguishing between the various classes. This concept was used in order to identify the spatial distribution of informative channels of the different cortical areas M1, S1 and the CS.

In all upcoming analyses, the $[\text{HFB}]_{\overline{B}}$ feature vector and the LDA classifier were used. The $[\text{HFB}]_{\overline{B}}$ feature vector was used for several reasons: Firstly, the $[\text{HFB}]_{\overline{B}}$ assigned indeed one feature to each channel and secondly, literature indicated that the modulations in the $[\text{HFB}]_{\overline{B}}$ show the highest spatial specificity. Since it can be observed from the results of the classifications using individual frequency bands (Section 3.4.3) that the classification performances between classification on the $[\alpha, \beta, \text{HFB}]_{\overline{B}}$ and the $[\text{HFB}]_{\overline{B}}$ feature vectors were highly similar, it could be argued that the results obtained in these sections generalized between classification processes on these two feature vectors. The rationale behind using the LDA classifier for these analyses stems from its high performance, observed in the results of the classification experiments in Sections 3.4.3 and 3.4.2. Only when the classification performance is high, it can be assumed that the estimation of channel importance is valid.

To calculate the weights of the classifier, only training (fitting) of the LDA classifier was performed, and no classification. For the `Matlab2019a` LDA classifier, the weights were stored in the `DeltaPredictor` variable. The resulting weights of the training process had an arbitrary unit with a lower boundary of 0 and no upper boundary (not specified by the `Matlab2019a` documentation). For this reason, the weights were normalized between 0 and 1 per participant and training run for all following spatial analyses.

3.4.6.1 Informative Areas for Distinguishing between Finger Movement and Rest

The first spatial analysis aimed to investigate whether the channels showing the highest R^2 values in Section 3.3.2 were also the channels that were most informative in distinguishing the movements of each of the fingers from rest. For this purpose, several binary LDA classifiers were trained to distinguish all trials of movement of each finger versus an equal number of rest trials (e.g. contralateral thumb versus rest, ipsilateral index finger versus rest, etc.).

3.4.6.2 Informative Areas for Distinguishing between Individual Finger Movement of the Same Laterality

The following spatial analysis aimed to determine which cortical areas where meaningful for distinguishing movement of the different fingers from the same hand. For this purpose, the LDA classifier was trained to distinguish movement trials of every finger against movement trials of the other fingers on the same hand in a binary scheme (e.g. ipsilateral thumb versus ipsilateral index and little finger, contralateral index finger versus contralateral thumb and little finger, etc.). To maintain a balance between training data of each class, trials of the contrasting fingers were sub-sampled and the training process was repeated 200 times to increase the likelihood that each trial was included in the training process at least once. The weights of the 200 training runs were averaged prior to normalization.

3.4.6.3 Informative Areas for Distinguishing between Contralateral and Ipsilateral Finger Movement

The last spatial analysis aimed to determine which cortical areas were meaningful for distinguishing between contralateral and ipsilateral finger movements. For this purpose, the LDA classifier was trained to distinguish all trials of movement of a specific contralateral finger against trials of the same ipsilateral finger movement separately in a binary scheme (e.g. ipsilateral thumb versus contralateral thumb, ipsilateral index finger versus contralateral index finger, etc.). Another training run was performed in which the LDA classifier was trained to distinguish all trials of all contralateral fingers from all trials of all ipsilateral fingers in a binary scheme (i.e. ipsilateral thumb, index and little finger all together versus contralateral thumb, index and little finger altogether).

3.5 Experiment II: Asynchronous Classification

As mentioned in the overview of experiments in Section 3.1, the goal of the asynchronous classification was to resemble the scenario of a real-life BCI were cues for finger movements are absent and movement is insead paced by the participant. The goal of a classifier in such a BCI is now to correctly classify movement of a certain finger when actual movement of that finger is performed (an IC event) and to classify episodes of rest in case there is no finger movement (the NC events). It should be underlined that the goal of this section was not to create the best possible performing asynchronous BCI for detecting contralateral and ipsilateral finger movement, but rather to evaluate the detection of both contralateral and ipsilateral finger movement in an asynchronous setting, mainly to determine whether ipsilateral finger movement could be correctly detected without a significant number of false positive detections during episodes of NC. For this purpose, the methodology for performing the asynchronous evaluation aimed at finding the most transparent and perhaps most pessimistic results, and not the best performance.

3.5.1 Approximation of an Asynchronous BCI

In this research, an asynchronous BCI setting was approximated by letting a classifier classify each one second window that was placed over each time point in the complete spectral ECoG data of both the contralateral run and the ipsilateral run (described by $\mathbf{P}_{\text{run}}$, defined in Section 3.2.3) of a participant, and saving the classifier output. This is schematically depicted in Figure 3.14 below.

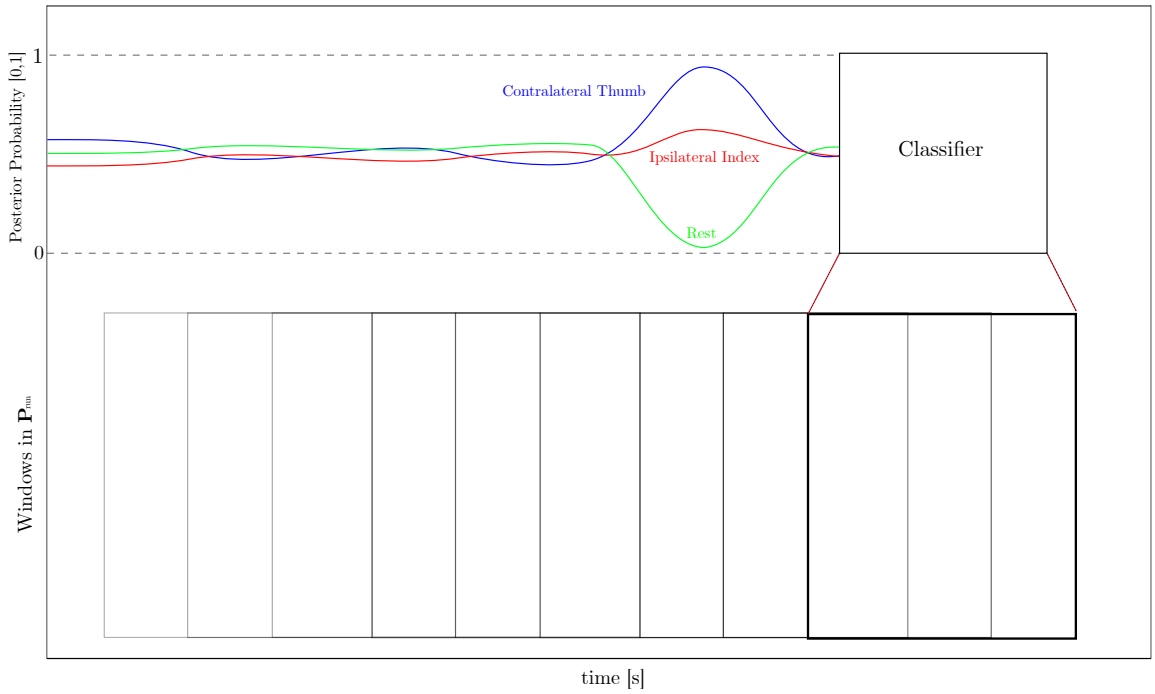

Figure 3.14: *A schematic representation of the classifier consecutively classifying each window in the spectral ECoG data* $\mathbf{P}_{run}$*. The outputted posterior probabilities of the classes at each window are concatenated to form traces as the classifier progresses in time. Here, the posterior probabilities corresponding to the contralateral thumb, ipsilateral index finger and rest classes are depicted. This instance shows that the classifier has passed a window to which a large posterior probability was assigned to the class of contralateral thumb movement.*

These traces of posterior probabilities for each class resulting from the classification of a complete run were compared to the dataglove signal of that same run, as depicted in Figure 3.15.

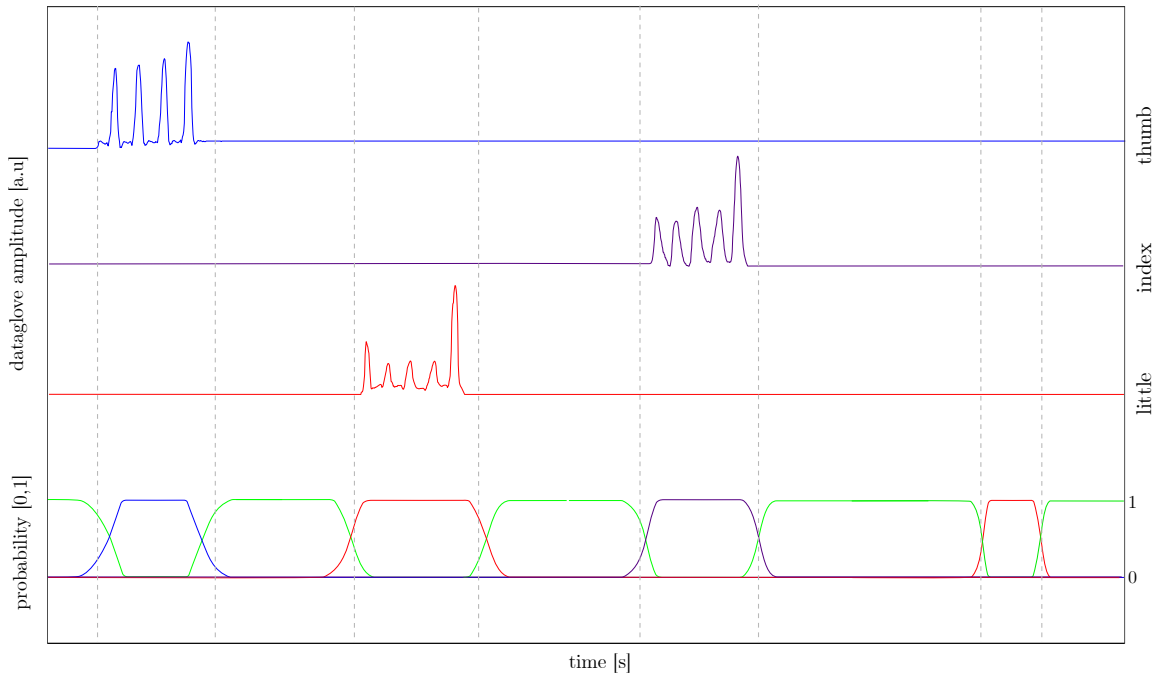

Figure 3.15: *A schematic representation of the approximation of a self paced asynchronous BCI. The dataglove signals for each finger are depicted in the top of the figure. The concatenated posterior probabilities for each finger are depicted in the bottom of the figure. Given that this figure represents a self-paced BCI, the movement cues are not present and the goal of the classifier is to correctly classify episodes of movement (IC). A measure for how confident a classifier is about whether there is movement of a certain finger, is the outputted posterior probability corresponding to that finger. This probability will theoretically be (close to) zero when there is no movement of that finger and (close to) one if there is. In this figure, the trace of the posterior probability of a finger is matched to the dataglove signal of that finger by color. The green trace denotes the posterior probability of rest, which is theoretically (close to) one during rest and (close to) zero during episodes of movement.*

In asynchronous BCIs, there are several parameters that govern whether a modulation in the control signal (here the increase of the posterior probability) will lead to an actual detection of movement. At first, a *threshold* is applied above which the posterior probability needs to rise before detection is considered. Secondly, the posterior probability needs to stay above this threshold for a certain amount of time to confidently and robustly label a detection. This amount of time is referred to as the *dwell time*. A last parameter is referred to as the *refractory period*, which denotes a period after which any rise in posterior probability - after a rise that has met the dwell time - will be ignored for a certain duration. Once a rise in posterior probability fits the criterion of the threshold and dwell time parameters, it is labeled as a movement detection. Once the detection of a specific finger movement takes place inside a movement episode of that specific finger, the detection is counted as a True Positive (TP). When the detection of a specific finger movement takes place outside a movement episode, the detection is labeled as a false positive. This is depicted schematically in Figure 3.16.

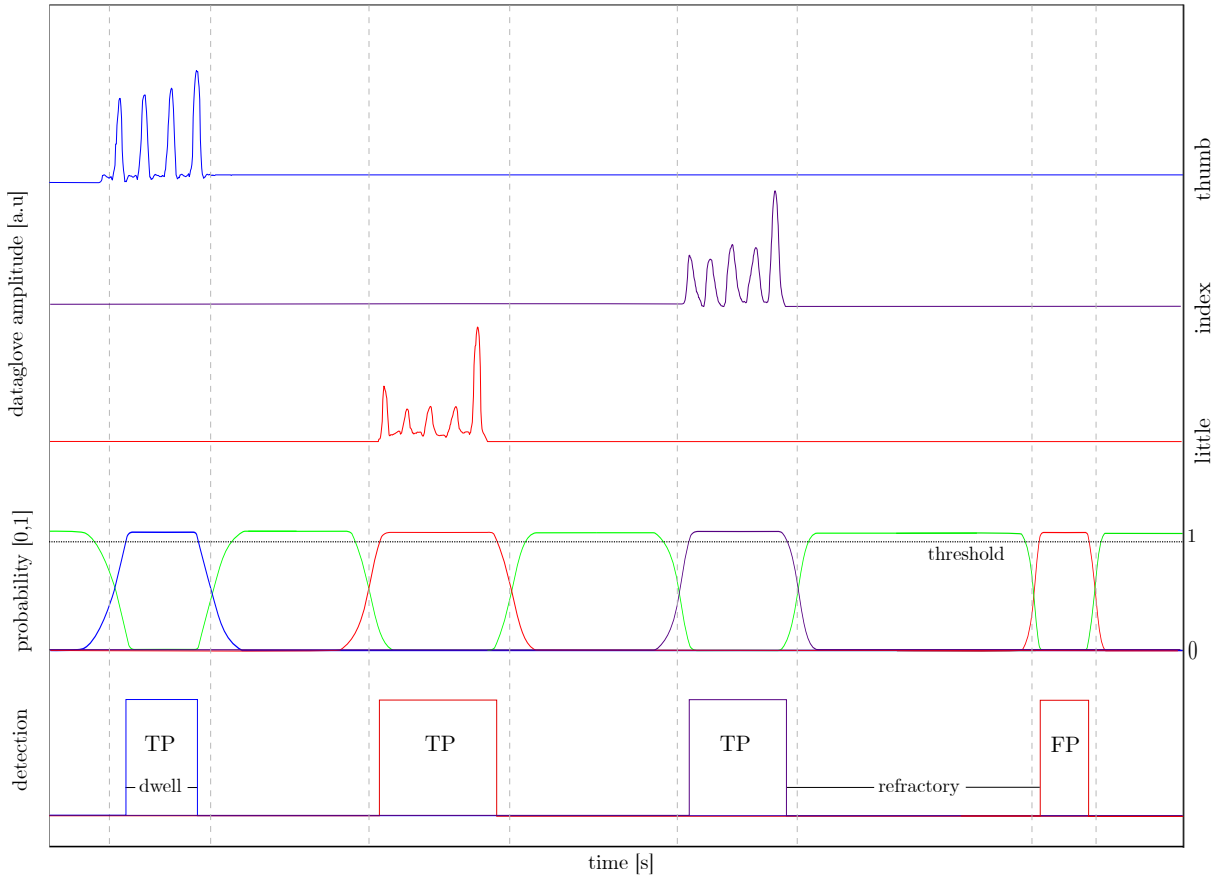

Figure 3.16: *A schematic representation of the detection of movement in an asynchronous BCI showing the detection threshold, the dwell time and the refractory period. The detections during and outside of movement events are indicated as true positives and false positives respectively.*

To evaluate the performance of an asynchronous BCI, literature has provided two suitable measures referred to as the event-based True Positive Rate (eb-TPR) for the evaluation of IC events, and the sample-based False Positive Rate (sb-FPR) for evaluation of NC events (Mason et al., 2006).

An eb-TP is counted when a detection of a finger movement is made inside an event where movement of that finger has taken place and the eb-TPR is expressed as a percentage of correctly detected movement events out of all movement events. In the case were more than one correct detection takes places during a movement event, it is necessary to count these as one detection in order to avoid a bias in the number of eb-TPs. Since this measure is often used for asynchronous BCIs with only two classes (one IC and one NC), literature does not describe the handling of detections of multiple (other) fingers within an movement event of one specific finger. In this research, such detections were counted as true positives, but they were considered as misclassifications as in the synchronous classification. As such, confusion matrices could be constructed during the asynchronous classification. Since these misclassifications can not be expressed as percentages in the confusion matrices, this research presented the number of eb-TPs as integers instead of the eb-TPR as a percentage.

Similarly, for the false positives, an eb-FPR can be calculated. However, the duration of NC events often vary largely (there may be a arbitrarily large time in between movements in BCI usage) and having to label a complete long NC event as a false positive when only a single false positive has occurred may provide a pessimistic view on performance. Therefore, the sample-based FPR (sb-FPR) can be used as an evaluation measures for NC episodes. During the calculation of this measure, the number of falsely

labeled IC samples within a NC event is divided by the total number of samples during all NC events and expressed as a percentage. In BCI research it is common to present the eb-TPR corresponding to a set sb-FPR of one percent (Bashashati et al., 2007). Since this research aimed to exactly investigate the occurrence of false positive detections (mainly for ipsilateral fingers), the sb-FPR measure was not used. Instead, the number of false positive detections during all NC events were provided as an integer since this provided a more transparent and practical performance measure to be used during NC events.

3.5.2 Feature Extraction and Preliminary Classification

The spectral data of both the contralateral and ipsilateral run $\mathbf{P}_{run}$ were extracted using the DFT as described in Section 3.2. This time however, the one second windows of ECoG data were not extracted at each sample of a run, but at every 0.01 seconds to enable a relatively quick computation during the asynchronous classification. Again, the dataglove data were up-sampled similarly as in section 3.2.4. The LDA classifier was selected for the asynchronous classification for several reasons. Firstly, its performance was high during the synchronous classification. Secondly, it has the ability to output a posterior probability distribution over classes instead of only class labels. Lastly, it has the ability to remain performing well with reduced data available for training, as shown in Section 3.4.4. To determine how classification was impacted by refraining from sub-sampling the rest trials and to determine whether the DFT computation at a different time resolution had any impact on the classification, again synchronous classification similar to Section 3.4.3 was performed. This time, sub-sampling of rest trials was thus not performed and all available trials of rest as noted in Table 3.2 were used in the classification process. The $[\alpha, \beta, \mathrm{HFB}]_{\overline{B}}$ feature vector was used to for this classification run.

For the asynchronous classification, a different LDA classifier was trained on the $[\alpha, \beta, \mathrm{HFB}]_{\overline{B}}$ feature vector. During this process, three-fold cross validation was applied. Here, every complete contralateral and ipsilateral run was divided in three parts each containing an equal number of trials for all fingers (10 trials per finger per fold) and rest (again not sub-sampled, 60 trials per fold). The LDA classifier was trained similarly as in Section 3.4.3 on the trials of all classes that were in the in total four folds (two folds from the contralateral run and two folds from the ipsilateral run). After training, each one second window placed at every 0.01 seconds in the remaining two folds (one from the contralateral run and one from the ipsilateral run) were classified to obtain the concatenated posterior probability distribution traces which the classifier outputted as it progressed over the windows. This process of cross validation was repeated three times so that every one second window of both the contralateral and the ipsilateral run of a participant was classified and the posterior probability traces for both runs had been obtained.

3.5.3 Postprocessing of Dataglove and Posterior Probability Traces

The dataglove signals showed significant amounts of noise and sensor drift and they were therefore unsuitable to directly use in the asynchronous evaluation. The dataglove signals corresponding to each finger $\mathbf{D}_v$ where therefore manually binarized to obtain $\mathbf{D}_{bin_v}$ as depicted in Figure 3.17. Visual inspection ensured that only confident movements were included and sensor noise was not labeled as movement. Corrections of movement were retained since finger movement had actually occurred, albeit not inside a trial. It is expected that movement will be detected by the classifier somewhat prior to the performed movement and likely similarly after the performed movement. To prevent these early and late detections that actually corresponded to the movement from being unnecessarily labeled as false positives, mercy windows of 200ms were added prior to and after each binary block of movement in the binarized dataglove signal movement $\mathbf{D}_{bin_v}$ as depicted in Figure 3.17.

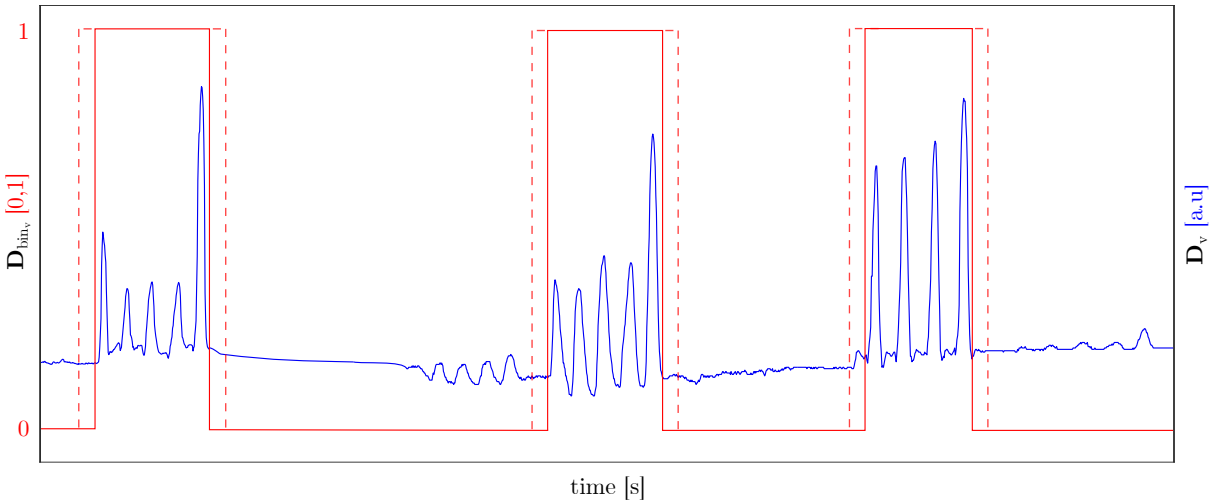

Figure 3.17: *Depiction of the binarization process of the noisy and drifted signal of* $\mathbf{D}_v$ *in blue, to obtain* $\mathbf{D}_{bin_v}$*, depicted in red. The introduced mercy windows are depicted by the dashed red lines.*

The number of movement events that were defined for each finger and participant from the binarized dataglove signals $\mathbf{D}_{bin_v}$ is presented in Table 3.5

Finger	**Participant P1**	**Participant P2**	**Participant P3**	**Participant P4**
Contralateral Thumb	30	30	31	30
Contralateral Index	30	30	30	30
Contralateral Little	30	30	31	30
Ipsilateral Thumb	29	29	30	27
Ipsilateral Index	30	30	30	26
Ipsilateral Little	30	30	30	28

Table 3.5: *The number of movement events for each participant and each finger during both the contralateral and ipsilateral task runs.*

An investigation of the outputted posterior probability traces of the classifier was performed. At first, it was expected that the increase of the posterior probability corresponding to a finger during movement of that finger was gradual, as depicted in the left hand figure of Figure 3.18. In contrast, the actual outputted posterior probability trace closely resembled a step function, as depicted in the right hand figure of Figure 3.18, where the

posterior probability increased strongly and quickly around the start of movement and similarly decreased strongly and quickly after movement.

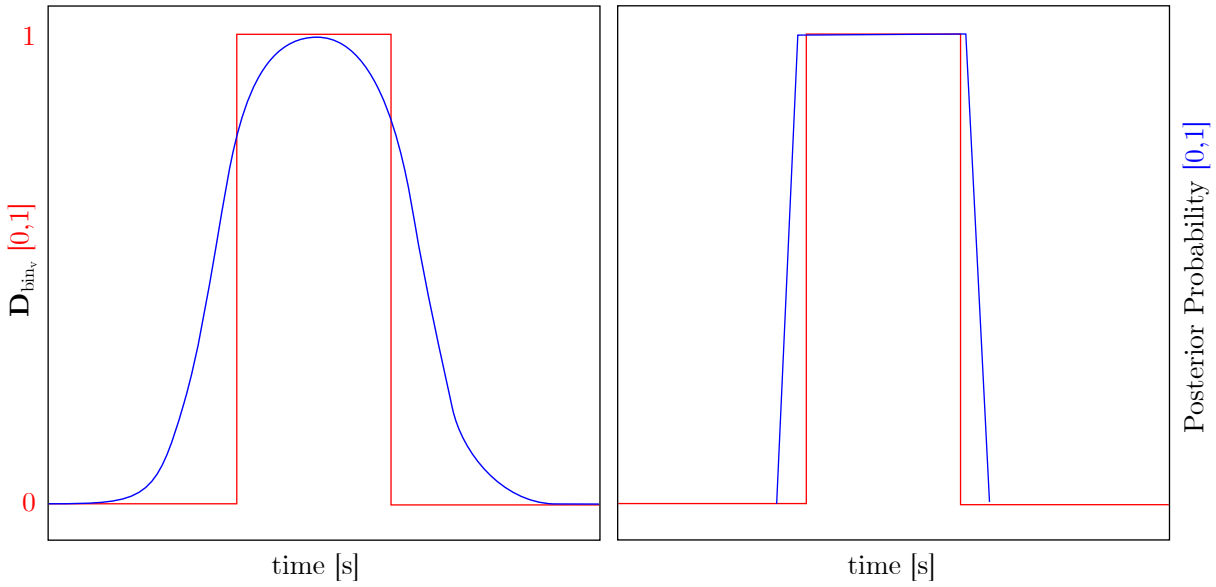

Figure 3.18: *The expected gradual posterior probability output belonging to an arbitrary finger is depicted in the left hand figure. The actual outputted posterior probability trace corresponding to an arbitrary finger is depicted in the right hand figure and depicts a more step function-like output.*

For this reason, the decision was made to binarize the classifier output completely. As such, the output of the classifier no longer consisted of traces of posterior probabilities for each class, but rather traces of ones and zeros for each class (forming traces that resembled block functions), corresponding to whether the one second windows were assigned to that specific class or not. This is schematically depicted in Figure 3.19 below.

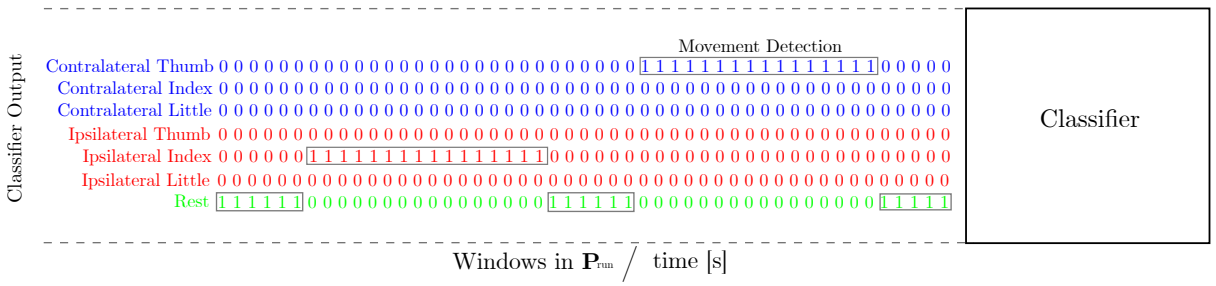

Figure 3.19: *Schematic depiction of the traces of ones and zeros outputted by the classifier for each class during the classification of each one second window in* $\mathbf{P}_{run}$.

This decision was preffered since it additionally circumvented the need to define a sensible value for the *threshold* parameter, since the classifier output were now binarized traces bound between with a value of either zero or one.

At this point, another phenomenon was observed. The classifier often outputted class labels corresponding to a detected finger only surrounding the beginning and ending of movement events of that specific finger. In the middle section of the movement event, the classifier outputted class labels corresponding to the rest class. Given that ipsilateral activity was occasionally confused with rest, several occurrences of outputted class labels for several ipsilateral fingers could also be found during that specific movement event. This is schematically depicted in Figure 3.20.

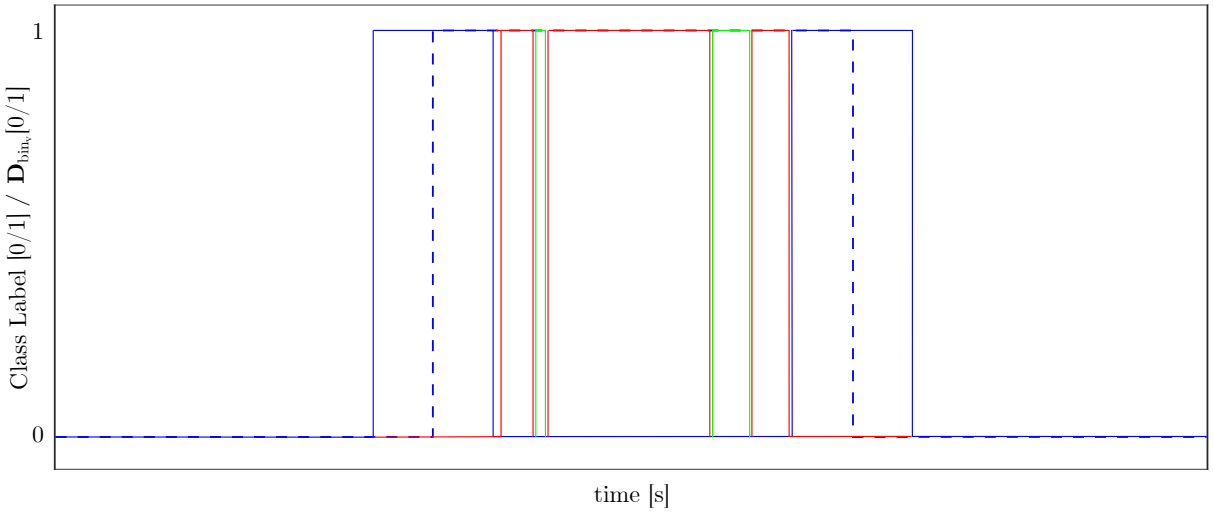

Figure 3.20: *The binarized dataglove signal denoting the movement event of an arbitrary finger, $\mathbf{D}_{bin_v}$, is depicted with the dashed blue line. The series of outputted class labels corresponding to that same arbitrary finger surrounding the beginning and ending of the movement event are depicted with the solid blue line. The occurrences of series of outputted class labels corresponding to rest and arbitrary ipsilateral fingers in the middle of the movement event are respectively denoted by the green and red lines.*

This phenomenon could be explained by considering that the beginning and ending of the movement episode constituted the moments at which finger flexion and finger extension respectively occurred. Because the finger movement performed by some participants was relatively slow, a brief period between flexion and extension existed where no actual movement took place. This is more easily visible when looking at the plots that denote the acceleration δ_{Z_v} in Figure 3.7. These brief intermittent periods of rest were subsequently detected by the classifier. This phenomenon may cause several misclassifications of rest and perhaps ipsilateral finger movement during other events of (contralateral or ipsilateral) finger movement. Such occurrences may normally be solved by issuing a refractory period (and possibly by setting an appropriate dwell time), but in this research the choice was explicitly made to not use any refractory period. This was done to be able to present the most transparent results as possible, in accordance with the statement made in the introductory paragraph of this section. Adding a refractory period can help to mitigate false positives (Townsend et al., 2004), while the goal of this section was actually to investigate in detail the occurrences of false positives. Additionally, this dataset was not designed for asynchronous evaluation and it may therefore not be suitable to introduce refractory periods since the movement events and inter-trial times are relatively constant and short. With this prior knowledge it is expected to see significant confusion between movement events and rest in the confusion matrices of this asynchronous classification.

3.5.4 Movement Detection in Asynchronous Classification

The moments in time at which the classifier outputted a class label corresponding to a finger, were the moments at which movement of that finger was detected by the classifier. Since the binarization of the classifier output circumvented the need to set a threshold parameter, the detection of events in this research was governed only by the dwell time parameter. The dwell time could in this research be approximated by counting how many one second windows spaced at 0.01 seconds had to consecutively labeled with the class label of a certain finger. Thus, if a finger movement that was detected by the classifier had to satisfy a dwell time of 0.12 seconds, then twelve consecutive one second windows spaced at 0.01 seconds had to be consecutively assigned the class label for that specific finger.

Detection of movement in this research therefore consisted of searching for the number '1' across all finger movement classes (and rest) in the output traces produced by the classifier at each one second window (see Figure 3.19), which denoted that the particular window was labeled as the class for which the '1' was found. When an arbitrary class label was found, the number of identically labeled consecutive windows was counted and the total number of consecutive identical class labels was multiplied with 0.01 to obtain the duration of the movement detection of that finger in seconds (each window was spaced at 0.01 seconds). The duration of the detected movement event in seconds was compared to the set dwell time in seconds. If the duration of the detected event was equal to or exceeded the set dwell time, it was registered as a movement detection, otherwise it was ignored.

The search for the number '1' in the output traces of the classifier across all classes was in this research performed with the same `MATLAB 2019a findpeaks` function that was used in Section 3.2. The minimum peak height parameter `MinPeakHeight` was set to one. To determine whether the detected movement satisfied the dwell time, the `MinPeakWidth` parameter was set to the number of consecutive 0.01 second windows that had to be assinged a 1. Thus, if the dwell time was 0.12, the `MinPeakWidth` parameter was set to 12.

A detected movement of an arbitrary finger was considered a true positive when it was located inside a movement event of that arbitrary finger, defined by the binarized dataglove signal. If the detected movement of an arbitrary finger was located inside the movement event of another finger that was not the arbitrary finger, it was counted as a true positive but considered as a misclassification and included in the confusion matrix. Events of rest were determined by the periods in the dataglove signal where no movement episodes of any finger were present and if the detected movement of an arbitrary finger was located inside such a rest event, it was counted as a false positive detection.

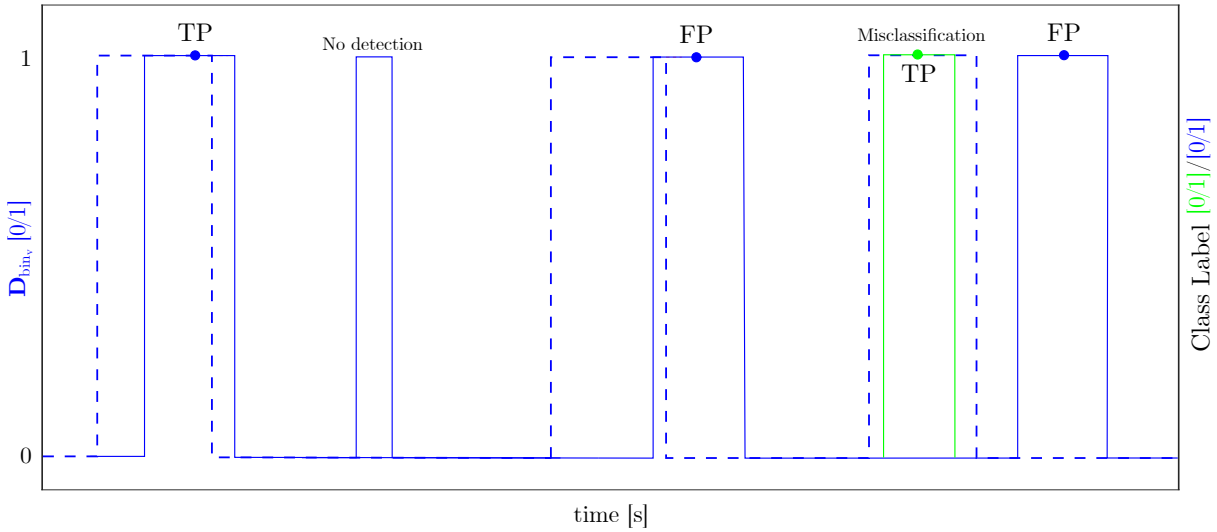

Figure 3.21: *The detection of peaks in the output trace of the classifier corresponding to an arbitrary finger, denoted with the solid blue line. An output trace of the classifier belonging to a different finger is depicted with the solid green line. The location of the found peaks in the middle of the detected movements are denoted with a dot. The location of this peak was co-registered with the binarized dataglove trace* $\mathbf{D}_{bin_v}$ *corresponding to the arbitrary finger, depicted with the dashed blue line. True positives were counted if the duration of the detected movement satisfied the set dwell time and if the peak in located in the middle of the detected movement fell within the boundaries of a movement event, regardless of which finger the output trace belonged to. False positives were counted if the peak satisfied the dwell time value but the peak fell outside the boundaries of a movement event. Peaks were not detected if they did not satisfy the dwell time value.*

3.5.5 Determination of Dwell Times

Firstly, an appropriate value of the dwell time had to be found. As a baseline, a dwell time of 0.01 seconds was selected. This was the smallest possible dwell time and was chosen to firstly determine whether all movement events of all fingers could be detected at all, and secondly to determine the largest number of false positive detections during rest that could possibly be attained. Afterwards, the dwell time was optimized for each separate finger of each participant by searching for a dwell time that minimized the number of false positive detections of that finger during episodes of rest while maintaining the maximum attainable number of true positives of that finger. For both dwell time settings, the number of true positive detections of that finger during movement events of only that finger was stored. Additionally, the number of false positives during periods of rest from the contralateral run and the ipsilateral run were separately determined.

3.5.6 Asynchronous Classification Runs

Afterwards, the actual asynchronous classification was performed twice with two different settings for the dwell time: one setting that was optimal for the detection of ipsilateral fingers and one setting that was optimal for contralateral fingers.

4 Results

4.1 Preliminary Data Analysis

4.1.1 Amplitudal Analysis: Visualization of Spectral Modulations

The visualization of the spectral modulations in the separate frequency bands and channels for a specific finger averaged over trials ($\mathbf{Z}_{\mathbf{P}_{v,\overline{Tv},\overline{B}}}$) is depicted for the thumb of participant P1 in Figure 4.1 below. The visualizations of $\mathbf{Z}_{\mathbf{P}_{v,\overline{Tv},\overline{B}}}$ corresponding to the remaining fingers of this participant as well as the fingers for the other participants are included in Figures H.1 through H.11 in Appendix H.

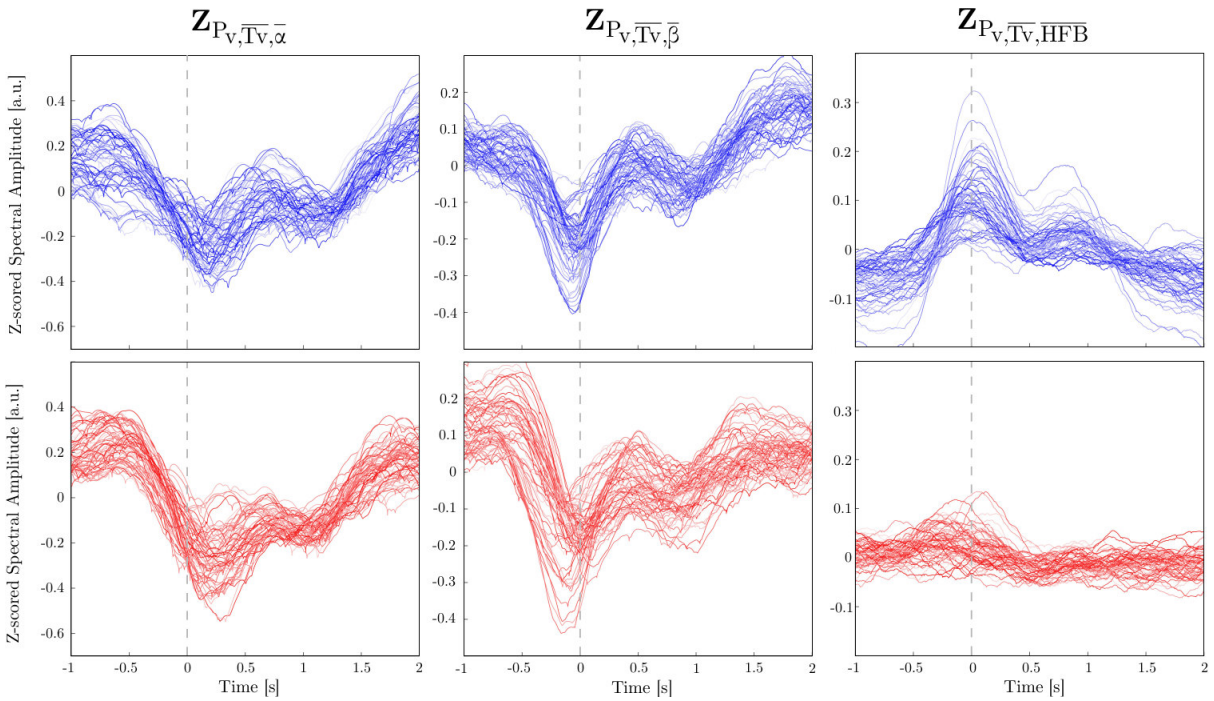

Figure 4.1: *Visualization of the spectral modulations represented by* $\mathbf{Z}_{\mathbf{P}_{v,\overline{Tv},\overline{B}}}$ *in the* α*,* β *and HFB frequency bands during movement of the thumb performed by participant P1. Modulations during contralateral thumb movement are depicted in blue and modulations during ipsilateral thumb movement are depicted in red. Each separate line denotes the signal of one channel. The dashed gray lines at t=0 seconds denote the movement marker position.*

The visualization of the spectral modulations in the separate frequency bands averaged over trials and channels for all fingers ($\mathbf{Z}_{\mathbf{P}_{v,\overline{Tv},\overline{B},\overline{E_f}}}$) is depicted for one of the participants in Figure 4.2 below. The visualizations of $\mathbf{Z}_{\mathbf{P}_{v,\overline{Tv},\overline{B},\overline{E_f}}}$ corresponding to the other participants are included in Figures I.1 through I.3 in Appendix I.

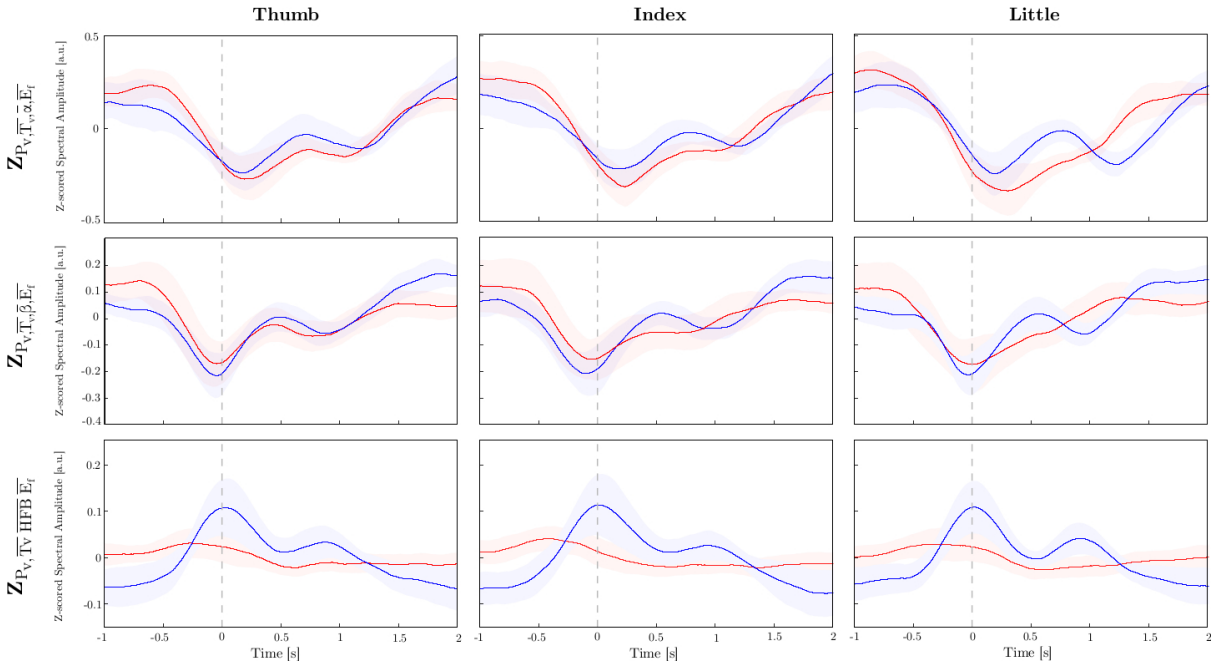

Figure 4.2: *Visualization of the spectral modulations of* $\mathbf{Z}_{\mathbf{P}_{v,\overline{T_v},\overline{B},\overline{E_f}}}$ *in the* α*,* β *and HFB frequency bands during movement of the thumb, index and little finger performed by participant P1. Modulations during contralateral finger movement are depicted in blue and modulations during ipsilateral finger movement are depicted in red. The solid lines denote the grand average signal and the shaded areas show the standard deviation of the signal. The dashed gray lines at t=0 seconds denote the movement marker positions.*

Several remarks can be made regarding the temporal aspects of spectral modulations of cortical activity resulting from contralateral and ipsilateral movement. In the HFB, the timing between channels seems to be less robust which is especially visible in the plots of $\mathbf{Z}_{\mathbf{P}_{v,\overline{T_v},\overline{B}}}$. From the plots of $\mathbf{Z}_{\mathbf{P}_{v,\overline{T_v},\overline{B},\overline{E_f}}}$ it can be seen that the peak of the spectral modulations in the HFB for ipsilateral movements occurs somewhat earlier. Any notable temporal differences between spectral modulations resulting from contralateral and ipsilateral movements were not visible in the α and β bands.

Some remarks regarding the amplitudal differences of spectral modulations resulting from contralateral and ipsilateral movement can additionally be made. No clear differences in amplitude of the spectral modluations in the α and β bands can be deduced, except for participant P4, for whom the amplitude of spectral modulations in these bands is smaller during ipsilateral movement. There are however clear differences in amplitudes of spectral modulations in the HFB. In this band, the amplitudes of the spectral modulations resulting from ipsilateral movement are smaller than the amplitudes of spectral modulations resulting from contralateral movement. This finding was consistent across all participants and all fingers.

4.1.2 Spatial Analysis: Channel R^2 Values

The spatial distributions of channel R^2 values in the α and β frequency bands plotted on the cortical surface of all participants are depicted in Figures J.1 through J.8 in Appendix J. The spatial distributions of channel R^2 values in the HFB plotted on the cortical surface of participants P1 and P2 are depicted below in Figures 4.3 through 4.4. The distribution of channel R^2 values in the HFB for the other participants are depicted in Figures K.1 through K.2 in Appendix K.

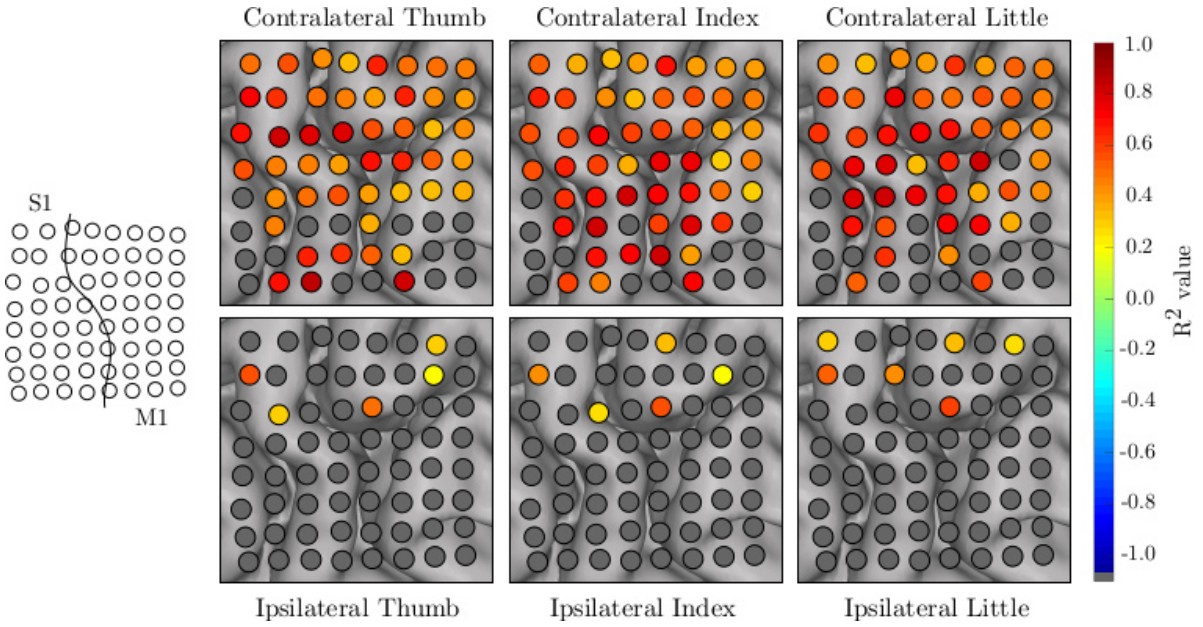

Figure 4.3: *Visualization of channel R^2 values in the HFB band for participant P1. Channels that showed no significant cortical activity as well as faulty channels are denoted in gray. This Figure caption holds for Figure 4.4 below.*

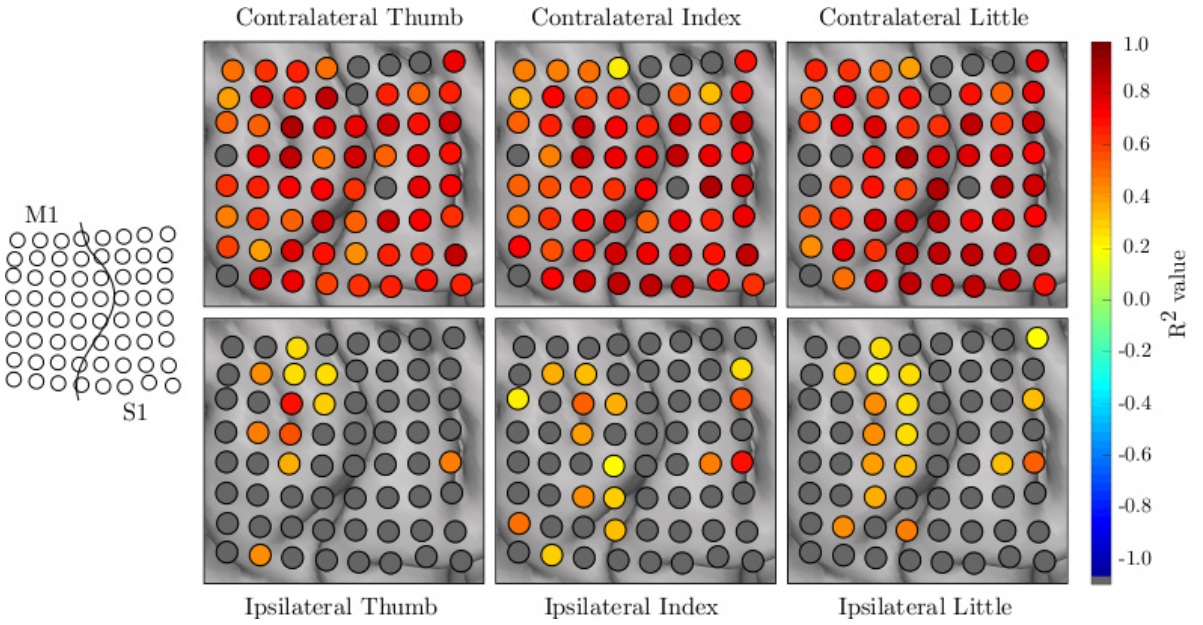

Figure 4.4: *Visualization of channel R^2 values in the HFB band for participant P2.*

In the α and β bands, there seems to be little difference between the number of channels that show significant cortical activity during ipsilateral movement with respect to contralateral movement. Especially for participants P1 and P3, the observed differences are minimal. For participant P2, no significant activity in the α and β bands is visible at

all. For participant P4, differences in the α band are slightly visible but clear differences are visible in the β band.

The most pronounced results can be found in the HFB. In this frequency band, the number of significantly channels resulting from ipsilateral movement is visibly smaller than the number of significantly activated channels during contralateral movement. Contralateral movement causes widespread cortical activity over M1 and S1 (with distinct hot-spots over S1) while ipsilateral cortical activity seems to manifest mostly over M1, a result that is consistent across participants.

4.1.3 Visualization of the Data Space

The low dimensional representations of $\mathbf{P}_{v,t,\overline{B}}$ obtained with t-SNE for participants P1 and P2 are depicted below in Figures 4.5 and 4.6. The visualizations of the other participants are included in Figures L.1 through L.2 in Appendix L.

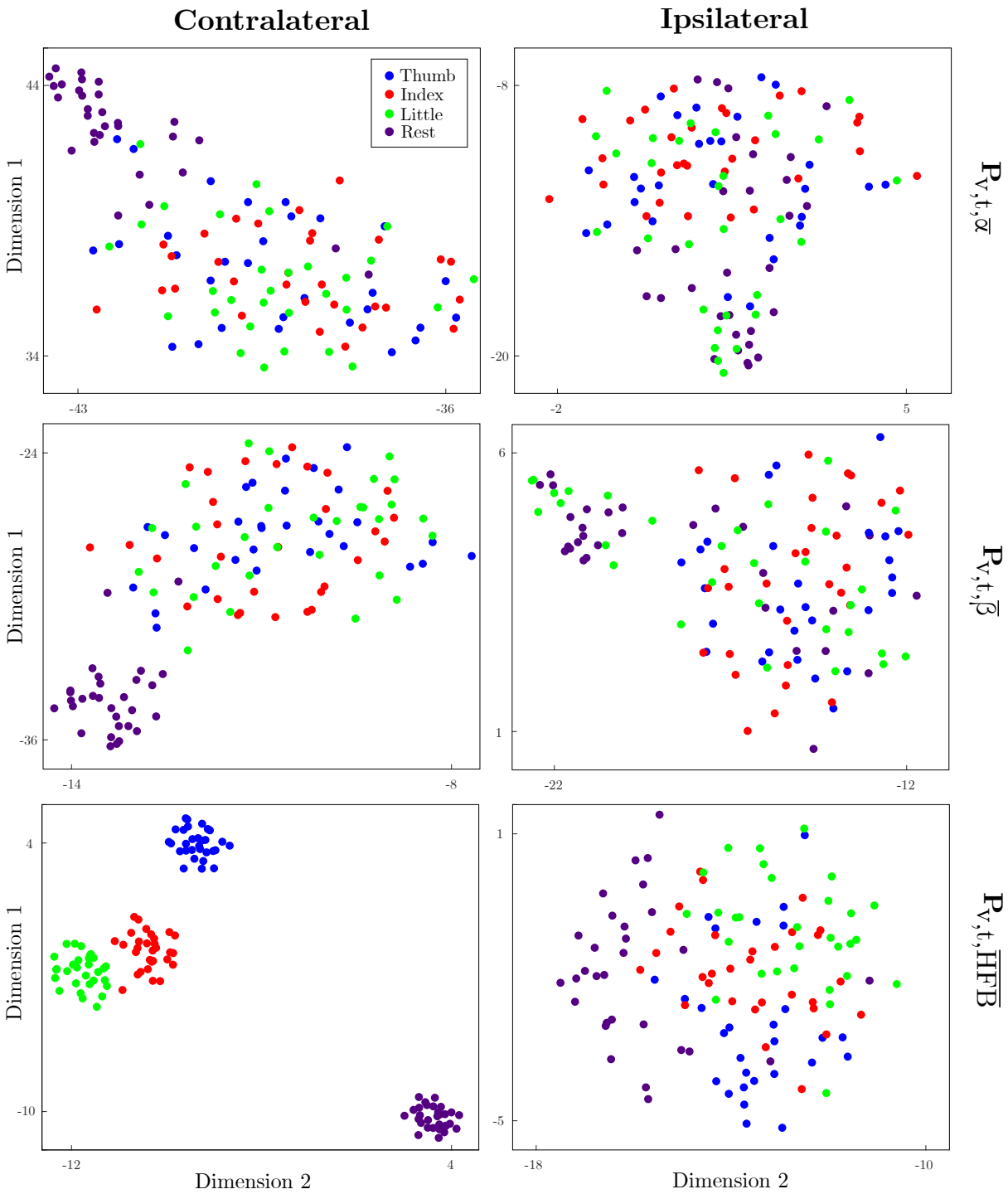

Figure 4.5: *Visualization of the low-dimensional data distribution formed by the t-SNE algorithm on the* $\mathbf{P}_{v,t,\overline{B}}$ *data for participant P1. The purple, blue, red and green dots indicate the datapoints corresponding to observations of rest, thumb movement, index finger movement and little finger movement respectively. This Figure caption holds for Figure 4.6 below.*

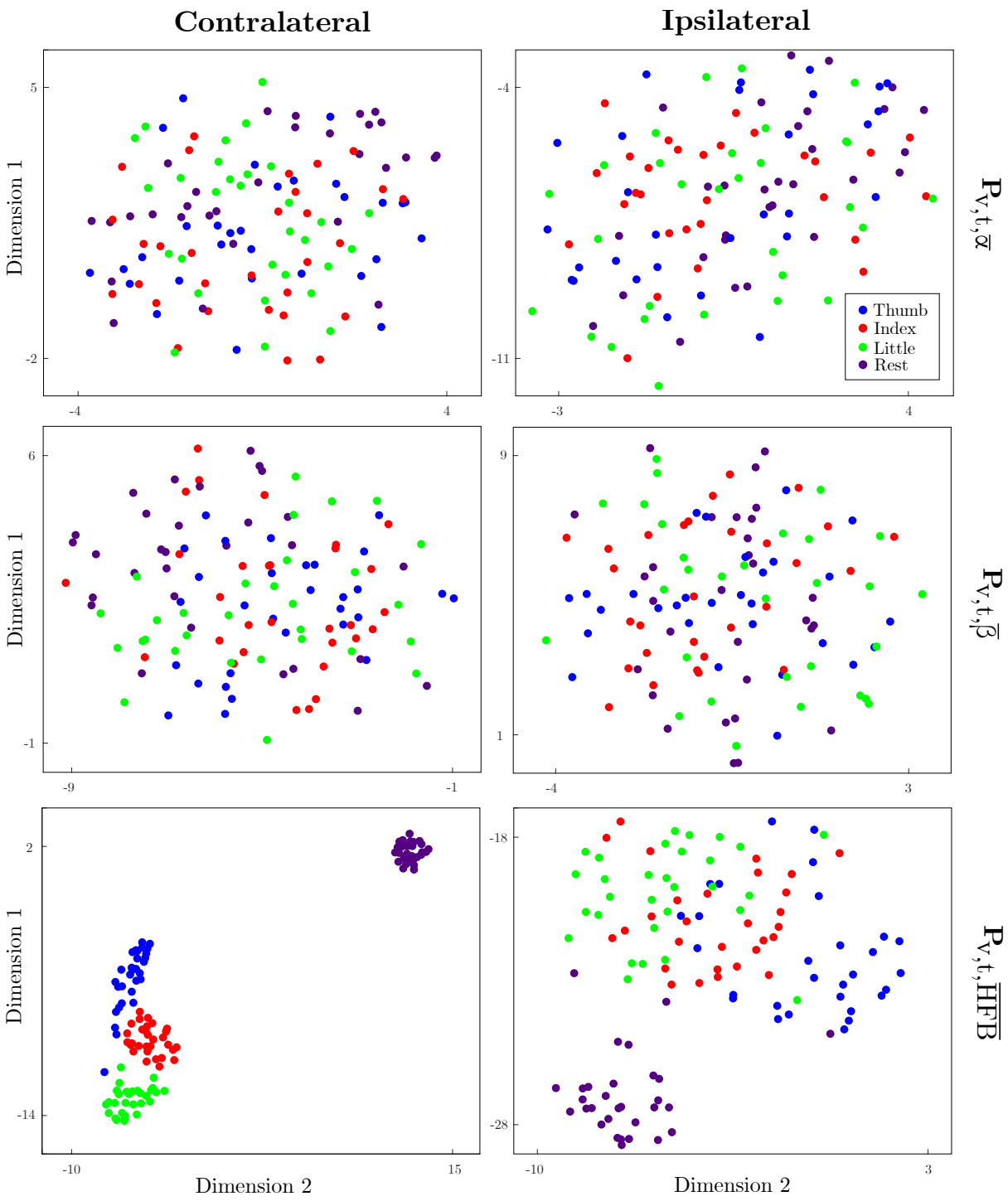

Figure 4.6: *Visualization of the low-dimensional data distribution formed by the t-SNE algorithm on the* $\mathbf{P}_{v,t,\overline{B}}$ *data for participant P2.*

The results obtained with this analysis allow to refine several early hypotheses. Firstly, from these results it appears that the α and β bands may serve as a good indicator for the differentiation of movement in general versus rest. The purple clusters, corresponding to observations of rest, are generally well separated from datapoints resembling movement of contralateral and ipsilateral fingers. The HFB might be an equally good indicator for the differentiation of movement in general versus rest, as again the purple datapoints corresponding to rest are clearly separated from the clusters of datapoints corresponding to contralateral and ipsilateral finger movements. Similarly, the HFB seems to hold the necessary information to effectively distinguish individual finger movements, as the results of the HFB show the strongest separation between clusters of datapoints corresponding to each of the individual finger movements.

These hypotheses asked for a systematic analysis of the contribution of the separate frequency bands on the classification of contralateral and ipsilateral finger movements and rest, which will be addressed in a later section.

It can additionally be observed that the separation between clusters of datapoints corresponding to observations of rest and datapoints corresponding to finger movements is generally smaller for ipsilateral fingers across all frequency bands. Secondly, the clusters of datapoints corresponding to observations of ipsilateral finger movement are generally less well separated. These insights contributed to an initial hypothesis that ipsilateral finger movements might be less well distinguished from rest and similarly less well distinguished from one another.

4.2 Experiment I: Synchronous Classification

4.2.1 Baseline Classification

The results of the performed hyper-parameter optimization prior to classification on the baseline feature vector are depicted in Tables 4.1 through 4.3.

	`Gamma`		`Delta`		Accuracy [%]		
Participant	Default	Optimized	Default	Optimized	Default	Optimized	Δ
P1	1	0.983	0	0.007	73.08	73.56	**+0.48**
P2	1	0.997	0	0.293	81.73	82.69	**+0.96**
P3	1	0.845	0	0.409	71.35	75.73	**+4.38**
P4	1	0.816	0	0.409	68.58	70.68	**+2.10**

Table 4.1: *Settings and results of the hyper-parameter optimization process for the LDA classifier on the baseline feature vector. The default value and optimized value for each hyper-parameter is listed. Along with these values, the obtained accuracies with the default values and the optimized values are listed. The gained accuracy in percent after hyper-parameter optimization is listed in the column Δ. This Table caption holds for Tables 4.2 through 4.6 which show the results of the hyper-parameter optimization processes for the other classifiers.*

	`BoxConstraint`		`KernelScale`		Accuracy [%]		
Participant	Default	Optimized	Default	Optimized	Default	Optimized	Δ
P1	1	37.24	1	0.001	72.60	78.85	**+6.25**
P2	1	186.85	1	15.42	70.19	71.29	**+1.10**
P3	1	120.90	1	38.12	72.33	75.09	**+2.67**
P4	1	46.66	1	4.00	67.02	70.16	**+3.14**

Table 4.2: *Settings and results of the hyper-parameter optimization process for the SVM classifier.*

	`NLearn`		`MinLeafSize`		Accuracy [%]		
Participant	Default	Optimized	Default	Optimized	Default	Optimized	Δ
P1	100	499	1	23	48.07	51.44	**+3.37**
P2	100	322	1	10	44.71	47.11	**+2.40**
P3	100	500	1	3	47.09	49.51	**+2.42**
P4	100	241	1	1	47.64	48.69	**+1.05**

Table 4.3: *Settings and results of the hyper-parameter optimization process for the RF classifier.*

Besides the expected increase in accuracy of several percent, no substantial increases in performances were attained which indicates that the default hyper-parameter values formed a valid initialization. Therefore, the default hyper-parameter values, identical across participants, were selected to favor comparability between participants.

The confusion matrices of the best performing classifier (LDA) are listed in Figure 4.7. The confusion matrices of the other classifiers are listed in Figures M.1 through M.3 in Appendix M.

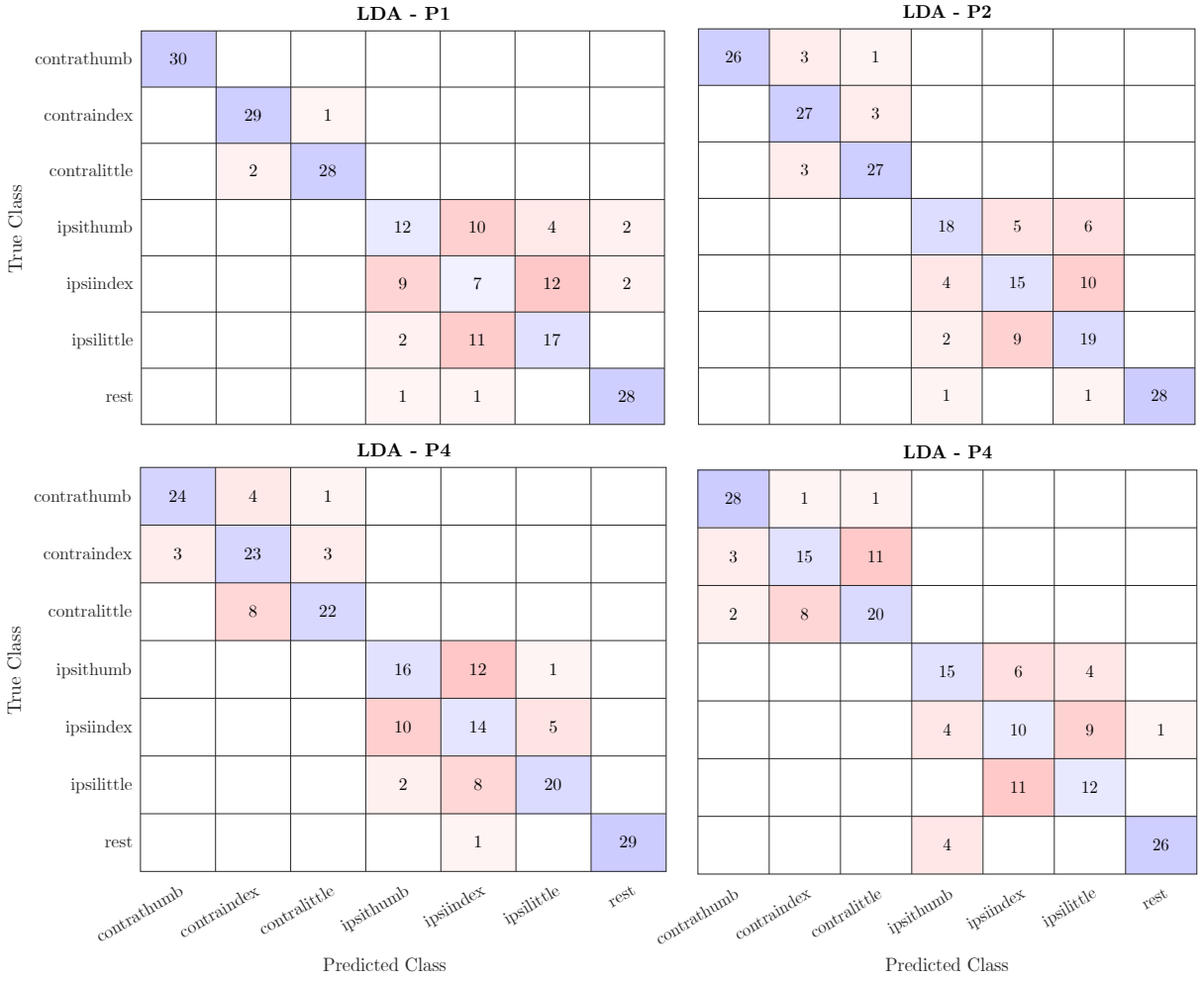

Figure 4.7: *Confusion matrices for the classification on the baseline feature vector with the LDA classifier for each participant individually.*

From these confusion matrices, it can be inferred that contralateral and ipsilateral fingers are never confused with each other. Moreover, contralateral fingers are less often confused with fingers from the same hand than ipsilateral fingers. Lastly, only ipsilateral fingers are confused with rest. These results are consistent across all participants.

4.2.2 Individual Frequency Band Classification

The results of the hyper-parameter optimization on the $[\alpha, \beta, \mathrm{HBF}]_{\overline{B}}$ feature vector prior to the classification on the individual frequency bands are depicted in Tables 4.4 through 4.6 below:

	`Gamma`		`Delta`		Accuracy [%]		
Participant	Default	Optimized	Default	Optimized	Default	Optimized	Δ
P1	1	0.433	0	0.003	81.73	82.69	**+0.96**
P2	1	0.329	0	0.000	86.06	87.02	**+0.96**
P3	1	0.693	0	0.000	81.55	87.02	**+5.47**
P4	1	0.000	0	0.000	72.25	76.44	**+4.19**

Table 4.4: *Settings and results of the hyper-parameter optimization process for the LDA classifier on the $[\alpha, \beta, HBF]_{\overline{B}}$ feature vector. The default value and optimized value for each hyper-parameter is listed. Along with these values, the obtained accuracies with the default values and the optimized values are listed. The gained accuracy in percent after hyper-parameter optimization is listed in the column Δ. This Table caption holds for Tables 4.5 through 4.6 below, which show the results of the hyper-parameter optimization processes for the other classifiers.*

	`BoxConstraint`		`KernelScale`		Accuracy [%]		
Participant	Default	Optimized	Default	Optimized	Default	Optimized	Δ
P1	1	0.00	1	0.25	79.33	83.65	**+4.32**
P2	1	0.00	1	0.31	86.54	88.46	**+1.92**
P3	1	986	1	113.88	84.46	85.44	**+0.98**
P4	1	0.00	1	0.15	74.87	78.01	**+3.14**

Table 4.5: *Settings and results of the hyper-parameter optimization process for the SVM classifier on the $[\alpha, \beta, HBF]_{\overline{B}}$ feature vector.*

	`NLearn`		`MinLeafSize`		Accuracy [%]		
Participant	Default	Optimized	Default	Optimized	Default	Optimized	Δ
P1	100	106	1	10	69.23	70.67	**+1.44**
P2	100	499	1	14	73.59	78.66	**+5.07**
P3	100	496	1	15	69.36	75.39	**+6.03**
P4	100	500	1	1	68.06	69.11	**+1.05**

Table 4.6: *Settings and results of the hyper-parameter optimization process for the RF classifier on the $[\alpha, \beta, HBF]_{\overline{B}}$ feature vector.*

Again, the hyper-parameter optimization procedures produced the expected increase in accuracy of several percent. No substantial increases in performances were attained. The default hyper-parameter values, identical across participants, were again selected for the classifiers.

Figure 4.8 shows the classification accuracies across participants on all the separate feature vectors, for each classifier separately.

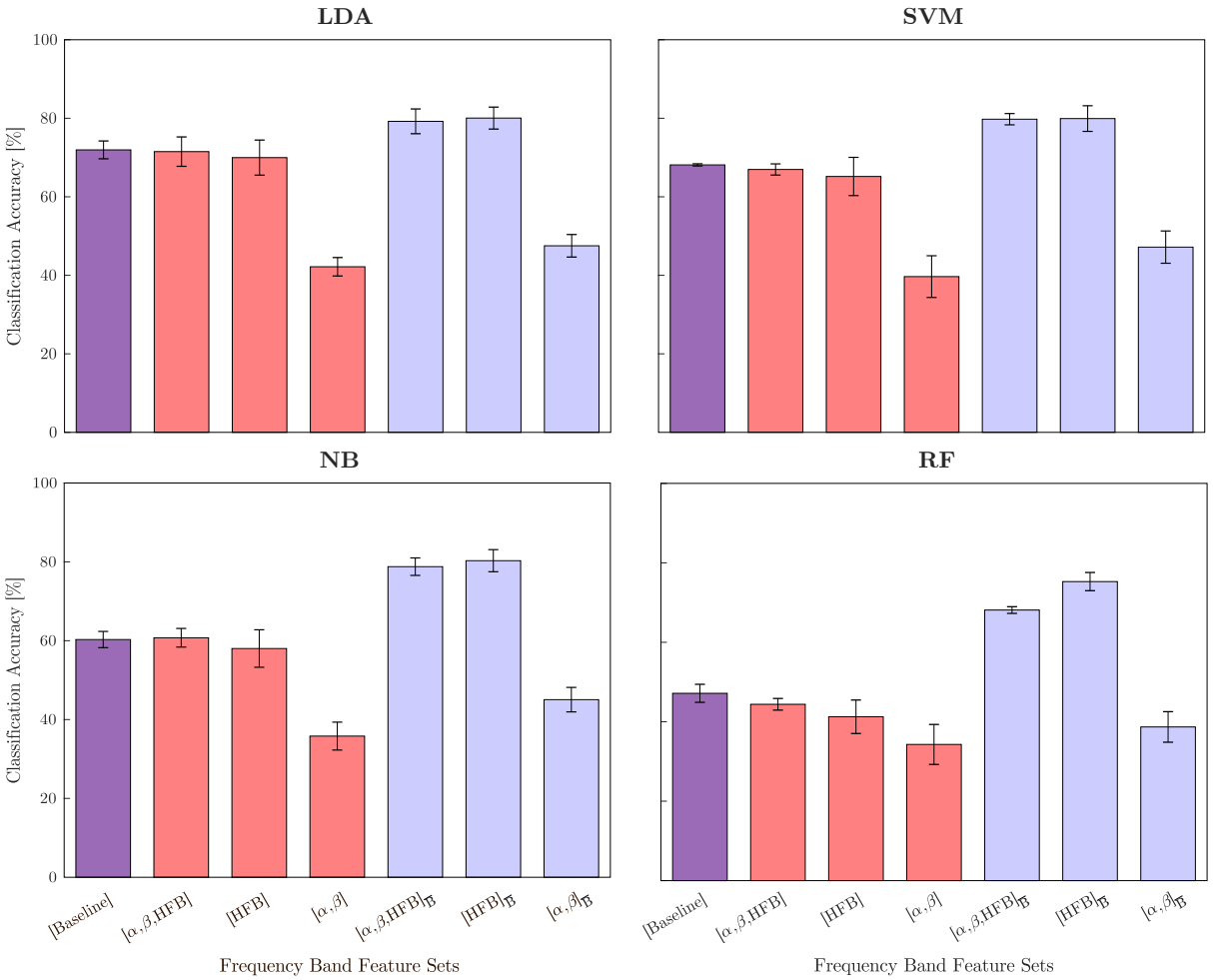

Figure 4.8: *Classification accuracies of the different classifiers on all available feature vectors, calculated across participants. The purple bar indicates the average accuracy obtained on the baseline feature vector. The red bars denote the average accuracies on the feature vectors with the various frequency bands, denoted by* $[\cdot]$*. The blue bars denote the average accuracy on the feature vectors containing the average values over the various frequency bands, denoted by* $[\cdot]_{\overline{B}}$*.*

These results show that the various finger movements can be as accurately classified from only the HFB as from the α, β and HFB frequency bands combined. Additionally, these results show that averaging over frequency bands increases performance, regardless of which (combinations of) frequency bands are used for classification. Both these results are consistent across participants and classifiers.

Figure 4.9 shows the attained averaged accuracies across participants on the baseline, $[\alpha, \beta, \text{HFB}]_{\overline{B}}$ and $[\text{HFB}]_{\overline{B}}$ feature vectors separately per classifier.

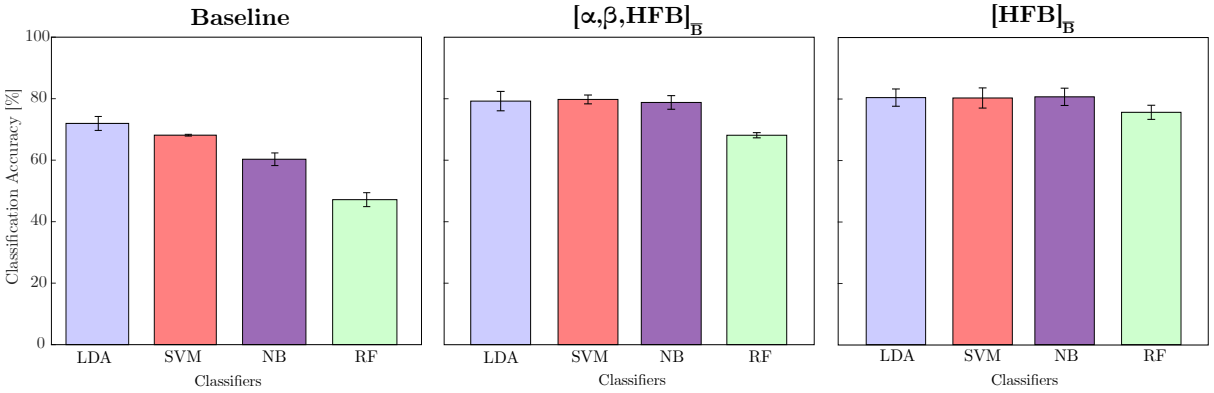

Figure 4.9: *The attained average accuracies across participants on the baseline feature vector as well as the attained average accuracies across participants on the* $[\alpha, \beta, HFB]_{\overline{B}}$ *and* $[HFB]_{\overline{B}}$ *feature vectors are depicted for each classifier separately.*

From these results it can be seen that the performances of the various classifiers on the classification of the $[\alpha, \beta, \text{HFB}]_{\overline{B}}$ and $[\text{HFB}]_{\overline{B}}$ feature vectors are on par, in contrast with the performance of the classifiers on the classification of the baseline feature vector, for which clear differences can be seen. The only exception to this statement has to be made for the RF classifier, which consistently performed less well than the other classifiers.

Figure 4.10 shows the highest obtained classification accuracies with the LDA classifier on the $[\alpha, \beta, \text{HFB}]_{\overline{B}}$ and $[\text{HFB}]_{\overline{B}}$ feature vectors separately per participant. The accuracies are compared to the empirical chance levels of classification at $p<0.05$, which were found to be 18.33 ($\pm$ 0.33) and 19.07 ($\pm$ 0.31) (Mean $\pm$ SD) for classification on the $[\alpha, \beta, \text{HFB}]_{\overline{B}}$ and $[\text{HFB}]_{\overline{B}}$ feature vector respectively.

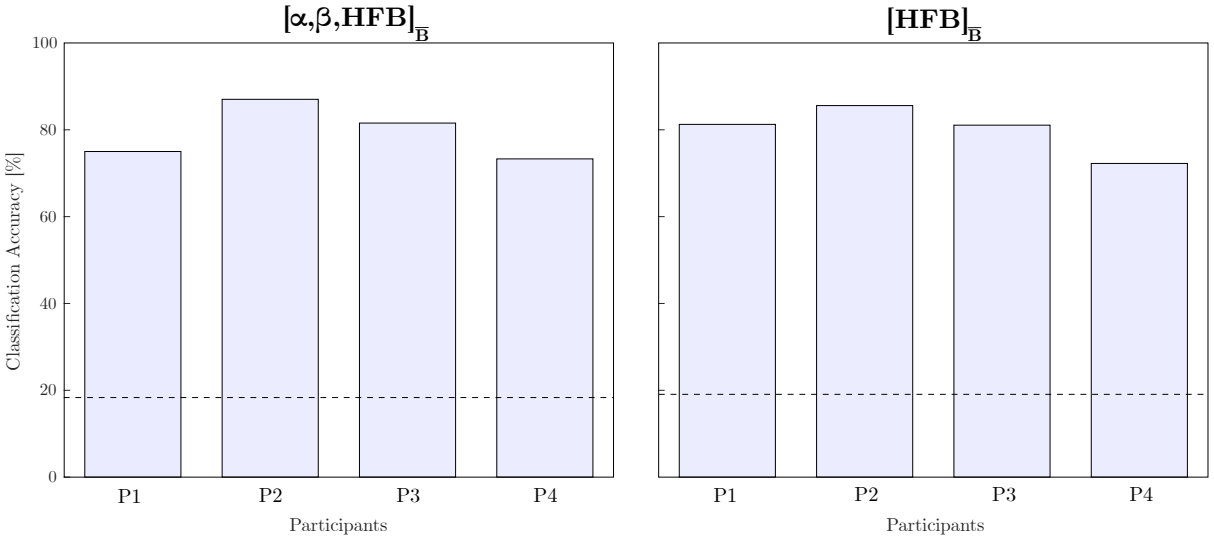

Figure 4.10: *Classification accuracies obtained per participant on the* $[\alpha, \beta, HFB]_{\overline{B}}$ *and* $[HFB]_{\overline{B}}$ *feature vectors respectively with the LDA classifier. The empirical chance level (*$p<0.05$*) is depicted by the horizontal black dotted line.*

This figure shows that the classification results attained by the LDA classifier on the $[\alpha, \beta, \text{HFB}]_{\overline{B}}$ and $[\text{HFB}]_{\overline{B}}$ feature vectors were significantly above chance level ($p<0.05$) for all participants. The confusion matrices of the LDA classifier on the $[\alpha, \beta, \text{HFB}]_{\overline{B}}$ and $[\text{HFB}]_{\overline{B}}$ feature vectors are depicted in Figures 4.11 and 4.12 respectively. The confusion matrices of the other classifiers on these feature vectors are listed in Figures O.1 through P.3 in Appendices O and P.

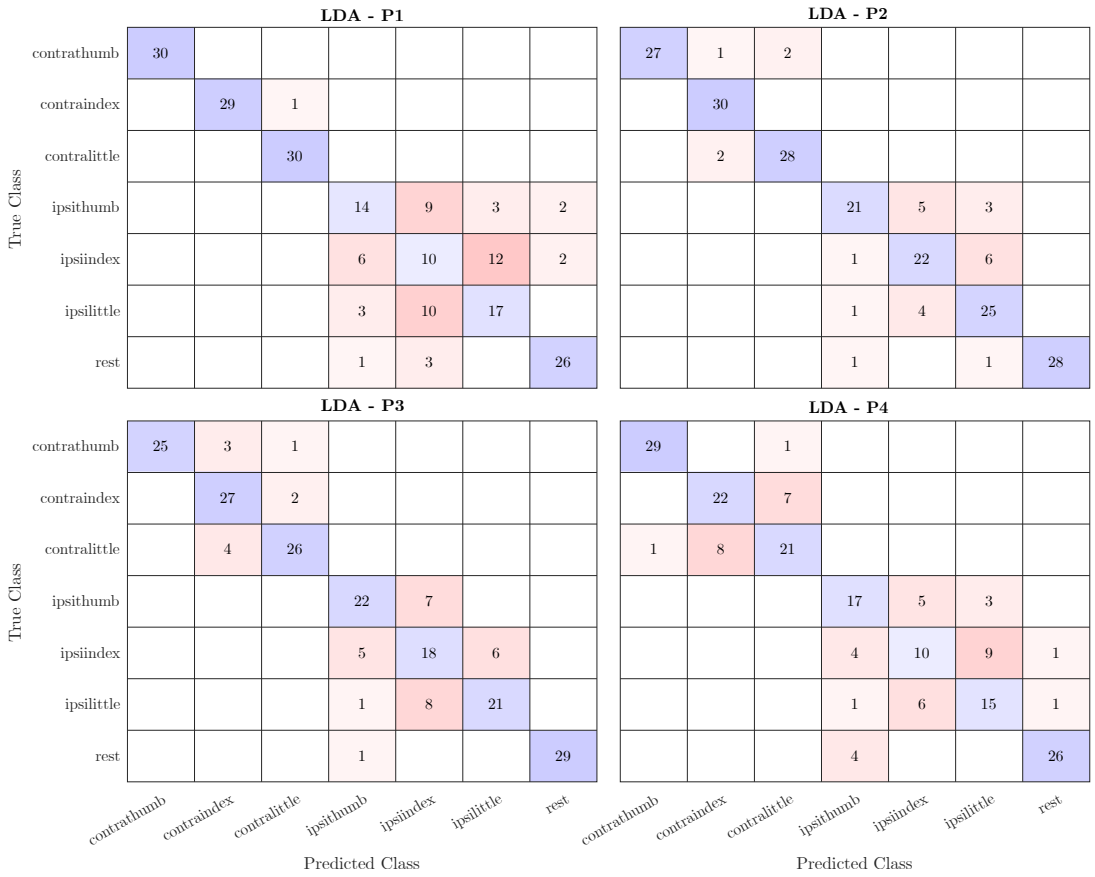

Figure 4.11: *Confusion matrices for the classification on the* $[\alpha, \beta, HFB]_{\overline{B}}$ *feature vector with the LDA classifier for each participant individually.*

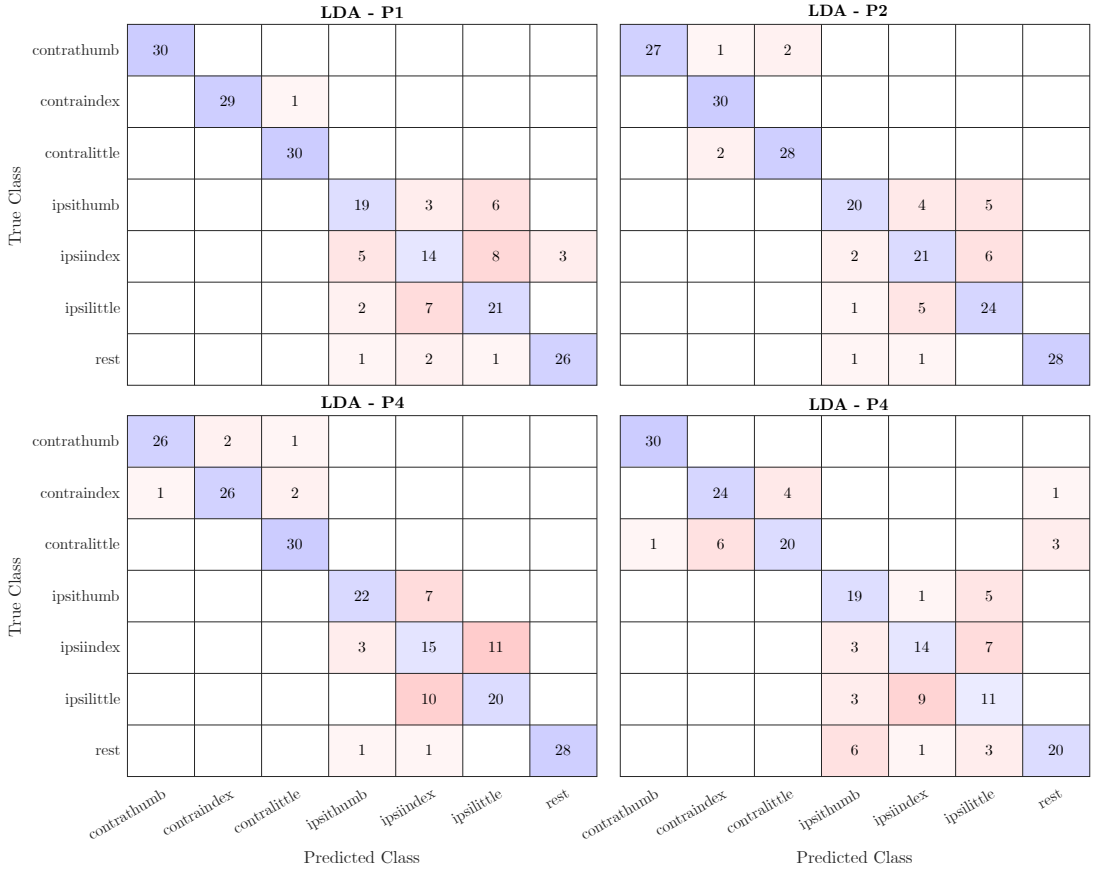

Figure 4.12: *Confusion matrices for the classification on the* $[HFB]_{\overline{B}}$ *feature vector with the LDA classifier for each participant individually.*

Similar to the results in Figure 4.7, it can be inferred from these confusion matrices that

contralateral and ipsilateral fingers are never confused with each other. Contralateral finger movements are again less often confused with fingers from the same hand than ipsilateral finger movements and only ipsilateral finger movements are confused with rest. These results are once more consistent across all participants.

There are minute differences in the confusions made between individual contralateral and ipsilateral finger movements between Figure 4.11 and Figure 4.12, but the overall classification accuracies are highly similar. Most importantly, the results from the classification on the $[\alpha, \beta, \text{HFB}]_{\overline{B}}$ feature vector show somewhat less confusion between ipsilateral finger movements and rest when compared to the results from the classification on the $[\text{HFB}]_{\overline{B}}$ feature vector. Additionally, for participant P4, the rest class is no longer confused with ipsilateral fingers as was the case with the classification on the $[\alpha, \beta, \text{HFB}]_{\overline{B}}$ feature vector. However, the rest class is confused with movement of some contralateral fingers during the classification on the $[\text{HFB}]_{\overline{B}}$ feature vector.

4.2.3 Required Training Data

The evolution of classification performances over the incremental reduction of the number of training observations in the baseline, $[\alpha, \beta, \text{HFB}]_{\overline{B}}$ and the $[\text{HFB}]_{\overline{B}}$ feature vectors are depicted below in Figures 4.13 through 4.15 for the LDA classifier. The results of the other classifiers on the various feature vectors are displayed in Figures Q.1 through S.3 in Appendices Q through S.

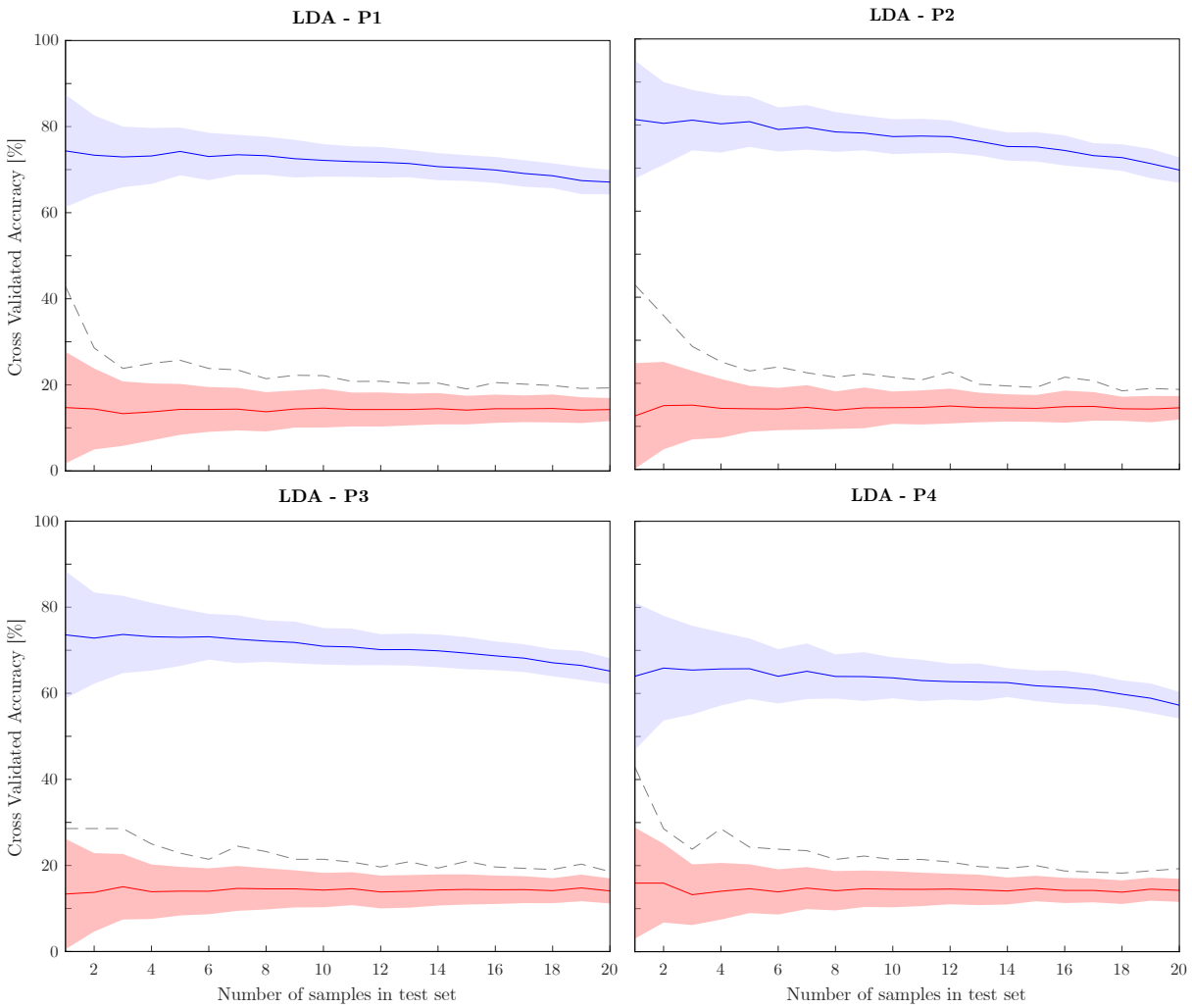

Figure 4.13: *The evolution of the classification performance with the incremental inclusion of trials of finger movement in the test set of the baseline feature vector. This figure shows the results obtained by the LDA classifier for every participant separately. The blue solid line and the blue shaded region respectively denote the classification accuracy on the baseline feature vector and standard deviation thereof. The red solid line and the red shaded region respectively denote the classification accuracy on random data and the standard deviation thereof. The gray dashed line shows the 95th percentile of the empirical chance level of classification at* $p < 0.05$. *This Figure caption holds for Figures 4.14 through 4.15, which show the results of the LDA classifier on the other feature vectors.*

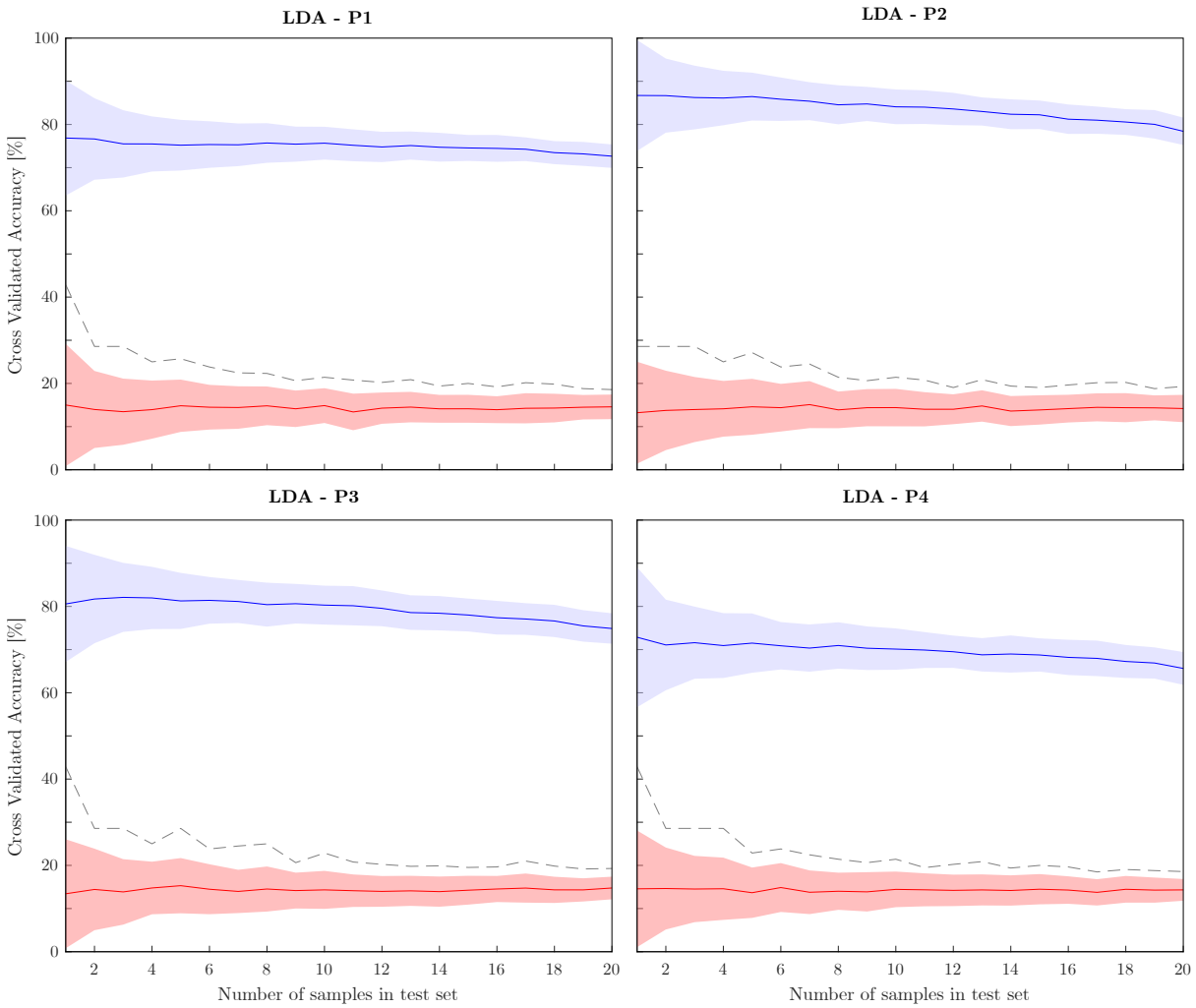

Figure 4.14: *The evolution of the classification performance with the incremental inclusion of trials of finger movement in the test set of the* $[\alpha, \beta, HFB]_{\overline{B}}$ *feature vector. This figure shows the results obtained by the LDA classifier for every participant separately.*

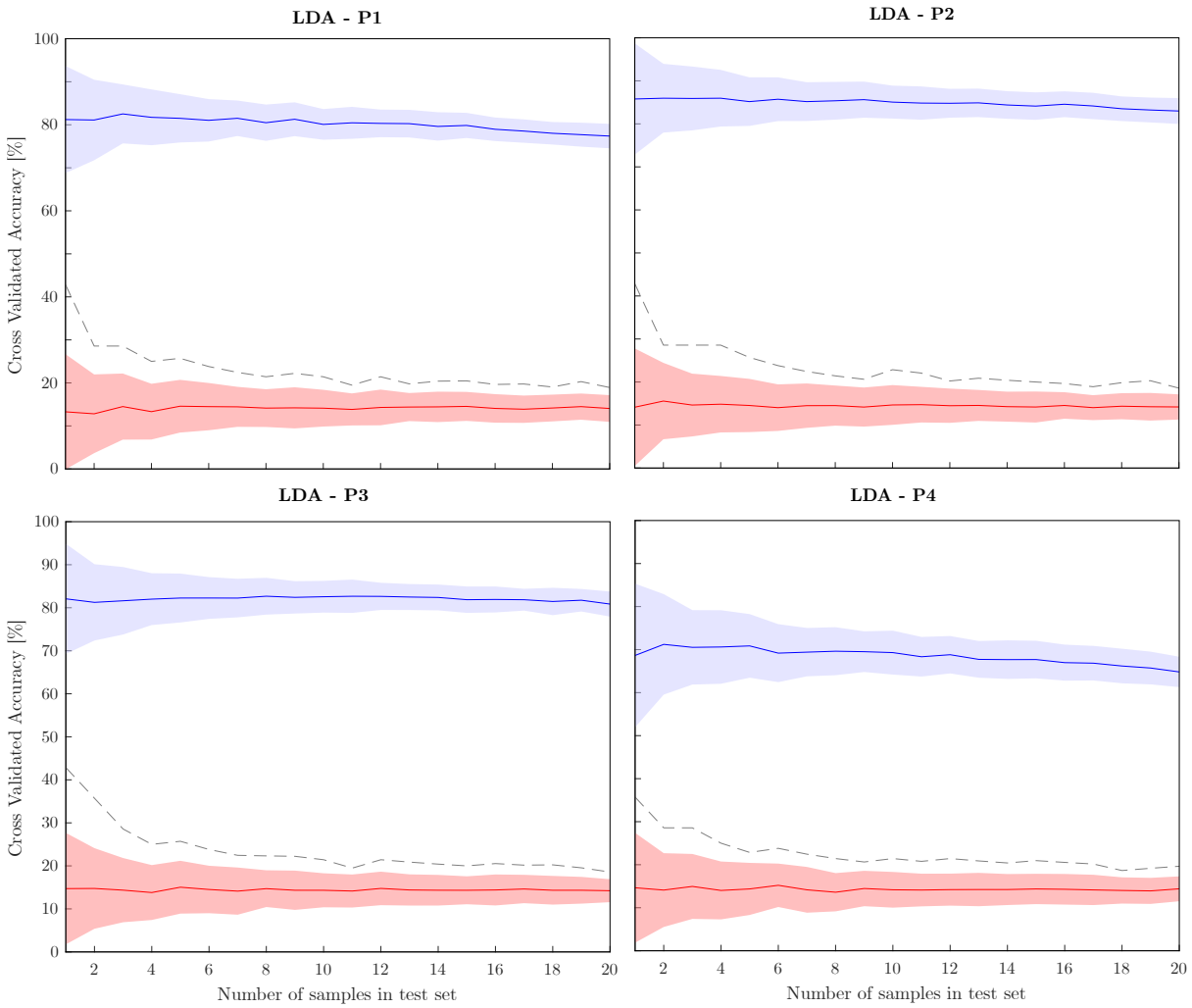

Figure 4.15: *The evolution of the classification performance with the incremental inclusion of trials of finger movement in the test set of the* $[HFB]_{\overline{B}}$ *feature vector. This figure shows the results obtained by the LDA classifier for every participant separately.*

Expectantly, the decrease in performance as an evolution of the number of used training samples is the most gradual for the feature vectors with the smaller numbers of features; especially the $[\text{HFB}]_{\overline{B}}$ features appear to be highly robust. This result is consistent across classifiers. Especially the LDA classifier demonstrates a relatively gradual decrease in performance across all feature vectors in comparison with the other classifiers, a result that is consistent across all feature vectors.

4.2.4 Time Lag Classification

The results of the time lag classification of contralateral finger movements with rest, ipsilateral finger movements with rest and the full classification with both contralateral and ipsilateral finger movements including rest are depicted below in Figure 4.16.

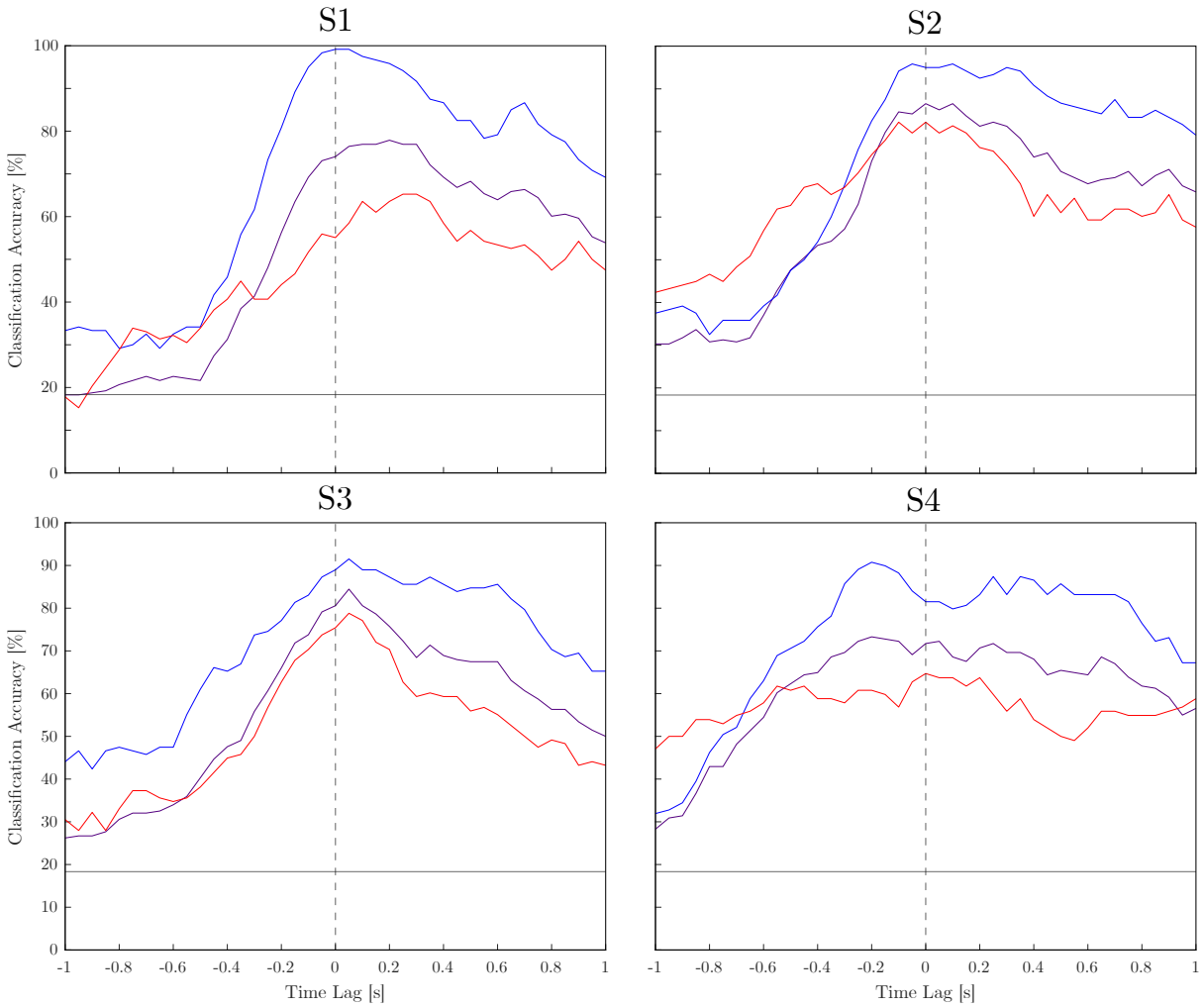

Figure 4.16: *The evolution of the classification performance over different time lags relative to the movement marker using the LDA classifier on the* $[\alpha, \beta, HFB]_{\overline{B}}$ *feature vector. The blue line denotes the classification performance on contralateral finger movements with rest. The red line denotes the classification performance on ipsilateral finger movements with rest. The purple line denotes the classification performance on both contralateral finger movements, ipsilateral finger movements and rest together. The gray dashed vertical line at t=0 seconds denotes the movement marker position and the gray horizontal line denotes the empirical chance level (*$p < 0.05$*) of classification.*

Based on these results, no clear statement on the influence of the reported earlier occurrence of cortical activity resulting from ipsilateral movements can be formulated; no clear peak in the classification performance of ipsilateral finger movements (purple line in Figure 4.16) could be observed prior to the movement marker. All classification accuracies are close to chance level prior to movement and peak close to the movement marker, after which a gradual decrease in classification performance can be observed. The results of participant P4 show a sustained performance long after movement onset but it is to be noted that this participant performed multiple finger movements in each trial.

4.2.5 Spatial Analysis: Relative Channel Importance

Before presenting the results of this spatial analysis, it must be mentioned that the channel weights presented in all subplots have been obtained from different classifier training schemes as described in Section 3.4.6. This means that the classifier weights were normalized with a different range during each training scheme. Therefore, the actual numerical values of the channel weights can not be compared between participants or different fingers of one participant. Only the spatial distribution of the most informative channels can be compared across participants and fingers.

4.2.5.1 Informative Areas for Distinguishing between Finger Movement and Rest

The spatial distributions of important channels for distinguishing between individual finger movements and rest are plotted on the cortical surfaces of participants P1 and P2 in Figures 4.17 through 4.18 below. The visualizations of the other participants are included in Figures T.1 through T.2 in Appendix T.

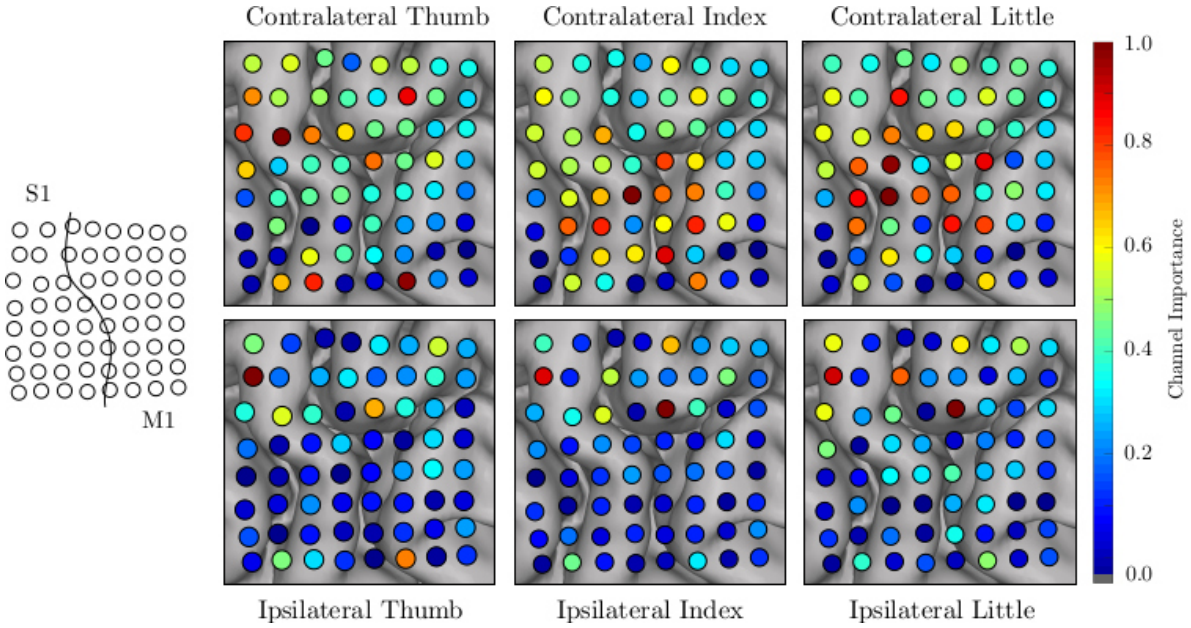

Figure 4.17: *The relative importance of channels in distinguishing between finger movement and rest for participant P1. Faulty channels are denoted in gray. Channels in red denote a relatively high channel importance and channels in blue denote a relatively low channel importance as indicated by the color bar. The inlay image at the far left depicts a schematic representation of the electrode grid placement with respect to S1 and M1, separated by a solid line representing the CS. This inlay serves as a reference for the exact electrode locations on the cortical surface. This caption holds for all figures in the upcoming spatial analyses.*

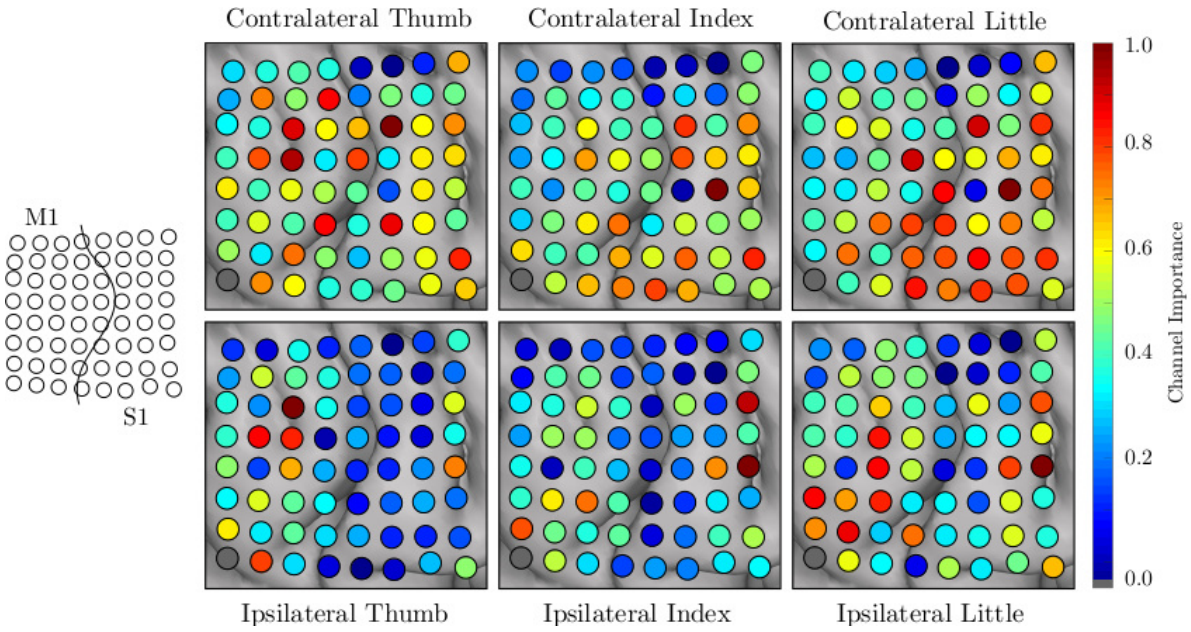

Figure 4.18: *The relative importance of channels in distinguishing between finger movement and rest for participant P2.*

When comparing these results with the results obtained in the analysis of channel R^2 values (Section 3.3.2), it can be seen that many of the channels that showed significant cortical activity during ipsilateral finger movement are indeed important for distinguishing between movements of those respective ipsilateral fingers and rest. Most of the channels that were important for distinguishing between movement of ipsilateral fingers and rest are clustered on M1 with several individual important channels located on S1. These results are consistent across participants.

When comparing the results corresponding to the distinction between contralateral finger movements and rest with the results obtained in the analysis of channel R^2 values (Section 3.3.2), several differences can be observed. While movement of contralateral fingers resulted in a widespread distribution of significantly activated channels across the SMC, the distribution of channels that are important for distinguishing contralateral finger movement from rest seem to be clustered mostly around the CS and S1. This result is consistent across all participants.

4.2.5.2 Informative Areas for Distinguishing between Individual Finger Movement of the Same Laterality

The spatial distributions of important channels for distinguishing between movement of a specific finger against movement of the other fingers of the same laterality are plotted on the cortical surfaces of participants P1 and P2 in Figures 4.19 through 4.20 below. The visualizations of the other participants are included in Figures U.1 through U.2 in Appendix U.

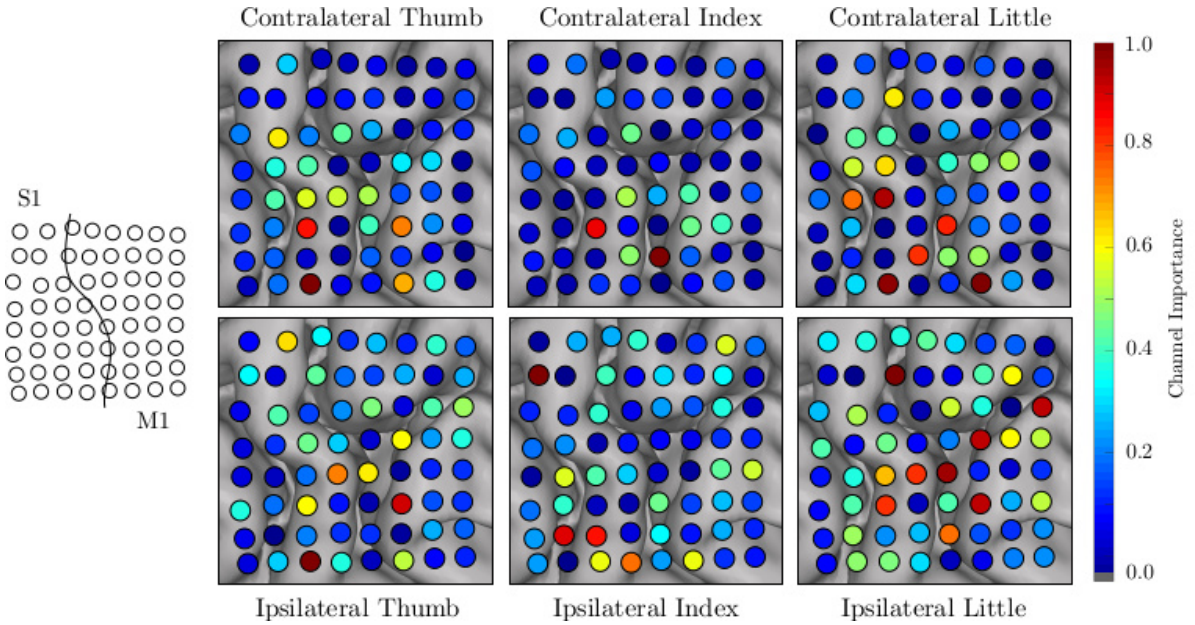

Figure 4.19: *The relative importance of channels in distinguishing between movement of a specific finger against movement of fingers of the same laterality for participant P1.*

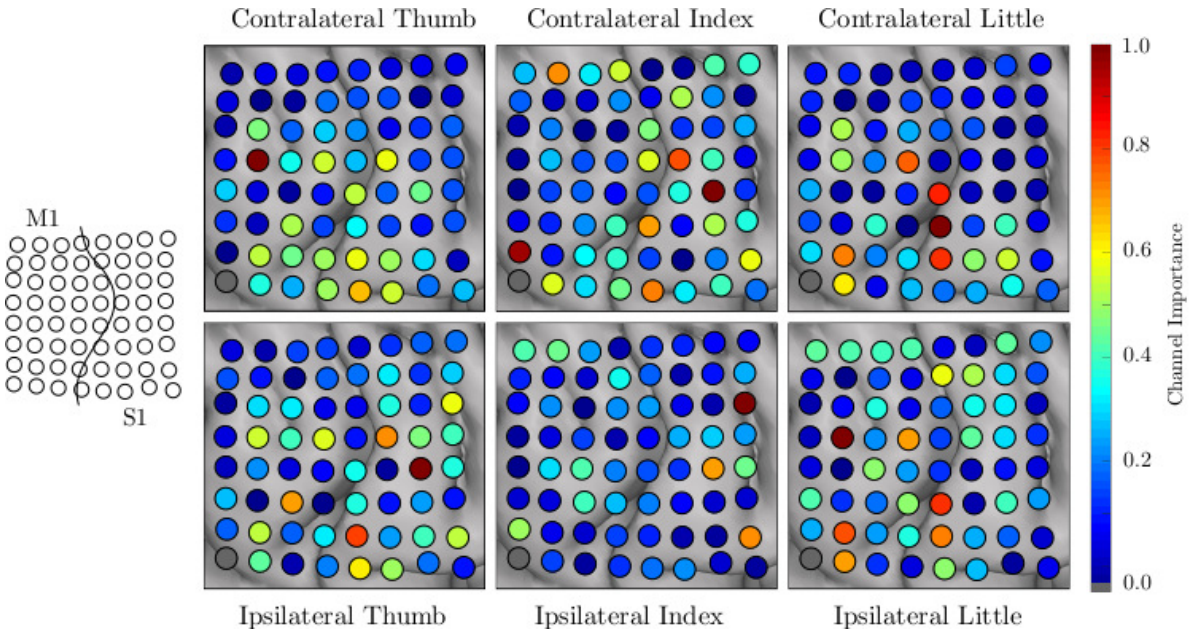

Figure 4.20: *The relative importance of channels in distinguishing between movement of a specific finger against movement of fingers of the same laterality for participant P2.*

Based on these results, it can be stated that mainly channels located over S1 and the CS are important for distinguishing between individual movements of contralateral fingers. Regarding the ability to distinguish between individual movements of ipsilateral fingers, several channels surrounding the CS and S1 seem to hold important information about finger specificity while these channels were not the channels which showed the most pronounced activation in Section 3.3.2 or which otherwise showed to be informative for distinguishing between movements of that certain finger and rest in in Section 3.4.6.2. These results were consistent across participants.

4.2.5.3 Informative Areas for Distinguishing between Contralateral and Ipsilateral Finger Movement

The spatial distributions of important channels for distinguishing between movement of pairs of contralateral and ipsilateral fingers are plotted on the cortical surfaces of partic-

ipants P1 and P2 in Figures 4.21 and 4.22 below. The results of the other participants are included in Figures V.1 through V.2 in Appendix V.

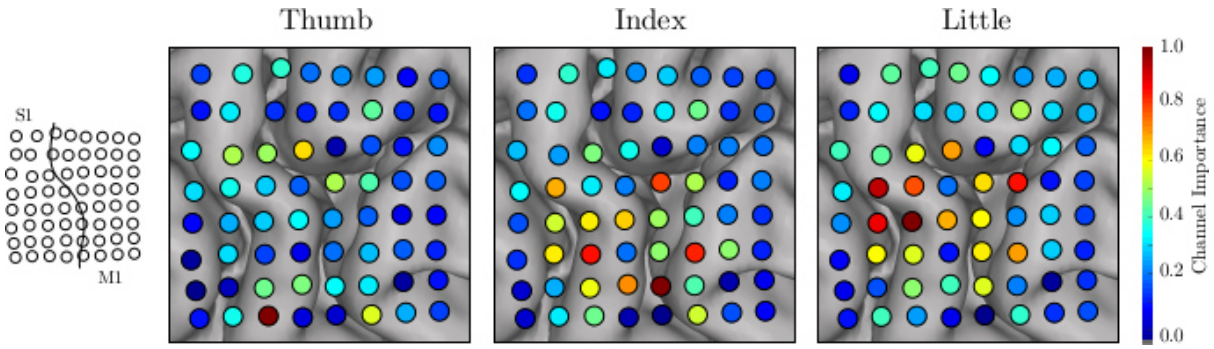

Figure 4.21: *The relative importance of channels in distinguishing between movements of contralateral and ipsilateral fingerpairs separately for participant P1.*

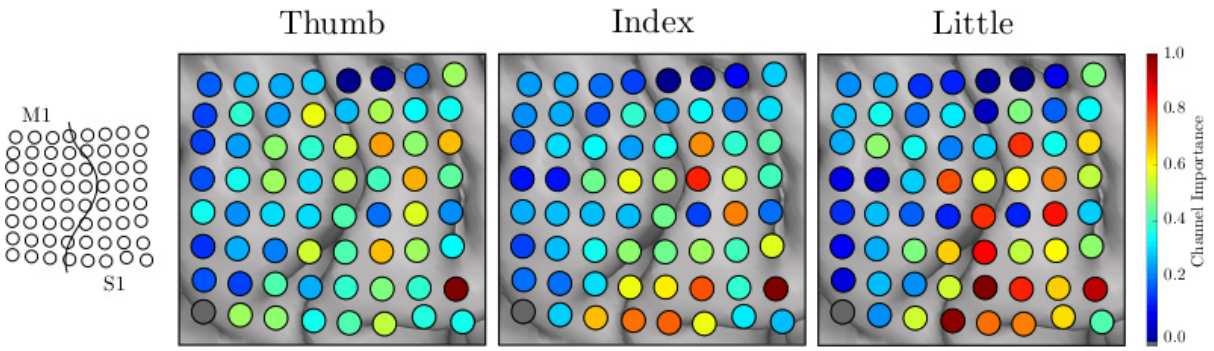

Figure 4.22: *The relative importance of channels in distinguishing between movements of contralateral and ipsilateral fingerpairs separately for participant P2.*

The spatial distributions of important channels for distinguishing between movement of all contralateral fingers versus movement of all ipsilateral fingers are plotted on the cortical surfaces of participants P1 and P2 in Figures 4.23 below. The results of the other participants are included in Figures W.1 through W.2 in Appendix W.

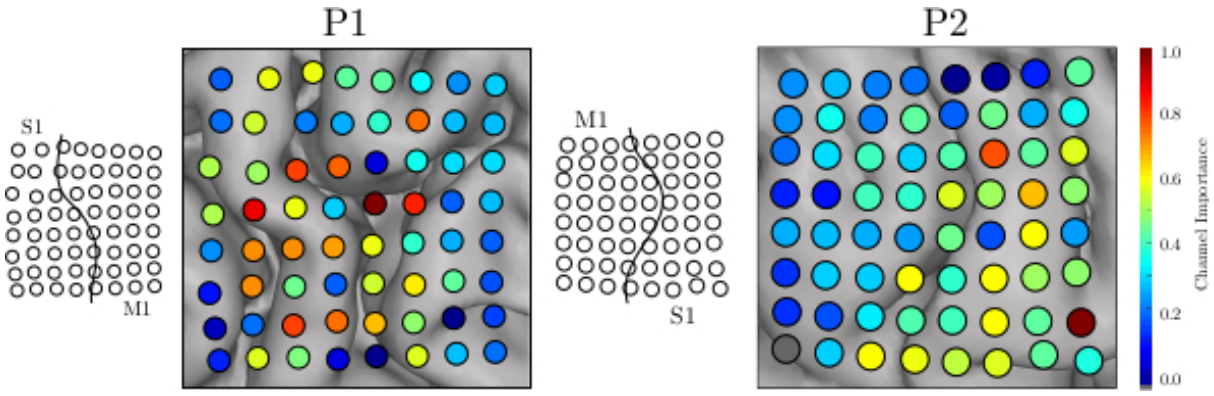

Figure 4.23: *The relative importance of channels in distinguishing between movement of all contralateral fingers versus movement of all ipsilateral fingers for participant P1 and P2.*

Based on the results obtained in this section, it can be stated that mainly channels located over S1 and the CS are important for distinguishing between movements of pairs of contralateral and ipsilateral fingers and for distinguishing between movements of contralateral and ipsilateral fingers in general.

4.3 Experiment II: Asynchronous Classification

4.3.1 Feature Extraction and Preliminary Classification

The result of the preliminary classification performed to investigate the influence of the alternative power extraction method and the inclusion of all available rest trials is depicted in Figure 4.24 below.

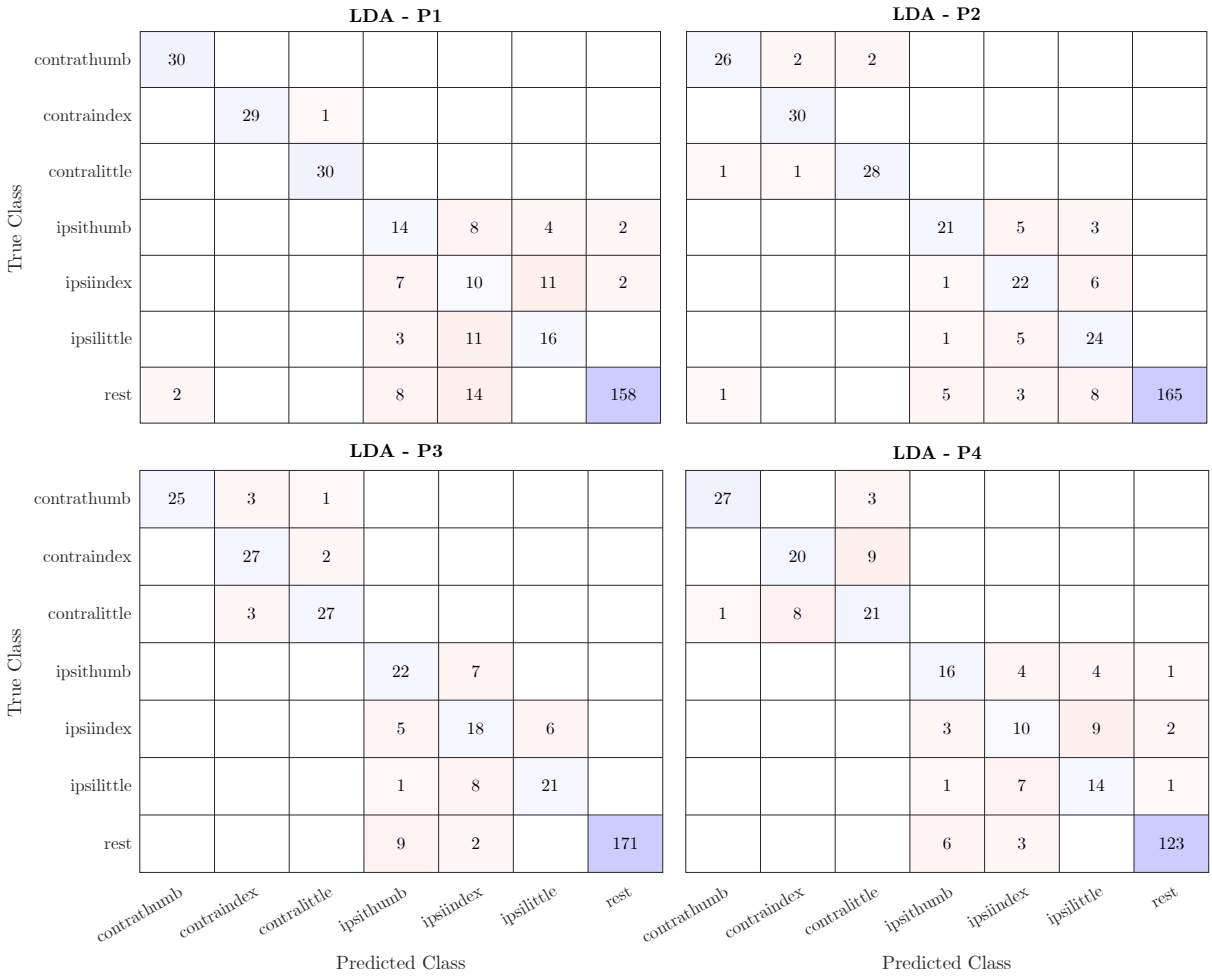

Figure 4.24: *Confusion matrices for the classification performed with the LDA classifier on the* $[\alpha, \beta, HFB]_{\overline{B}}$ *feature vector which was created using a different power extraction method and which additionally included all available rest trials. The results for each participant are depicted separately.*

When comparing these results with the results obtained during the synchronous classification (Section 3.4.3), little differences in the classification of contralateral finger movements can be observed. Only several trials of contralateral finger movement were confused differently for participants P2 through P4. For participants P1 and P2, several false positive detections of contralateral thumb movement can be noted. These confusions of contralateral finger movement with rest had not occurred in the results of Section 3.4.3. For the classification of ipsilateral finger movement, a slight and expected increase in the number of confusions between ipsilateral finger movements and trials of rest are notable. Based on these results, there is no indication that the imbalanced training data resulting from the inclusion of all available trials of rest negatively impacts classification performance. Similarly, there seems to be no negative influence of the reduced time resolution with which the DFT was performed.

4.3.2 Determination of Dwell Times

The results of the comparison between the baseline dwell time of 0.01 seconds and the optimal dwell times are depicted in Tables 4.7 through 4.10.

Finger	**Baseline Dwell Time**				**Optimized Dwell**				
	TP	$FP_{rest_{contra}}$	$FP_{rest_{ipsi}}$	FP_{Total}	Dwell Time	TP	$FP_{rest_{contra}}$	$FP_{rest_{ipsi}}$	FP_{Total}
Contra Thumb	30	1	2	3	0.30	30	0	1	1
Contra Index	30	2	1	3	0.29	30	0	0	0
Contra Little	30	6	2	8	0.28	30	3	2	5
Ipsi Thumb	29	137	72	209	0.07	29	104	55	159
Ipsi Index	29	198	78	276	0.22	29	106	38	144
Ipsi Little	25	52	9	61	0.03	25	47	8	55

Table 4.7: *The number of true positive detections and false positive detection per finger separately, listed for both the baseline dwell time and the optimized dwell time for that finger. For both dwell time settings, the number of true positive detections of the specific finger during movement events of only that finger are listed under the TP column. Additionally, the number of false positive detections during periods of rest in the contralateral run and ipsilateral run are separately listed in the columns denoted by $FP_{rest_{contra}}$ and $FP_{rest_{ipsi}}$ respectively. The total number of false positive detections during rest periods in both runs is listed under the column denoted by FP_{Total}. This Table caption holds for Tables 4.8 through 4.10 which show the results for the other participants.*

Finger	**Baseline Dwell**				**Optimized Dwell**				
	TP	$FP_{rest_{contra}}$	$FP_{rest_{ipsi}}$	FP_{Total}	Dwell Time	TP	$FP_{rest_{contra}}$	$FP_{rest_{ipsi}}$	FP_{Total}
Contra Thumb	30	1	10	11	0.17	30	1	7	8
Contra Index	30	2	0	2	0.30	30	0	0	0
Contra Little	29	1	0	1	0.33	29	1	0	1
Ipsi Thumb	29	27	84	111	0.25	29	6	28	34
Ipsi Index	29	96	28	124	0.12	29	64	12	79
Ipsi Little	30	121	39	160	0.15	30	66	17	83

Table 4.8: *Baseline and optimized dwell times and the corresponding number of true positives and false positives for each finger of participant P2.*

Finger	**Baseline Dwell**				**Optimized Dwell**				
	TP	$FP_{rest_{contra}}$	$FP_{rest_{ipsi}}$	FP_{Total}	Dwell Time	TP	$FP_{rest_{contra}}$	$FP_{rest_{ipsi}}$	FP_{Total}
Contra Thumb	31	22	0	22	0.27	31	9	0	9
Contra Index	30	0	0	0	0.16	30	0	0	0
Contra Little	31	5	0	5	0.20	31	3	0	3
Ipsi Thumb	27	49	93	142	0.14	27	18	73	91
Ipsi Index	25	35	18	53	0.02	25	34	17	51
Ipsi Little	28	26	8	34	0.13	28	13	4	17

Table 4.9: *Baseline and optimized dwell times and the corresponding number of true positives and false positives for each finger of participant P3.*

Finger	Baseline Dwell				Optimized Dwell				
	TP	$FP_{rest_{contra}}$	$FP_{rest_{ipsi}}$	FP_{Total}	Dwell Time	TP	$FP_{rest_{contra}}$	$FP_{rest_{ipsi}}$	FP_{Total}
Contra Thumb	30	46	0	46	0.53	30	2	0	2
Contra Index	30	6	0	6	0.13	30	2	0	2
Contra Little	30	13	0	13	0.27	30	1	0	1
Ipsi Thumb	27	39	142	181	0.23	27	3	61	64
Ipsi Index	24	1	63	64	0.06	24	1	55	56
Ipsi Little	26	17	33	50	0.05	26	6	20	26

Table 4.10: *Baseline and optimized dwell times and the corresponding number of true positives and false positives for each finger of participant P4.*

Several observations can be made based on these results. Firstly, when equipping the baseline dwell time, all available events of contralateral finger movement (which were listed in Table 3.5) were detected for all participants, with the only exception being one trial of contralateral little finger movement for participant P2. For ipsilateral fingers, several trials of finger movements were not detected at all. This is apparent in the results of all participants but was most notable in the results of participant P3. Secondly, when using the baseline dwell time, the number of false positives is much larger for ipsilateral fingers than for contralateral fingers, with the number of false positives exceeding the number of true positives for several ipsilateral fingers. This is visible in the results of all participants. The only contralateral fingers for which a large number of false positive detections took place were the contralateral thumbs of participants P3 and P4. Lastly, for participants P1 through P3, many of the false positive detections of ipsilateral finger movement occurred during rest periods of the contralateral run instead of during rest periods in the ipsilateral run.

After optimizing the dwell time for each finger individually, several changes could be noted. The number of false positives for contralateral fingers decreased where possible. The most notable decrease in the number of false positives could be observed for the contralateral thumbs of participants P3 and P4. For the ipsilateral fingers, a decrease in the number of false positives was similarly notable. Most notably, the ipsilateral thumb still showed a large number of false positives for all participants. Only for participant P2, the number of false positive detections of ipsilateral thumb movements was somewhat similar to the number of true positives for that finger. For the other participants, the number of false positive detections of ipsilateral thumb movement still strongly exceeded the number of true positives for that finger. The results for the ipsilateral index and little fingers were less consistent across participants, but in several cases the number of false positives exceeded the number of true positives for these fingers. Such observations could not be made for any of the contralateral fingers for any of the participants. Additionally, the optimal dwell times for contralateral fingers were on average higher than the optimal dwell times for ipsilateral fingers with optimal dwell times of (0.27 ± 0.01) seconds and (0.12 ± 0.01) seconds respectively (Mean $\pm$ SD across participants).

4.3.3 Asynchronous Classification Runs

The asynchronous classification was performed twice with two different settings for the dwell time. At first, the dwell time was set to match the optimal dwell time for ipsilateral fingers at 0.15 seconds. Afterwards, a dwell time that corresponded to the optimal dwell time for contralateral fingers was employed, namely 0.30 seconds. The results of these classifications are depicted in Figures 4.25 and 4.26 respectively.

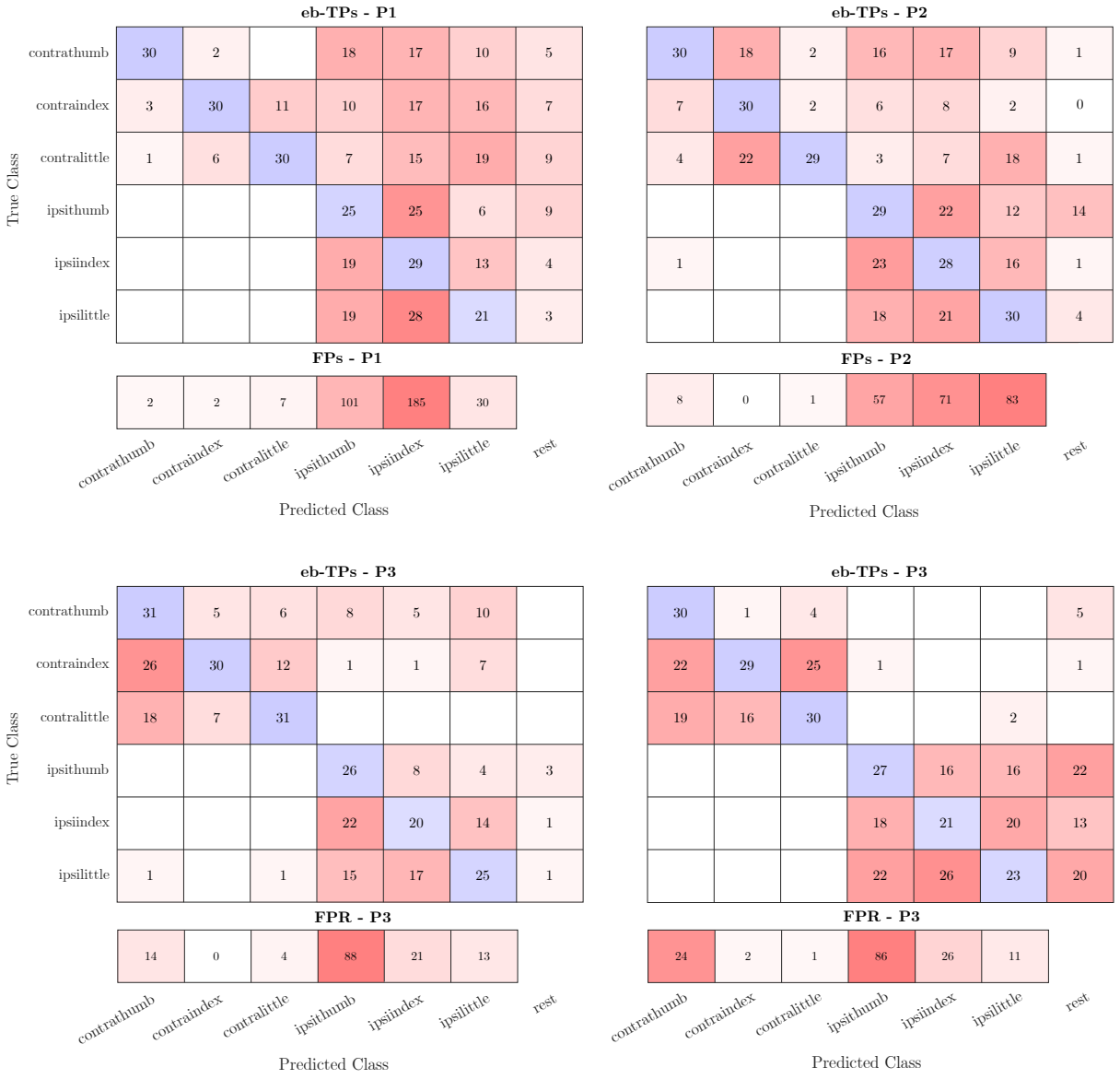

Figure 4.25: *The results of the asynchronous classification run with a dwell time setting of 0.15 seconds. The confusion matrices correspond to the true positive detections of finger movement events and misclassifications between contralateral and ipsilateral finger movement events. The number of false positives that occurred during periods of rest in both the contralateral and the ipsilateral task run are included below each confusion matrix. The results are presented for each participant separately.*

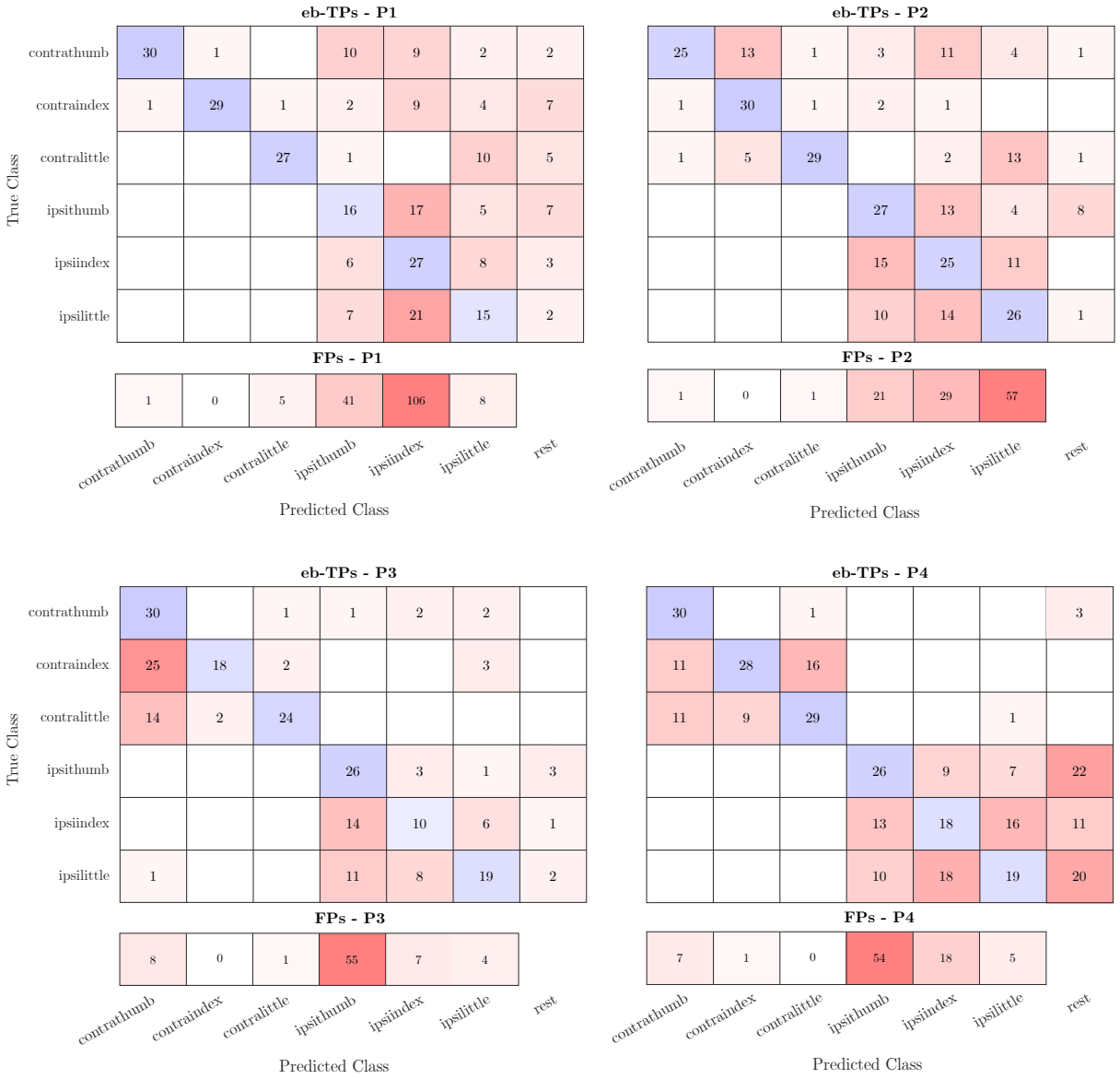

Figure 4.26: *The results of the asynchronous classification run with a dwell time setting of 0.30 seconds. The confusion matrices correspond to the true positive detections of finger movement events and misclassifications between contralateral and ipsilateral finger movement events. The number of false positives that occurred during periods of rest in both the contralateral and the ipsilateral task run are included below each confusion matrix. The results are presented for each participant separately.*

The results of both asynchronous classification runs runs show several similarities. At first, the phenomena described in Figure 3.20 are visible throughout these results: Firstly, misclassifications between the rest class and both contralateral and ipsilateral movement events occurred as can be deducted from the confusion matrices. This effect was somewhat more pronounced for ipsilateral finger movement events than for contralateral finger movement events, especially for participant P4. The misclassifications of rest events during movement episodes of fingers of both lateralities does not further impact the current results and they will not be discussed further. Secondly, misclassifications of ipsilateral movement during contralateral movement events occurred regularly, but almost no misclassifications of contralateral movement occurred during ipsilateral movement events. Increasing the dwell time from 0.15 seconds to 0.30 seconds decreased the occurrence of both these types of misclassifications.

Increasing the dwell time additionally reduced the overall number of confusions between movement events of contralateral and ipsilateral finger movements, visible in

the off-diagonal entries of the confusion matrices in Figures 4.25 and 4.26.

When considering the false positive detections of finger movement events during rest, one largely clear observation can be made based on Figures 4.25 and 4.26: the number of false positive detections was severely larger for ipsilateral finger movements than for contralateral finger movements. Increasing the dwell time from 0.15 seconds to 0.30 seconds reduced the number of false positive detections for both contralateral and ipsilateral fingers, but did impact the detectability of the movement events for some fingers. This was most notable for the ipsilateral fingers, meaning that some trials of ipsilateral finger movement were not detected at all. After increasing the dwell time, the number of false positives was still considerably larger for ipsilateral finger movements than for contralateral finger movements and generally, the best detectable ipsilateral fingers were also exactly the fingers associated with the largest number of false positives during rest.

5 Discussion

This research has investigated the possibility to classify both contralateral and ipsilateral individual finger movements from the SMC of a single hemisphere with the aid of several experiments, of which the results and implications will be discussed in more detail in this chapter.

5.1 Preliminary Data Analysis

Prior to the classification experiments, a preliminary analysis was carried out in Section 3.3 to determine whether the reports surrounding cortical activity resulting from contralateral and ipsilateral finger movements found in the literature review, coincided with the dataset that was employed in this study.

5.1.1 Spatial Aspects of Cortical Activity

Various fMRI studies showed that cortical activity resulting from ipsilateral movement was either absent (e.g. (Ehrsson et al., 2000) (Singh et al., 1998)), or showed a smaller spatial extent with respect to cortical activity resulting from contralateral movement (e.g. (Hanakawa et al., 2005) (Baraldi et al., 1999)), although overlap was visible (e.g. (Horenstein et al., 2009) (Verstynen et al., 2005)). The spatial specificity of the fMRI BOLD signal is highly similar to the spatial specificity of cortical activity in the HFB measured in ECoG signals (Siero et al., 2014). Indeed, a reduced spatial extent of cortical activity in the HFB resulting from ipsilateral movement was similarly described in ECoG studies (e.g. (Zanos et al., 2009), (Jin et al., 2016)). This research gathered more evidence for the above mentioned findings in literature. The spatial analysis that handled the distribution of significantly activated channels (Section 3.3.2) showed that the spatial extent of cortical activity resulting from ipsilateral finger movements was smaller with respect to that of cortical activity resulting from contralateral finger movement. Cortical activity resulting from ipsilateral finger movement was clustered mostly in M1, similar to the findings of (Verstynen et al., 2005) and (Horenstein et al., 2009)). Cortical activity resulting from contralateral finger movements was found spread over the whole SMC (similar to the findings of (Jin et al., 2016) and (Scherer et al., 2009)), with especially channels over S1 showing strong cortical activity. A reduced spatial extent of cortical activity resulting from ipsilateral fingers movements with respect to that of contralateral finger movements in the α and β bands could not be reliably determined with the results of this research. It is to be noted that for participant P2, very little significantly activated channels could be observed in the α and β band. Additionally, for participant P4, several positive correlations in the β band are visible. It is at this point unknown whether these unexpected results are attributable to individual cortical characteristics, the use of anti-epileptic or surgery related drugs, the mental state or other the pathology of the participants.

In hindsight, the apparent similarity between cortical activity resulting from ipsilateral finger movement and cortical activity resulting from contralateral finger

movement appears to be mostly dependent on the available measurement resolution. The observed neural pattern similarity of Fujiwara et al. (Fujiwara et al., 2017) could have been attributed to the fact that their study employed clinical ECoG grids, which are arguably less suitable for discerning fine differences in cortical activity. Additionally, their study employed a more brisk hand movement task which may have resulted in activation over a broader cortical area than one would otherwise observe by using a finer finger movement task. The results of the spatial analysis that handled the distribution of significantly activated channels (Section 3.3.2) are more in line with the findings of Zanos and colleagues (Zanos et al., 2009), who similarly employed a higher density electrode grid for one participant and subsequently noted unique locations of pronounced cortical activity resulting from ipsilateral movement with respect to the locations of cortical activity resulting from contralateral movement.

5.1.2 Spectral Aspects of Cortical Activity

Although the spatial distribution of the HFB and BOLD signals can be compared, much discussion still exists on the comparison of the signal envelopes between HFB and BOLD signals. Therefore, the findings from the ECoG, EEG and MEG studies surrounding the signal envelope of spectral modulations in the various frequency bands will be compared with the findings of the amplitudal analysis carried out in Section 3.3.1. This research has provided further evidence to support the findings of a smaller amplitude of spectral modulations in the HFB resulting from ipsilateral movement in contrast of those resulting from contralateral movement. (e.g. (Jin et al., 2016) (Wisneski et al., 2008)). The comparison of the amplitudes of spectral modulations after averaging over channels as in Section 3.3.1 may have been somewhat misleading since including the channels which show no significant activation in the averaging process automatically leads to a reduced average amplitude. However, in the figures that show the amplitudes of modulations for each channel separately (Section 3.3.1), the relatively smaller amplitudes of spectral modulations in the HFB resulting from ipsilateral finger movement with respect to those resulting from contralateral finger movement are still apparent. Reports of smaller amplitudes of spectral modulations in the α and β bands resulting from ipsilateral finger movement with respect to those resulting from contralateral finger movement (e.g. (Formaggio et al., 2008) (Muthuraman et al., 2012)) were only visible for participant P4 and can therefore not be confidently underlined with the findings of this research.

5.2 Experiment I: Synchronous Classification

After establishing that cortical activity resulting from both contralateral and ipsilateral finger movements was present over the SMC, the sub research question that handled the actual classification of this activity could be addressed. This first sub research question was formulated as follows:

What performance can be attained on the classification of contralateral and ipsilateral individual finger movements in a synchronous setting?

This question was formulated such that the results could build upon the findings of Scherer et al. (Scherer et al., 2009), who had only provided results on the classification of movement from several contralateral fingers versus movement of several ipsilateral fingers. These incomplete results called for a more realistic evaluation of the decodability of individual contralateral and ipsilateral finger movements with the addition of a rest class.

5.2.1 Classification Results

Based on the confusion matrices depicted in Section 3.4.3, individual movements of both contralateral and ipsilateral fingers along with periods of rest can be classified with a performance significantly above chance level ($p<0.05$) for all participants with an average accuracy of 79.22 ± 6.30 (Mean ± SD) over participants. This research has shown that individual contralateral finger movements (excluding rest) can be classified with an average accuracy of 90.75% ± 7.68 (Mean ± SD) over participants. Individual ipsilateral finger movements (excluding rest) were classified with an average accuracy of 65.00% ± 6.16 (Mean ± SD) over participants. The accuracies obtained on the classification of individual contralateral finger movements in related research can be calculated by taking the lower and upper boundaries of accuracies of the ECoG studies that have handled classification of *Individual Finger Movement* in Table E.1 in Section 2.5. These results were on average 66.75% ± 32.97 (Mean ± SD) using similar frequency band features and classifiers. When comparing the obtained performances of this research with the results from related research, it can be stated that the average accuracy obtained on the classification of contralateral finger movement in this research is in the higher registers of related research. The accuracies obtained on the classification of ipsilateral finger movements were lower than those obtained on the classification of contralateral finger movement, which is in accordance with related research on classifying contralateral and ipsilateral movement (e.g. (Diedrichsen et al., 2013) Jin et al. (2016) (Fujiwara et al., 2017)). The differences in performance between the classification of contralateral and ipsilateral finger movements in this research were however larger, which is something that could be attributed to the fact that these former studies employed a brisker movement task. No performance benchmark for the classification of individual ipsilateral finger movements could be deduced from related research, but the accuracies obtained in this research from the classification of ipsilateral finger movements are on par with accuracies for classifying contralateral finger movements in related research. Trials of ipsilateral finger movement were additionally confused with trials of rest, which was not observed for contralateral finger movements.

Although still no concrete answer can be given regarding the discussion on the influence of electrode grid density, it is likely that the high classification accuracies obtained in this research can be related to the usage of HD electrode grids. Especially accurate placement of these grids over the SMC can contribute to high classification accuracies (Bleichner et al., 2016). A third factor that may have contributed to the high classification performance is the fact that the task performance of the participants was generally good. The number of bad trials was low across participants and the error bars on the deflection amplitudes of cued fingers (Section 3.2.4) showed little variance of finger deflection amplitudes during the movement task. For this reason, it can be stated that there was high consistency in the execution of the movement task by the participants, which can be beneficial for the overall classification performance (Bleichner et al., 2014).

Lastly, when observing the confusion matrices depicted in Section 3.4.3, it can be deduced that contralateral finger movements can be excellently distinguished from ipsilateral finger movements, with an accuracy of 100% for all participants. These results are comparable with the results of Scherer and colleagues (Scherer et al., 2009) who have classified two binary schemes of contralateral finger movements versus ipsilateral finger movements. The accuracies attained in those classification schemes ranged between 94.7% and 100.0%. The observant reader might have noticed that the contralateral and ipsilateral task runs have been recorded on different days for two of the participants, which may cause some bias in the signal due to the re-initialization of hardware or the

selection of different reference electrodes. It can therefore be argued that the ability to distinguish contralateral and ipsilateral finger movements might be attributed to systematic differences in the ECoG data of the separate runs. However, an excellent performance on the classification of contralateral versus ipsilateral finger movements was also observed in the results of the participants for which the runs were recorded on identical days. Additionally, The use of the DFT as power extraction method may be especially suitable for eliminating signal biases such as a Direct Current (DC) biases. For these reasons, it can be argued that the results in this research are true. For future research it is nevertheless recommended to combine trials of both contralateral and ipsilateral finger movement in one task run to completely rule out the possibility of such a phenomenon.

5.2.2 Contribution of Frequency Bands

Prior to the actual classification, Section 3.3.3 described the low-dimensional visualization of the high-dimensional ECoG data. Several hypotheses were formulated with these results and as a subsequently, the contribution of the individual frequency bands in the classification process was assessed. For participant P4, some confusion of contralateral fingers with rest occurred after leaving the α and β bands out of the classification process. This finding may support the literature finding that the α and β bands serve as a robust indicator of a general cognitive state of movement (e.g (Onaran et al., 2011) (Hotson et al., 2016)). Solely features from the HFB were as effective for the accurate classification of individual contralateral and ipsilateral finger movements including rest as features from the α, β and HFB frequency bands together. This finding indicates that the HFB indeed held information around finer aspects related to finger movement (e.g. (Onaran et al., 2011) (Wissel et al., 2013)). Additionally, the HFB seems to similarly serve as a robust indicator of a movement state. This research confirmed that these discussed literature findings do not only hold for cortical activity resulting from contralateral finger movement, but also for cortical activity resulting from ipsilateral finger movement, for which little literature evidence could be found. The finding that solely the HFB contains enough information for accurate decoding of both contralateral and ipsilateral finger movements may be especially beneficial for eventual BCI users with LIS, for whom the ability to modulate the α and β bands might be impacted by their lesion (Freudenburg et al., 2019). As a final remark, averaging over frequency bins resulted in a strong increase in performance for all frequency bands and participants. This increase can most likely be attributed to the reduction of dimensionality and the cancellation of noise inside the various individual frequency bins through averaging.

Several anomalies in the low-dimensional visualizations in Section 3.3.3 must be discussed. One of the subplots for participant P4 (Figure L.2 in Appendix L, sub-figure for contralateral HFB) shows two separated clusters of observations corresponding to trials of rest. This anomaly could be explained by the fact that t-SNE uses a gradient descent method which can converge at different and possibly locally optimal solutions. Therefore, visualizations can differ every time the analysis is performed. Such a separation of clusters of datapoints corresponding to rest trials was namely not observed in the corresponding subplot for ipsilateral HFB, for which the same rest trials were used. The plots of the datapoints in the α and β bands belonging to participant P2 (Figure 4.6) showed no formations of separate clusters for any of the observations corresponding to rest or finger movement. This can be explained by the fact that there was no significant cortical activity in these frequency bands for this participant (Figures J.3 and J.4 in Appendix J).

5.3 Experiment II: Asynchronous Classification

After the classification of contralateral and ipsilateral finger movements in an synchronous fashion was handled, further evaluation in an asynchronous setting was required. Therefore, the second sub research question was formulated as follows:

1.2 What performance can be attained on the classification of contralateral and ipsilateral individual finger movements in an asynchronous setting?

Theoretically, any arbitrarily complex BCI with a large number of parameters and filtering stages may have performed well on the classification of contralateral and ipsilateral finger movements. The application of such a sophisticated system would however have masked the phenomenon that was precisely the subject of this research; namely the hypothesized occurrence of false positive detections of mainly ipsilateral finger movements. By implementing the simplest approximation of an asynchronous BCI, this research has provided other (future) researchers with an honest and transparent ground truth and a clear presentation of the obstacles to overcome.

The results of the asynchronous classification were in line with the hypothesis in the discussion section of the literature review (Section 2.8). The number of false positive detections during episodes of rest were especially high for the ipsilateral fingers. The number of false positive detections of ipsilateral finger movement during periods of rest for were at best 106, 57, 55 and 54 for different fingers of participants P1 through P4 respectively, when employing a dwell time of 0.30 seconds. The number of false positive detections of contralateral fingers during episodes of rest using the same dwell time were at best 5, 1, 8 and 7 for different finger of participants P1 through P4 respectively. Considering that the two movement tasks performed by the participants combined took roughly 20 minutes, the number of false positive detections of ipsilateral finger movement is relatively large for such a short time span.

5.4 Comparison of Experiment Results

The last sub research question was intended to compare the performance attained on the synchronous classification with the performance attained on the asynchronous classification and was formulated as follows:

1.3 Do the attained performances on the classification of contralateral and ipsilateral individual finger movements differ between synchronous and asynchronous settings and what can explain possible differences?

The large differences in the methodologies of the synchronous and asynchronous classifications make a one-on-one numerical comparison between results difficult. However, the largest difference that can be observed between the results of the synchronous classification and the asynchronous classification is the strongly exacerbated number of false positive detections of ipsilateral finger movements during the asynchronous evaluation. During the experiment handling synchronous classification, several misclassifications between ipsilateral finger movements and trials of rest were already visible. However, the synchronous classification constituted the classification of at most 300 one-second windows corresponding to each of the trials of finger movement or rest, which were additionally aligned and processed perfectly with use of the movement markers. During the asynchronous classification, around 40.000 to 45.000 one-second windows were classified for each contralateral and ipsilateral run separately in which the windows

contained ECoG signals corresponding to various stages of finger movement, rest and everything in between.

One note of criticality surrounding the differences in the classification process between the synchronous and asynchronous cases must be addressed. Firstly, it can be observed that there was a large class imbalance during the training the asynchronous case (Section 3.5.2). One could argue that as a result, the classifier would be biased to the majority class. However, as mentioned, a proportional increase in the number of confusions of ipsilateral fingers with rest were not observed in Figure 4.24. Still, this class imbalance may have caused a bias towards the rest class during the asynchronous evaluation which could imply that the number of false positive detections of ipsilateral finger movements could have been larger if the classes were balanced. In this research, this did not impact the final outcome of this research since a large number of false positives was still observed and the initial hypotheses remained confirmed, but for future research, it can be recommended to retain the class balance.

Comparison of the confusion matrices of the synchronous classification and those of the asynchronous classification is even more difficult. The confusion matrices of the asynchronous classification demonstrated that still a fairly large number - much larger than in the synchronous evaluation - of misclassifications between movement events of the fingers took place. The initial investigation of the posterior probabilities (Figure 3.20) already provided clarification towards this phenomenon and most of the misclassifications can be attributed to the fact that the asynchronous classification was highly simplistic. Therefore, an in depth comparison between the confusion matrices of the synchronous and asynchronous experiments can be explained with this reason and further comparison is disappointingly not possible. The confusion matrices of the asynchronous evaluation do show that the movement events of each finger can be accurately detected in the asynchronous setting (based on the true positive detections on the diagonals of these confusion matrices), although for now this largely depends on the selected dwell time. By comparing the diagonals of the confusion matrices and the number of false positive detections corresponding to the two asynchronous classification runs with different settings of the dwell times (Figures 4.25 and 4.26), it can additionally be seen that balancing the reliable detection of ipsilateral finger movements with the number of false positive detections of ipsilateral finger movements poses a difficult trade-off.

The best way to compare the obtained results in both experiments is therefore to consider them as extensions of one another. The results of synchronous classification portray the most optimistic view regarding the true positive detections of contralateral and ipsilateral finger movement and the results of the asynchronous classification portray the most pessimistic view regarding the false positive detections of contralateral and ipsilateral finger movements. One note of criticality must be made; during the synchronous classification, bad trials were visually rejected which naturally introduced a slightly positive bias in the results. It is however expected that this bias is not extremely large, since only a small number of finger movement trials were rejected as can be seen from Table 3.2.

5.5 Implications, Limitations and Recommendations

The results obtained in this research need to be put into a broader context and this section will be devoted to discussing possible explanations and implications surrounding the

results obtained in this research. This section will additionally address further limitations of this research, which will subsequently be transformed into recommendations for future work. To provide overview, the implications, limitations and recommendations have been combined per topic and are handled in that order.

5.5.1 Somatotopy and the Relative Importance of the Cortical Areas

The notion that the spatially focal HFB was important in the classification process asks for the re-visitation of a question that was posed in the discussion of the literature review in Section 2.8, namely the question whether the notion of a somatotopy is required for the correct classification of finger movements. It is to be noted that the question whether good classification results are causal with - or even correlated with - the notion of a distinct somatotopy can definitely not be answered with the results of this research. Among more reasons, the main limitation is that even though HD electrode grids with 3-4 mm inter-electrode spacing were used in this study, the spatial sampling of these electrode grids is still rather coarse and sparse in comparison to fMRI and therefore a true somatotopy is difficult to establish by using ECoG.

However, several insights contributed to the believe that at least some spatial ordering of finger representations was required for accurate classification and that therefore the related research on somatotopy should be discussed in light of the obtained results of this research. Firstly, the spatially focal HFB was required for accurate classification and even more importantly, classification could be equally well performed using only features from the HFB with respect to using features from the α, β and HFB frequency bands. Secondly, the findings surrounding finger somatotopy in the literature review (Section 2.3) were based on the cortical regions that expressed the most activity during movement of a specific finger. Based on the results of the first spatial analysis into the relevant cortical areas (Section 3.4.6.1) it could be inferred that the channels that showed the most activation were also the most relevant ones for the classification of finger movements versus rest. Therefore, several insights from the classification results and the subsequent spatial analysis carried out in Section 3.4.6 deserve some more attention.

Literature on somatotopy for contralateral finger movement described widespread cortical activity across the SMC, similarly to the results of the Channel R^2 analysis (Section 3.3.2) of this study. Literature on somatotopy noted a more ordered and segregated somatotopy in S1 with respect to M1, suggesting that the processing of sensory information occurs at a more specific level (Schellekens et al., 2018). The discussion section of the literature review (Section 2.8) therefore posed the question whether HD electrode grids could possibly capitalize on this fine segregation in S1 because these grids would allow for recording of smaller and more finger specific neuronal populations. Whether there is direct causality or not, the results of the spatial analysis in Section 3.3.2 did show that the channels over S1 show strong cortical activity during during contralateral finger movement. Similarly, the channels that were relevant for the classification of contralateral finger movement versus rest were mainly located on S1 and several channels that are important for distinguishing between individual contralateral finger movements (Section 3.4.6.1) were similarly located on S1 and the CS. Both these results were consistent across participants.

Literature on somatotopy for ipsilateral finger movement was scarce and could not establish a finger somatotopy in S1 due to the absence of significant cortical activity (e.g. (Hlustik, 2001), (Stippich et al., 2007)). In M1, only a rough somatotopy was observed in literature due to the reduced cortical activity resulting from ipsilateral

movement and the brisk movement task employed (e.g. (Alkadhi et al., 2002) (Alkadhi et al., 2000)). The relatively small amount of cortical activity in S1 for ipsilateral fingers was similarly observed in this study (Section 3.3.2) but the results do show that the patterns of cortical activity resulting from individual ipsilateral finger movements were unique in M1 and over several channels in S1. The spatial analysis in Section 3.4.6.2 showed that important channels for distinguishing between individual contralateral and ipsilateral fingers were located mainly over S1 and the CS. Given that the cortical activity resulting from ipsilateral fingers was most pronounced on M1 and not S1, the claim by Scherer and colleagues (Scherer et al., 2009) that the good differentiation of contralateral versus ipsilateral finger movements in their binary classification scheme being mostly due to a difference in amplitude can be supported with these results. To go further on this claim, the results of this research indicate that the classification decision between movement of contralateral and ipsilateral fingers seemed to be mostly based on an amplitude difference in S1. Given the apparent importance of S1, it might be an interesting target for the decoding contralateral and ipsilateral finger movements on a smaller scale, which was an additional aspect of the problem statement from Section 2.8, which was later deemed outside of the scope of this research.

The are several factors that can help explain the importance of S1 beyond its role in the processing of sensory information. These factors are important because it can be argued that BCI performance may be positively influenced by the processing of sensory feedback resulting from muscle movement in able-bodied participants (e.g. (Branco et al., 2017) (Chestek et al., 2013)), who have been included in this research. Naturally, such feedback processing mechanisms would be absent in participants with LIS, who must resort solely to attempted movement. For that reason, S1 has been the subject of research that aimed to find answers regarding its possible active role during voluntary movement. The best known active role of S1 can be considered the generation and sending of efference copies (Cullen, 2004) during movement, for which some evidence was also found in an ECoG study (Sun et al., 2015). Additionally, one study demonstrated that cortical stimulation of S1 can result in movement of the limbs (Nii et al., 1996), which supports the claim that S1 may play a role during active movement. Adding to that, other studies have shown that the segregated finger representations of S1 (and M1), that are potentially valuable to the good classification results of this research, have been conserved in paralyzed individuals and individuals with amputated limbs (Bruurmijn et al., 2017). The activity in S1 (and additionally M1) appears to also be retained during attempted movement (Hotz-Boendermaker et al., 2008) (Cramer et al., 2005), which may suggest that the findings in this research obtained from able-bodied participants may generalize for lesional BCI users as well.

5.5.2 The Effects of Reduced Cortical Activity

So far, it appears likely that the ability to distinguish finger movements is related to a somatotopic representation of fingers on the cortical surface. However, the plausibility of this theory seems debatable when the detection of ipsilateral finger movements is concerned. It is expected that any somatotopy would appear in those regions that show most cortical activity, but based on the results of this research, this did not seem to hold for ipsilateral fingers. The spatial analysis carried out in Section 3.4.6.2 showed indeed that distinction of individual ipsilateral finger movements did not solely rely on the channels that showed the most (or even significant) activation when comparing these with the results of Section3.3.2. Apparently, finding unique hotspots of cortical activity in M1 resulting from ipsilateral finger movement was not a good enough premise for accurate classification of movements of these fingers. This implies that there is not much distinguishable power in the overlapping cortical activity (resulting from both

contralateral and ipsilateral finger movements) in M1 and that therefore several channels in the CS and in S1 are required to reliably distinguish individual ipsilateral finger movements.

For the classification of ipsilateral finger movements, this finding has some implications. If the classifier assigns a high importance to one of these non-significantly activated channels during training, it seems logical that any non-significant and therefore non-task related stray activity occurring over these electrodes would contribute to false positive detections. During the classification attempts in this research, the classifier was trained on all available channels, including the non-significantly activated channels. This did not seem to be problematic during the classification of contralateral fingers, for which a large number of significantly activated channels were found. However, in hindsight it may have posed issues for the classification of ipsilateral finger movements, for which there were generally more non-significantly activated channels than there were significantly activated channels. This additionally may have caused the difficulties in detecting these ipsilateral finger movements, resulting in missed detections of movement events during the asynchronous evaluation. It must be mentioned that the spatial distribution of cortical activity in Section 3.3.2 shows a rather black and white view of which channels show activity. There might reasonably be task-related activity over the non-significant electrodes that was simply not pronounced enough to survive the fairly strict Bonferroni corrected threshold. But, as the methodology dictates, any non-significant activity should be regarded as noise and it can therefore be argued that non-significant stray activity may have played a role in the creation of false positive detections during the classification of especially ipsilateral finger movements. A notable example comes from the results of the dwell time optimization step during the asynchronous classification (Section 4.3.2). It can be seen that false positive detections of ipsilateral finger movements did not only occur in episodes of rest from the ipsilateral run, but it appeared that a significant amount of false positives also occurred during the rest episodes of the contralateral run. When observing the fact that misclassifications with rest and ipsilateral fingers occurred right in between flexion and extension of contralateral fingers (schematically depicted by Figure 3.20), it is highly plausible that stray activity resulting from the onset or completion of contralateral movement with a subsequent smaller amplitude and spatial distribution could trigger false positive detections of ipsilateral finger movement. A striking example is the ipsilateral thumb of participant P4, for which no significantly activated channels were found in the spatial analysis of Section 3.3.2 (Figure K.2). The spatial analysis in Section 3.4.6.1 for this finger (Figure T.2) showed consequently that the classifier was forced to base classification decisions over the complete set of non-significantly activated channels.

One critical note should be placed surrounding the identification of important channels. It might at first seem curious that the spatial analyses showed in a several occasions that individual channels were highly important and that the respective neighboring electrodes were not relevant, for example in Figure 4.17. It is reasonable to assume that neighboring channels in ECoG grids are highly correlated and these results may therefore be unexpected. However, in the spatial analysis of Section 3.3.2, several individual channels could be identified that showed a high R^2 value without its neighbors showing significant activation. This could be discussed in light of the distinct characteristic of HD electrode grids to measure smaller populations neurons with a more specific function. Also, especially when cortical activity of several finger movements overlap over channels, the classifier will be forced to focus on minute and detailed differences between these channels, which could result in only several scattered channels to be highly important.

From a machine learning point of view, especially the small number of signifi-

cantly activated channels can have a negative impact on the classification results. Basing classification decisions on numerous channels that show no significant activity implies that there may simply be little informative features to be used in the classification process. This in turn helps towards explaining why ipsilateral finger movements could not be reliably distinguished from rest but also not be reliably distinguished from one another. Simply put, if there is no cortical activity, a classifier has nothing to pick up on and a harsh theoretical upper limit to the decodability of especially ipsilateral finger movements may well exist.

Since a researcher can hardly dictate where and when cortical activity appears, the insight of the previous paragraph begs the question whether the SMC was the most suitable candidate in the search for cortical activity resulting from ipsilateral finger movement. Several studies handled in the literature review have mentioned that cortical activity resulting from ipsilateral movement might manifest outside the SMC as well. Berlot and colleagues (Berlot et al., 2018) mentioned in their fMRI study that contralateral activity showed the strongest representation in S1, which was observed in this study, but that ipsilateral activity showed the strongest representation in the Premotor (PM) cortex and the Posterior Parietal Cortex (PPC). Also Wisneski and colleagues (Wisneski et al., 2008) showed in their ECoG study that cortical activity resulting from ipsilateral finger movement can be found in areas outside the SMC, such as again the PM cortex or other non-sensorimotor areas which are left unspecified by the authors. Additionally, Fujiwara and colleagues include the PM cortex in their work (Fujiwara et al., 2017) which handles the classification of ipsilateral hand movements. Since the electrode grids employed in this study did not extent to those areas, nothing can be said about the ability to decode from these areas based on the results of this study. However, a word of caution must be issued when embarking on the search for cortical activity resulting from movement outside areas that are known to be associated with movement. It might become difficult to interpret and discuss the exact neurological underpinning and reliability of this found cortical activity. Nevertheless, it can be argued that for some machine learning or BCI research, the neurophysiological function of cortical activity might be somewhat less relevant if good classification accuracy in those regions can be reliably obtained.

5.5.3 Classifiers and the Classification Approach

Simple and linear classifiers have been employed in this research for several distinct reasons. Especially the high dimensionality and the small amount of training data available made these classifiers a suitable choice. Additionally, the application of simple classifiers allowed for the desired white box classification approach with which inferences about some of the underlying neurological phenomena contributing to the results gained in this research could be made. Especially the spatial analyses of Section 3.4.6 using the weights of the LDA classifier provided several interesting insights and helped explain the obtained results. The LDA classifier was mostly used in this research because of its architectural simplicity in comparison to the ECOC-SVM and its ability to work well despite a reduced amount of training data with respect to the RF and NB classifiers (Section 3.4.4). The ability of the LDA to work with little training data may be devoted to the fact that its covariance matrix was completely diagonalized and therefore relatively easy to estimate. Additionally, the LDA uses only the pooled covariance matrix computed based on observations from all classes. This allowed the classifier to use all data for the robust estimation of the covariance matrix. Lastly, the success of the linear hyperplanes employed by several of the classifiers might be attributed to the fact that their generalization ability is high in the case of little data, which in turn made the classifier less susceptible to outliers.

The LDA, SVM and NB classifiers all seemed to perform well and notably, the only non-linear classifier that was employed consistently showed a lower performance. One possible explanation could be that the amount of training data was indeed too little to adequately train the classifier. The combination of a small number of training samples and a high dimensionality of the feature space can cause the more complex RF model to overfit. The question whether linear classifiers are unconditionally better than non-linear classifiers in BCI research was already discussed with the article of Marjaninejad and colleagues (Marjaninejad et al., 2017) and naturally, still no conclusive answer can be provided based on the results of this research. The possible advantages of the non-linear variant of the LDA, the Quadratic Discriminant Analysis (QDA) classifier can however be discussed. This classifier was not employed in this research due to the resulting singular covariance matrices after training, to be attributed to too little training data. However, a strong benefit of the QDA could be that it does not use the same covariance matrix for all classes but instead computes these for each class separately. In reality, the covariance matrices of the different classes may indeed not be similar at all, especially for movement and rest, so that the usage of QDA might yield better classification scores and possibly even help mitigating the observed false positives. This notion could hold for non-linear classifiers in general, of which the complex decision boundary may function well in modeling fine differences between cortical activity resulting from ipsilateral finger movement and rest.

Although the use of complex non-linear and modern classifiers may be tempting, the largest impeding factor in BCI research and ECoG research (including this research) in particular remains the scarcity of data and participants. The scarcity of data may be limiting and frustrating at times, but one must not forget that this type of research is performed for and with human beings. The author of this research has attended one of the surgeries required for the implantation of the ECoG grid and has further personally witnessed at first hand the burden of data collection for the already ill participants suffering from not only their epilepsy but also from the consequences of the surgery they underwent. Foremost, gratefulness should here be expressed to all the participants in this research for their courage, time and effort. Naturally, a higher number of participants would have strengthened the results especially in a statistical sense and could have helped to better explain the variance in classification scores, but four participants can be already considered as a relatively large number of participants in ECoG literature. It is imaginable that home usage of a BCI would allow for the collection of more data over time, enabling the use of more complex classifiers. But for most research, including this one, the matter of data scarcity will likely remain prominent and researchers must therefore be pragmatical in their choice of classification strategy.

The above paragraph should also serve as an encouragement that machine learning in BCI research should mainly remain a means towards an end and not an end in itself. Therefore, researchers should also attempt to investigate possibilities for improvement in the broadest range of the classification pipeline, starting with the preprocessing and feature extraction stages and ending with the deployment of classifiers. The influence of the preprocessing and feature extraction procedure of this research also deserves some discussion. Here, rather wide one second Hanning windows were used to ensure that at least a complete flexion of the finger was included in the window. However, because the window was centered around the peak of movement, it is reasonable to assume that the windows included a significant amount of rest signal prior to movement. In hindsight, this could have been disadvantageous for the feature extraction of ipsilateral fingers with less pronounced activity. Also, the relatively wide window setting may have masked the possible influence of the earlier occurrence of ipsilateral activity in the time lag classification in Section 3.4.5. The fact that classification in Section 3.4.5 was above

chance level even half a second before movement can similarly be contributed to the fact that half of the window centered around -0.5 seconds included signal corresponding to movement onset. Additionally, the steep increase of the posterior probability in the asynchronous evaluation (Figure 3.18) can be attributed to the wide window setting. Selection of a more narrow window may have lead to a more gradual increase of posterior probability which in turn could have effected the detection process. Although determining the optimal window length can be considered as a form of hyper-parameter optimization, the exact windowing approach could be more thoroughly investigated. For example, in the time frame during which this research was carried out, an article was published that effectively included temporal successions of cortical signals in the classification process, which increased classification performance for finger movement with a similar simple LDA classifier (Gruenwald et al., 2019) that was highly successful in this research.

Similarly, there still exists a myriad of features, feature extraction techniques, dimensionality reduction techniques, noise mitigation techniques and classifiers that can be employed, of which Table E.1 shows only a small collection. Most interesting is that these techniques have proven to be successful for classification or regression of contralateral finger movement, but have not yet been applied towards the decoding of ipsilateral finger movement. An investigation into the application of these options might therefore be an interesting quest.

The usage of machine learning methods here can be discussed in the light of the thought that only synchrony of man and machine can lead to optimal BCI usage. In terms of this research, that was of an exploratory nature, any hyper-parameter optimization was not performed to favor generalizability and comparability of results across participants. But however important generalization is for research and however noble the quest for a "one size fits all" BCI may be, this research has shown that increase in performance may be possible with further optimization of several parameters in the classification pipeline. Firstly, the hyper-parameter optimization in Sections 3.4.2 and 3.4.3 show that tuning hyper-parameters can increase decoding performance. The actual validation of those settings must then however be appropriately determined, as the hyper-parameter search in this research was only used as a sanity check. Secondly, the cortical structure and occurrence of cortical activity varies strongly across participants and therefore the search for informative participant-specific frequency modulations and locations thereof may be fruitful (Scherer et al., 2009). This research has shown that feature extraction could even be dependent on participant-specific temporal aspects of cortical activity (Section 3.4.5).

5.5.4 Modeling of the NC State

The modeling of the NC state as performed in this research also deserves some discussion. Section 2.9 already discussed the difficulty of accurately modeling the NC state since it factually constitutes everything that is not an IC state. However, in this research it was decided to model an NC state (by means of taking one second windows in a rest trial as depicted in Figure 3.8 for several reasons. Firstly, these observations of rest were required to calculate the channel R^2 values in the spatial analysis (Section 3.3.2). Secondly, this research aimed to quantify the number of confusions with rest in the synchronous classification, for which observations of rest were required. These same trials of rest were later used to calculate the channel importance in the spatial analysis of Section 3.4.6.

If the NC state was not accurately modeled by these rest trials, this would have strong consequences for all analyses performed in this research. In this dataset, the time

in between trials was relatively short and this research was not able to rule out the possibility that several frequency components such as the β rebound or other sustained presence of cortical activity (described in Section 2.4.2) may have bled into the one second windows placed in the rest trials. Additionally, signal components related to the anticipation of movement (e.g. (Kornhuber and Deecke, 1965)) may have been present throughout the runs since it this research employed an event-based task design (Olman et al., 2012b). It is debatable whether similar activity in the HFB would be included, since that component was strongly time-locked to movement (e.g. (Talakoub et al., 2017) (Huo et al., 2010)), but especially the combination of sustained cortical activity in the α and/or β bands with an absence or scarcity of cortical activity in the HFB in trials of rest does resemble the cortical activity resulting from ipsilateral finger movement. In that sense, bad modeling of the NC state may actually cause additional false positive detections of finger movement.

The above scenario is however highly speculative and this research did not attempt to establish the true extent to which this phenomenon may have taken place. Rather, good care was taken to select one second windows that contained only rest and were surrounded by rest as much as possible. Additionally, this research investigated whether the set of sub-sampled rest trials were representative with respect to all available rest trials by refraining from sub-sampling of rest trials in the classification prior to the asynchronous classification (Figure 4.24). These results showed that the amount of confusions of ipsilateral finger movements with rest did not increase proportionally to the increas in the number of rest trials in the classification process. Therefore, it can be argued that the NC state was modeled fairly well by these rest trials.

Nevertheless, it may advisable for the future researcher to think about whether he or she wants to model a NC state at all. The direct seven-class classification employed in this research required the classifier to always choose one class at every observation since it simply cannot output no class label at all. Similarly, the posterior probability distribution outputted over all classes should sum to one and this distribution rarely showed a scenario in which equal probabilities over the movement classes were assigned (Figure 3.20). If the rest class was not included, the classifier would have been forced to make a choice out of the remaining six classes (which constituted finger movement) at every observation. In the case of periods of rest, the classifier would have likely picked the class that most resembled rest out of the classes it can choose from, which would likely be one of the ipsilateral finger movement classes. This would have potentially caused even more false positive detections and as such, the modeling of an NC state was clearly a necessity with this approach. In hindsight, a completely different approach to the asynchronous classification could have been handled that circumvented the need to model an NC state altogether. An example would be to use a number of 1-class SVMs that are trained only on the class they have to detect, so that classification becomes a matter of anomaly detection instead of assigning a specific class label to each window.

5.5.5 Creation of a Dataset for an Asynchronous Evaluation

This research has shown that fair accuracy can be obtained for the classification of contralateral and ipsilateral finger movements during a synchronous evaluation. It is needless to mention that especially the decodability of ipsilateral finger movements should from now on only be mainly evaluated in an asynchronous setting to determine how well the false positive detections related to movements of these fingers can be mitigated.

As mentioned in the discussion of the literature review (Section 2.8) this dataset

was not purposely designed for an asynchronous evaluation. Therefore, the most important step towards future research is the recording of a dataset that is suitable for the classification of contralateral and ipsilateral finger movements in an asynchronous setting. The first recommendation towards this dataset is to increase the duration of movement events. Since the movement task equipped in this research dictated mostly one finger flexion and extension, the movement events were of relatively short duration. Most BCI datasets for asynchronous evaluations include (attempted) movement events of several seconds (e.g. (Blankertz et al., 2007) (Brunner et al., 2008) (Leeb et al., 2008)). The dwell times in this research were relatively short with a minimum of 0.02 and a maximum of 0.53 seconds. Such short dwell times were dictated by the short movement periods but could be responsible for a portion of false positives. Longer (attempted) movement events could enable longer dwell times so that noisy detections need not to be counted as a false positives. Especially for ipsilateral finger movements, which appeared to be more difficult to detect, this could be beneficial.

The second recommendation to be made for this dataset has regard to the NC events. The dataset of this research contained relatively short periods of NC (rest). The possibility that false positives for ipsilateral fingers may be caused by stray activity prior to and following finger movement has already been discussed, but with the short and fixed inter-trial times in between movements of this dataset, it can not be certainly determined whether the occurrences of false positives for ipsilateral fingers would only occur prior to and shortly following contralateral or ipsilateral finger movement. It would be advisable to determine whether the false positive detections of ipsilateral finger movements would spontaneously occur after much longer periods of rest of several seconds or even minutes. If this is not the case, it could put the results of this research in a different perspective and the problem of false positives may be partially mitigated by using for example a refractory period. The fixed inter-trial time of the employed data set in this research also explains why any refractory period was not introduced in this research. A fixed refractory period with the length of the inter-trial time could theoretically have mitigated the occurrence of all false positives which would provide highly masked results. Although the refractory period may good for mitigating false positives and misclassifications of multiple fingers during movement events, they should be used with caution for the above mentioned reason. In real life BCI situations, periods of NC would have a more variable duration and the determination of a refractory period will be not as straightforward. The variable length of NC episodes could additionally provide the future researcher with more possibilities to model and evaluate an NC state in different ways and aid in determining whether modeling an NC would be a logic approach in the first place.

The creation of such a dataset will first be limited to an event-related task design with executed movement. A task design with imagined movement or a self paced task design would require feedback to the user for which first a reasonable working system for the detection of (mainly ipsilateral) fingers is required.

5.5.6 Alternative Classification Strategy

It is worthwhile to shortly spark a brainstorm surrounding an alternative classification strategy for the classification of contralateral and ipsilateral finger movements. This research has not further explored the possibilities mentioned in Section 2.5.3 regarding the use of pragmatical constraints or hierarchical classification, but such constraints may be valuable in this scenario. One possible option for an asynchronous BCI employing these constraints would be a multi-stage classifier specifically designed for the classification of contralateral and ipsilateral finger movements. As seen from the confusion matrices of

the synchronous classification (Section 3.4.3), contralateral and ipsilateral finger movements could be well distinguished from each other. Contralateral and ipsilateral finger movements could possibly be well distinguished from rest by using only those channels that showed significant cortical activity. Two separate classifiers could be trained on the subsets of significantly activated channels for each laterality and could, during the classification, jointly first place a decision on whether there was movement or not and afterwards decide on which finger was moved, in a hierarchical fashion. This could circumvent the problem that may arise when a classifier has been trained on a lot of non-significant channels. Further decreasing the number of electrodes in the classification process has the additional benefit that the dimensionality of the data is lowered. To what extent the discarding of non-significant electrodes influences the ability to accurately distinguish individual contralateral and ipsilateral fingers should then naturally be first investigated, but removing non-significant channels during classifier training is an otherwise known and used methodology (e.g. (Salari et al., 2019)).

5.5.7 Exploiting Knowledge of Underlying Neurophysiology

This research has not further investigated the neurological processes and functional roles that govern cortical activity resulting from contralateral and ipsilateral finger movements. This topic was outside the scope of this research and for that reason discussion of this topic might become more speculative than factual. However, if properly investigated, knowledge on this matter could have provided another layer of depth in this discussion. For this reason, some of the insights - mostly related to cortical activity resulting from ipsilateral movements - are worth mentioning while refraining from directly relating them to the results obtained in this research.

Several articles in the literature review have argued that ipsilateral cortical activity plays an active role rather than a passive role during voluntary movement. Literature reported that cortical activity resulting from ipsilateral movement was mostly seen during active movement tasks and not during passive tactile stimulation (e.g. (Berlot et al., 2018) (Singh et al., 1998) (Li et al., 1996)). Several other articles argued that ipsilateral activity may play a supportive role during voluntary movement of limbs of the opposite laterality, contributing to the precision of those movements (e.g. (Ehrsson et al., 2000) (Verstynen et al., 2005)). Such a theory would fit with the matter of handedness, where it was reported that ipsilateral cortical activity was most pronounced during non-dominant hand movements (e.g. (Kobayashi et al., 2003), (Singh et al., 1998)). Also, an earlier occurrence of ipsilateral activity (e.g. (Wisneski et al., 2008), (Leuthardt et al., 2009)) suggests that ipsilateral activity may even play a role in movement planning, perhaps supported by the findings that ipsilateral activity was found in the PM cortex (e.g. (Berlot et al., 2018) (Wisneski et al., 2008)).

There similarly is debate about the functional relation between contralateral and ipsilateral activity in the two hemispheres. Some research shows that fibers in the Corpus Callosum (CC) connect the motor cortices of different hemispheres and one can therefore investigate how activity in the motor cortex of a single hemisphere is related to activity in the laterally opposite motor cortex (Wahl et al., 2007). The research by Berlot and colleagues (Berlot et al., 2018) suggests that the motor cortices of the two hemispheres reflect different functional processes during unilateral movement and activity in M1 of a single hemisphere is not likely to be attributed by passive spillover from the laterally opposite motor cortex. Although these examples again focuses on two hemispheres instead of one, more investigation into the specific underlying phenomena that generate cortical activity in M1 (and S1) of a single hemisphere during ipsilateral and contralateral finger movement may have enabled a more thorough discussion on

the matter why M1 was did not appear to be the most informative cortical area for distinguishing ipsilateral and contralateral finger movement. Similarly, such research could provide more clarification as to why S1 was an important cortical area in this research. Furthermore, the knowledge of the underlying neurophysiological principles could have aided with explaining several observations in this research, such as the variances in the classification accuracies for ipsilateral finger movements or the question as to why the spectral and spatial differences between cortical activity resulting from contralateral and ipsilateral finger movement mostly manifested only in the HFB.

This knowledge could be applied practically as well. Firstly, if ipsilateral activity indeed plays an active role during voluntary movement, this might support that ipsilateral cortical activity could potentially also be modulated by individuals with LIS or lesional BCI users in general, which can serve as a motivation to perform further research into the topic of decoding ipsilateral finger movements. Secondly, the matter of handedness could not be further clarified by the results of this research, but if handedness is in some way related the amount of cortical activity resulting from ipsilateral finger movements, then knowledge about this could aid in the decision on which hemisphere the electrode grid should be placed. Similarly, if cortical activity resulting from ipsilateral movement is related to movement planning (Wisneski et al., 2008), then a small extension of the grid over the SMC towards the PM cortex might possibly be beneficial. Lastly, if the amount of ipsilateral cortical activity is indeed dependent on the task complexity (perhaps in a supportive manner as described above) (e.g. (Ehrsson et al., 2000), (Huo et al., 2010), (Verstynen et al., 2005)), issuing a different and perhaps more complex finger movement task might yield more cortical activity and possibly better decoding results.

5.5.8 Experiments with End Users

First, further research should investigate what quantitative performance can be attained on the classification of contralateral and ipsilateral finger movements. More specifically, research should first further investigate how well especially the false negative (i.e. missed detections) and false positive detections mainly associated with ipsilateral finger movement can be mitigated. Afterwards, the true extent to which contralateral and ipsilateral finger movements can be used as a viable control signal must be determined more qualitatively. One important measure of qualitative performance is the opinion of the final user and the requirements dictated by the final application. Firstly, experiments with lesional users, such as individuals with LIS, can provide a definitive answer whether the findings of this research generalize during attempted movement instead of actual performed movement, as was discussed earlier. Secondly, during such experiments, the final user him- or herself can determine what level of performance is acceptable, depending on the final application. It is imaginable that some critical tasks such as wheelchair control require a reliable detection with zero false positives and zero false negatives. Any false positive detections during such a critical control task can impose risk to the user, which is understandably unacceptable. Although false negative detections might influence the perceived smoothness of operations and thus be frustrating for users, they might be preferable over false positive detections in a critical control task such as wheelchair control. Other tasks such as control of a speller or computer program may be less performance critical and may provide a safer testing environment. If it indeed appears that there is a limit to the attainable performance on the classification of ipsilateral fingers, they could perhaps still be used in a more supportive fashion, or during tasks that require less frequent control, for example performing a right mouse click in addition to a left mouse click, which is used more often. Although it is yet too early to speculate about the eventual possibilities, it can be stated that even if (attempted) movement of only a single ipsilateral finger

could be used in BCI control, this would already help not only the UMCU, but the BCI community and end users towards a BCI with more degrees of freedom.

6 Conclusion

The main research question of this research was formulated as:

To what extent can contralateral and ipsilateral individual finger movements both be accurately classified from the SMC of a single hemisphere?

Based on the results of the synchronous classification, it can be stated that contralateral and ipsilateral fingers along with periods of rest can be classified from the SMC of a single hemisphere with accuracies significantly above chance level ($p<0.05$) for all participants. The average attained accuracy of 79.22 ± 6.30 across participants lies only slightly lower than the definition of accurate classification accuracy of 85% (Vansteensel et al., 2016a). By performing an asynchronous classification, this research has on the other hand identified the occurrence of a large number of false positive detections for mainly ipsilateral finger movements which forms a key obstacle to overcome in future research. With these results, this research has build further on the results of Scherer and colleagues, Jin and colleagues and Fujiwara and colleagues ((Scherer et al., 2009), (Jin et al., 2016),(Fujiwara et al., 2017)) and shows that the results of these authors presented an optimistic view on the decodability of mainly ipsilateral movement. This research has provided further directions that future research could take, after which it should become more clear to what extent both contralateral and ipsilateral finger movements can be used as a viable control signal for a reliable BCI with more degrees of freedom.

References

Acharya, S., Fifer, M. S., Benz, H. L., Crone, N. E., and Thakor, N. V. (2010). Electrocorticographic amplitude predicts finger positions during slow grasping motions of the hand. *Journal of Neural Engineering*, 7(4):046002.

Alkadhi, H., Crelier, G. R., Hotz Boendermaker, S., Hepp-Reymond, M. C., and Kollias, S. S. (2002). Somatotopy in the ipsilateral primary motor cortex. *NeuroReport*, 13(16):2065–2070.

Alkadhi, H., Kollias, S. S., Crelier, G. R., Golay, X., Hepp-Reymond, M. C., and Valavanis, A. (2000). Reproducibility of Primary Motor Cortex Somatotopy Under Controlled Conditions. *American Journal of Neuroradiology*, 21(8):1423–1433.

Ang, K. K., Guan, C., Chua, K. S. G., Ang, B. T., Kuah, C. W. K., Wang, C., Phua, K. S., Chin, Z. Y., and Zhang, H. (2011). A Large Clinical Study on the Ability of Stroke Patients to Use an EEG-Based Motor Imagery Brain-Computer Interface. *Clinical EEG and Neuroscience*, 42(4):253–258.

Bai, O., Lin, P., Vorbach, S., Li, J., Furlani, S., and Hallett, M. (2007). Exploration of computational methods for classification of movement intention during human voluntary movement from single trial EEG. *Clinical Neurophysiology*, 118(12):2637–2655.

Baraldi, P., Porro, C. A., Serafini, M., Pagnoni, G., Murari, C., Corazza, R., and Nichelli, P. (1999). Bilateral representation of sequential finger movements in human cortical areas. *Neuroscience letters*, 269(2):95–98.

Bashashati, A., Ward, R. K., and Birch, G. E. (2007). Towards development of a 3-state self-paced brain-computer interface. *Computational intelligence and neuroscience*, 2007.

Bauer, G., Gerstenbrand, F., and Rumpl, E. (1979). Varieties of the locked-in syndrome. *Journal of Neurology*, 221(2):77–91.

Beisteiner, R., Gartus, A., Erdler, M., Mayer, D., Lanzenberger, R., and Deecke, L. (2004). Magnetoencephalography indicates finger motor somatotopy. *European Journal of Neuroscience*, 19(2):465–472.

Berlot, E., Prichard, G., O'Reilly, J., Ejaz, N., and Diedrichsen, J. (2018). Ipsilateral finger representations in the sensorimotor cortex are driven by active movement processes, not passive sensory input. *Journal of Neurophysiology*, 121(2):418–426.

Besle, J., Sánchez-Panchuelo, R. M., Bowtell, R., Francis, S., and Schluppeck, D. (2014). Event-related fMRI at 7T reveals overlapping cortical representations for adjacent fingertips in S1 of individual subjects. *Human Brain Mapping*, 35(5):2027–2043.

Birbaumer, N. (2006). Breaking the silence: Brain-computer interfaces (BCI) for communication and motor control. In *Psychophysiology*, volume 43, pages 517–532. John Wiley & Sons, Ltd (10.1111).

Blankenburg, F., Ruben, J., Meyer, R., Schwiemann, J., and Villringer, A. (2003). Evidence for a rostral-to-caudal somatotopic organization in human primary somatosensory cortex with mirror-reversal in areas 3b and 1. *Cerebral cortex (New York, N.Y. : 1991)*, 13(9):987–993.

Blankertz, B., Dornhege, G., Krauledat, M., Müller, K.-R., and Curio, G. (2007). The non-invasive berlin brain–computer interface: fast acquisition of effective performance in untrained subjects. *NeuroImage*, 37(2):539–550.

Blaus, B. (2014). Medical Gallery of Blausen Medical.

Bleichner, M. G., Freudenburg, Z. V., Jansma, J. M., Aarnoutse, E. J., Vansteensel, M. J., and Ramsey, N. F. (2016). Give me a sign: decoding four complex hand gestures based on high-density ECoG. *Brain Structure and Function*, 221(1):203–216.

Bleichner, M. G., Jansma, J. M., Sellmeijer, J., Raemaekers, M., and Ramsey, N. F. (2014). Give me a sign: Decoding complex coordinated hand movements using high-field fMRI. *Brain Topography*, 27(2):248–257.

Bodison, S. (2017). Neuroimaging.

Bougrain, L., Liang, N., Inria, C., and University-loria, N. (2009). Band-specific features improve Finger Flexion Prediction from ECoG. *Jornadas Argentinas sobre Interfaces Cerebro Computadora*, 2009:1–4.

Branco, M. P., Freudenburg, Z. V., Aarnoutse, E. J., Bleichner, M. G., Vansteensel, M. J., and Ramsey, N. F. (2017). Decoding hand gestures from primary somatosensory cortex using high-density ECoG. *NeuroImage*, 147:130–142.

Branco, M. P., Freudenburg, Z. V., Aarnoutse, E. J., Vansteensel, M. J., and Ramsey, N. F. (2018a). Optimization of sampling rate and smoothing improves classification of high frequency power in electrocorticographic brain signals. *Biomedical Physics and Engineering Express*, 4(4):045012.

Branco, M. P., Leibbrand, M., Vansteensel, M. J., Freudenburg, Z. V., and Ramsey, N. F. (2018b). Gridloc: An automatic and unsupervised localization method for high-density ecog grids. *NeuroImage*, 179:225–234.

Breiman, L. (2001). Random forests. *Machine learning*, 45(1):5–32.

Brunner, C., Leeb, R., Müller-Putz, G., Schlögl, A., and Pfurtscheller, G. (2008). Bci competition 2008–graz data set a. *Institute for Knowledge Discovery (Laboratory of Brain-Computer Interfaces), Graz University of Technology*, 16.

Bruurmijn, M. L., Pereboom, I. P., Vansteensel, M. J., Raemaekers, M. A., and Ramsey, N. F. (2017). Preservation of hand movement representation in the sensorimotor areas of amputees. *Brain*, 140(12):3166–3178.

Bundy, D. T., Pahwa, M., Szrama, N., and Leuthardt, E. C. (2016). Decoding three-dimensional reaching movements using electrocorticographic signals in humans. *Journal of Neural Engineering*, 13(2).

Bundy, D. T., Szrama, N., Pahwa, M., and Leuthardt, E. C. (2018). Unilateral, 3D Arm Movement Kinematics Are Encoded in Ipsilateral Human Cortex. *The Journal of Neuroscience*, 38(47):10042–10056.

Chen, W., Liu, X., and Litt, B. (2014). Logistic-weighted regression improves decoding of finger flexion from electrocorticographic signals. In *2014 36th Annual International Conference of the IEEE Engineering in Medicine and Biology Society, EMBC 2014*, pages 2629–2632.

Chestek, C. A., Gilja, V., Blabe, C. H., Foster, B. L., Shenoy, K. V., Parvizi, J., and Henderson, J. M. (2013). Hand posture classification using electrocorticography signals in the gamma band over human sensorimotor brain areas. *Journal of Neural Engineering*, 10(2):026002.

Cho, S., Kim, J. A., Hwang, D.-U., and Han, S. K. (2004). Single Trial Discrimination between Right and Left Hand Movement-Related EEG Activity. *IEEE Transactions on Biomedical Engineering*, pages 255–262.

Cincotti, F., Kauhanen, L., Aloise, F., Palomäki, T., Caporusso, N., Jylänki, P., Mattia, D., Babiloni, F., Vanacker, G., Nuttin, M., Marciani, M. G., and Millán, J. d. R. (2007). Vibrotactile Feedback for Brain-Computer Interface Operation. *Computational Intelligence and Neuroscience*, 2007.

Combrisson, E. and Jerbi, K. (2015). Exceeding chance level by chance: The caveat of theoretical chance levels in brain signal classification and statistical assessment of decoding accuracy. *Journal of neuroscience methods*, 250:126–136.

Cramer, S. C., Finklestein, S. P., Schaechter, J. D., Bush, G., and Rosen, B. R. (1999). Activation of distinct motor cortex regions during ipsilateral and contralateral finger movements. *Journal of neurophysiology*, 81(1):383–7.

Cramer, S. C., Lastra, L., Lacourse, M. G., and Cohen, M. J. (2005). Brain motor system function after chronic, complete spinal cord injury. *Brain*, 128(12):2941–2950.

Crone, N. (1998). Functional mapping of human sensorimotor cortex with electrocorticographic spectral analysis. II. Event-related synchronization in the gamma band. *Brain*, 121(12):2301–2315.

Cullen, K. E. (2004). Sensory signals during active versus passive movement. *Current opinion in neurobiology*, 14(6):698–706.

Dalal, S. S., Guggisberg, A. G., Edwards, E., Sekihara, K., Findlay, A. M., Canolty, R. T., Berger, M. S., Knight, R. T., Barbaro, N. M., Kirsch, H. E., and Nagarajan, S. S. (2008). Five-dimensional neuroimaging: Localization of the time-frequency dynamics of cortical activity. *NeuroImage*, 40(4):1686–1700.

Dechent, P. and Frahm, J. (2003). Functional somatotopy of finger representations in human primary motor cortex. *Human Brain Mapping*, 18(4):272–283.

Delgado Saa, J. F., De Pesters, A., and Cetin, M. (2016). Asynchronous decoding of finger movements from ECoG signals using long-range dependencies conditional random fields. *Journal of Neural Engineering*, 13(3):036017.

Diedrichsen, J., Wiestler, T., and Krakauer, J. W. (2013). Two distinct ipsilateral cortical representations for individuated finger movements. *Cerebral Cortex*, 23(6):1362–1377.

Do, T. N., Lenca, P., Lallich, S., and Pham, N. K. (2010). Classifying very-high-dimensional data with random forests of oblique decision trees. In *Studies in Computational Intelligence*, volume 292, pages 39–55. Springer, Berlin, Heidelberg.

Ehrsson, H. H., Fagergren, A., Jonsson, T., Westling, G., Johansson, R. S., and Forssberg, H. (2000). Cortical activity in precision- versus power-grip tasks: an fMRI study. *Journal of neurophysiology*, 83(1):528–536.

Ejaz, N., Hamada, M., and Diedrichsen, J. (2015). Hand use predicts the structure of representations in sensorimotor cortex. *Nature Neuroscience*, 18(7):1034–1040.

Elango, V., Patel, A. N., Miller, K. J., and Gilja, V. (2017). Sequence Transfer Learning for Neural Decoding. *bioRxiv*, page 210732.

Elgharabawy, A. and Wahed, M. A. (2017). Decoding of finger movement using kinematic model classification and regression model switching. In *2016 8th Cairo International Biomedical Engineering Conference, CIBEC 2016*, pages 84–89. IEEE.

Elghrabawy, A. and Wahed, M. A. (2012). Prediction of five-class finger flexion using ECoG signals. In *2012 Cairo International Biomedical Engineering Conference, CIBEC 2012*, pages 1–5.

Erbil, N. and Ungan, P. (2007). Changes in the alpha and beta amplitudes of the central EEG during the onset, continuation, and offset of long-duration repetitive hand movements. *Brain research*, 1169:44–56.

Evgeniou, T. and Pontil, M. (1999). Support vector machines: Theory and applications. In *Advanced Course on Artificial Intelligence*, pages 249–257. Springer.

Fifer, M. S., Mollazadeh, M., Acharya, S., Thakor, N. V., and Crone, N. E. (2011). Asynchronous decoding of grasp aperture from human ECoG during a reach-to-grasp task. In *Proceedings of the Annual International Conference of the IEEE Engineering in Medicine and Biology Society, EMBS*, pages 4584–4587. IEEE.

Fisher, R. A. (1936). The use of multiple measurements in taxonomic problems. *Annals of eugenics*, 7(2):179–188.

Flamary, R. and Rakotomamonjy, A. (2012). Decoding finger movements from ECoG signals using switching linear models. *Frontiers in Neuroscience*, 6(MAR).

Flint, R. D., Rosenow, J. M., Tate, M. C., and Slutzky, M. W. (2017). Continuous decoding of human grasp kinematics using epidural and subdural signals. *Journal of Neural Engineering*, 14(1):016005.

Formaggio, E., Storti, S. F., Avesani, M., Cerini, R., Milanese, F., Gasparini, A., Acler, M., Pozzi Mucelli, R., Fiaschi, A., and Manganotti, P. (2008). EEG and fMRI coregistration to investigate the cortical oscillatory activities during finger movement. *Brain Topography*, 21(2):100–111.

Freudenburg, Z. V., Branco, M. P., Leinders, S., van der Vijgh, B. H., Pels, E. G., Denison, T., van den Berg, L. H., Miller, K. J., Aarnoutse, E. J., Ramsey, N. F., et al. (2019). Sensorimotor ecog signal features for bci control: A comparison between people with locked-in syndrome and able-bodied controls. *Frontiers in neuroscience*, 13.

Fujiwara, Y., Matsumoto, R., Nakae, T., Usami, K., Matsuhashi, M., Kikuchi, T., Yoshida, K., Kunieda, T., Miyamoto, S., Mima, T., Ikeda, A., and Osu, R. (2017). Neural pattern similarity between contra- and ipsilateral movements in high-frequency band of human electrocorticograms. *NeuroImage*, 147:302–313.

Gerloff, C., Hummel, F., and Dichgans, J. (2000). Ipsilateral sensorimotor cortex activation during movement sequences of increasing complexity: Representation of movement complexity or memory load? *Mov Disorders*, 15((Suppl 3)):90.

Graimann, B., Allison, B., and Pfurtscheller, G. (2009). *Brain–Computer Interfaces: A Gentle Introduction*. Springer.

Gruenwald, J., Znobishchev, A., Kapeller, C., Kamada, K., Scharinger, J., and Guger, C. (2019). Time-variant linear discriminant analysis improves hand gesture and finger movement decoding for invasive brain-computer interfaces. *Frontiers in neuroscience*, 13:901.

Hämäläinen, M., Hari, R., Ilmoniemi, R. J., Knuutila, J., and Lounasmaa, O. V. (1993). Magnetoencephalography—theory, instrumentation, and applications to noninvasive studies of the working human brain. *Reviews of Modern Physics*, 65(2):413–497.

Hamzelou, J. (2016). Nog even en we communiceren van brein tot brein.

Hanakawa, T., Parikh, S., Bruno, M. K., and Hallett, M. (2005). Finger and face representations in the ipsilateral precentral motor areas in humans. *Journal of neurophysiology*, 93(5):2950–2958.

Hazrati, M. K. and Hofmann, U. G. (2012). Decoding finger movements from ECoG signals using Empirical Mode Decomposition. *Biomedizinische Technik*, 57(SUPPL. 1 TRACK-F):650–653.

Henry, J. C. (2006). Electroencephalography: Basic Principles, Clinical Applications, and Related Fields, Fifth Edition. *Neurology*, 67(11):2092–2092.

Hermes, D., Miller, K. J., Noordmans, H. J., Vansteensel, M. J., and Ramsey, N. F. (2010). Automated electrocorticographic electrode localization on individually rendered brain surfaces. *Journal of neuroscience methods*, 185(2):293–298.

Hermiz, J., Rogers, N., Kaestner, E., Ganji, M., Cleary, D. R., Carter, B. S., Barba, D., Dayeh, S. A., Halgren, E., and Gilja, V. (2018). Sub-millimeter ECoG pitch in human enables higher fidelity cognitive neural state estimation. *NeuroImage*, 176:454–464.

Hill, N. J., Gupta, D., Brunner, P., Gunduz, A., Adamo, M. A., Ritaccio, A., and Schalk, G. (2012). Recording human electrocorticographic (ecog) signals for neuroscientific research and real-time functional cortical mapping. *JoVE (Journal of Visualized Experiments)*, page e3993.

Hlustik, P. (2001). Somatotopy in Human Primary Motor and Somatosensory Hand Representations Revisited. *Cerebral Cortex*, 11(4):312–321.

Horenstein, C., Lowe, M. J., Koenig, K. A., and Phillips, M. D. (2009). Comparison of unilateral and bilateral complex finger tapping-related activation in premotor and primary motor cortex. *Human Brain Mapping*, 30(4):1397–1412.

Hotson, G., McMullen, D. P., Fifer, M. S., Johannes, M. S., Katyal, K. D., Para, M. P., Armiger, R., Anderson, W. S., Thakor, N. V., Wester, B. A., and Crone, N. E. (2016). Individual finger control of a modular prosthetic limb using high-density electrocorticography in a human subject. *Journal of Neural Engineering*, 13(2):026017.

Hotz-Boendermaker, S., Funk, M., Summers, P., Brugger, P., Hepp-Reymond, M.-C., Curt, A., and Kollias, S. S. (2008). Preservation of motor programs in paraplegics as demonstrated by attempted and imagined foot movements. *Neuroimage*, 39(1):383–394.

Huo, X., Xiang, J., Wang, Y., Kirtman, E. G., Kotecha, R., Fujiwara, H., Hemasilpin, N., Rose, D. F., and Degrauw, T. (2010). Gamma oscillations in the primary motor cortex studied with MEG. *Brain & development*, 32(8):619–624.

Jiang, T., Jiang, T., Wang, T., Mei, S., Liu, Q., Li, Y., Wang, X., Prabhu, S., Sha, Z., and Ince, N. F. (2018). Investigation of the Influence of ECoG Grid Spatial Density on Decoding Hand Flexion and Extension. In *Proceedings of the Annual International Conference of the IEEE Engineering in Medicine and Biology Society, EMBS*, volume 2018-July, pages 3052–3055.

Jin, Y., Lu, M., Wang, X., Zhang, S., Zhu, J., and Zheng, X. (2016). Electrocorticographic signals comparison in sensorimotor cortex between contralateral and ipsilateral hand movements. In *Proceedings of the Annual International Conference of the IEEE Engineering in Medicine and Biology Society, EMBS*, volume 2016-Octob, pages 1544–1547.

Jochumsen, M., Rovsing, C., Rovsing, H., Niazi, I. K., Dremstrup, K., and Kamavuako, E. N. (2017). Classification of Hand Grasp Kinetics and Types Using Movement-Related Cortical Potentials and EEG Rhythms. *Computational intelligence and neuroscience*, 2017:7470864.

Jurafsky, D. and Martin, J. H. (2008). Speech and language processing: An introduction to speech recognition, computational linguistics and natural language processing. *Upper Saddle River, NJ: Prentice Hall*.

Kaufman, I. C. (1950). The Cerebral Cortex of Man: A Clinical Study of Localization of Function. *American Journal of Psychiatry*, 108(2):153–153.

Kauhanen, L., Nykopp, T., and Sams, M. (2006). Classification of single MEG trials related to left and right index finger movements. *Clinical Neurophysiology*, 117(2):430–439.

Kim, S. G., Ashe, J., Georgopoulos, A. P., Merkle, H., Ellermann, J. M., Menon, R. S., Ogawa, S., and Ugurbil, K. (1993). Functional imaging of human motor cortex at high magnetic field. *Journal of neurophysiology*, 69(1):297–302.

Kim, S. G., Richter, W., and Uğurbil, K. (1997). Limitations of temporal resolution in functional MRI. *Magnetic resonance in medicine*, 37(4):631–6.

Kobayashi, M., Hutchinson, S., Schlaug, G., and Pascual-Leone, A. (2003). Ipsilateral motor cortex activation on functional magnetic resonance imaging during unilateral hand movements is related to interhemispheric interactions. *NeuroImage*, 20(4):2259–70.

Kolasinski, J., Makin, T. R., Jbabdi, S., Clare, S., Stagg, C. J., and Johansen-Berg, H. (2016). Investigating the Stability of Fine-Grain Digit Somatotopy in Individual Human Participants. *Journal of Neuroscience*, 36(4):1113–1127.

Kornhuber, H. H. and Deecke, L. (1965). Hirnpotentialänderungen bei willkürbewegungen und passiven bewegungen des menschen: Bereitschaftspotential und reafferente potentiale. *Pflüger's Archiv für die gesamte Physiologie des Menschen und der Tiere*, 284(1):1–17.

Kubánek, J., Miller, K. J., Ojemann, J. G., Wolpaw, J. R., and Schalk, G. (2009). Decoding flexion of individual fingers using electrocorticographic signals in humans. *Journal of Neural Engineering*, 6(6).

Kübler, A., Furdea, A., Halder, S., Hammer, E. M., Nijboer, F., and Kotchoubey, B. (2009). A Brain-Computer Interface Controlled Auditory Event-Related Potential (P300) Spelling System for Locked-In Patients. *Annals of the New York Academy of Sciences*, 1157(1):90–100.

Kübler, A., Nijboer, F., Mellinger, J., Vaughan, T. M., Pawelzik, H., Schalk, G., McFarland, D. J., Birbaumer, N., and Wolpaw, J. R. (2005). Patients with ALS can use sensorimotor rhythms to operate a brain-computer interface. *Neurology*, 64(10):1775–7.

Kuo, C.-C., Luu, P., Morgan, K. K., Dow, M., Davey, C., Song, J., Malony, A. D., and Tucker, D. M. (2014). Localizing Movement-Related Primary Sensorimotor Cortices with Multi-Band EEG Frequency Changes and Functional MRI. *PLoS ONE*, 9(11):e112103.

Leeb, R., Brunner, C., Müller-Putz, G., Schlögl, A., and Pfurtscheller, G. (2008). Bci competition 2008–graz data set b. *Graz University of Technology, Austria*, pages 1–6.

Leuthardt, E. C., Freudenberg, Z., Bundy, D., and Roland, J. (2009). Microscale recording from human motor cortex: implications for minimally invasive electrocorticographic brain-computer interfaces. *Neurosurgical Focus*, 27(1):E10.

Li, A., Yetkin, F. Z., Cox, R., and Haughton, V. M. (1996). Ipsilateral hemisphere activation during motor and sensory tasks. *AJNR. American journal of neuroradiology*, 17(4):651–5.

Li, Y., Zhang, S., Jin, Y., Cai, B., Controzzi, M., Zhu, J., Zhang, J., and Zheng, X. (2017). Gesture Decoding Using ECoG Signals from Human Sensorimotor Cortex: A Pilot Study. *Behavioural Neurology*, 2017:1–12.

Li, Z.-M., Dun, S., Harkness, D. A., and Brininger, T. L. (2016). Motion Enslaving among Multiple Fingers of the Human Hand. *Motor Control*, 8(1):1–15.

Liang, N. and Bougrain, L. (2012). Decoding finger flexion from band-specific ecog signals in humans. *Frontiers in Neuroscience*.

Liao, K., Xiao, R., Gonzalez, J., and Ding, L. (2014). Decoding individual finger movements from one hand using human EEG signals. *PLoS ONE*, 9(1).

Liao, X., Yao, D., Wu, D., and Li, C. (2007). Combining spatial filters for the classification of single-trial EEG in a finger movement task. *IEEE Transactions on Biomedical Engineering*, 54(5):821–831.

Liu, Y., Coon, W., De Pesters, A., Brunner, P., and Schalk, G. (2015). The effects of spatial filtering and artifacts on electrocorticographic signals. *Journal of neural engineering*, 12(5):056008.

Liu, Y. and Sharma, M. (2010). Decoding ipsilateral finger movements from ECoG signals in humans. *Advances in ...*, pages 1–9.

Logothetis, N. K., Pauls, J., Augath, M., Trinath, T., and Oeltermann, A. (2001). Neurophysiological investigation of the basis of the fMRI signal. *Nature*, 412(6843):150–157.

Lotze, M., Erb, M., Flor, H., Huelsmann, E., Godde, B., and Grodd, W. (2000). fMRI evaluation of somatotopic representation in human primary motor cortex. *NeuroImage*, 11(5 I):473–481.

Maaten, L. v. d. and Hinton, G. (2008). Visualizing data using t-sne. *Journal of machine learning research*, 9(Nov):2579–2605.

Marjaninejad, A., Taherian, B., and Valero-Cuevas, F. J. (2017). Finger movements are mainly represented by a linear transformation of energy in band-specific ECoG signals. In *Proceedings of the Annual International Conference of the IEEE Engineering in Medicine and Biology Society, EMBS*, pages 986–989. IEEE.

Martuzzi, R., van der Zwaag, W., Farthouat, J., Gruetter, R., and Blanke, O. (2014). Human finger somatotopy in areas 3b, 1, and 2: A 7T fMRI study using a natural stimulus. *Human Brain Mapping*, 35(1):213–226.

Mason, S., Kronegg, J., Huggins, J., Fatourechi, M., and Schlögl, A. (2006). Evaluating the performance of self-paced brain computer interface technology. *Neil Squire Soc., Vancouver, BC, Canada, Tech. Rep.*

Mason, S. G. and Birch, G. E. (2000). A brain-controlled switch for asynchronous control applications. *IEEE Transactions on Biomedical Engineering*, 47(10):1297–1307.

Meier, J. D., Aflalo, T. N., Kastner, S., and Graziano, M. S. A. (2008). Complex Organization of Human Primary Motor Cortex: A High-Resolution fMRI Study. *Journal of Neurophysiology*, 100(4):1800–1812.

Miller, K. J., Leuthardt, E. C., Schalk, G., Rao, R. P. N., Anderson, N. R., Moran, D. W., Miller, J. W., and Ojemann, J. G. (2007). Spectral changes in cortical surface potentials during motor movement. *The Journal of neuroscience : the official journal of the Society for Neuroscience*, 27(9):2424–32.

Miller, K. J., Zanos, S., Fetz, E. E., den Nijs, M., and Ojemann, J. G. (2009). Decoupling the Cortical Power Spectrum Reveals Real-Time Representation of Individual Finger Movements in Humans. *Journal of Neuroscience*, 29(10):3132–3137.

Muthuraman, M., Arning, K., Govindan, R. B., Heute, U., Deuschl, G., and Raethjen, J. (2012). Cortical representation of different motor rhythms during bimanual movements. *Experimental brain research*, 223(4):489–504.

Nakanishi, Y., Yanagisawa, T., Shin, D., Chen, C., Kambara, H., Yoshimura, N., Fukuma, R., Kishima, H., Hirata, M., and Koike, Y. (2014). Decoding fingertip trajectory from electrocorticographic signals in humans. *Neuroscience Research*, 85:20–27.

Nambu, I., Hagura, N., Hirose, S., Wada, Y., Kawato, M., and Naito, E. (2015). Decoding sequential finger movements from preparatory activity in higher-order motor regions: A functional magnetic resonance imaging multi-voxel pattern analysis. *European Journal of Neuroscience*, 42(10):2851–2859.

Nii, Y., Uematsu, S., Lesser, R. P., and Gordon, B. (1996). Does the central sulcus divide motor and sensory functions: Cortical mapping of human hand areas as revealed by electrical stimulation through subdural grid electrodes. *Neurology*, 46(2):360–367.

Nijboer, F., Furdea, A., Gunst, I., Mellinger, J., McFarland, D. J., Birbaumer, N., and Kübler, A. (2008). An auditory brain–computer interface (BCI). *Journal of Neuroscience Methods*, 167(1):43–50.

Nirkko, A. C., Ozdoba, C., Redmond, S. M., Bürki, M., Schroth, G., Hess, C. W., and Wiesendanger, M. (2001). Different ipsilateral representations for distal and proximal movements in the sensorimotor cortex: Activation and deactivation patterns. *NeuroImage*, 13(5):825–835.

Oldfield, R. C. (1971). The assessment and analysis of handedness: the edinburgh inventory. *Neuropsychologia*, 9(1):97–113.

Olman, C. A., Pickett, K. A., Schallmo, M. P., and Kimberley, T. J. (2012a). Selective BOLD responses to individual finger movement measured with fMRI at 3T. *Human Brain Mapping*, 33(7):1594–1606.

Olman, C. A., Pickett, K. A., Schallmo, M.-P., and Kimberley, T. J. (2012b). Selective bold responses to individual finger movement measured with fmri at 3t. *Human brain mapping*, 33(7):1594–1606.

Onaran, I., Ince, N. F., and Cetin, A. E. (2011). Classification of multichannel ECoG related to individual finger movements with redundant spatial projections. In *Proceedings of the Annual International Conference of the IEEE Engineering in Medicine and Biology Society, EMBS*, pages 5424–5427.

Oostenveld, R., Fries, P., Maris, E., and Schoffelen, J.-M. (2011). Fieldtrip: open source software for advanced analysis of meg, eeg, and invasive electrophysiological data. *Computational intelligence and neuroscience*, 2011:1.

Overduin, S. A. and Servos, P. (2004). Distributed digit somatotopy in primary somatosensory cortex. *NeuroImage*, 23(2):462–472.

Pan, G., Li, J. J., Qi, Y., Yu, H., Zhu, J. M., Zheng, X. X., Wang, Y. M., and Zhang, S. M. (2018). Rapid decoding of hand gestures in electrocorticography using recurrent neural networks. *Frontiers in Neuroscience*, 12(AUG).

Pels, E. G., Aarnoutse, E. J., Ramsey, N. F., and Vansteensel, M. J. (2017). Estimated Prevalence of the Target Population for Brain-Computer Interface Neurotechnology in the Netherlands. *Neurorehabilitation and Neural Repair*, 31(7):677–685.

Penfield, W. and Boldrey, E. (1937). Somatic motor and sensory representation in the cerebral cortex of man as studied by electrical stimulation. *Brain*, 60(4):389–443.

Pfannmöller, J. P., Greiner, M., Balasubramanian, M., and Lotze, M. (2016). High-resolution fMRI investigations of the fingertip somatotopy and variability in BA3b and BA1 of the primary somatosensory cortex. *Neuroscience*, 339:667–677.

Pfurtscheller, G., Stancák, A., and Neuper, C. (1996). Post-movement beta synchronization. A correlate of an idling motor area? *Electroencephalography and Clinical Neurophysiology*, 98(4):281–293.

Pires, G., Nunes, U., and Castelo-Branco, M. (2007). Single-Trial EEG Classification of Movement Related Potential. In *2007 IEEE 10th International Conference on Rehabilitation Robotics*, pages 569–574. IEEE.

Purves, D., Augustine, G. J., Fitzpatrick, D., Hall, W. C., Lamantia, A. S., and White, L. E. (2011). *Neuroscience*. sinauer, 5th editio edition.

Quandt, F., Reichert, C., Hinrichs, H., Heinze, H. J., Knight, R. T., and Rieger, J. W. (2012). Single trial discrimination of individual finger movements on one hand: A combined MEG and EEG study. *NeuroImage*, 59(4):3316–3324.

Rau, C., Plewnia, C., Hummel, F., and Gerloff, C. (2003). Event-related desynchronization and excitability of the ipsilateral motor cortex during simple self-paced finger movements. *Clinical neurophysiology : official journal of the International Federation of Clinical Neurophysiology*, 114(10):1819–1826.

Rousseau, M. C., Baumstarck, K., Alessandrini, M., Blandin, V., Billette De Villemeur, T., and Auquier, P. (2015). Quality of life in patients with locked-in syndrome: Evolution over a 6-year period. *Orphanet Journal of Rare Diseases*, 10(1):88.

Saa, J., Christen, A., Martin, S., Pasley, B., BioRxiv, R. K., and 2018, U. (2018). Coherence-based spectro-spatial fillters for stimulus features prediction from electrocorticographic recordings. *biorxiv.org*, page 481572.

Salari, E., Freudenburg, Z., Branco, M., Aarnoutse, E., Vansteensel, M., and Ramsey, N. (2019). Classification of articulator movements and movement direction from sensorimotor cortex activity. *Scientific reports*, 9(1):1–12.

Salyers, J. B., Dong, Y., and Gai, Y. (2018). Continuous Wavelet Transform for Decoding Finger Movements from Singe-Channel EEG. *IEEE Transactions on Biomedical Engineering*, 66(6):1588–1597.

Samiee, S., Hajipour, S., and Shamsollahi, M. B. (2010). Five-class finger flexion classification using ECoG signals. In *2010 International Conference on Intelligent and Advanced Systems, ICIAS 2010*, pages 1–4. IEEE.

Sanchez Panchuelo, R. M., Besle, J., Schluppeck, D., Humberstone, M., and Francis, S. (2018). Somatotopy in the Human Somatosensory System. *Frontiers in human neuroscience*, 12:235.

Sanes, J. N. and Donoghue, J. P. (2002). Plasticity and Primary Motor Cortex. *Annual Review of Neuroscience*, 23(1):393–415.

Sanes, J. N. and Schieber, M. H. (2001). Orderly Somatotopy in Primary Motor Cortex: Does It Exist? *NeuroImage*, 13(6):968–974.

Schalk, G. (2010). Can Electrocorticography (ECoG) Support Robust and Powerful Brain-Computer Interfaces? *Frontiers in Neuroengineering*, 3:9.

Schellekens, W., Petridou, N., and Ramsey, N. F. (2018). Detailed somatotopy in primary motor and somatosensory cortex revealed by Gaussian population receptive fields. *NeuroImage*, 179(June):337–347.

Schendel, A. A., Nonte, M. W., Vokoun, C., Richner, T. J., Brodnick, S. K., Atry, F., Frye, S., Bostrom, P., Pashaie, R., Thongpang, S., Eliceiri, K. W., and Williams, J. C. (2014). The effect of micro-ECoG substrate footprint on the meningeal tissue response. *Journal of neural engineering*, 11(4):046011.

Scherer, R., Zanos, S. P., Miller, K., Rao, R. P. N., and Ojemann, J. G. (2009). Classification of contralateral and ipsilateral finger movements for electrocorticographic brain-computer interfaces. *Neurosurgical Focus*, 27(1):E12.

Shen, G., Zhang, J., Wang, M., Lei, D., Yang, G., Zhang, S., and Du, X. (2014). Decoding the individual finger movements from single-trial functional magnetic resonance imaging recordings of human brain activity. *The European journal of neuroscience*, 39(12):2071–2082.

Shenoy, P., Miller, K. J., Ojemann, J. G., and Rao, R. P. (2007). Finger movement classification for an electrocorticographic BCI. In *Proceedings of the 3rd International IEEE EMBS Conference on Neural Engineering*, pages 192–195. IEEE.

Siero, J. C. W., Hermes, D., Hoogduin, H., Luijten, P. R., Ramsey, N. F., and Petridou, N. (2014). BOLD matches neuronal activity at the mm scale: A combined 7T fMRI and ECoG study in human sensorimotor cortex. *NeuroImage*, 101:177–184.

Singh, L. N., Higano, S., Takahashi, S., Abe, Y., Sakamoto, M., Kurihara, N., Furuta, S., Tamura, H., Yanagawa, I., Fujii, T., Ishibashi, T., Maruoka, S., and Yamada, S. (1998). Functional MR imaging of cortical activation of the cerebral hemispheres during motor tasks. *AJNR. American journal of neuroradiology*, 19(2):275–280.

Stippich, C., Blatow, M., Durst, A., Dreyhaupt, J., and Sartor, K. (2007). Global activation of primary motor cortex during voluntary movements in man. *NeuroImage*, 34(3):1227–1237.

Stringer, E. A., Chen, L. M., Friedman, R. M., Gatenby, C., and Gore, J. C. (2011). Differentiation of somatosensory cortices by high-resolution fMRI at 7T. *NeuroImage*.

Sun, H., Blakely, T. M., Darvas, F., Wander, J. D., Johnson, L. A., Su, D. K., Miller, K. J., Fetz, E. E., and Ojemann, J. G. (2015). Sequential activation of premotor, primary somatosensory and primary motor areas in humans during cued finger movements. *Clinical Neurophysiology*, 126(11):2150–2161.

Talakoub, O., Marquez-Chin, C., Popovic, M. R., Navarro, J., Fonoff, E. T., Hamani, C., and Wong, W. (2017). Reconstruction of reaching movement trajectories using electrocorticographic signals in humans. *PloS one*, 12(9):e0182542.

Talakoub, O., Popovic, M., Navaro, J., Hamani, C., Fonoff, E., and Wong, W. (2014). Temporal alignment of electrocorticographic recordings for upper limb movement. *Frontiers in neuroscience*, 8:431.

Tanaka, K., Matsunaga, K., and Wang, H. (2005). Electroencephalogram-based control of an electric wheelchair. *IEEE Transactions on Robotics*, 21(4):762–766.

Townsend, G., Graimann, B., and Pfurtscheller, G. (2004). Continuous EEG Classification During Motor Imagery—Simulation of an Asynchronous BCI. *IEEE Transactions on Neural Systems and Rehabilitation Engineering*, 12(2):258–265.

Vansteensel, M. J., Pels, E. G., Bleichner, M. G., Branco, M. P., Denison, T., Freudenburg, Z. V., Gosselaar, P., Leinders, S., Ottens, T. H., Van Den Boom, M. A., et al. (2016a). Fully implanted brain–computer interface in a locked-in patient with als. *New England Journal of Medicine*, 375(21):2060–2066.

Vansteensel, M. J., Pels, E. G. M., Bleichner, M. G., Branco, M. P., Denison, T., Freudenburg, Z. V., Gosselaar, P., Leinders, S., Ottens, T. H., Van Den Boom, M. A., Van Rijen, P. C., Aarnoutse, E. J., and Ramsey, N. F. (2016b). Fully Implanted Brain-Computer Interface in a Locked-In Patient with ALS. *The New England journal of medicine*, 375(21):2060–2066.

Verstynen, T., Diedrichsen, J., Albert, N., Aparicio, P., and Ivry, R. B. (2005). Ipsilateral Motor Cortex Activity During Unimanual Hand Movements Relates to Task Complexity. *Journal of Neurophysiology*, 93(3):1209–1222.

Wahl, M., Lauterbach-Soon, B., Hattingen, E., Jung, P., Singer, O., Volz, S., Klein, J. C., Steinmetz, H., and Ziemann, U. (2007). Human motor corpus callosum: topography, somatotopy, and link between microstructure and function. *Journal of neuroscience*, 27(45):12132–12138.

Waldert, S., Braun, C., Preissl, H., Birbaumer, N., Aertsen, A., and Mehring, C. (2007). Decoding performance for hand movements: EEG vs. MEG. *Conference proceedings : ... Annual International Conference of the IEEE Engineering in Medicine and Biology Society. IEEE Engineering in Medicine and Biology Society. Annual Conference*, 2007:5346–5348.

Waldert, S., Preissl, H., Demandt, E., Braun, C., Birbaumer, N., Aertsen, A., and Mehring, C. (2008). Hand Movement Direction Decoded from MEG and EEG. *Soc Neuroscience*.

Wang, B. (2018). Openwater Portable MRI will be 1000 times Cheaper with 1 million times the resolution.

Wang, P. T., King, C. E., McCrimmon, C. M., Lin, J. J., Sazgar, M., Hsu, F. P., Shaw, S. J., Millet, D. E., Chui, L. A., Liu, C. Y., Do, A. H., and Nenadic, Z. (2016). Comparison of decoding resolution of standard and high-density electrocorticogram electrodes. *Journal of Neural Engineering*, 13(2):026016.

Wang, Y. and Witten, I. (1999). Pace Regression.

Wang, Z. (2011). Anatomically Constrained Decoding of Finger Flexion from Electrocorticographic Signals. In *Advances in Neural Information Processing Systems 24*, pages 1–9.

Wang, Z., Ji, Q., Miller, K. J., and Schalk, G. (2010). Decoding finger flexion from electrocorticographic signals using a sparse gaussian process. In *Proceedings - International Conference on Pattern Recognition*, pages 3756–3759.

Weibull, A., Björkman, A., Hall, H., Rosén, B., Lundborg, G., and Svensson, J. (2008). Optimizing the mapping of finger areas in primary somatosensory cortex using functional MRI. *Magnetic Resonance Imaging*, 26(10):1342–1351.

Wisneski, K. J., Anderson, N., Schalk, G., Smyth, M., Moran, D., and Leuthardt, E. C. (2008). Unique cortical physiology associated with ipsilateral hand movements and neuroprosthetic implications. *Stroke*, 39(12):3351–3359.

Wissel, T., Pfeiffer, T., Frysch, R., Knight, R. T., Chang, E. F., Hinrichs, H., Rieger, J. W., and Rose, G. (2013). Hidden Markov model and support vector machine based decoding of finger movements using electrocorticography. *Journal of Neural Engineering*, 10(5).

WMA (2013). World Medical Association Declaration of Helsinki: Ethical Principles for Medical Research Involving Human Subjects. *JAMA*, 310(20):2191–2194.

Wolpaw, J. R., Birbaumer, N., McFarland, D. J., Pfurtscheller, G., and Vaughan, T. M. (2002). Brain–computer interfaces for communication and control. *Clinical Neurophysiology*, 113(6):767–791.

Wu, X., Chen, K., Liu, Y., Long, Z., Wen, X., Jin, Z., and Yao, L. (2008). Ipsilateral brain deactivation specific to the nondominant hand during simple finger movements. *Neuroreport*, 19(4):483–486.

Xiao, R. and Ding, L. (2013). Evaluation of EEG Features in Decoding Individual Finger Movements from One Hand. *Computational and Mathematical Methods in Medicine*, 2013:1–10.

Xiao, R. and Ding, L. (2015). EEG resolutions in detecting and decoding finger movements from spectral analysis. *Frontiers in Neuroscience*, 9(SEP).

Xie, Z., Schwartz, O., and Prasad, A. (2018). Decoding of finger trajectory from ECoG using deep learning. *Journal of Neural Engineering*, 15(3):036009.

Yanagisawa, T., Hirata, M., Saitoh, Y., Goto, T., Kishima, H., Fukuma, R., Yokoi, H., Kamitani, Y., and Yoshimine, T. (2011). Real-time control of a prosthetic hand using human electrocorticography signals. *Journal of Neurosurgery*, 114(6):1715–1722.

Yang, Y., Chevallier, S., Wiart, J., and Bloch, I. (2014). Time-frequency optimization for discrimination between imagination of right and left hand movements based on two bipolar electroencephalography channels. *Eurasip Journal on Advances in Signal Processing*, 2014(1).

Yong, L., Xiaorong, G., Hesheng, L., and Shangkai, G. (2004). Classification of Single-Trial Electroencephalogram During Finger Movement. *IEEE Transactions on Biomedical Engineering*, 51(6):1019–1025.

Yousry, T., Schmid, U. D., Alkadhi, H., Schmidt, D., Peraud, A., Buettner, A., and Winkler, P. (1997). Localization of the motor hand area to a knob on the precentral gyrus. A new landmark. *Brain*, 120(1):141–157.

Yu, W. S., van Duinen, H., and Gandevia, S. C. (2009). Limits to the Control of the Human Thumb and Fingers in Flexion and Extension. *Journal of Neurophysiology*, 103(1):278–289.

Yuan, H. and He, B. (2014). Brain-computer interfaces using sensorimotor rhythms: current state and future perspectives. *IEEE transactions on bio-medical engineering*, 61(5):1425–35.

Zang, Y., Jia, F., Weng, X., Li, E., Cui, S., Wang, Y., Hazeltine, E., and Ivry, R. (2003). Functional organization of the primary motor cortex characterized by event-related fMRI during movement preparation and execution. *Neuroscience letters*, 337(2):69–72.

Zanos, S., Miller, K. J., and Ojemann, J. G. (2009). Electrocorticographic spectral changes associated with ipsilateral individual finger and whole hand movement. *2008 30th Annual International Conference of the IEEE Engineering in Medicine and Biology Society*, pages 5939–5942.

A Electrode Grid Layout

P1

8	7	6	5	4	3	2	1
12	11	10	9	52	51	50	49
20	19	18	17	16	15	14	13
24	23	22	21	56	55	54	53
32	31	30	29	28	27	26	25
44	43	42	41	40	39	38	37
36	35	34	33	60	59	58	57
48	47	46	45	64	63	62	61

P2

1	49	13	53	25	57	37	61
2	50	14	54	26	58	38	62
3	51	15	55	27	59	39	63
4	52	16	56	28	60	40	64
5	9	17	21	29	33	34	45
6	10	18	22	30	34	42	46
7	11	19	23	31	35	43	47
8	12	20	24	32	36	44	48

Figure A.1: *Electrode Grid Numbering and Layout for participants P1 and P2. Channels over the CS are depicted in gray, channels over S1 are depicted in blue and channels over M1 are depicted in red. Faulty are depicted in a wave pattern.*

P3

113	114	115	116	117	118	119	120	121	122	123	124	125	126	127	128
97	98	99	100	101	102	103	104	105	106	107	108	109	110	111	112
81	82	83	84	85	86	87	88	89	90	91	92	93	94	95	96
65	66	67	68	69	70	71	72	73	74	75	76	77	78	79	80
49	50	51	52	53	54	55	56	57	58	59	60	61	62	63	64
33	34	35	36	37	38	39	40	41	42	43	44	45	46	47	48
17	18	19	20	21	22	23	24	25	26	27	28	29	30	31	32
1	2	3	4	5	6	7	8	9	10	11	12	13	14	15	16

Figure A.2: *Electrode Grid Numbering and Layout for participant P3. Channels over the CS are depicted in gray, channels over S1 are depicted in blue and channels over M1 are depicted in red. Channels indicated in white are those that fall in neither M1, S1 or the CS. Faulty channels are depicted in a wave pattern.*

P4

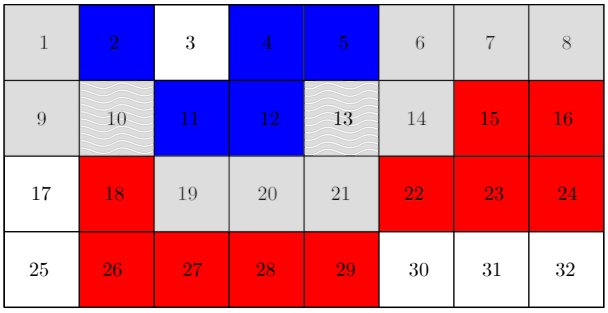

Figure A.3: *Electrode Grid Numbering and Layout for participant P4. Channels over the CS are depicted in gray, channels over S1 are depicted in blue and channels over M1 are depicted in red. Faulty channels are depicted in a wave pattern.*

B Elaboration on Inclusion Criteria

This appendix provides an elaboration on the decisions that were involved in constructing the inclusion criteria. These are summed up per inclusion criterium.

- **Date**: Articles focusing on physiological processes may be older articles, as they portray results about the brain that may not change significantly over time (such as definition of Brodmann areas). To include these articles, no lower boundary on the publication year was set. However, articles related to classification or other computerized methods quickly outdate given the rapid increase of computing power and classification possibilities. Therefore, the choice was made to only include articles from the year 2000.

- **Participants**: Studies that use data acquired from healthy participants are naturally included. Studies with epilepsy patients are expected since much of the ECoG research is performed with participants that required ECoG electrode implantation for the localization of epilepsy foci. Studies with epilepsy participants are therefore included but it is important that task data has not been recorded shortly after or before an epilepsy attack or that the epileptic focus area does not extend to the SMC. Studies handling neurological damage of the cortical matter of interest (resulting from stroke or bleeding for example) should be excluded since these damages may affect patterns of cortical activity and cortical organization. However, studies handling individuals with amputated limbs or individuals with paralysis (such as those who suffer from ALS) are included. A low number of participants is expected for ECoG studies, therefore no lower boundary for the number of participants was set. Non-human primate studies were considered, but it was not known whether the results would generalize and therefore it was decided to exclude those studies

- **Methodology**: The movement during tasks should be measured with a data glove, EMG measurements or similar techniques so that obtained results can be precisely aligned with the movement. Studies with purely qualitative methodologies (free unrecorded movement) will be excluded. Studies that focus solely on bimanual movement were excluded since unimanual movement is researched in this review. Only studies that recorded hand and finger movement were included. However, studies with attempted movement from individuals with amputated limbs or paralysis were included, since studies with these patients were included as defined by the inclusion criterion "participants" above.

- **Language**: This study field was not so small that articles from other languages had to be considered. Therefore, it was decided for the sake of transparency to only include articles written in English.

- **Literature types**: Literature from peer-reviewed (Scopus, Embase, Pubmed, Google Scholar) and non-peer reviewed sources (BioRxiv) were included. The one exception was made for BioRxiv in order to include relevant articles that had not yet been published.

- **Modality**: Articles using ECoG, fMRI, EEG and MEG were included. Studies that combine two or more of the abovementioned modalities were also included and were even highly favorable. Needle electrodes and other techniques such as fNIRS have been considered, but in order to avoid too many comparisons between modalities the focus was lain on these four modalities since it was expected that the majority of publications would use one of these modalities.

C Keyword Combinations with Boolean Operators

Below in Table C.1, the keywords that were used during the literature search are organized and grouped per concept, so that clustered groups of words or separate words can be used to define search queries for the databases with a boolean (OR, AND, NOT) structure.

Concept	**Keywords and Search Terms**
Imaging modality	(Functional magnetic resonance imaging OR fMRI OR MRI) (ECoG, OR electrocorticography) (electroencephalography OR EEG OR iEEG OR intracranial OR EEG) (magnetoencephalography OR MEG)
Cortical areas	(Primary somatosensory cortex OR sensory cortex OR s1 OR postcentral gyrus) (Primary motor cortex OR motor cortex OR m1 OR precentral gyrus) (Sensorimotor cortex OR SMC)
Decoding and Classification	(encoding OR decoding OR classification) (mapping OR somatotopy OR somatotopic OR representation)
Movement	(finger OR hand OR gesture OR unimanual OR movement)
Laterality	(contralateral OR ipsilateral)
Participant type	Human
Study type	Comparing

Table C.1: *Keywords and search terms for the literature search grouped in a boolean structure per concept*

D Search Queries

Including all search terms and bridging all categories with an OR operator				
(functional magnetic resonance imaging OR fmri OR mri) OR (electrocorticography OR ecog) OR (encephalography OR eeg OR ieeg OR intracranial eeg) OR (micro array OR needle) OR (magnetoencephalography OR meg) AND (Primary somatosensory cortex OR sensory cortex OR s1 OR postcentral gyrus) OR (Primary motor cortex OR motor cortex OR m1 OR precentral gyrus) OR (Sensorimotor cortex OR SMC) OR (encoding OR decoding OR classification) OR (mapping OR somatotopy OR somatotopic OR representation) OR (finger OR hand OR gesture OR unimanual) OR (Contralateral AND Ipsilateral)				
Scopus	Pubmed	Embase	Biorxiv	Google Scholar
4,602,818	2,055,920	1,557,773	-	-
Query much too broad and too long for biorxiv and google scholar				

Including all search terms and bridging all categories with an AND operator				
(functional magnetic resonance imaging OR fmri OR mri) OR (electrocorticography OR ecog) OR (encephalography OR eeg OR ieeg OR intracranial eeg) OR (micro array OR needle) OR (magnetoencephalography OR meg) AND (Primary somatosensory cortex OR sensory cortex OR s1 OR postcentral gyrus) AND (Primary motor cortex OR motor cortex OR m1 OR precentral gyrus) AND (Sensorimotor cortex OR SMC) AND (encoding OR decoding OR classification) AND (mapping OR somatotopy OR somatotopic OR representation) AND (finger OR hand OR gesture OR unimanual) AND (Contralateral AND Ipsilateral)				
Scopus	Pubmed	Embase	Biorxiv	Google Scholar
1	0	0	-	-
Query much too narrow and too long for biorxiv and google scholar				

Including all articles which handle finger mapping or classification in any of the brain areas
(functional magnetic resonance imaging OR fmri OR mri) OR (electrocorticography OR ecog) OR (encephalography OR eeg OR ieeg OR intracranial eeg) OR (micro array OR needle) OR (magnetoencephalography OR meg) OR (encoding OR decoding OR classification) OR (mapping OR somatotopy OR somatotopic OR representation) AND (finger OR hand OR gesture OR unimanual) AND (Contralateral AND Ipsilateral) OR (Primary

somatosensory cortex OR sensory cortex OR s1 OR postcentral gyrus) OR (Primary motor cortex OR motor cortex OR m1 OR precentral gyrus) OR (Sensorimotor cortex OR SMC)				
Scopus	Pubmed	Embase	Biorxiv	Google Scholar
3,481	214,294	122,917	-	-
Query much too broad and too long for biorxiv and google scholar				

Including all articles which handle finger mapping and classification in any of the brain areas				
(functional magnetic resonance imaging OR fmri OR mri) OR (electrocorticography OR ecog) OR (encephalography OR eeg OR ieeg OR intracranial eeg) OR (micro array OR needle) OR (magnetoencephalography OR meg) AND (encoding OR decoding OR classification) AND (mapping OR somatotopy OR somatotopic OR representation) AND (finger OR hand OR gesture OR unimanual) AND (Contralateral AND Ipsilateral) OR (Primary somatosensory cortex OR sensory cortex OR s1 OR postcentral gyrus) OR (Primary motor cortex OR motor cortex OR m1 OR precentral gyrus) OR (Sensorimotor cortex OR SMC)				
Scopus	Pubmed	Embase	Biorxiv	Google Scholar
95	214,055	122,523	-	-
Query much too broad and too long for biorxiv and google scholar				

Including all articles which handle finger mapping or classification in the specific brain areas
(functional magnetic resonance imaging OR fmri OR mri) OR (electrocorticography OR ecog) OR (encephalography OR eeg OR ieeg OR intracranial eeg) OR (micro array OR needle) OR (magnetoencephalography OR meg) OR (encoding OR decoding OR classification) OR (mapping OR somatotopy OR somatotopic OR representation) AND (finger OR hand OR gesture OR unimanual) AND (Contralateral AND Ipsilateral) AND (Primary somatosensory cortex OR sensory cortex OR s1 OR postcentral gyrus) AND (Primary motor cortex OR motor cortex OR m1 OR precentral gyrus) OR (Sensorimotor cortex OR SMC)

Scopus	Pubmed	Embase	Biorxiv	Google Scholar
19	16,349	17,345	-	-
Query much too broad and too long for biorxiv and google scholar				

Including all articles which handle finger mapping and classification in the specific brain areas				
(functional magnetic resonance imaging OR fmri OR mri) OR (electrocorticography OR ecog) OR (encephalography OR eeg OR ieeg OR intracranial eeg) OR (micro array OR needle) OR (magnetoencephalography OR meg) AND (encoding OR decoding OR classification) AND (mapping OR somatotopy OR somatotopic OR representation) AND (finger OR hand OR gesture OR unimanual) AND (Contralateral AND Ipsilateral) OR (Primary somatosensory cortex OR sensory cortex OR s1 OR postcentral gyrus) OR (Primary motor cortex OR motor cortex OR m1 OR precentral gyrus) OR (Sensorimotor cortex OR SMC)				
Scopus	Pubmed	Embase	Biorxiv	Google Scholar
95	214,055	122,523	-	-
Query much too broad and too long for biorxiv and google scholar				

Including all articles which handle finger mapping in the specific brain areas				
(functional magnetic resonance imaging OR fmri OR mri) OR (electrocorticography OR ecog) OR (encephalography OR eeg OR ieeg OR intracranial eeg) OR (micro array OR needle) OR (magnetoencephalography OR meg) AND (mapping OR somatotopy OR somatotopic OR representation) AND (finger OR hand OR gesture OR unimanual) AND (Contralateral AND Ipsilateral) AND (Primary somatosensory cortex OR sensory cortex OR s1 OR postcentral gyrus) AND (Primary motor cortex OR motor cortex OR m1 OR precentral gyrus) OR (Sensorimotor cortex OR SMC)				
Scopus	Pubmed	Embase	Biorxiv	Google Scholar

5	16,288	17,500	-	-
Query much too broad and too long for biorxiv and google scholar				

Including all articles which handle decoding in the specific brain areas				
(functional magnetic resonance imaging OR fmri OR mri) OR (electrocorticography OR ecog) OR (encephalography OR eeg OR ieeg OR intracranial eeg) OR (micro array OR needle) OR (magnetoencephalography OR meg) AND (encoding OR decoding OR classification) AND (finger OR hand OR gesture OR unimanual) AND (Contralateral AND Ipsilateral) AND (Primary somatosensory cortex OR sensory cortex OR s1 OR postcentral gyrus) AND (Primary motor cortex OR motor cortex OR m1 OR precentral gyrus) OR (Sensorimotor cortex OR SMC)				
Scopus	Pubmed	Embase	Biorxiv	Google Scholar
1	16,243	17,493	-	-
Query much too broad and too long for biorxiv and google scholar				

All modalities, but only focussing on decoding and classification of movements of contralateral and ipsilateral, not minding the brain regions.				
(functional magnetic resonance imaging OR fmri OR mri) OR (electrocorticography OR ecog) OR (encephalography OR eeg OR ieeg OR intracranial eeg) OR (micro array OR needle) OR (magnetoencephalography OR meg) AND (encoding OR decoding OR classification) AND (finger OR hand OR gesture OR unimanual) AND (Contralateral AND Ipsilateral)				
Scopus	Pubmed	Embase	Biorxiv	Google Scholar
34	39	34	-	-
Query returns a decent number of results, the query is still too long for biorxiv and scholar				

Only ecog and only focussing on decoding and classification of movements of contralateral and ipsilateral, not minding the brain regions.

(electrocorticography OR ecog) AND (encoding OR decoding OR classification) AND (finger OR hand OR gesture OR unimanual) AND (contralateral AND ipsilateral) OR (primary AND somatosensory AND cortex OR sensory AND cortex OR s1 OR postcentral AND gyrus) OR (primary AND motor AND cortex OR motor AND cortex OR m1 OR precentral AND gyrus) OR (sensorimotor AND cortex OR smc)				
Scopus	Pubmed	Embase	Biorxiv	Google Scholar
26	27,094	30,789	-	-
Query returns a decent number of results, the query is still too long for biorxiv and scholar				

Only fmri and only focussing on decoding and classification of movements of contralateral and ipsilateral, not minding the brain regions.				
(functional magnetic resonance imaging OR fmri OR mri) AND (encoding OR decoding OR classification) AND (finger OR hand OR gesture OR unimanual) AND (contralateral AND ipsilateral) OR (primary AND somatosensory AND cortex OR sensory AND cortex OR s1 OR postcentral AND gyrus) OR (primary AND motor AND cortex OR motor AND cortex OR m1 OR precentral AND gyrus) OR (sensorimotor AND cortex OR smc)				
Scopus	Pubmed	Embase	Biorxiv	Google Scholar
77	27,065	30,802	-	-
Query returns a decent number of results, the query is still too long for biorxiv and scholar				

Focusing on the mapping or somatotopy of fingers including all modalities and not specifing brain areas				
mapping OR *somatotopy* OR *representation* AND *finger* AND (*ecog* OR *fmri* OR *mico array* OR *eeg* OR *meg*)				
Scopus	Pubmed	Embase	Biorxiv	Google Scholar
68	313	428	0	48,100
Query returns a decent number of results				

Focusing on the mapping or somatotopy of fingers and hand including all modalities and not specifing brain areas				
mapping OR *somatotopy* OR *representation* AND *finger* OR *hand* AND (*ecog* OR *fmri* OR *mico* AND *array* OR *eeg* OR *meg*)				
Scopus	Pubmed	Embase	Biorxiv	Google Scholar
191	2,826	134	0	140,000
Query returns a decent number of results				

Focusing finger activation on ipsilateral and contralateral including all modalities				
finger AND (ecog OR fmri OR eeg OR meg OR micro AND array) AND ipsilateral AND contralateral				
Scopus	Pubmed	Embase	Biorxiv	Google Scholar
2	2	2	0	7,340
Query returns a decent number of results				

Attempt to look at the difference between contralateral and ipsilateral for the brain areas				
motor cortex AND sensory cortex AND contralateral AND ipsilateral AND finger				
Scopus	Pubmed	Embase	Biorxiv	Google Scholar
69	4	4	11	29,600
Query returns a decent number of results				

Looks at decoding of finger or hand or gestures from any modality, but looking at ipsilateral and contralateral

Decoding OR classification AND finger OR hand OR gesture AND (ecog OR fmri OR eeg OR meg OR electrode array) AND ipsilateral AND contralateral				
Scopus	Pubmed	Embase	Biorxiv	Google Scholar
0	342	468	1	29,600
Query returns a decent number of results				

Strictly decoding or classification focused on ecog and on fingers				
finger AND decoding OR classification AND ecog				
Scopus	Pubmed	Embase	Biorxiv	Google Scholar
65	284	933	17	5,360

Decoding of fingers with any modality but including ipsilateral and contralateral				
finger AND decoding OR classification AND ecog OR fmri OR eeg OR needle OR micro array OR meg) AND ipsilateral AND contralateral				
Scopus	Pubmed	Embase	Biorxiv	Google Scholar
0	1387	2052	0	12,200

Classification or decoding with any technique but including the terms of the brain areas				
finger AND decoding OR classification AND ecog OR fmri OR eeg OR needle OR micro array OR meg AND ipsilateral AND contralateral AND sensory cortex AND motor cortex				
Scopus	Pubmed	Embase	Biorxiv	Google Scholar

0	9	10	4	4,220

Classification or decoding with any technique but including the terms of the brain areas				
(*functional* AND *magnetic* AND *resonance* AND *imaging* OR *fmri* OR *mri* OR *electrocorticography* OR *ecog* OR *encephalography* OR *eeg* OR *ieeg* OR *intracranial* AND *eeg* OR *micro* AND *array* OR *needle* OR *magnetoencephalography* OR *meg*) AND (*encoding* OR *decoding* OR *classification*) AND (*finger* OR *hand* OR *gesture*)				
Scopus	Pubmed	Embase	Biorxiv	Google Scholar
2	129	160	-	4,220

E Classification Attempts in Literature

Author	Modality	Task	Features	Classifier
Contralateral Hand	(Li et al., 2017) (Branco et al., 2018a) (Pan et al., 2018) (Branco et al., 2017) (Bundy et al., 2016) (Fifer et al., 2011) (Jiang et al., 2018) (Chestek et al., 2013) (Bleichner et al., 2016) (Talakoub et al., 2017)	(Bleichner et al., 2014)	(Waldert et al., 2007) (Flint et al., 2017) (Waldert et al., 2008)	(Waldert et al., 2008)
Contralateral Fingers	(Liang and Bougrain, 2012) (Saa et al., 2018) (Flamary and Rakotomamonjy, 2012) (Yang et al., 2014) (Elango et al., 2017) (Nakanishi et al., 2014) (Elghrabawy and Wahed, 2012) (Hazrati and Hofmann, 2012) (Wang et al., 2010) (Kubánek et al., 2009) (Wang, 2011) (Bougrain et al., 2009) (Chen et al., 2014) (Xie et al., 2018) (Elgharabawy and Wahed, 2017) (Marjaninejad et al., 2017) (Samiee et al., 2010) (Delgado Saa et al., 2016) (Shenoy et al., 2007) (Hotson et al., 2016) (Acharya et al., 2010) (Yanagisawa et al., 2011) (Wissel et al., 2013) (Liao et al., 2007)	(Nambu et al., 2015) (Formaggio et al., 2008) (Shen et al., 2014)	(Xiao and Ding, 2015) (Quandt et al., 2012) (Liao et al., 2014)	-
Ipsilateral Hand	-	-	-	-
Ipsilateral Fingers	(Liu and Sharma, 2010) (Non-Reproducible Results)	-	-	-
Contralateral and Ipsilateral Hands	(Jin et al., 2016) (Fujiwara et al., 2017)	-	(Cho et al., 2004)	-
Contralateral and Ipsilateral Fingers	(Scherer et al., 2009)	(Diedrichsen et al., 2013)	(Pires et al., 2007) (Liao et al., 2007)	(Kauhanen et al., 2006)

Table E.1: *Overview of literature handling decoding of hand and finger movements sorted per category and per measurement modality*

F Visualizations of Conjoined Movements

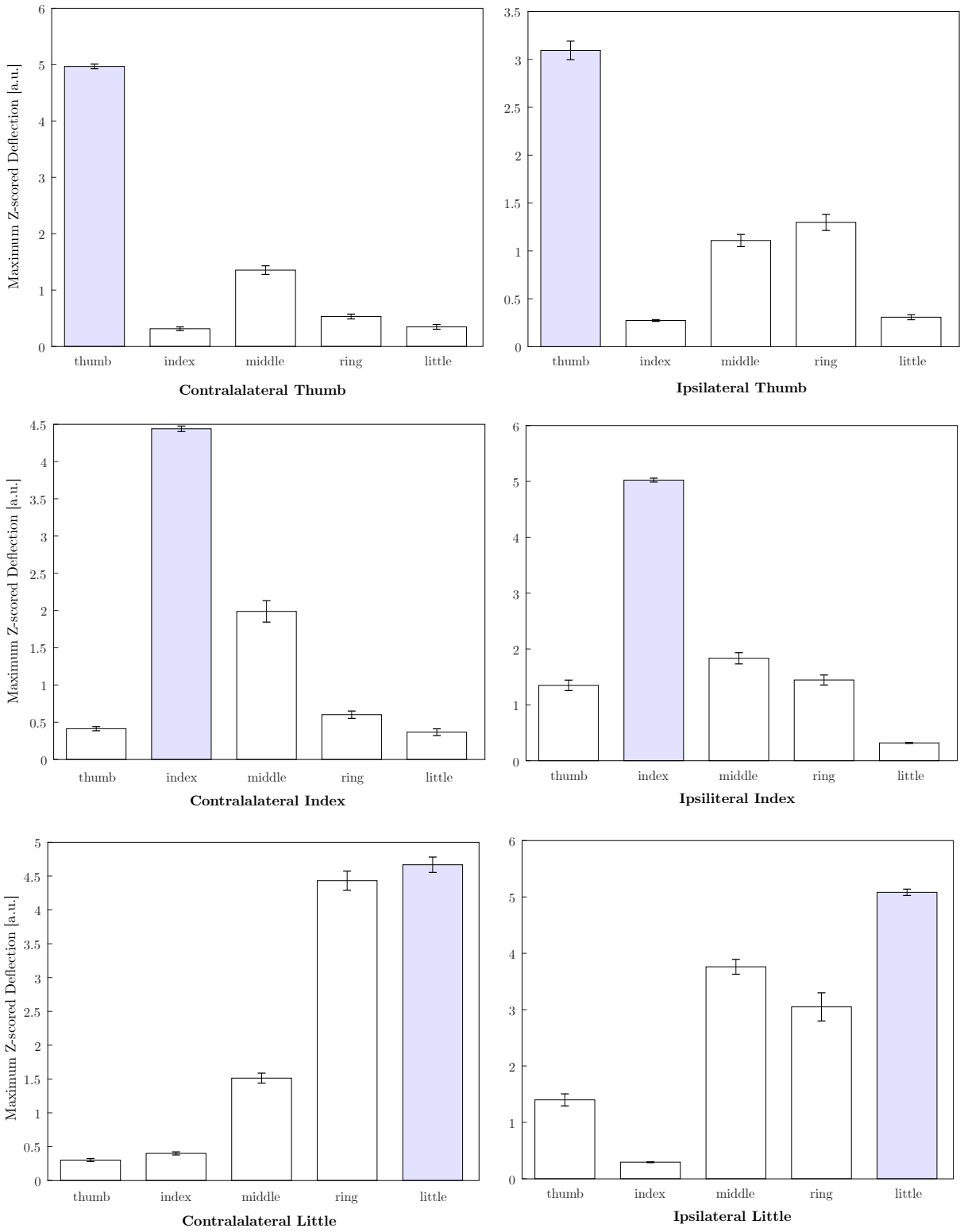

Figure F.1: *The amount of conjoined movement of non-cued fingers during movement of a cued finger for participant P1.*

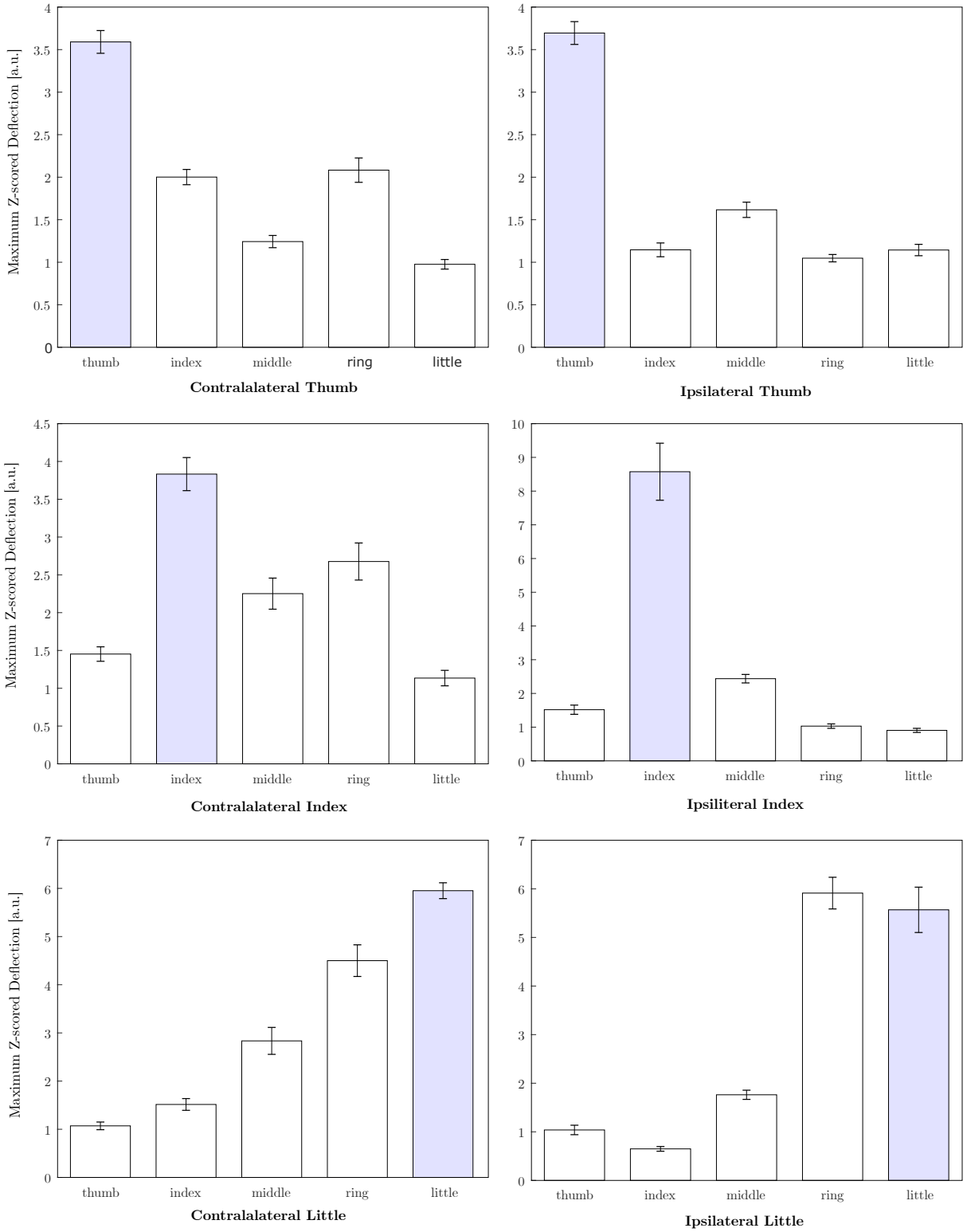

Figure F.2: *The amount of conjoined movement of non-cued fingers during movement of a cued finger for participant P2.*

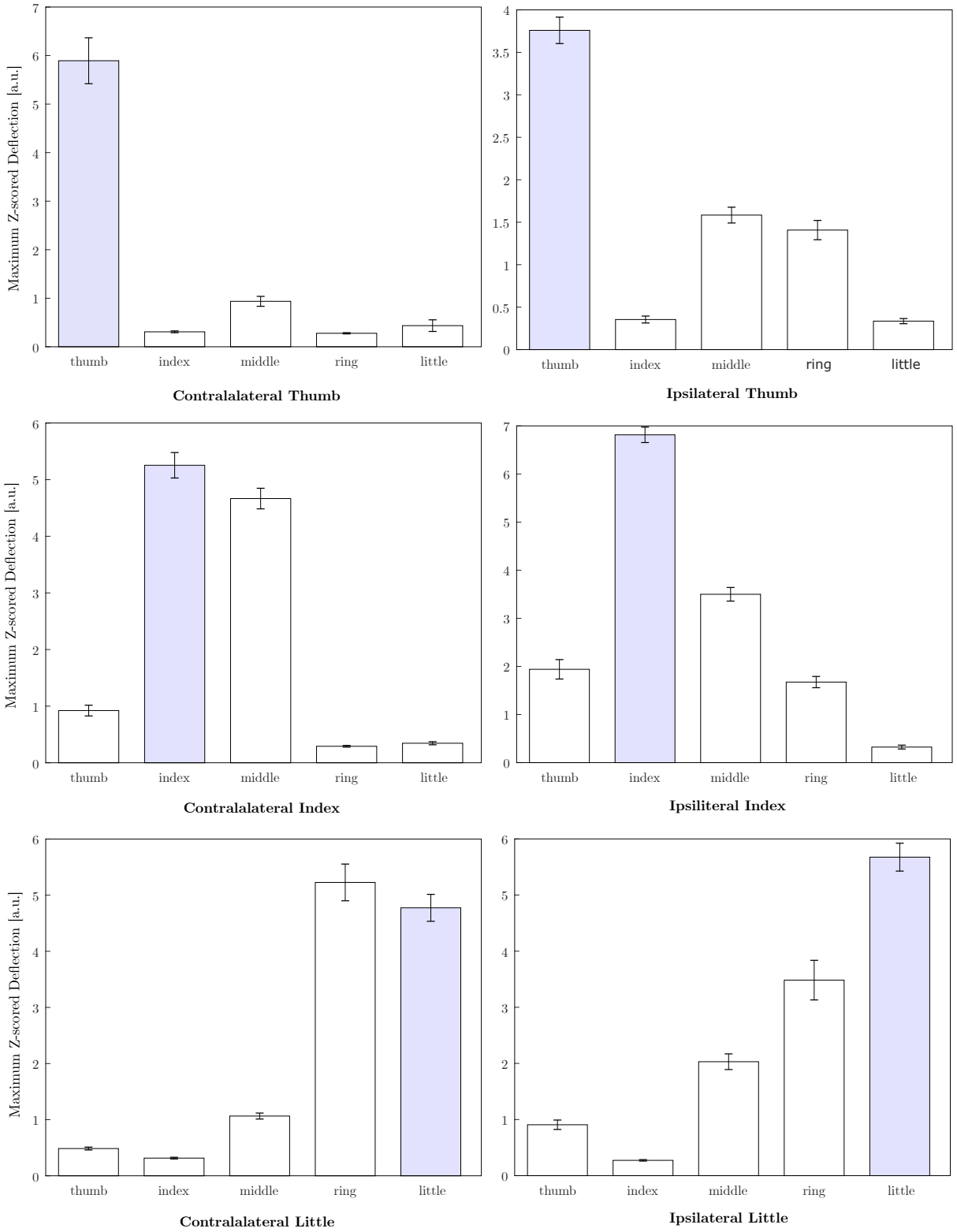

Figure F.3: *The amount of conjoined movement of non-cued fingers during movement of a cued finger for participant P3.*

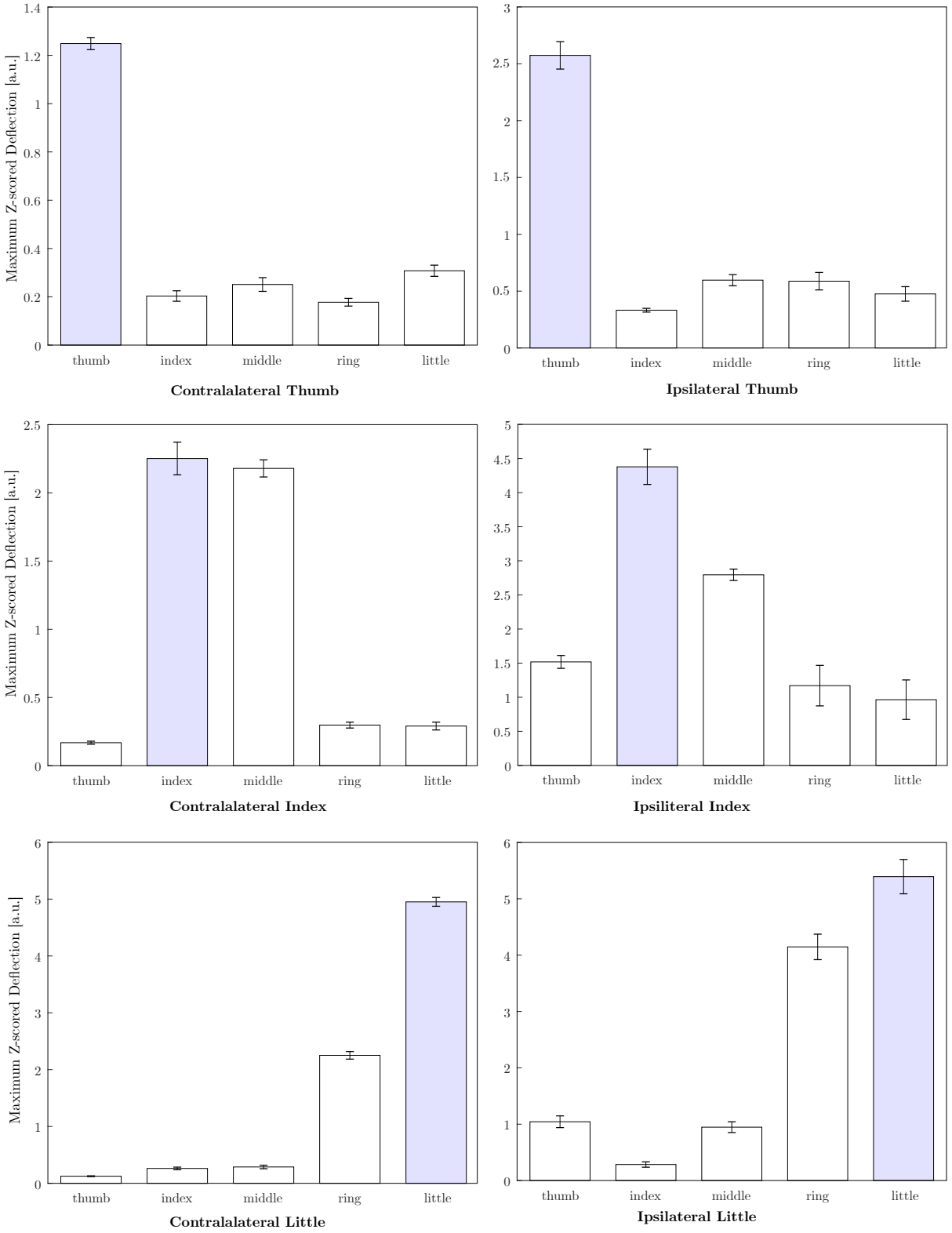

Figure F.4: *The amount of conjoined movement of non-cued fingers during movement of a cued finger for participant P4.*

G ANOVA Comparison of Conjoined Movements

For the ANOVA test, the H_0 hypothesis denoted that the means of the maximum movement amplitudes of the cued finger and the specific non-cued finger was equal ($\mu_{cued} = \mu_{non-cued}$. If the H_0 hypothesis could be rejected, the alternative hypothesis H_a could be accepted, which denoted that the movement amplitude of the cued finger was significantly larger than that of the non-cued finger. The significance level was set at α <0.01 and was Bonferroni corrected for multiple comparisons between the fingers.

Subj.	**Cued**	**CT**	**CI**	**CM**	**CR**	**CL**	**IT**	**II**	**IM**	**IR**	**IL**
1	CT	-	< 0.01	< 0.01	< 0.01	< 0.01	-	-	-	-	-
	CI	< 0.01	-	< 0.01	< 0.01	< 0.01	-	-	-	-	-
	CL	< 0.01	< 0.01	< 0.01	**0.6355**	-	-	-	-	-	-
	IT	-	-	-	-	-	-	< 0.01	< 0.01	< 0.01	< 0.01
	II	-	-	-	-	-	< 0.01	-	< 0.01	< 0.01	< 0.01
	IL	-	-	-	-	-	< 0.01	< 0.01	< 0.01	< 0.01	-
2	CT	-	< 0.01	< 0.01	< 0.01	< 0.01	-	-	-	-	-
	CI	< 0.01	-	< 0.01	< 0.01	< 0.01	-	-	-	-	-
	CL	< 0.01	< 0.01	< 0.01	< 0.01	-	-	-	-	-	-
	IT	-	-	-	-	-	-	< 0.01	< 0.01	< 0.01	< 0.01
	II	-	-	-	-	-	< 0.01	-	< 0.01	< 0.01	< 0.01
	IL	-	-	-	-	-	< 0.01	< 0.01	< 0.01	< 0.01	-
3	CT	-	< 0.01	< 0.01	< 0.01	< 0.01	-	-	-	-	-
	CI	< 0.01	-	**0.0283**	< 0.01	< 0.01	-	-	-	-	-
	CL	< 0.01	< 0.01	**0.832**	< 0.01	-	-	-	-	-	-
	IT	-	-	-	-	-	-	< 0.01	< 0.01	< 0.01	< 0.01
	II	-	-	-	-	-	< 0.01	-	< 0.01	< 0.01	< 0.01
	IL	-	-	-	-	-	< 0.01	< 0.01	< 0.01	< 0.01	-
4	CT	-	< 0.01	< 0.01	< 0.01	< 0.01	-	-	-	-	-
	CI	< 0.01	-	**1.0000**	< 0.01	< 0.01	-	-	-	-	-
	CL	< 0.01	< 0.01	< 0.01	< 0.01	-	-	-	-	-	-
	IT	-	-	-	-	-	-	< 0.01	< 0.01	< 0.01	< 0.01
	II	-	-	-	-	-	< 0.01	-	< 0.01	< 0.01	< 0.01
	IL	-	-	-	-	-	< 0.01	< 0.01	< 0.01	< 0.01	-

Table G.1: P-values of the one-way ANOVA between the cued finger and non-cued fingers. The abbreviations for the fingers are defined as Contralateral thumb (CT), Contralateral Index (CI), Contralateral Middle (CM), Contralateral Ring (CR), Contralateral Little (CL), Ipsilateral Thumb (IT), Ipsilateral Index (II), Ipsilateral Middle (IM), Ipsilateral Ring (IR) and Ipsilateral Little (IL) The "cued" column shows which finger was cued and the columns following it show with which finger the one-way ANOVA comparison was performed. Note that the dataglove was only placed on one hand during the contralateral and ipsilateral tasks and therefore, contralateral and ipsilateral fingers could not be compared. If the the p-value was smaller than $1x10^{-4}$, it is noted in this table as < 0.01. P-values that were larger than the confidence value α of 0.01 are indicated in bold.

H Visualizations of the $\mathbf{Z}_{\mathbf{P}_{v,\overline{Tv},\overline{B}}}$ Spectral Power Modulations

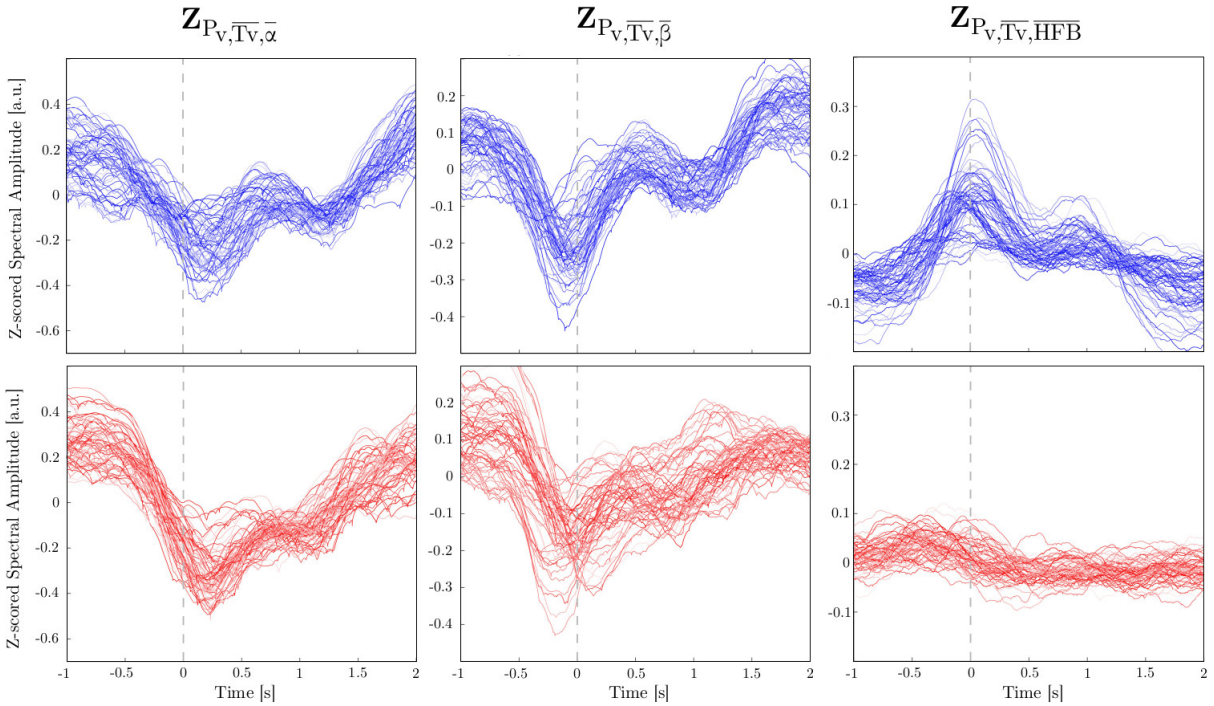

Figure H.1: *Visualization of the spectral modulations represented by* $\mathbf{Z}_{\mathbf{P}_{v,\overline{Tv},\overline{B}}}$ *in the* α*,* β *and HFB frequency bands during movement of the index finger performed by participant P1. Modulations resulting from contralateral index finger movement are depicted in blue and modulations resulting from ipsilateral index finger movement are depicted in red. Each separate line denotes the signal of one channel. The dashed gray lines at t=0 seconds denote the movement marker position. This Figure caption holds for the following figures in this Appendix, which show the results for the other participants.*

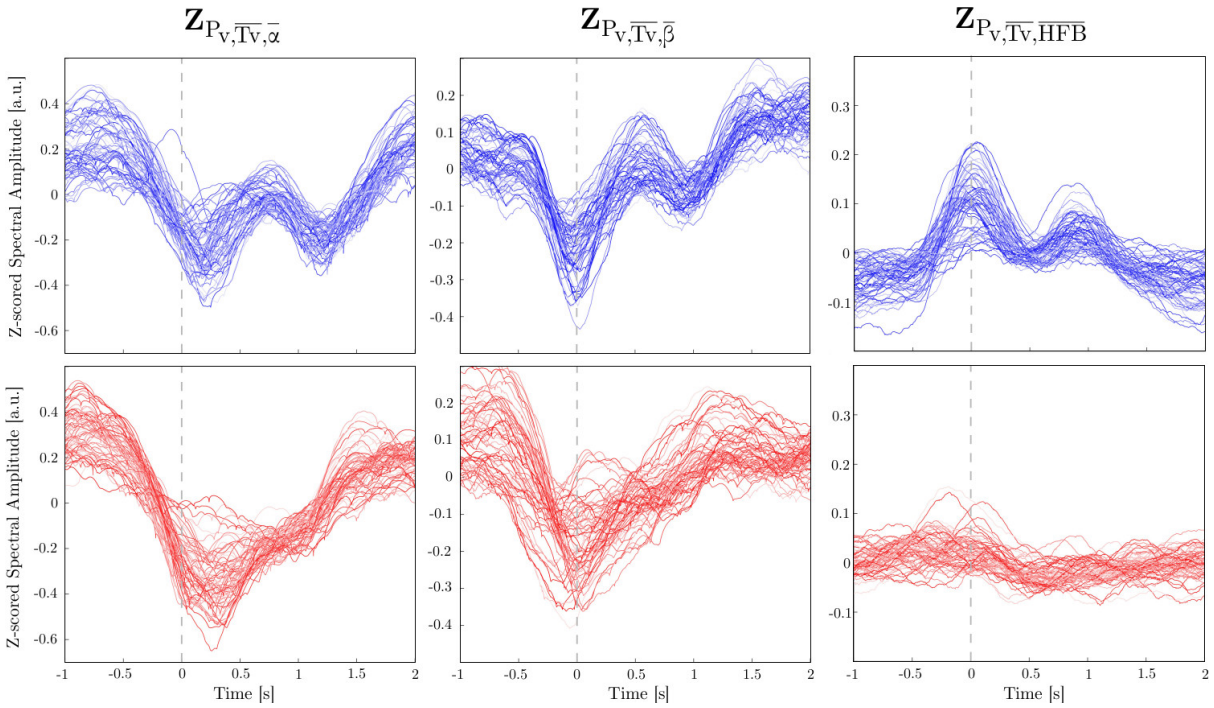

Figure H.2: *Visualization of the spectral modulations represented by* $\mathbf{Z}_{\mathbf{P}_{v,\overline{Tv},\overline{B}}}$ *in the* α*,* β *and HFB frequency bands during movement of the little finger performed by participant P1.*

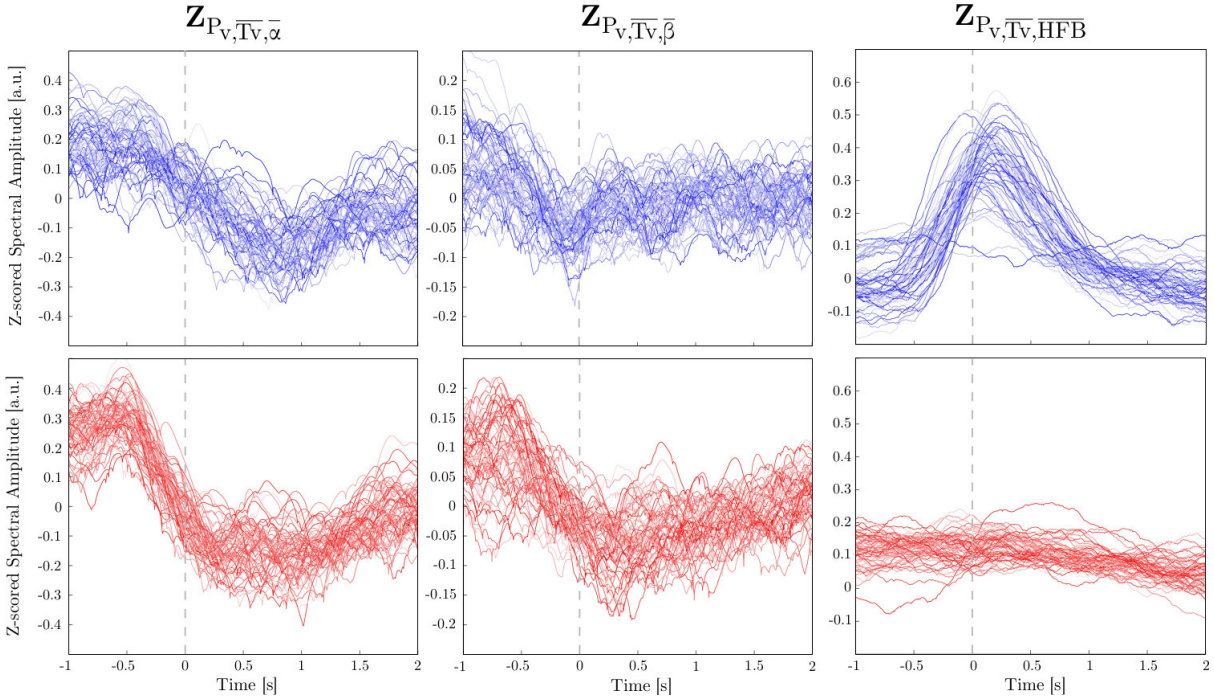

Figure H.3: *Visualization of the spectral modulations represented by* $\mathbf{Z}_{\mathbf{P}_{v,\overline{Tv},\overline{B}}}$ *in the* α*,* β *and HFB frequency bands during movement of the thumb performed by participant P2.*

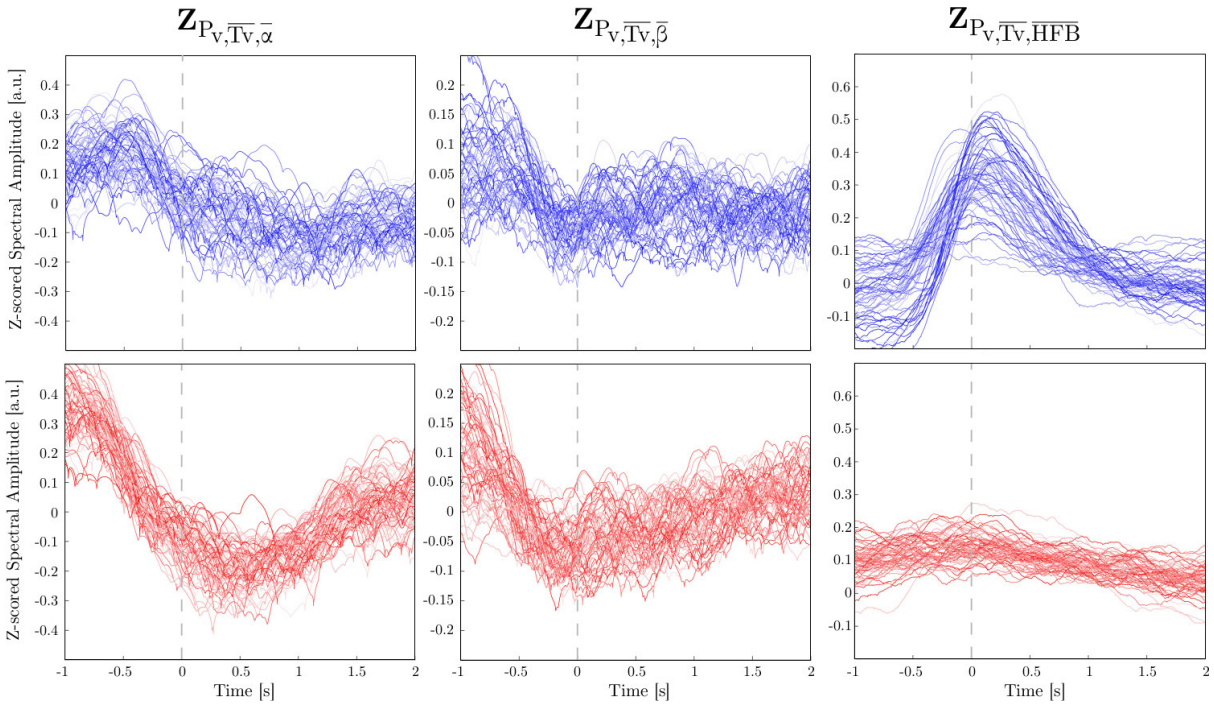

Figure H.4: *Visualization of the spectral modulations represented by* $\mathbf{Z}_{\mathbf{P}_{v,\overline{Tv},\overline{B}}}$ *in the* α*,* β *and HFB frequency bands during movement of the index finger performed by participant P2.*

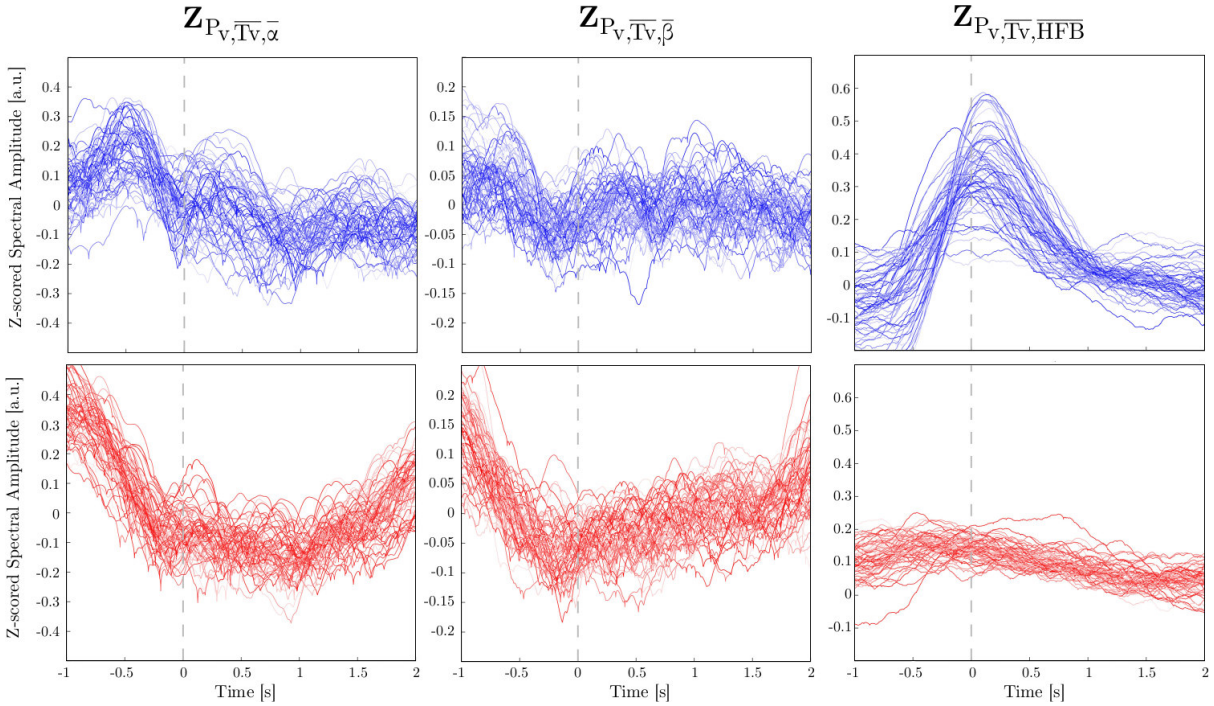

Figure H.5: *Visualization of the spectral modulations represented by* $\mathbf{Z}_{\mathbf{P}_{v,\overline{Tv},\overline{B}}}$ *in the* α*,* β *and HFB frequency bands during movement of the little finger performed by participant P2.*

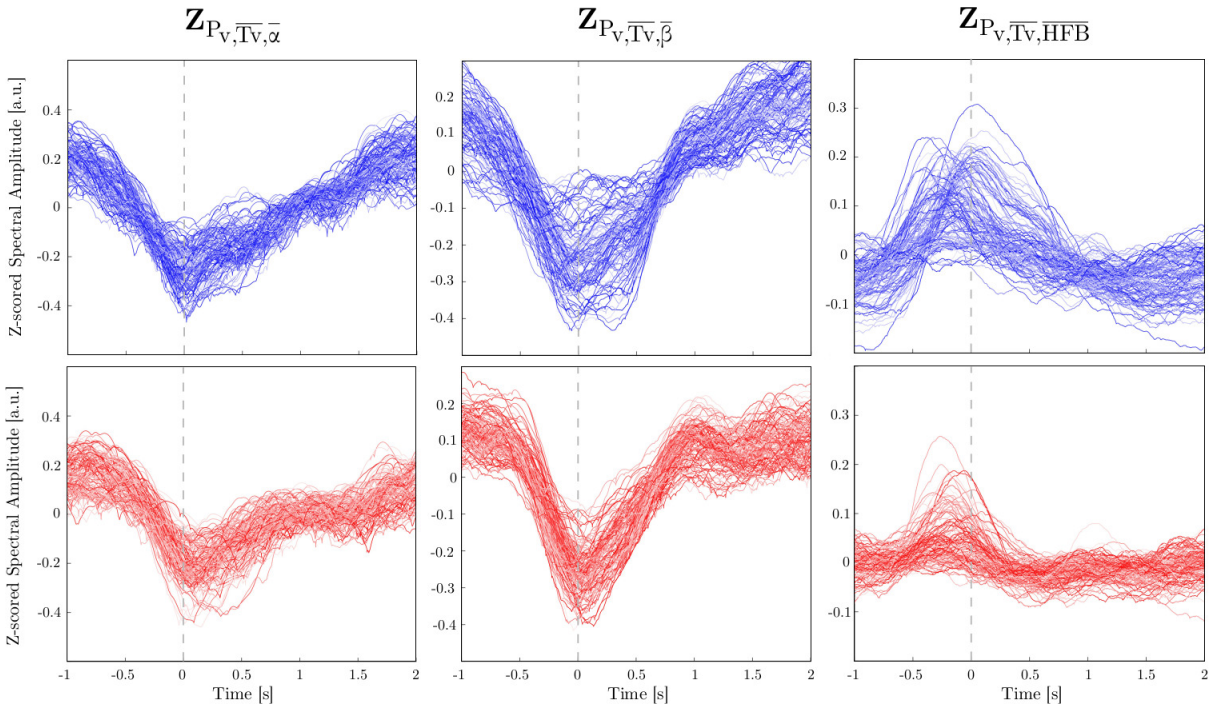

Figure H.6: *Visualization of the spectral modulations represented by* $\mathbf{Z}_{\mathbf{P}_{v,\overline{Tv},\overline{B}}}$ *in the* α*,* β *and HFB frequency bands during movement of the thumb performed by participant P3.*

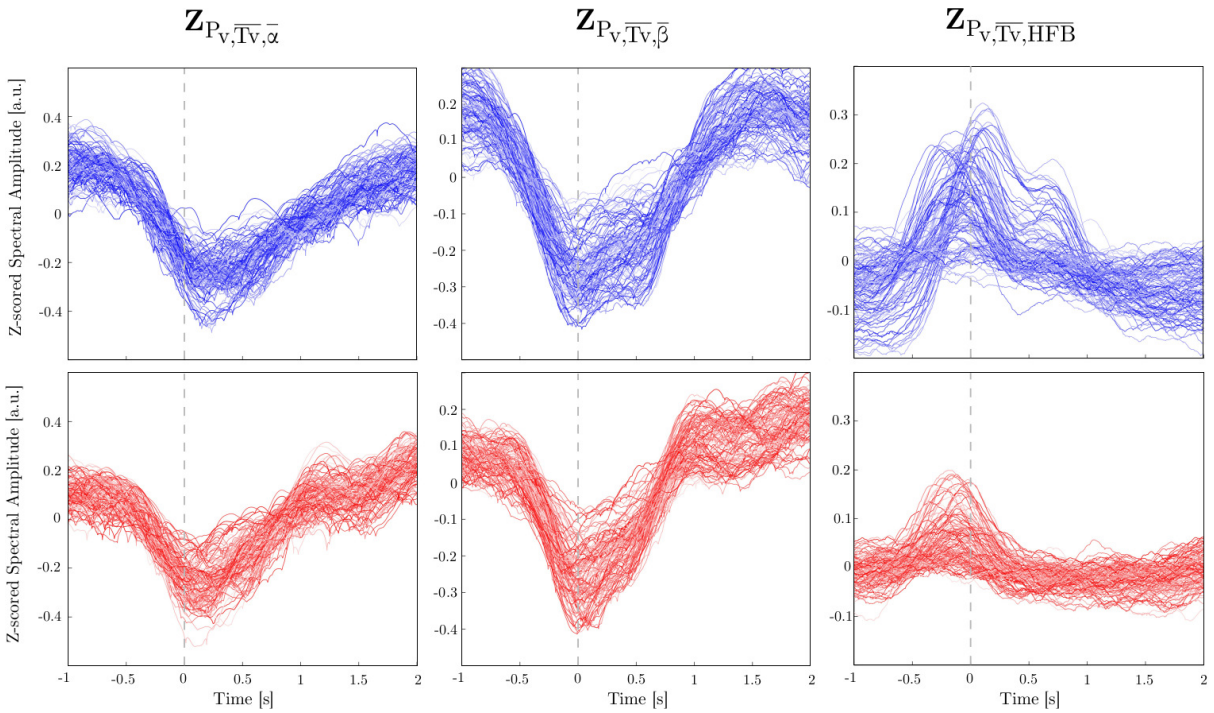

Figure H.7: *Visualization of the spectral modulations represented by* $\mathbf{Z}_{\mathbf{P}_{v,\overline{Tv},\overline{B}}}$ *in the* α*,* β *and HFB frequency bands during movement of the index finger performed by participant P3.*

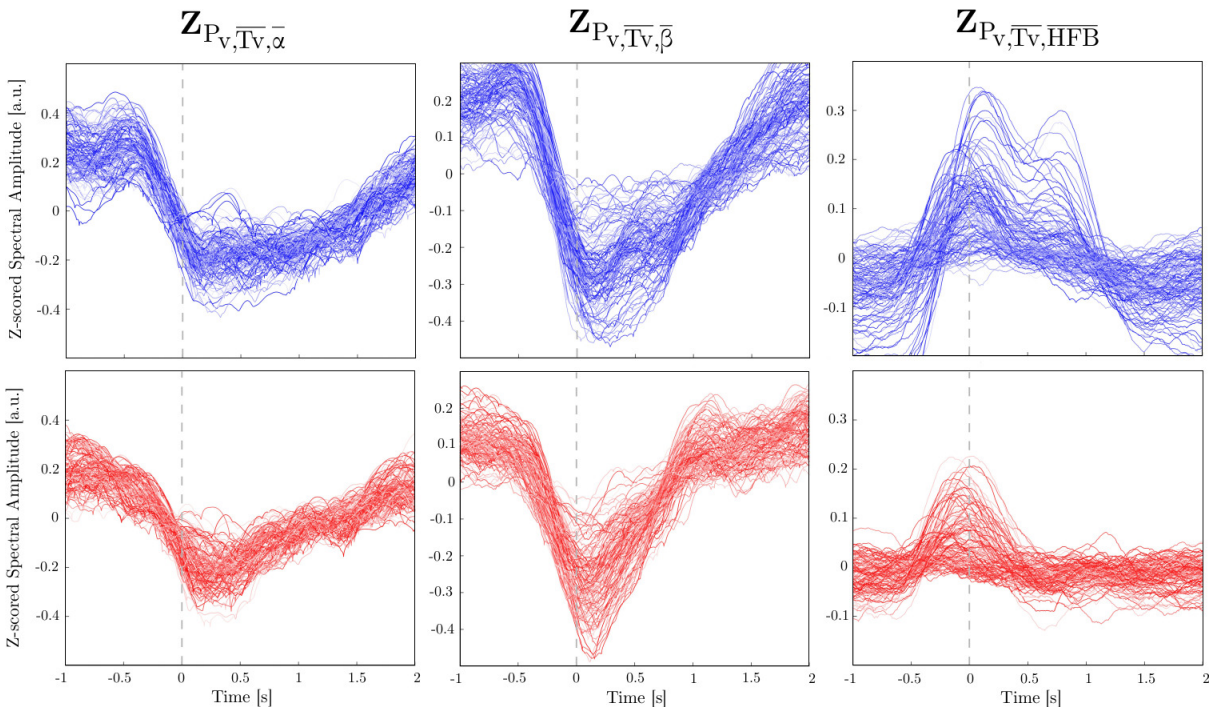

Figure H.8: *Visualization of the spectral modulations represented by* $\mathbf{Z}_{\mathbf{P}_{v,\overline{Tv},\overline{B}}}$ *in the* α*,* β *and HFB frequency bands during movement of the little finger performed by participant P3.*

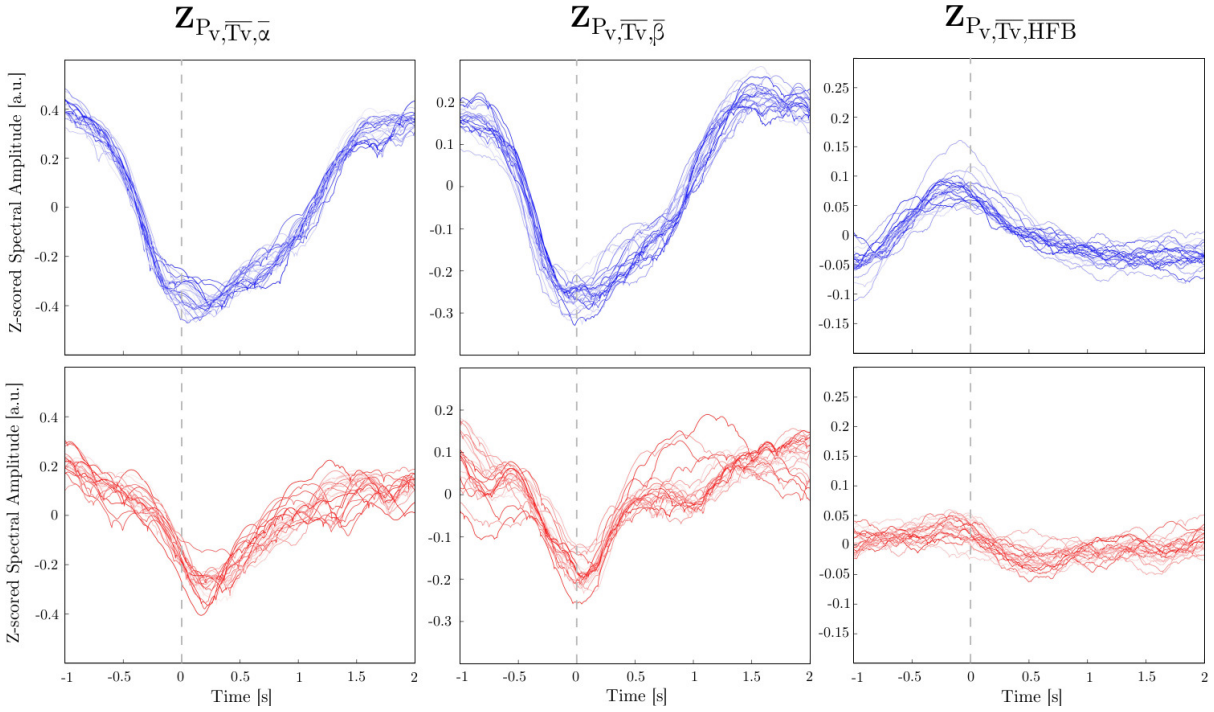

Figure H.9: *Visualization of the spectral modulations represented by* $\mathbf{Z}_{\mathbf{P}_{v,\overline{Tv},\overline{B}}}$ *in the* α*,* β *and HFB frequency bands during movement of the thumb performed by participant P4.*

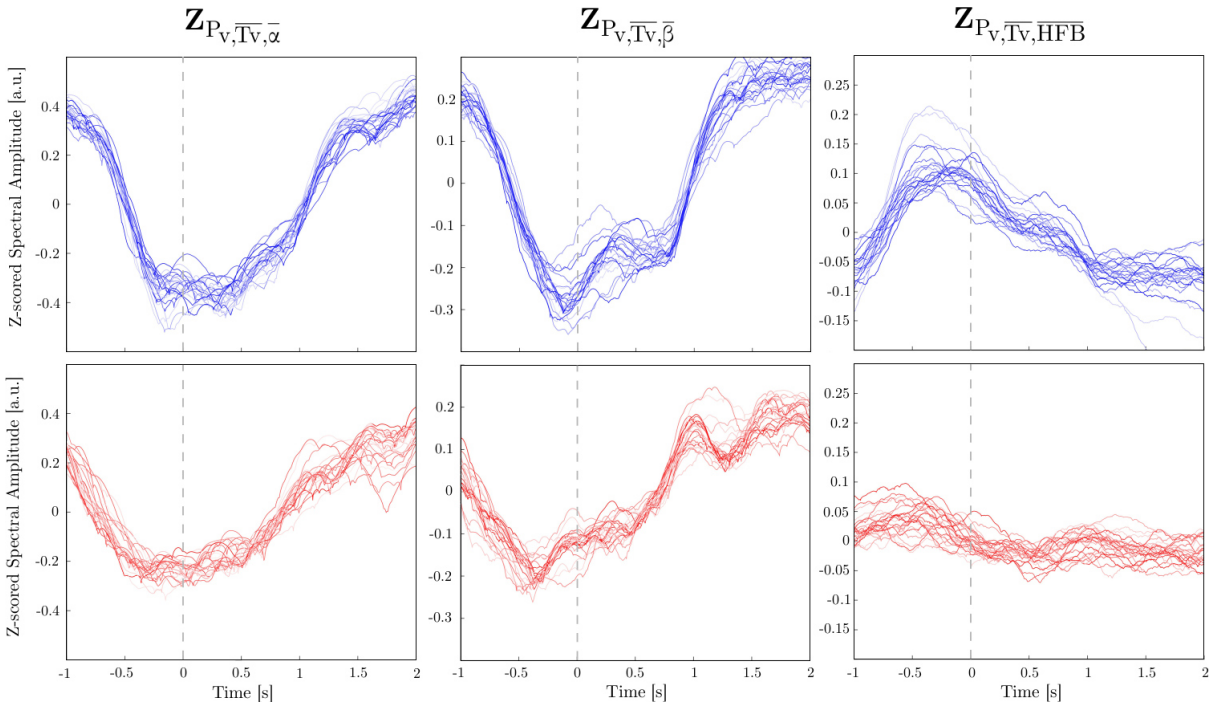

Figure H.10: *Visualization of the spectral modulations represented by* $\mathbf{Z}_{\mathbf{P}_{v,\overline{Tv},\overline{B}}}$ *in the* α*,* β *and HFB frequency bands during movement of the index finger performed by participant P4.*

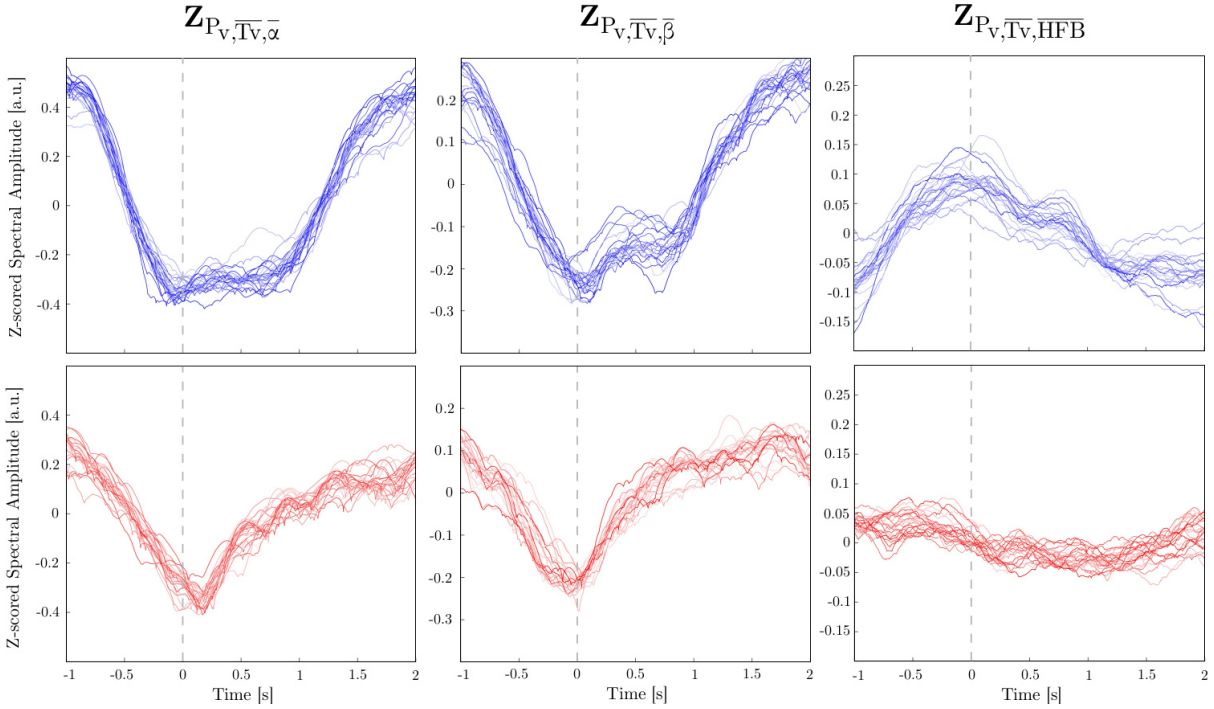

Figure H.11: *Visualization of the spectral modulations represented by* $\mathbf{Z}_{\mathbf{P}_{v,\overline{Tv},\overline{B}}}$ *in the* α*,* β *and HFB frequency bands during movement of the little finger performed by participant P4.*

I Visualizations of the $\mathbf{Z_P}_{v,\overline{Tv},\overline{B},\overline{E_f}}$ Spectral Power Modulations

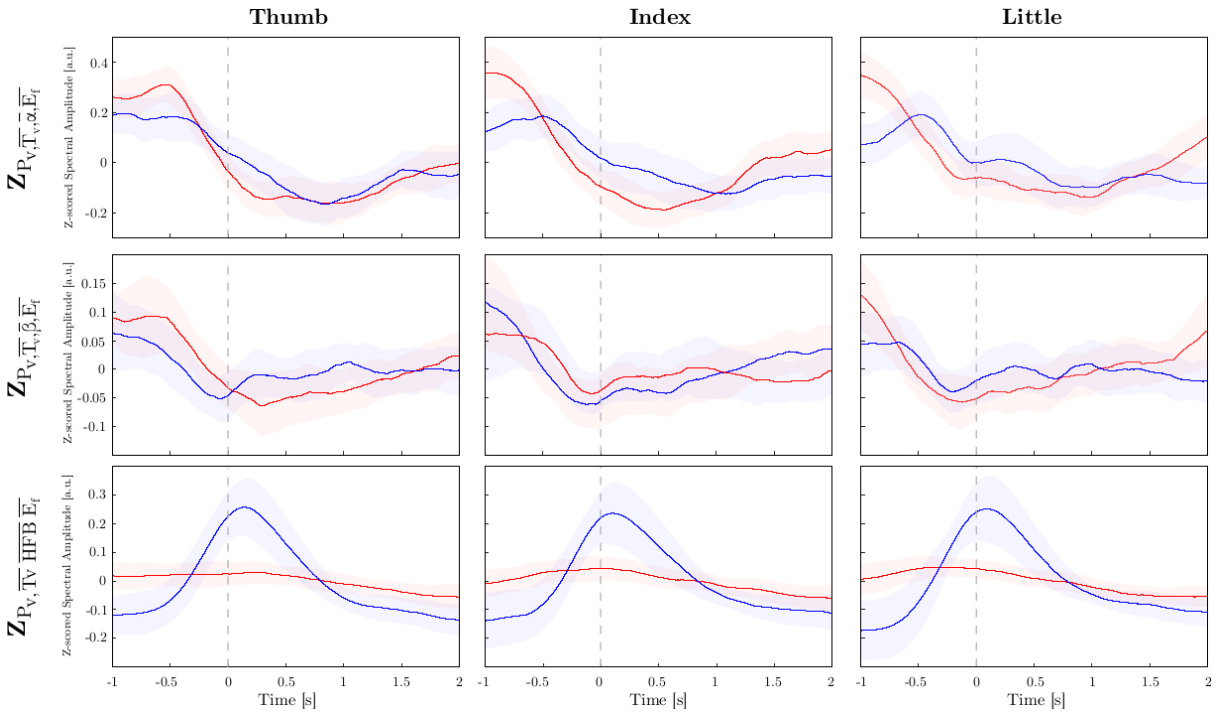

Figure I.1: *Visualization of the spectral modulations of* $\mathbf{Z}_{\mathbf{P}_{v,\overline{Tv},\overline{B},\overline{E_f}}}$ *in the* α*,* β *and HFB frequency bands during movement of the thumb, index and little finger performed by participant P2. Modulations during contralateral finger movement are depicted in blue and modulations during ipsilateral finger movement are depicted in red. The solid lines denote the grand average signal and the shaded areas show the standard deviation of the signal. The dashed gray lines at t=0 seconds denote the movement marker positions. This caption holds for the other figures in this Appendix, which denote the results for the other participants.*

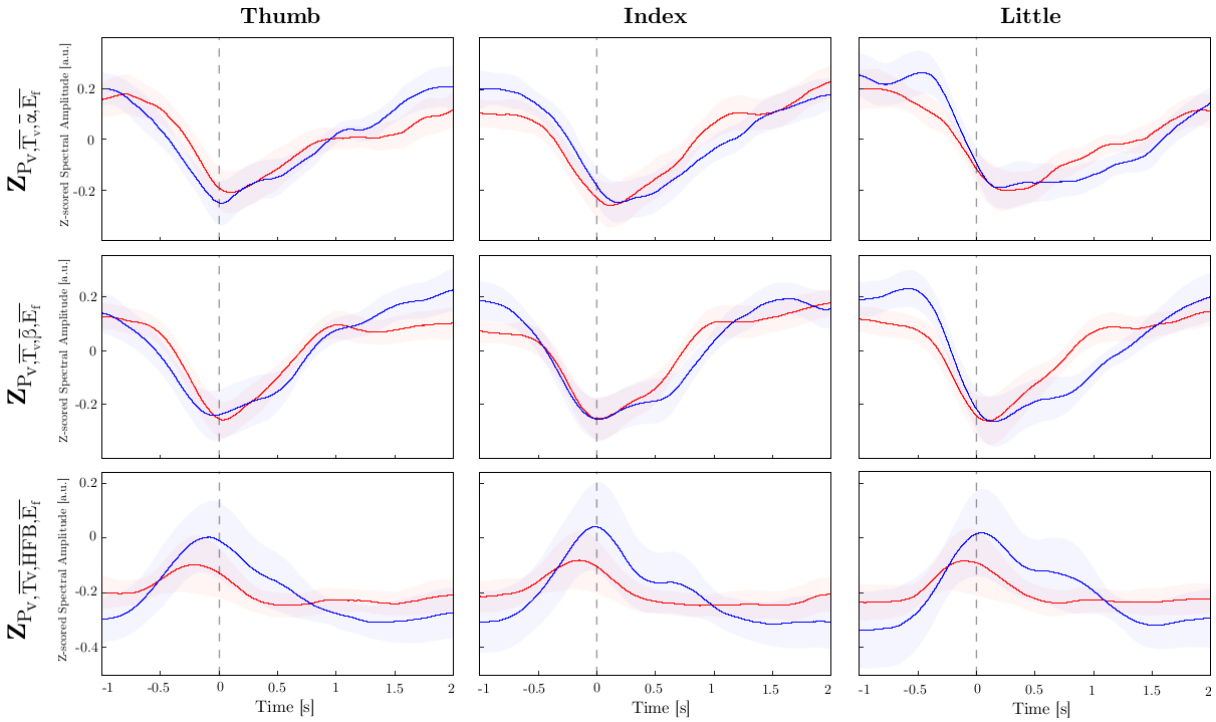

Figure I.2: *Visualization of the spectral modulations of* $\mathbf{Z}_{\mathbf{P}_{v,\overline{Tv},\overline{B},\overline{E_f}}}$ *in the* α*,* β *and HFB frequency bands for participant P3.*

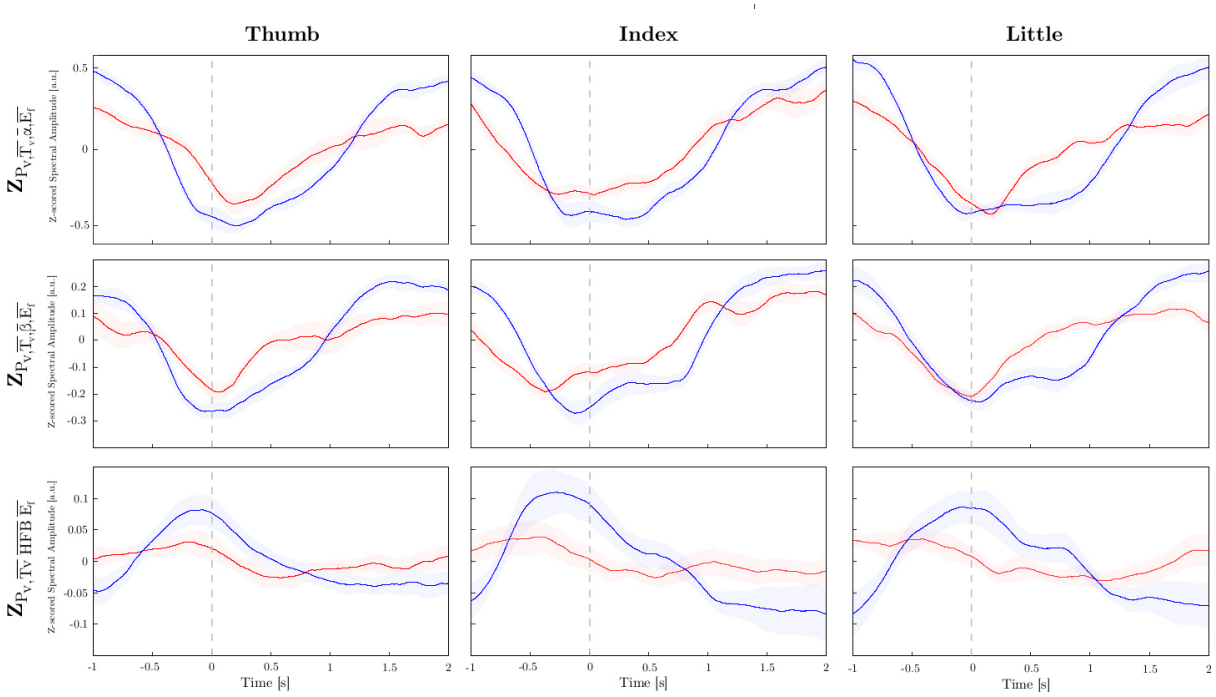

Figure I.3: *Visualization of the spectral modulations of* $\mathbf{Z}_{\mathbf{P}_{v,\overline{Tv},\overline{B},\overline{E_f}}}$ *in the* α*,* β *and HFB frequency bands for participant P4.*

J Channel R^2 Values in the α and β Bands

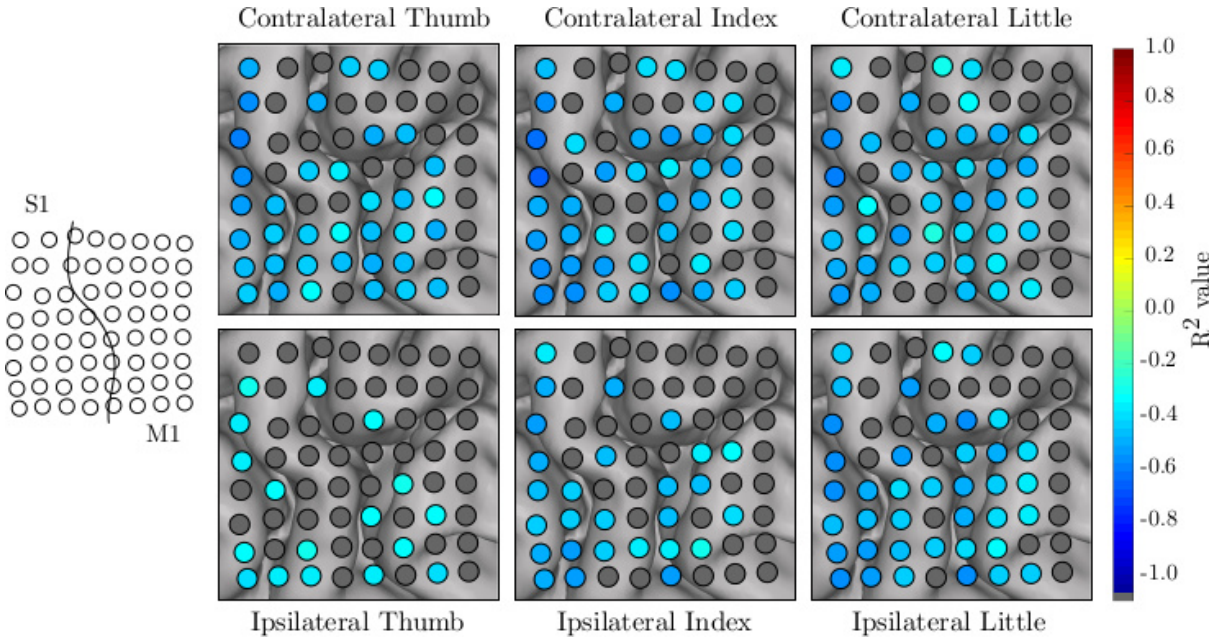

Figure J.1: *Visualization of channel R^2 Values in the α band for Participant P1. Channels that showed no significant cortical activity as well as faulty channels are denoted in gray. This Figure caption holds for the other figures in this Appendix.*

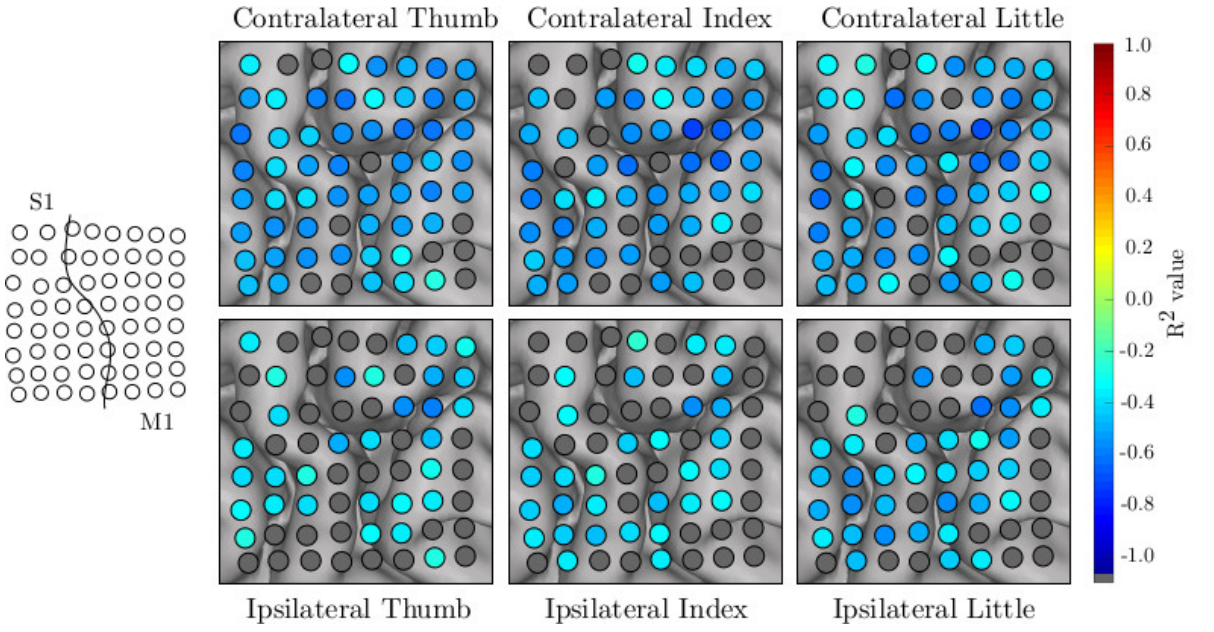

Figure J.2: *Visualization of channel R^2 Values in the β band for Participant P1.*

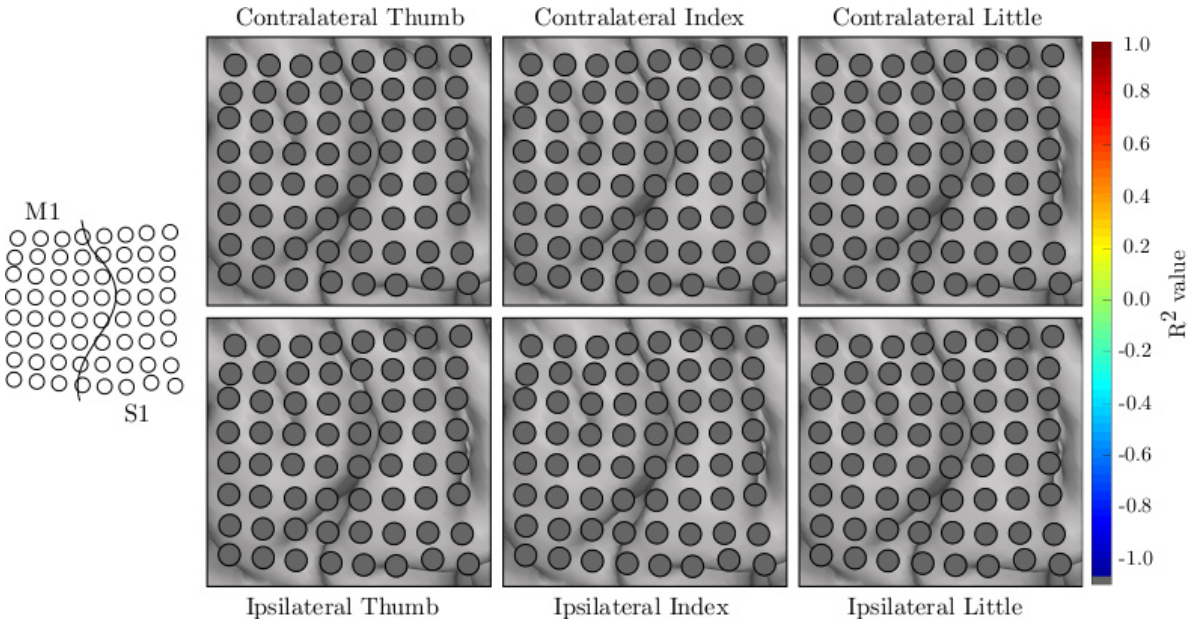

Figure J.3: *Visualization of channel R^2 Values in the α band for Participant P2.*

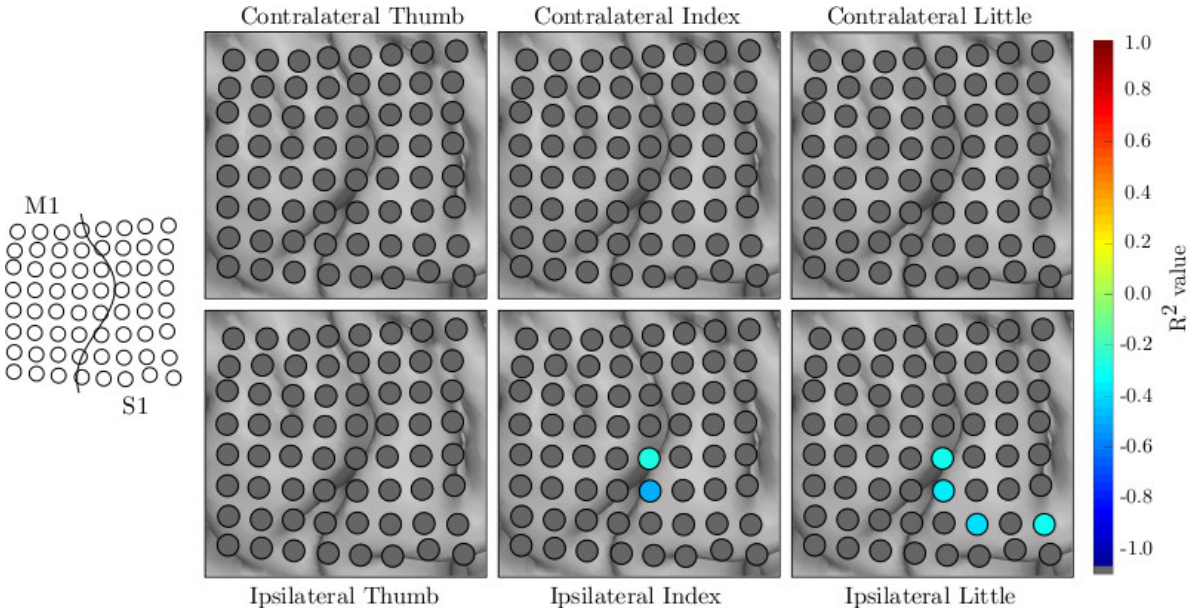

Figure J.4: *Visualization of channel R^2 Values in the β band for Participant P2.*

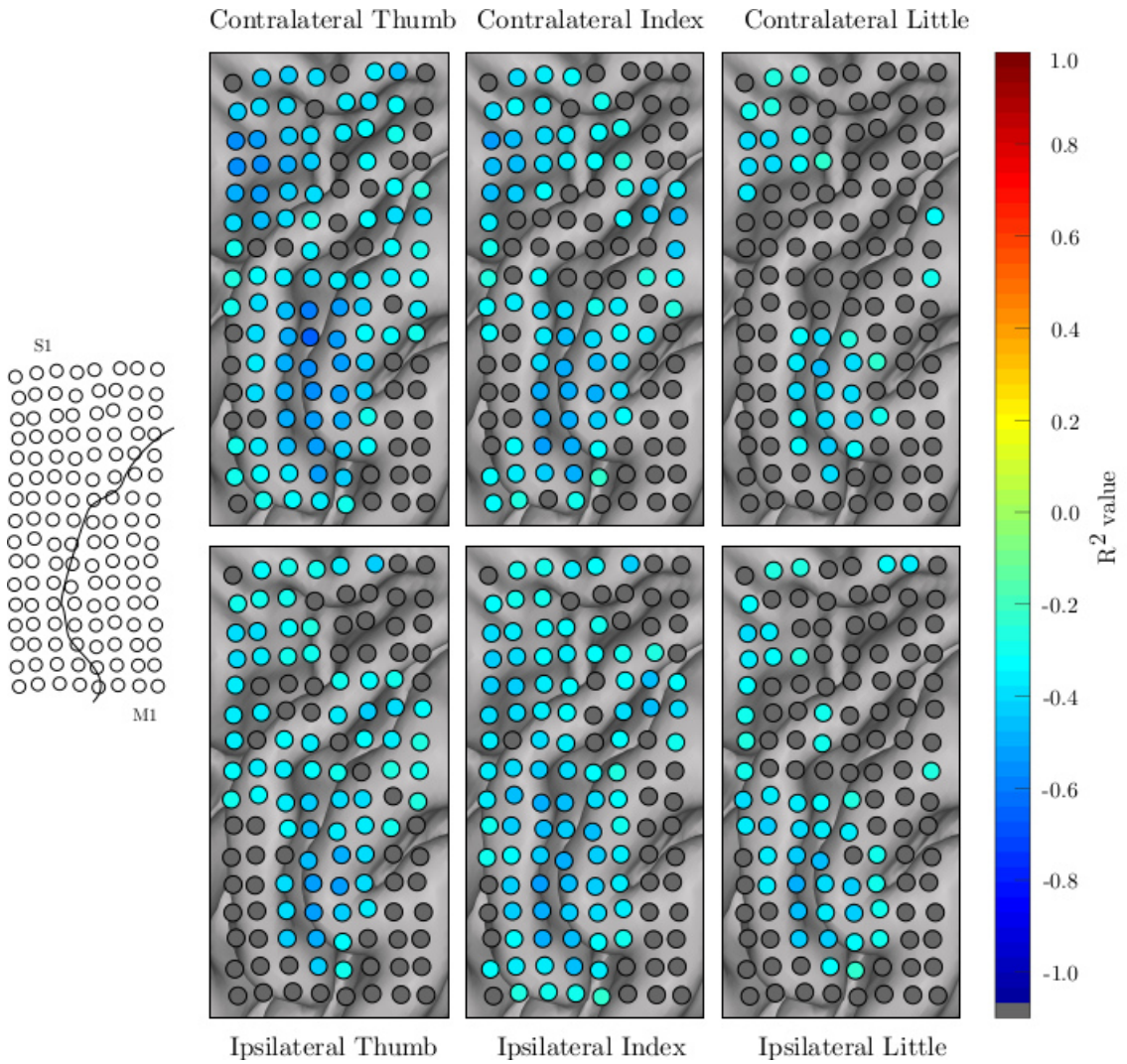

Figure J.5: *Visualization of channel R^2 Values in the α band for Participant P3.*

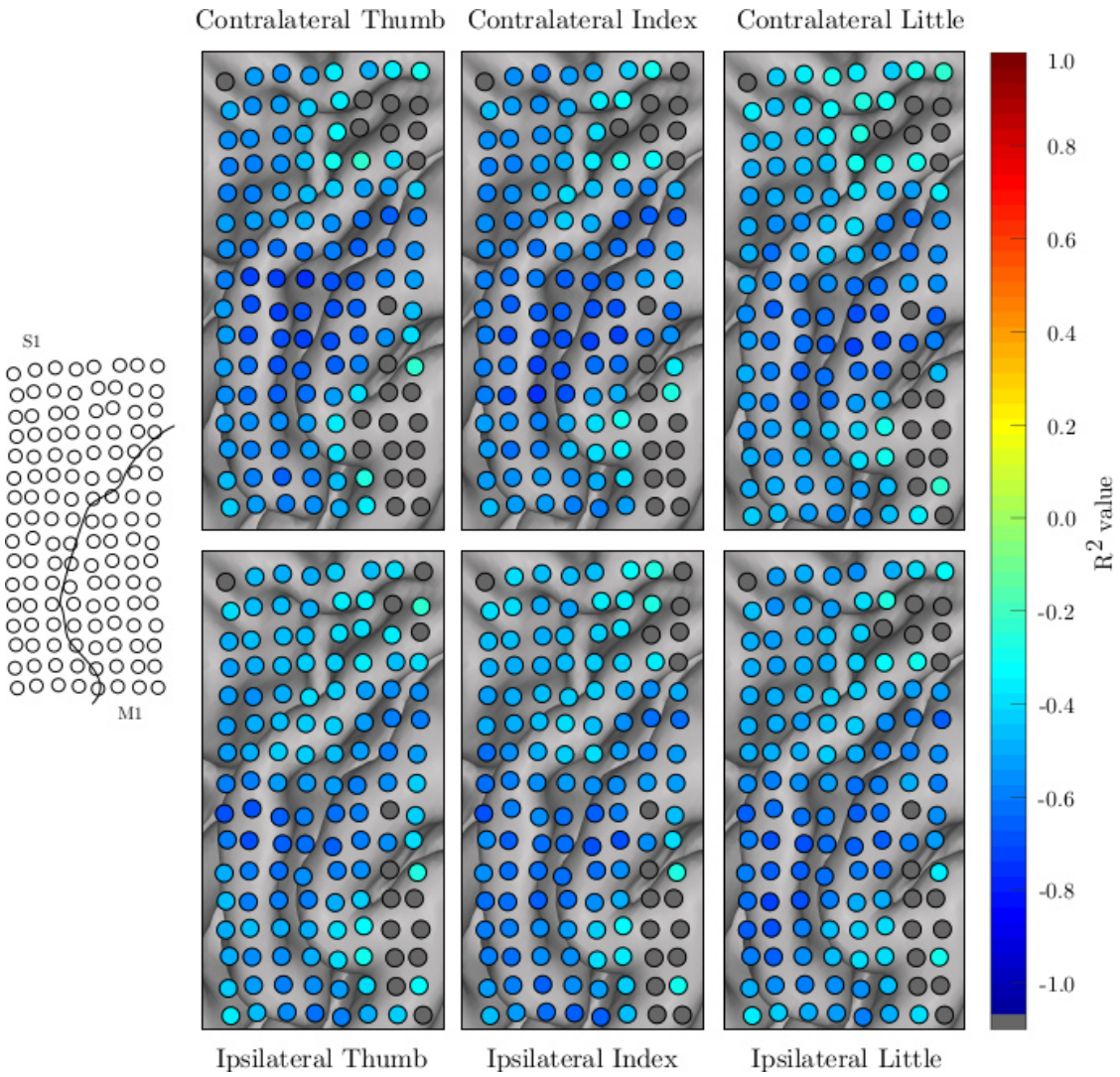

Figure J.6: *Visualization of channel R^2 Values in the β band for Participant P3.*

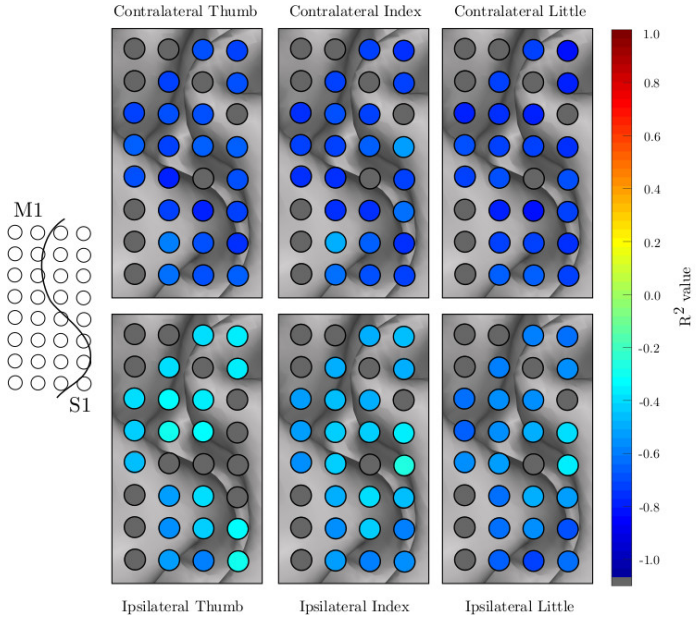

Figure J.7: *Visualization of channel R^2 Values in the α band for Participant P4.*

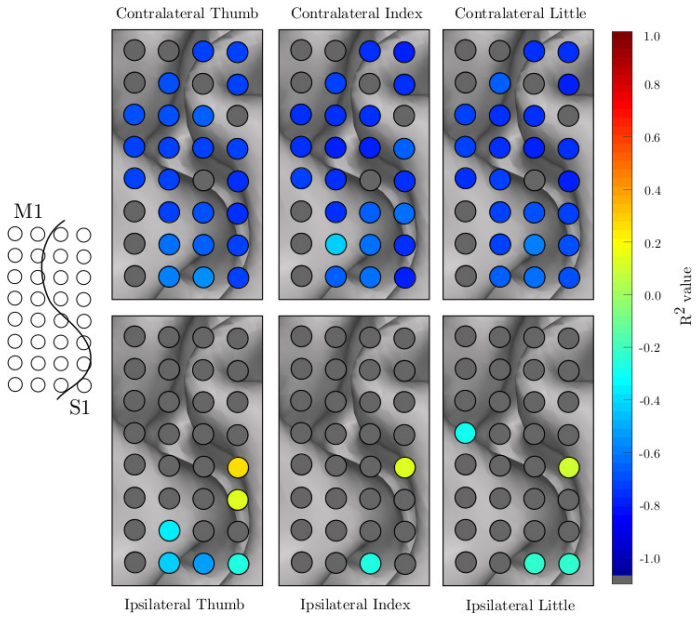

Figure J.8: *Visualization of channel R^2 Values in the β band for Participant P4.*

K Channel R^2 Values in the HFB

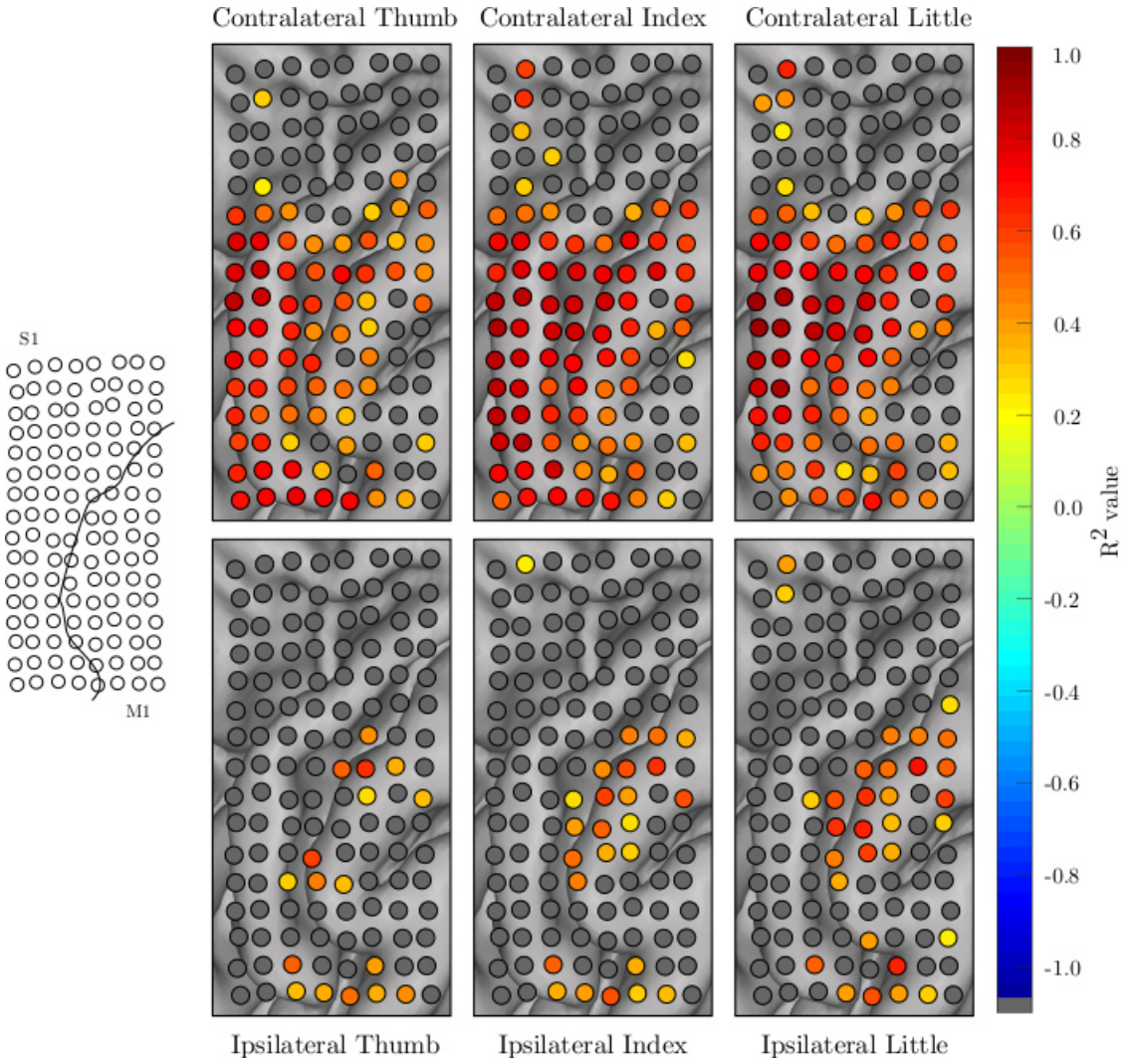

Figure K.1: *Visualization of channel R^2 values in the HFB band for participant P3. Channels that showed no significant cortical activity as well as faulty channels are denoted in gray. This Figure caption holds for the other figure in this appendix, which portrays the results for participant P4.*

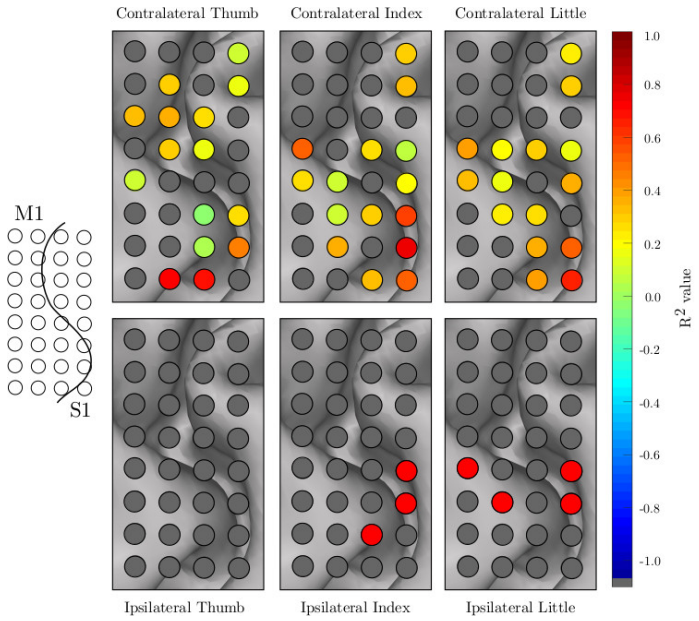

Figure K.2: *Visualization of channel R^2 Values in the HFB band for participant P4.*

L Low Dimensional t-SNE Visualizations of $\mathbf{P}_{v,t,\overline{B}}$

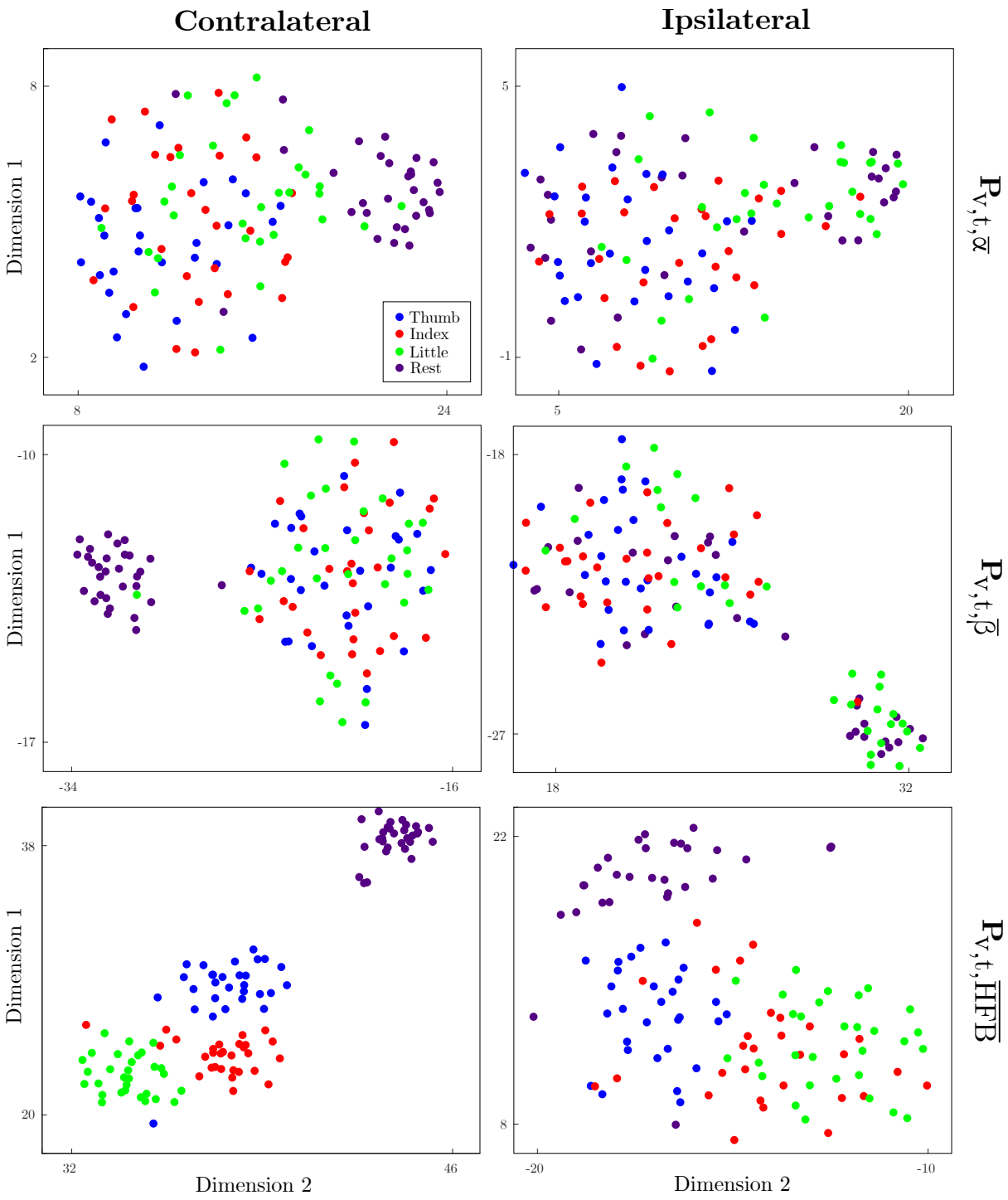

Figure L.1: *Visualization of the low-dimensional data distribution formed by the t-SNE algorithm on the* $\mathbf{P}_{v,t,\overline{B}}$ *data for participant P3. The purple, blue, red and green dots indicate the datapoints corresponding to trials of rest, thumb movement, index finger movement and little finger movement respectively. This Figure caption holds the other figure in this Appendix, which shows the result for participant P4.*

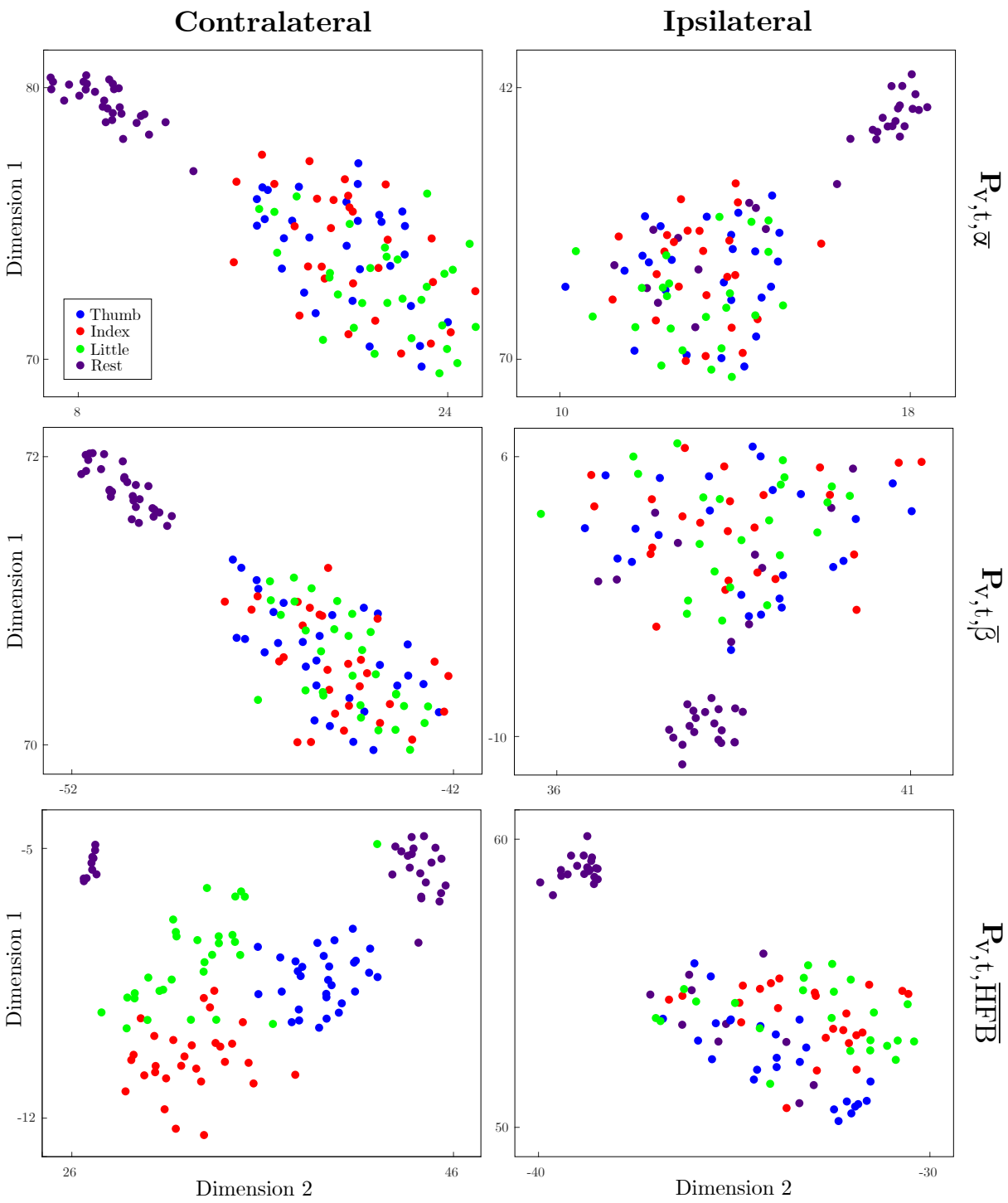

Figure L.2: *Visualization of the low-dimensional data distribution formed by the t-SNE algorithm on the* $\mathbf{P}_{v,t,\overline{B}}$ *data for participant P4.*

M Confusion Matrices Baseline Classification

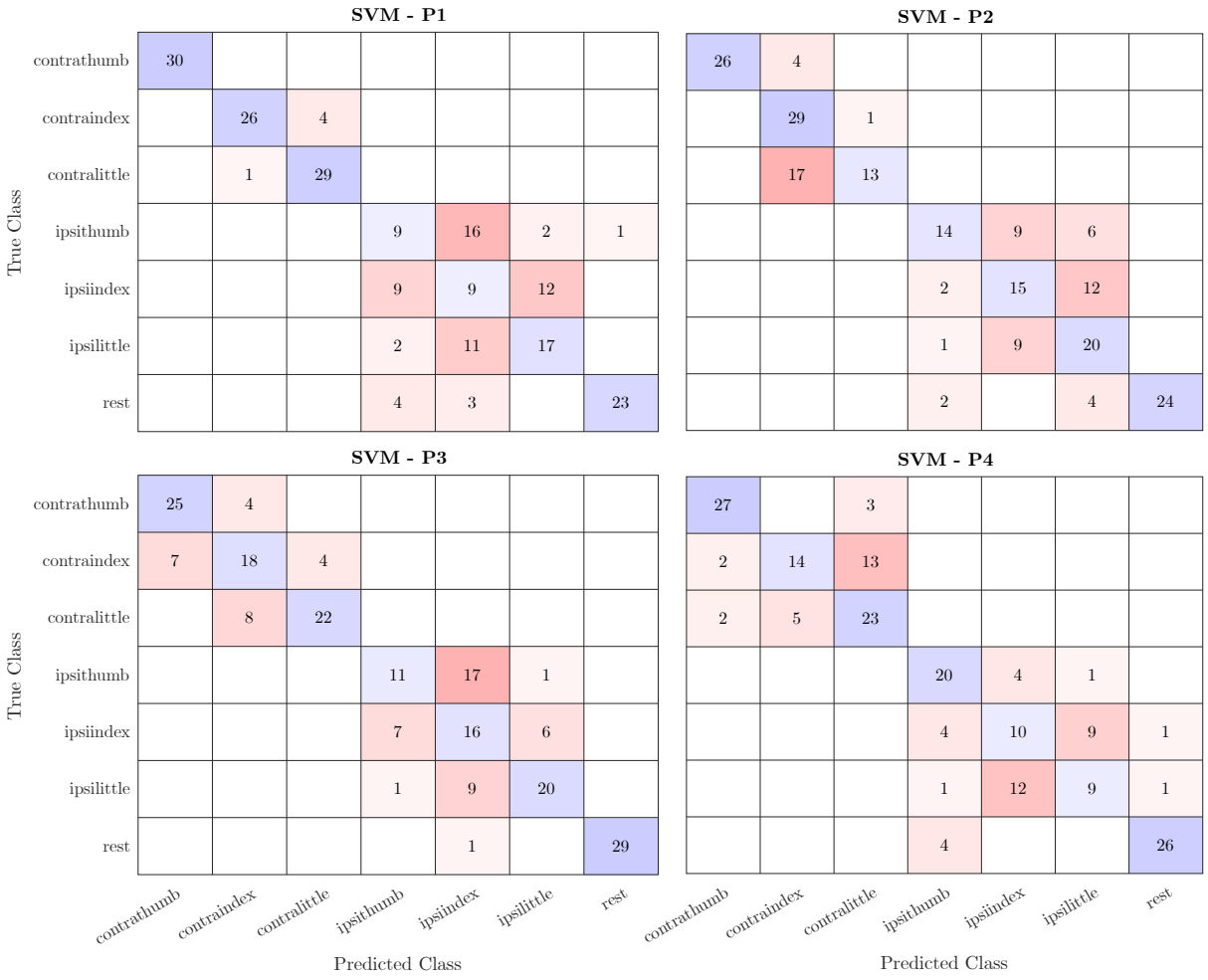

Figure M.1: *Confusion matrices for the classification on the baseline feature vector with the SVM classifier for each participant individually.*

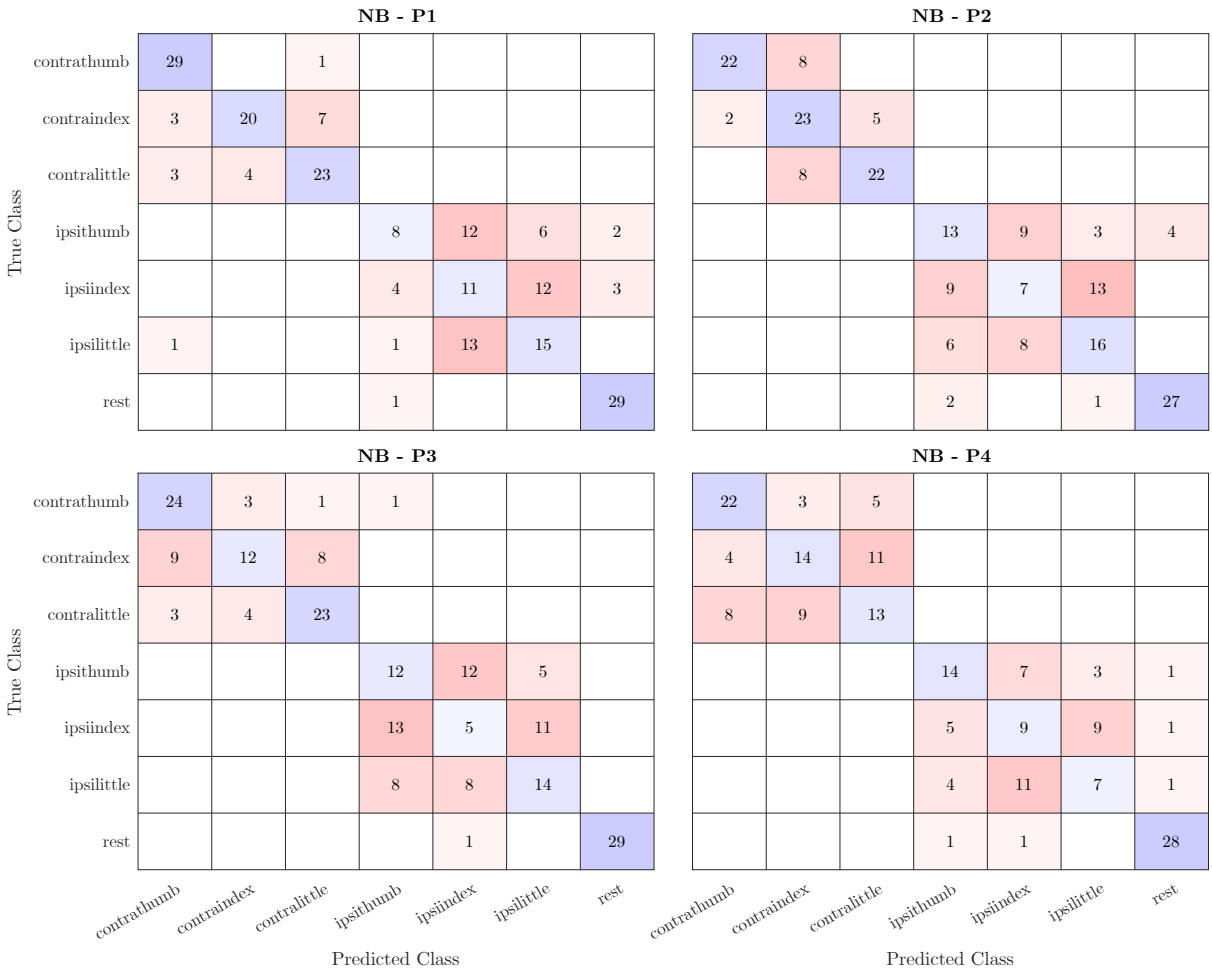

Figure M.2: *Confusion matrices for the classification on the baseline feature vector with the NB classifier for each participant individually.*

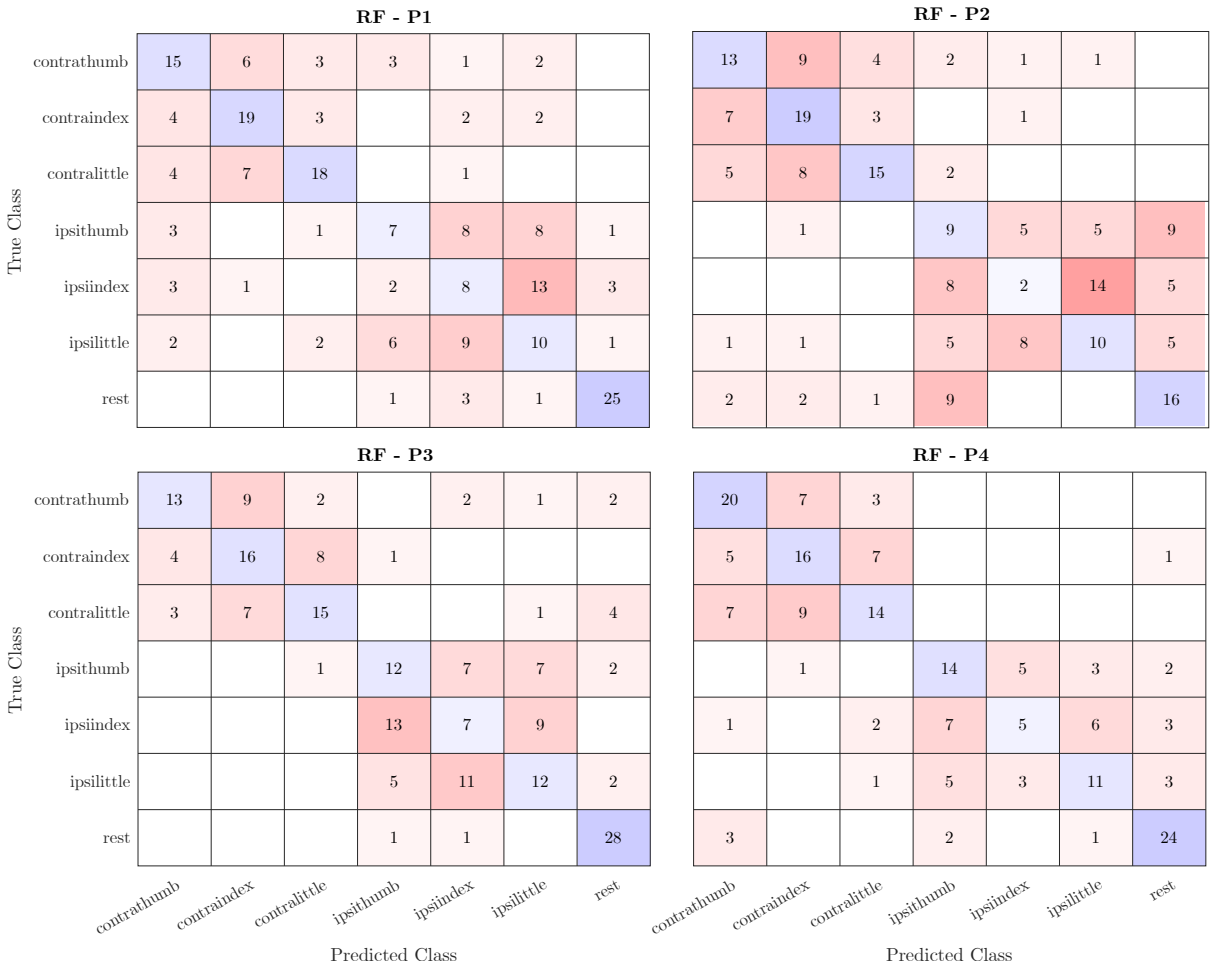

Figure M.3: *Confusion matrices for the classification on the baseline feature vector with the RF classifier for each participant individually.*

N Overview of Classification Accuracies

Participant	**LDA**	**SVM**	**NB**	**RF**	**LDA**	**SVM**	**NB**	**RF**
	Baseline				$[\alpha, \beta, \text{HFB}]$			
P1	73.08	68.75	64.90	49.04	73.56	69.23	63.94	43.27
P2	76.92	67.79	62.50	40.38	79.81	69.23	63.94	48.56
P3	71.84	68.45	57.76	50.00	70.87	66.02	61.17	41.75
P4	65.97	67.54	56.02	49.21	61.78	63.35	53.93	43.98
	$[\alpha, \beta]$				[HFB]			
P1	44.23	47.60	38.94	39.42	72.60	68.75	64.90	44.23
P2	37.02	26.92	25.96	22.12	78.85	75.96	64.42	50.96
P3	39.81	34.95	35.92	30.58	70.87	63.11	58.25	31.07
P4	47.64	49.21	42.41	45.03	57.59	52.88	44.50	38.74
	$[\alpha, \beta, \text{HFB}]_{\overline{B}}$				$[\alpha, \beta]_{\overline{B}}$			
P1	75.00	78.37	75.48	75.48	47.60	48.56	47.12	38.94
P2	87.02	82.69	85.10	85.10	42.30	36.54	39.42	28.85
P3	81.55	81.55	78.64	78.64	44.66	47.09	40.78	39.32
P4	73.30	76.44	75.92	75.92	55.50	56.54	52.88	47.64
	$[\text{HFB}]_{\overline{B}}$							
P1	81.25	76.92	80.29	74.52				
P2	85.58	86.54	87.02	78.37				
P3	81.07	83.98	80.58	79.13				
P4	72.25	72.25	73.30	69.11				

Table N.1: Overview of the classification accuracies of all classifiers on the different feature vectors per participant separately.

O Confusion Matrices on the $[\alpha, \beta, \mathbf{HFB}]_{\overline{B}}$ Feature Vector

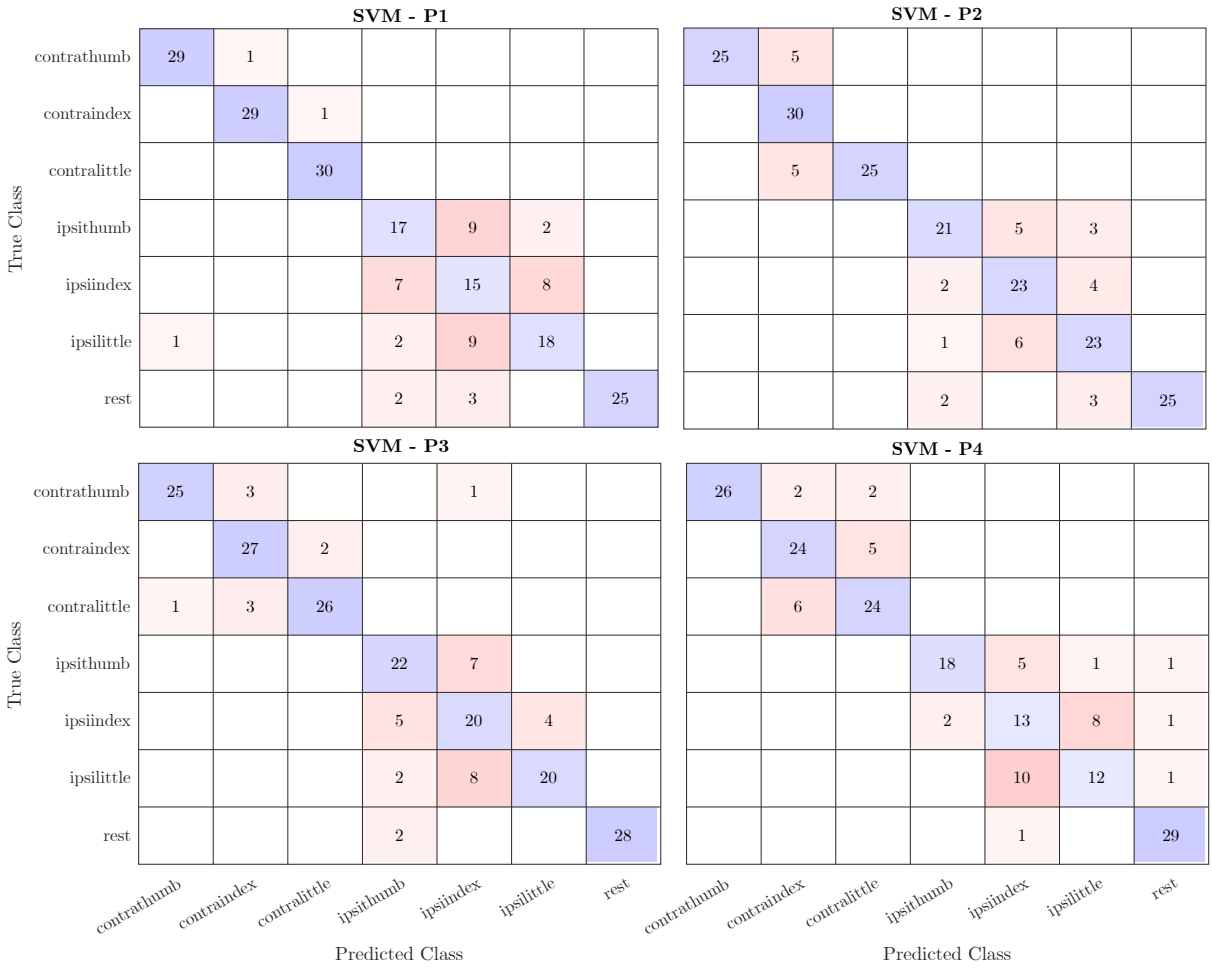

Figure O.1: *Confusion matrices for the classification performed with the SVM classifier for each participant individually on the* $[\alpha, \beta, HFB]_{\overline{B}}$ *feature vector.*

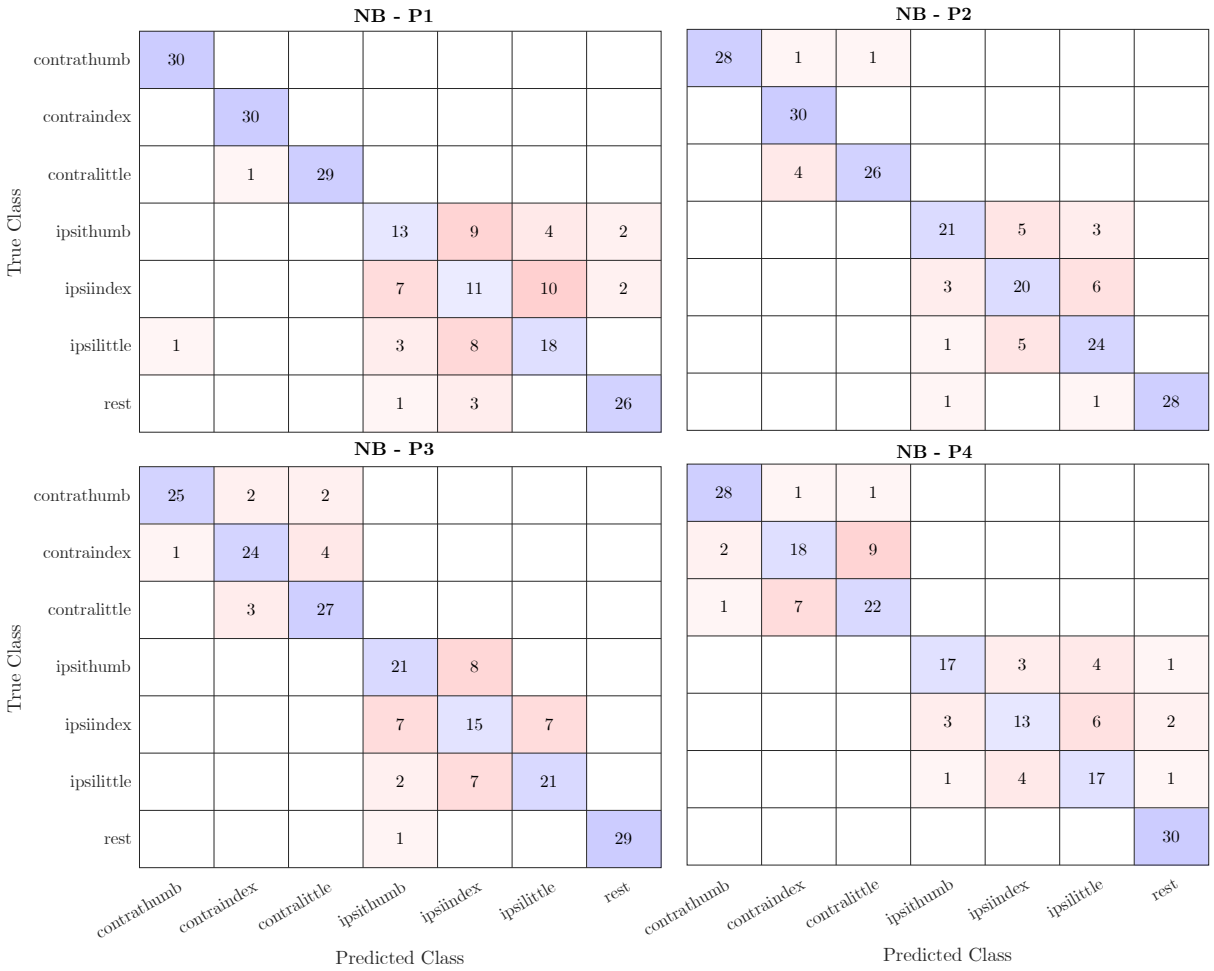

Figure O.2: *Confusion matrices for the classification performed with the NB classifier for each participant individually on the* $[\alpha, \beta, HFB]_{\overline{B}}$ *feature vector.*

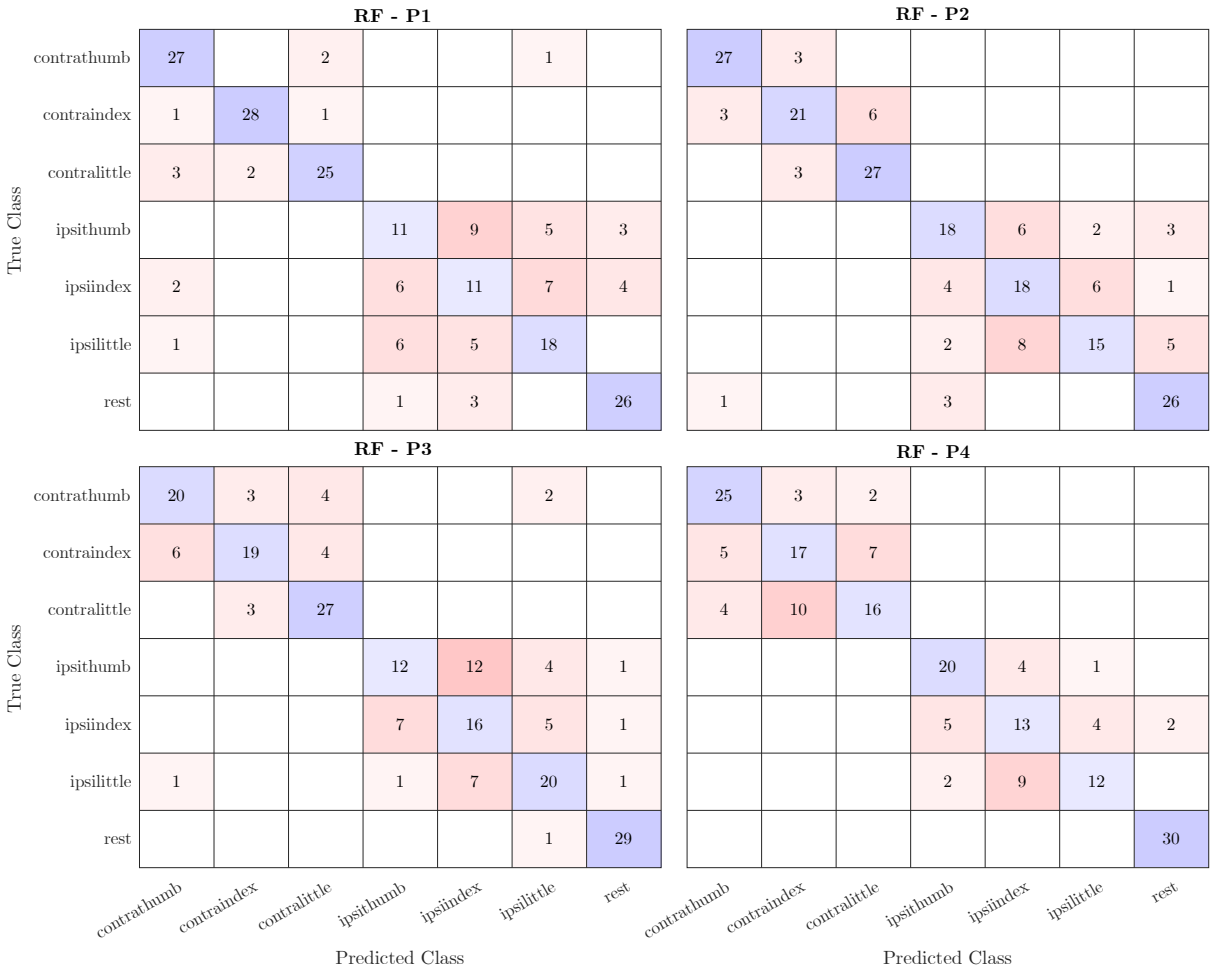

Figure O.3: *Confusion matrices for the classification performed with the RF classifier for each participant individually on the* $[\alpha, \beta, HFB]_{\overline{B}}$ *feature vector.*

P Confusion Matrices on the $[\mathbf{HFB}]_{\overline{B}}$ Feature Vector

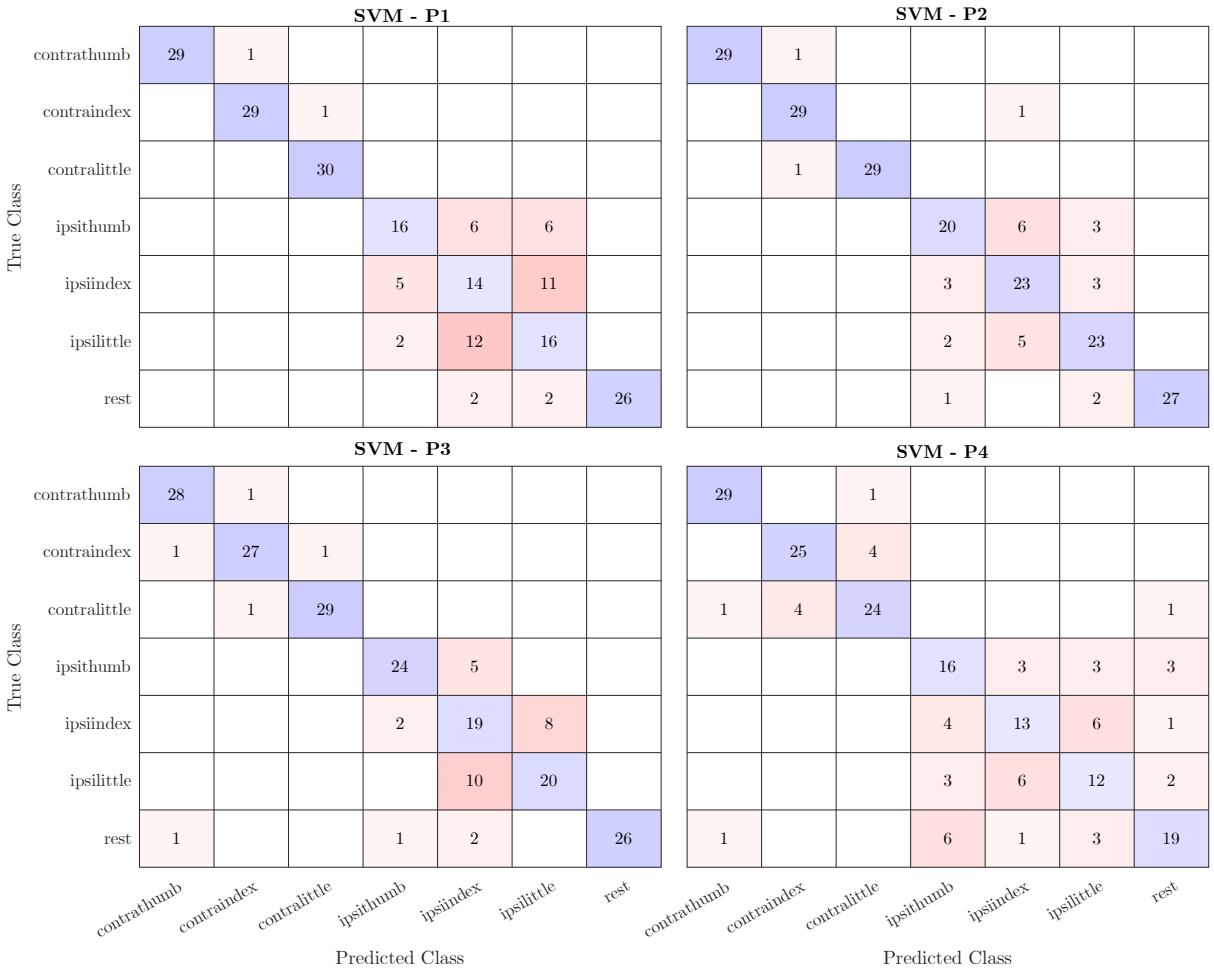

Figure P.1: *Confusion matrices for the classification performed with the SVM classifier for each participant individually on the* $[HFB]_{\overline{B}}$ *feature vector.*

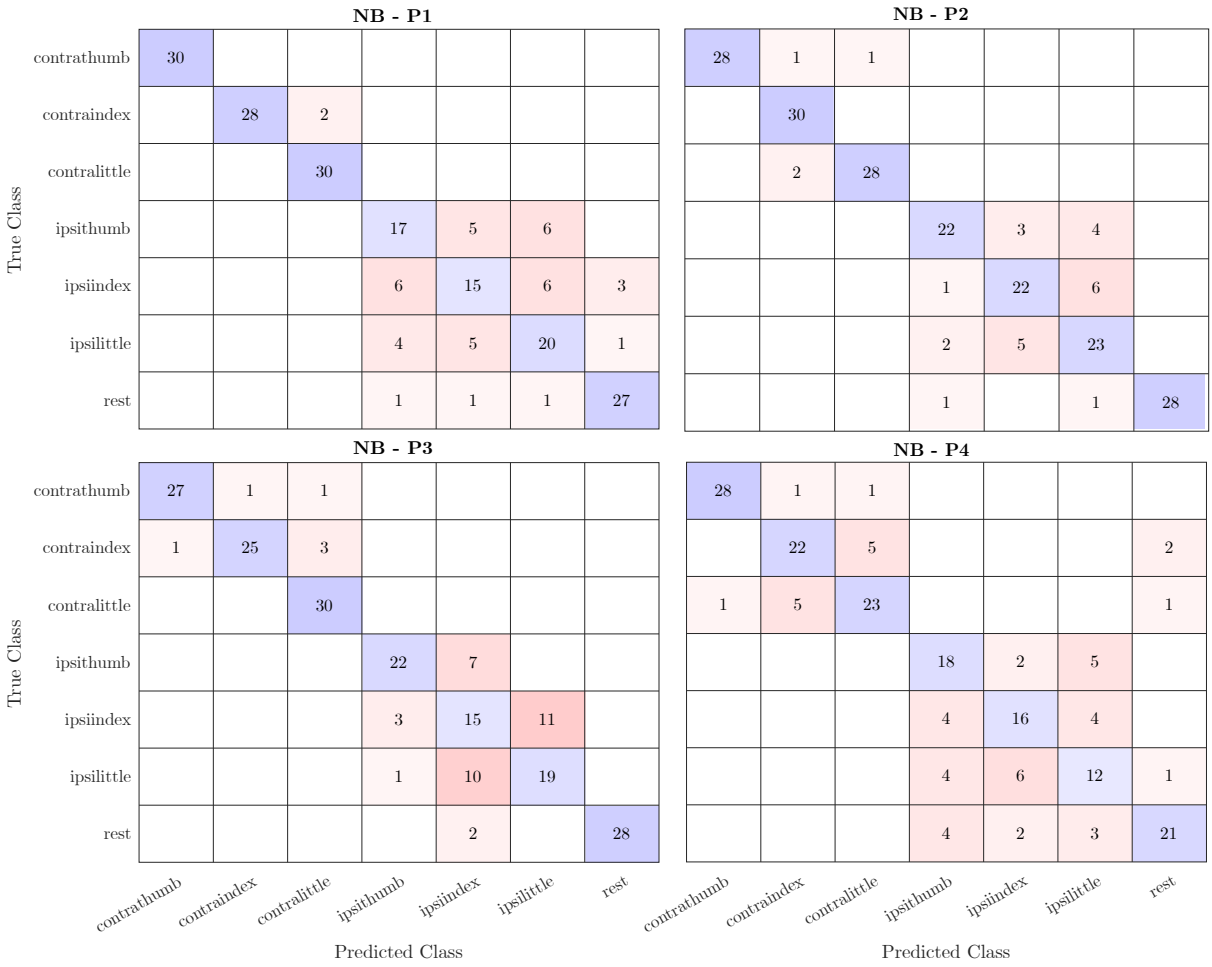

Figure P.2: *Confusion matrices for the classification performed with the NB classifier for each participant individually on the* $[HFB]_{\overline{B}}$ *feature vector.*

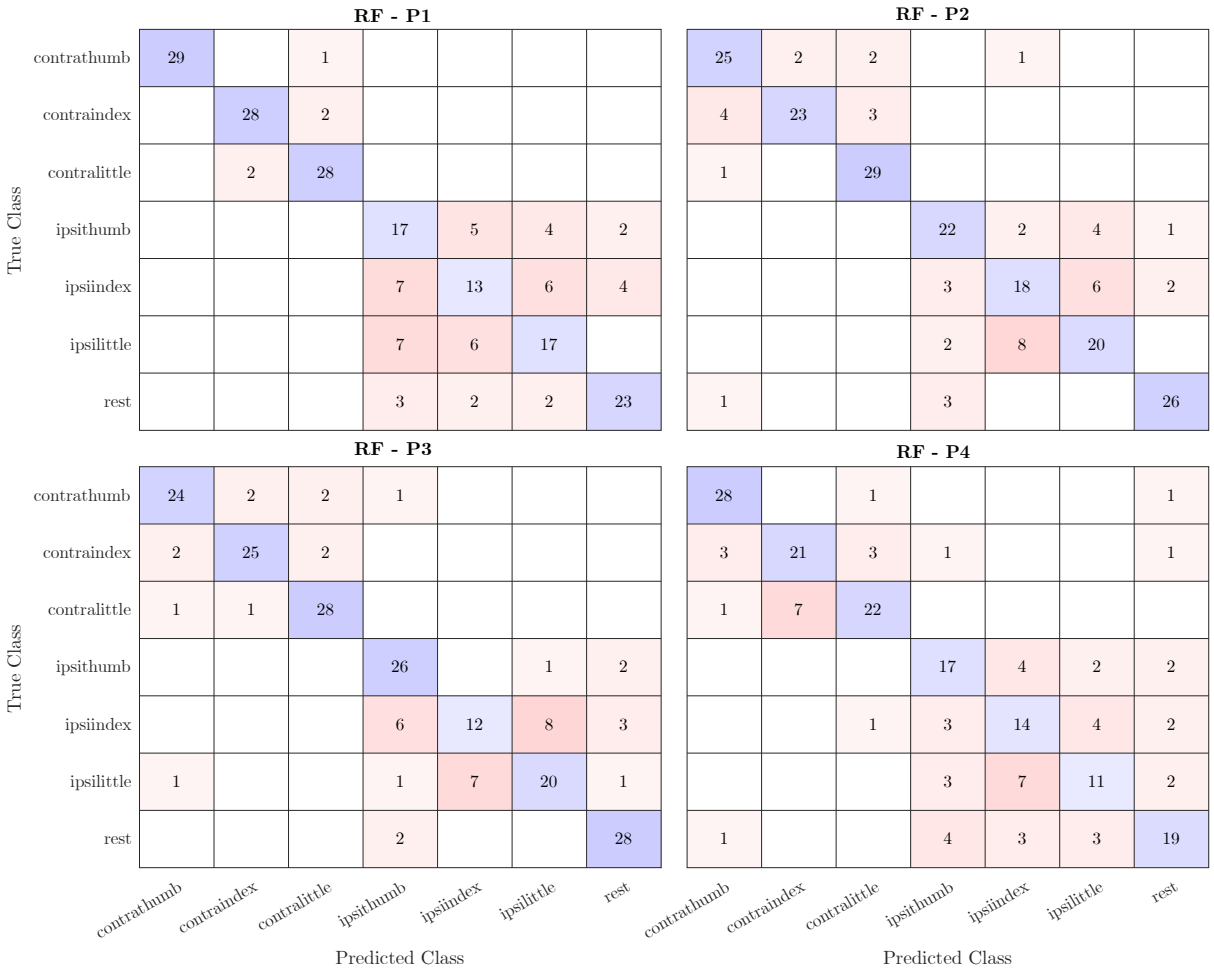

Figure P.3: *Confusion matrices for the classification performed with the RF classifier for each participant individually on the* $[HFB]_{\overline{B}}$ *feature vector.*

Q Required Training Data: Baseline feature vector

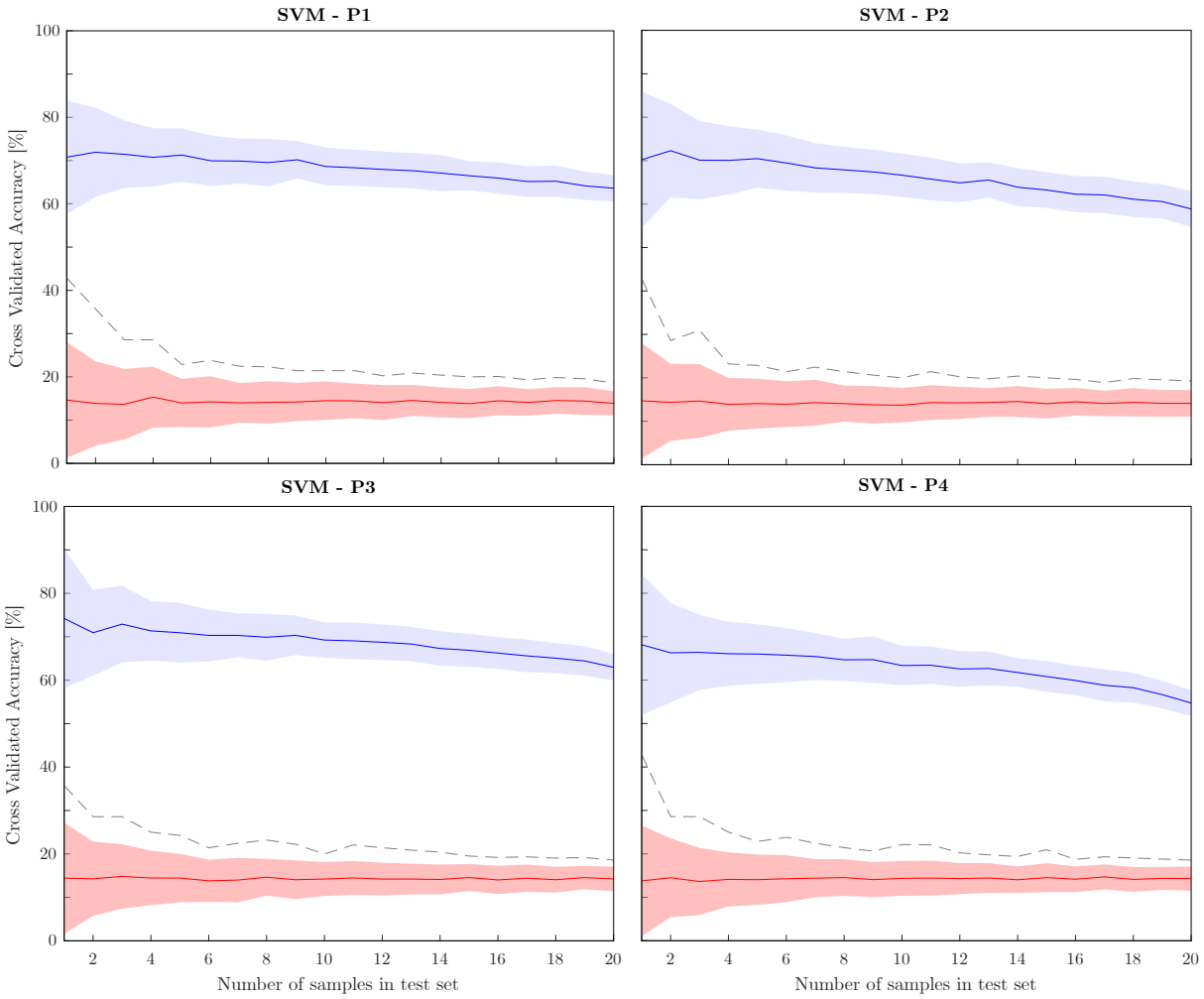

Figure Q.1: *The evolution of the classification performance with the incremental inclusion of trials of finger movement in the test set of the baseline feature vector. This figure shows the results obtained by the SVM classifier for every participant separately. The blue solid line and the blue shaded region respectively denote the classification accuracy on the baseline feature vector and standard deviation thereof. The red solid line and the red shaded region respectively denote the classification accuracy on random data and the standard deviation thereof. The gray dashed line shows the 95th percentile of the empirical chance level of classification at* $p < 0.05$*. This Figure caption holds for the other figures in this Appendix, which show the results for the other classifiers.*

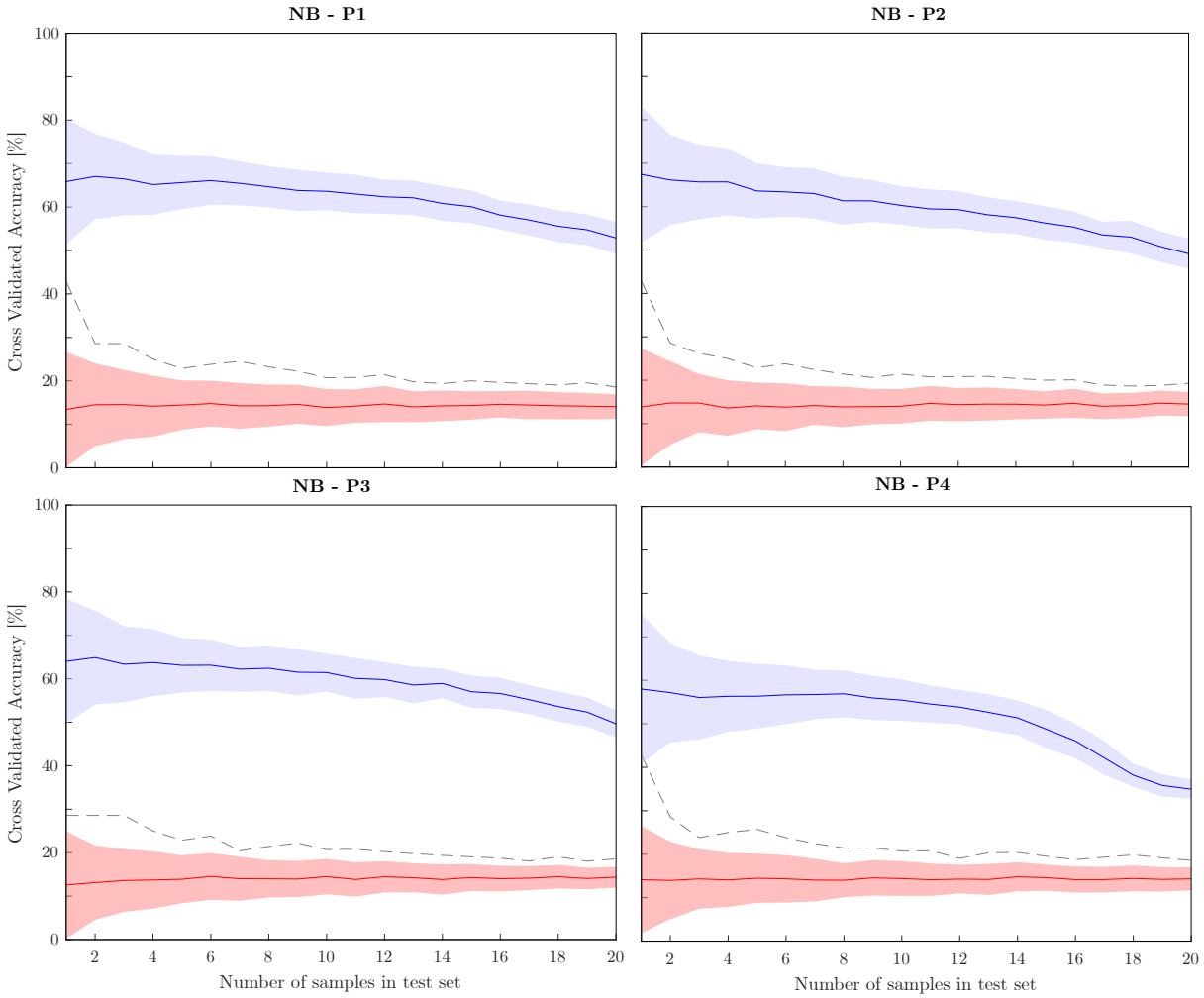

Figure Q.2: *The evolution of the classification performance with the incremental inclusion of trials of finger movement in the test set of the baseline feature vector. This figure shows the results obtained by the NB classifier for every participant separately.*

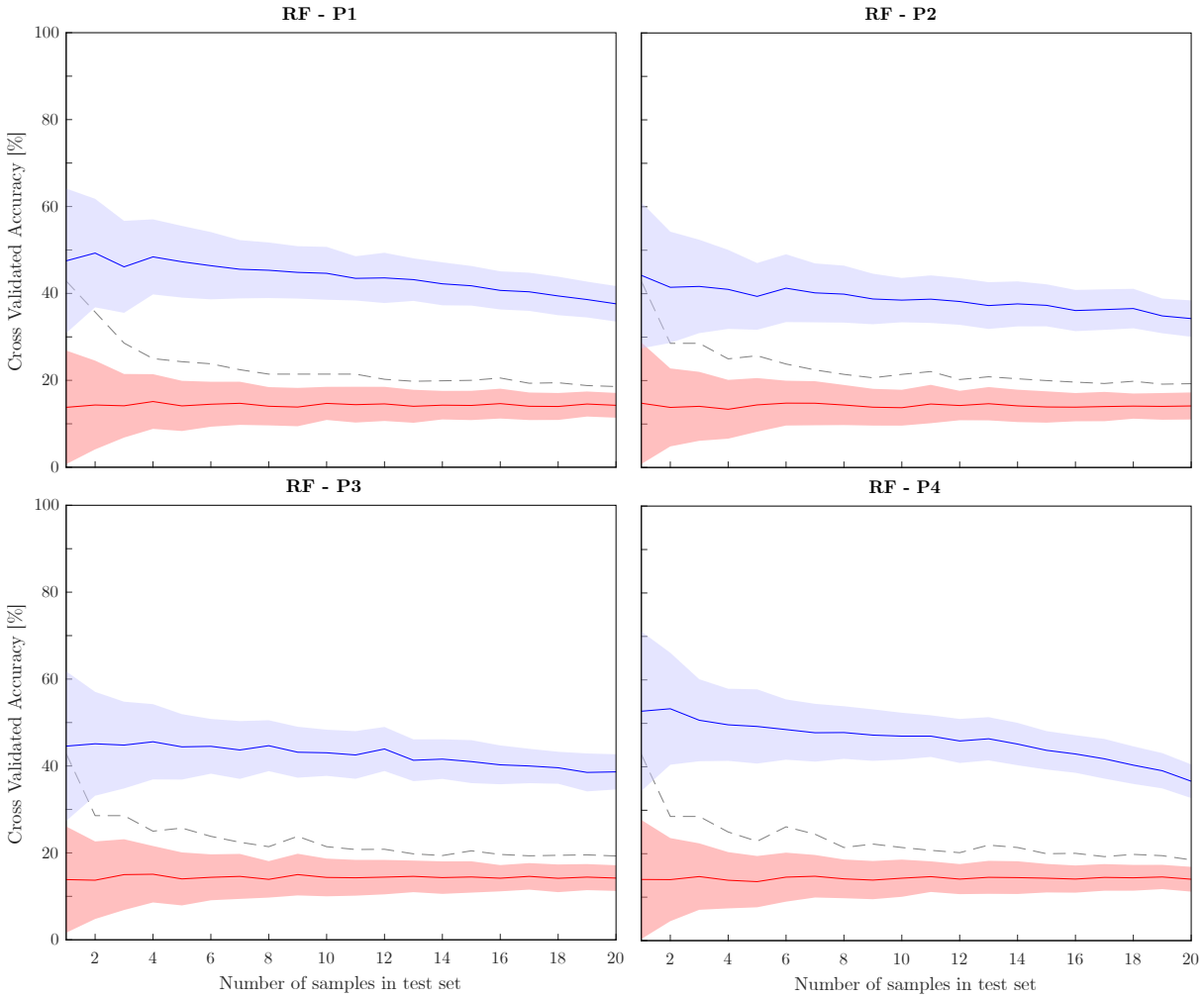

Figure Q.3: *The evolution of the classification performance with the incremental inclusion of trials of finger movement in the test set of the baseline feature vector. This figure shows the results obtained by the RF classifier for every participant separately.*

R Required Training Data: $[\alpha, \beta, \mathbf{HFB}]_{\overline{B}}$ feature vector

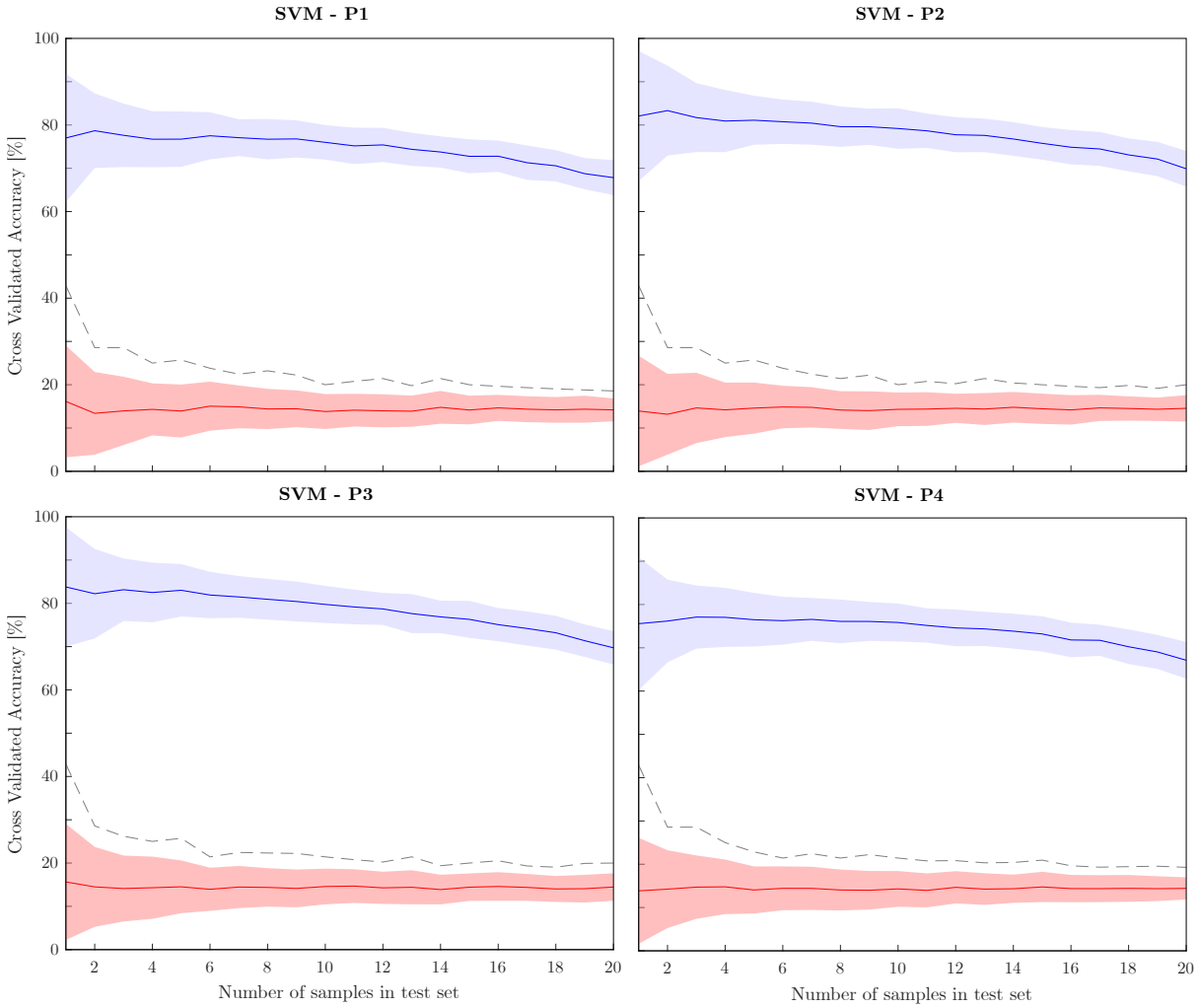

Figure R.1: *The evolution of the classification performance with the incremental inclusion of trials of finger movement in the test set of the* $[\alpha, \beta, HFB]_{\overline{B}}$ *feature vector. This figure shows the results obtained by the SVM classifier for every participant separately. The blue solid line and the blue shaded region respectively denote the classification accuracy on the baseline feature vector and standard deviation thereof. The red solid line and the red shaded region respectively denote the classification accuracy on random data and the standard deviation thereof. The gray dashed line shows the 95th percentile of the empirical chance level of classification at* $p < 0.05$*. This Figure caption holds for the other figures in this Appendix, which shows the results for the other classifiers.*

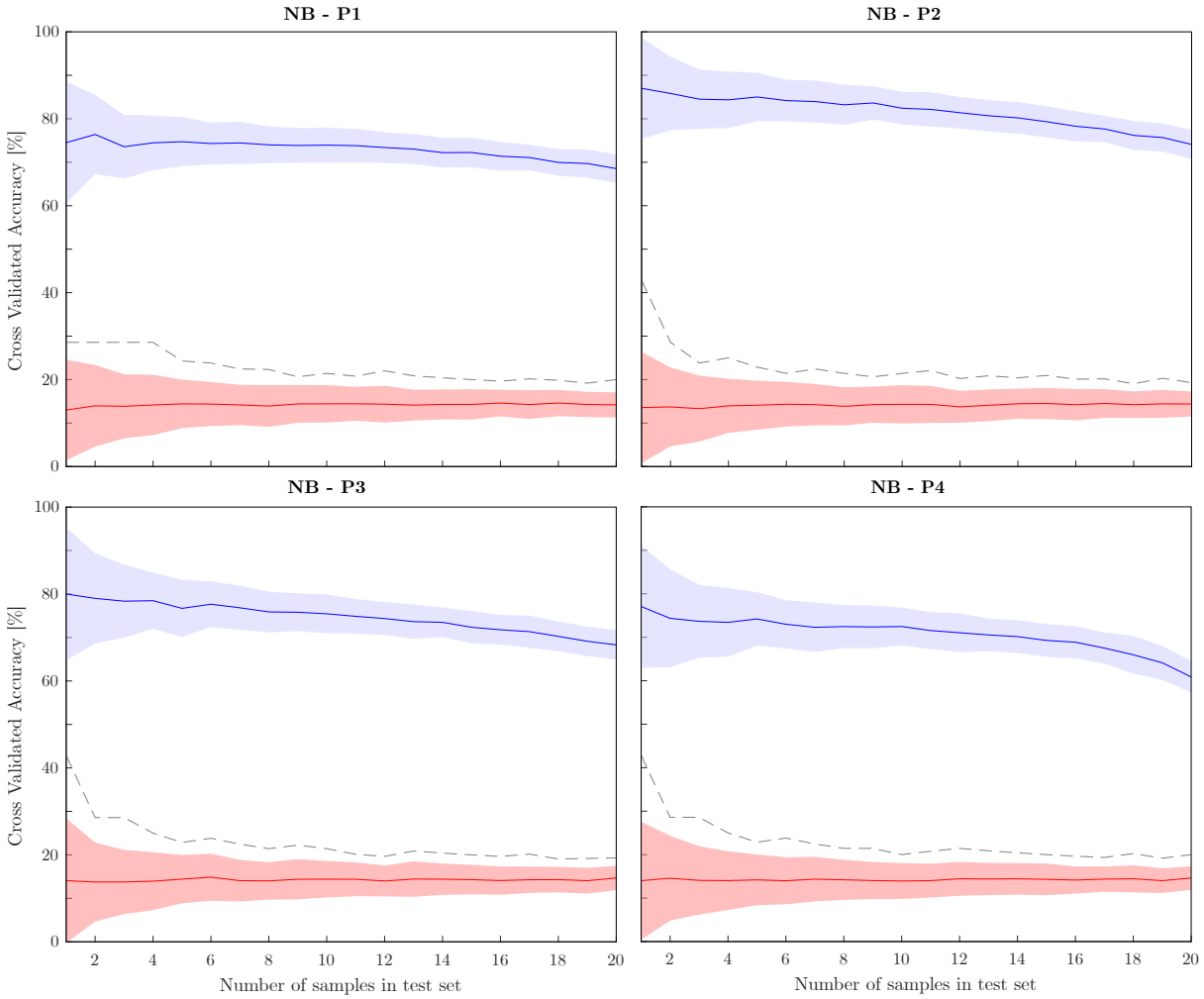

Figure R.2: *The evolution of the classification performance with the incremental inclusion of trials of finger movement in the test set of the* $[\alpha, \beta, HFB]_{\overline{B}}$ *feature vector. This figure shows the results obtained by the NB classifier for every participant separately.*

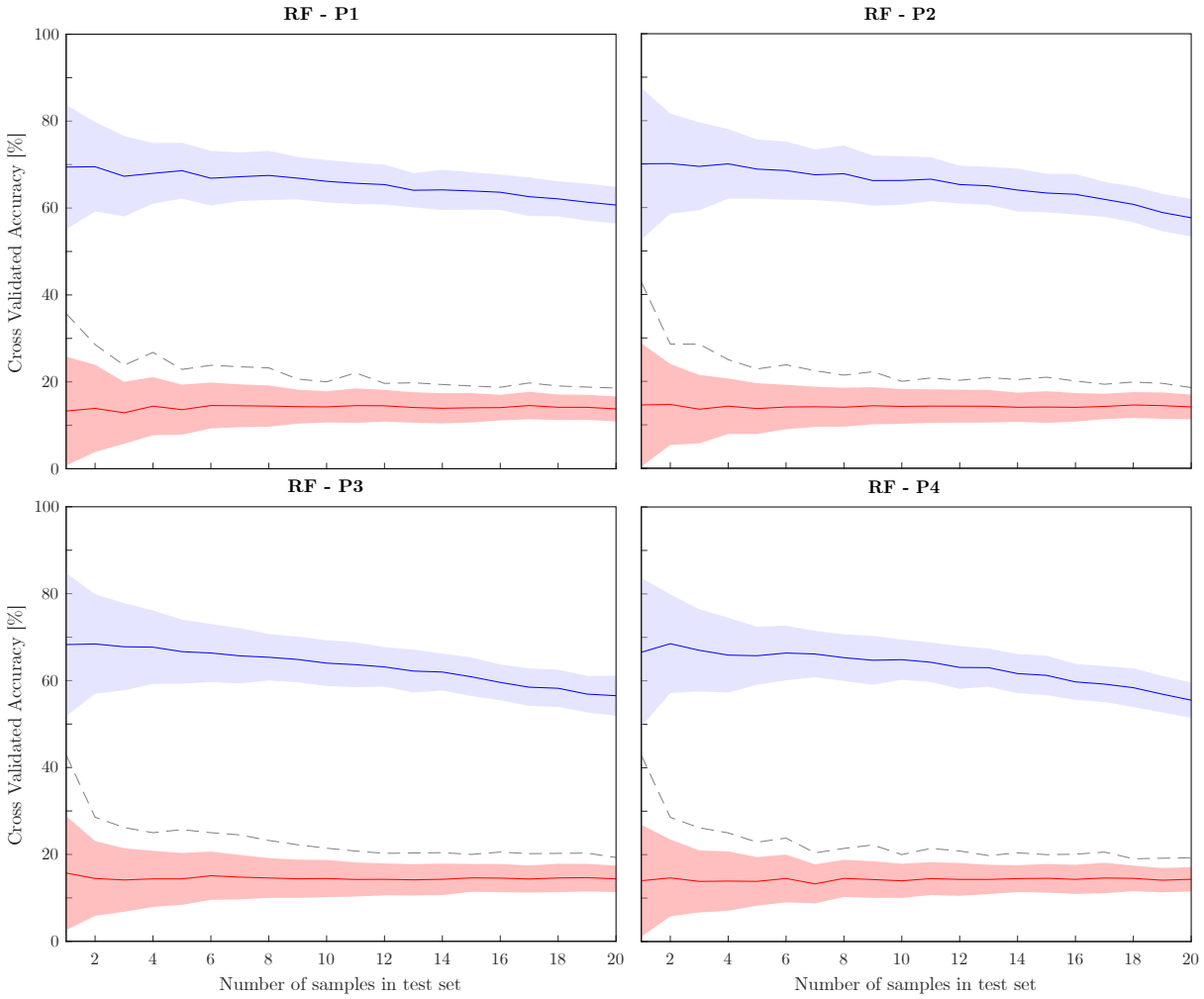

Figure R.3: *The evolution of the classification performance with the incremental inclusion of trials of finger movement in the test set of the* $[\alpha, \beta, HFB]_{\overline{B}}$ *feature vector. This figure shows the results obtained by the RF classifier for every participant separately.*

S Required Training Data: $[\mathbf{HFB}]_{\overline{B}}$ feature vector

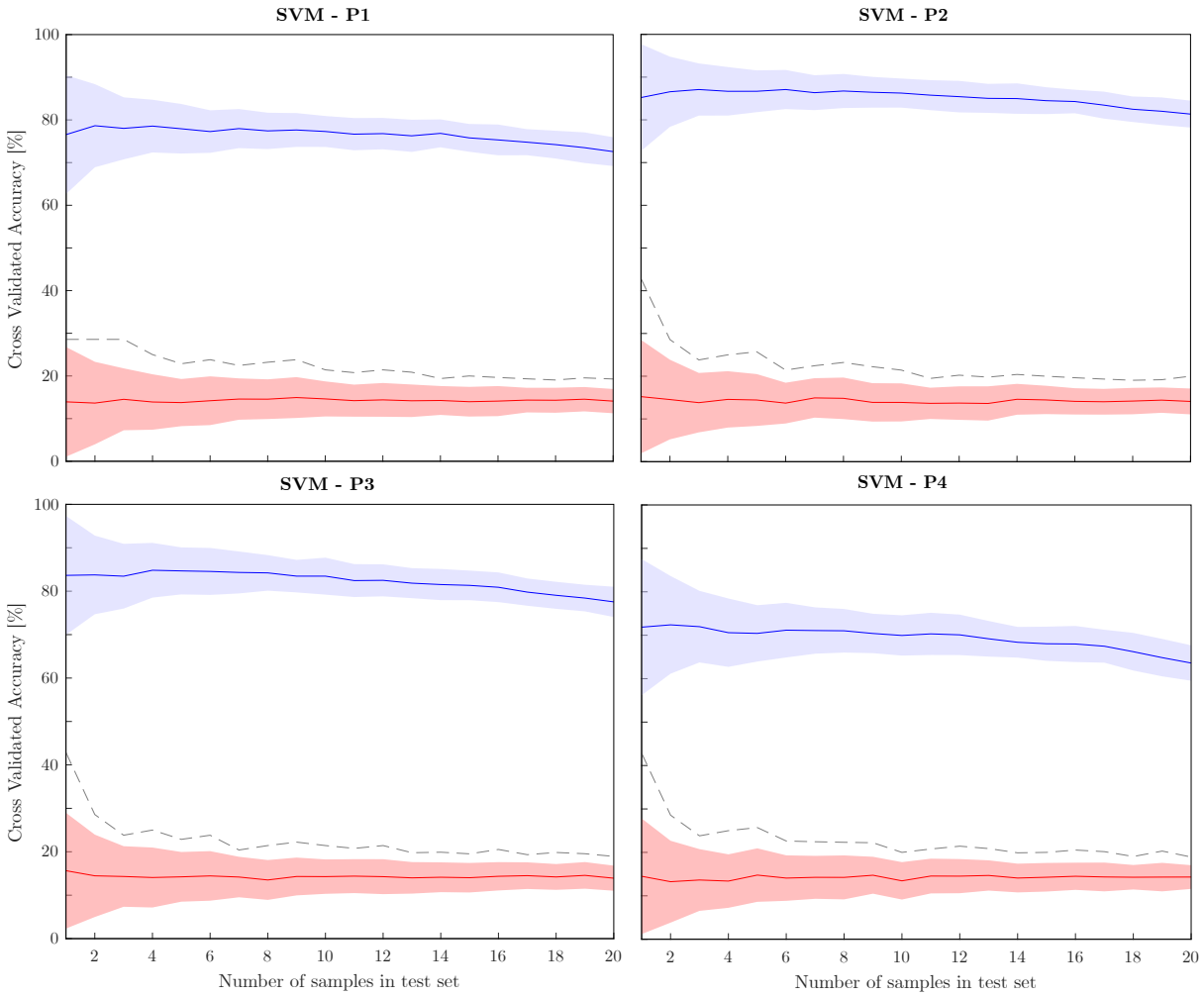

Figure S.1: *The evolution of the classification performance with the incremental inclusion of trials of finger movement in the test set of the $[HFB]_{\overline{B}}$ feature vector. This figure shows the results obtained by the SVM classifier for every participant separately. The blue solid line and the blue shaded region respectively denote the classification accuracy on the baseline feature vector and standard deviation thereof. The red solid line and the red shaded region respectively denote the classification accuracy on random data and the standard deviation thereof. The gray dashed line shows the 95th percentile of the empirical chance level of classification at $p < 0.05$. This Figure caption holds for the other figures in this Appendix, which shows the results for the other classifiers*

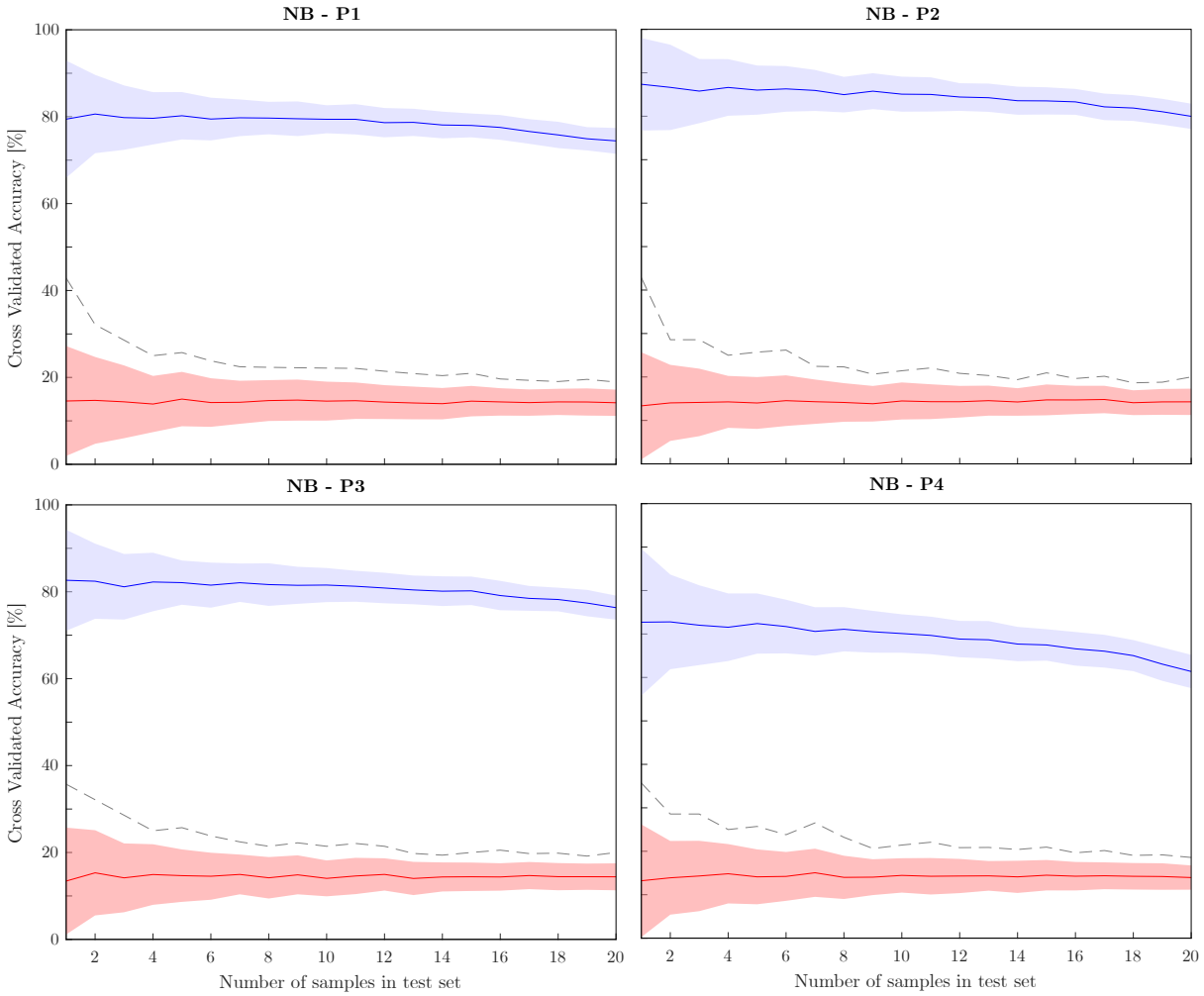

Figure S.2: *The evolution of the classification performance with the incremental inclusion of trials of finger movement in the test set of the* $[HFB]_{\overline{B}}$ *feature vector. This figure shows the results obtained by the NB classifier for every participant separately.*

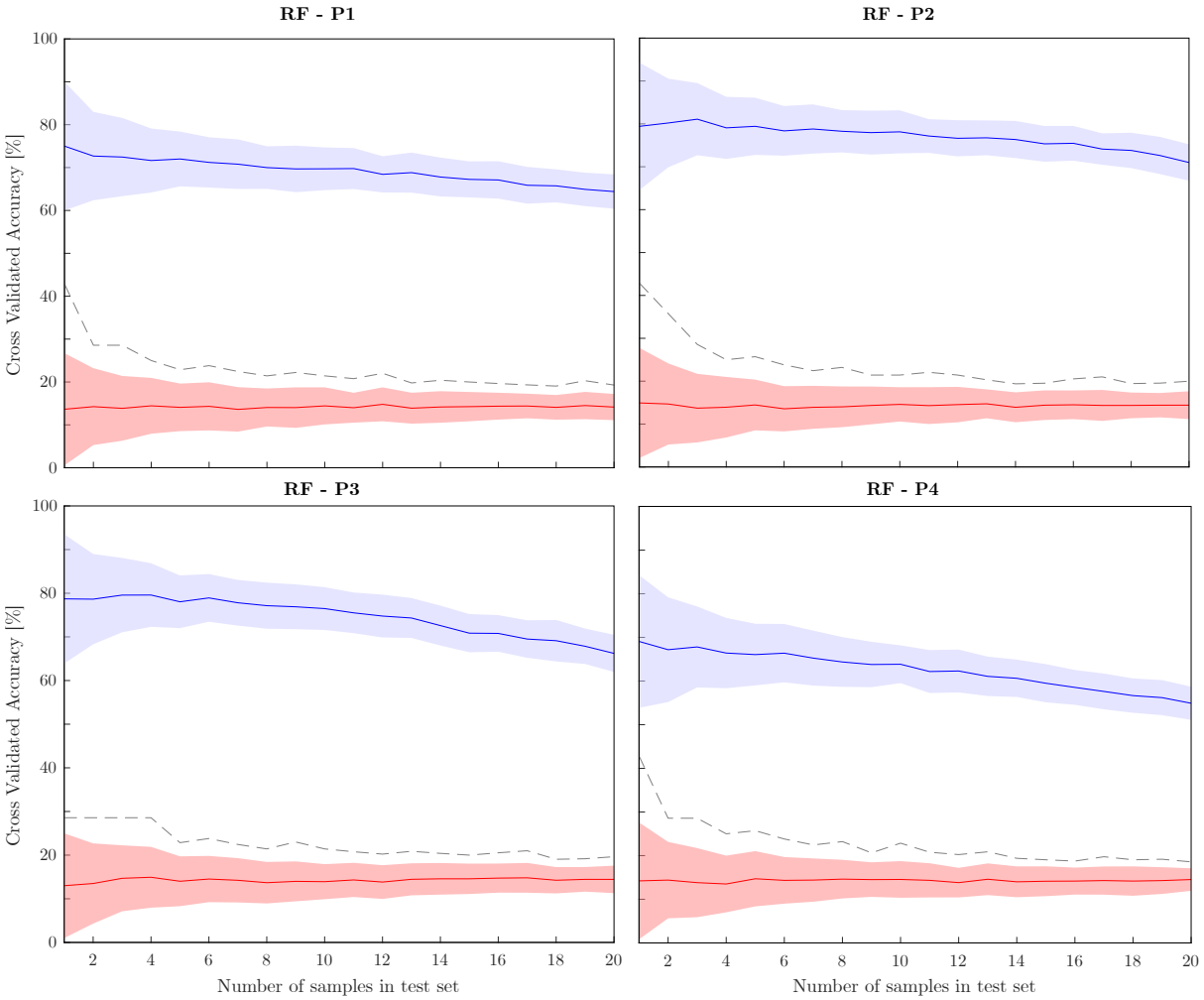

Figure S.3: *The evolution of the classification performance with the incremental inclusion of trials of finger movement in the test set of the* $[HFB]_{\overline{B}}$ *feature vector. This figure shows the results obtained by the RF classifier for every participant separately.*

T Spatial Analysis: Informative Areas for Distinguishing between Finger Movement and Rest

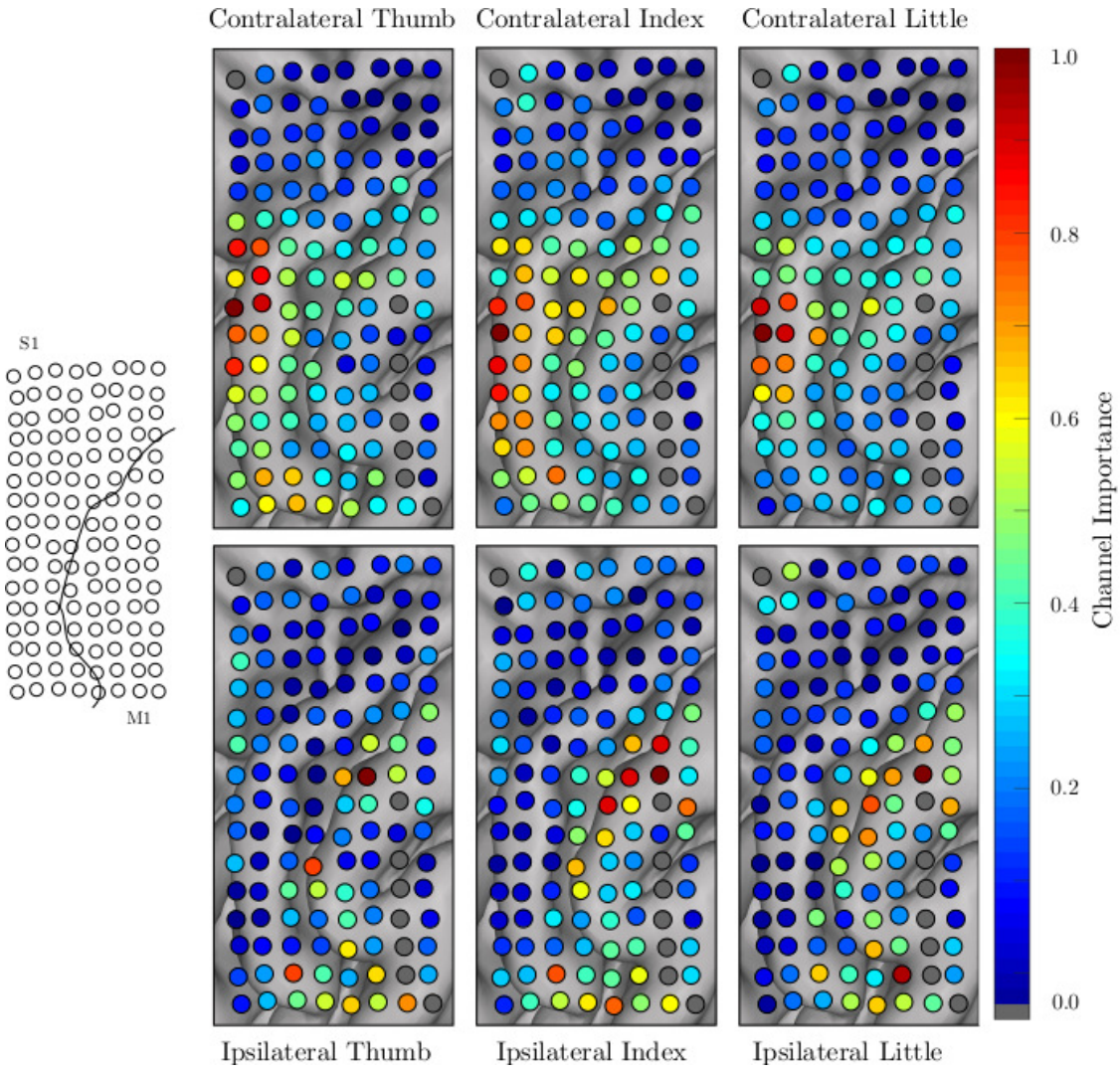

Figure T.1: *Relative channel importance for distinguishing between finger movement and rest for participant P3. Faulty channels are denoted in gray. Channels in red denote a relatively high channel importance and channels in blue denote a relatively low channel importance as indicated by the color bar. The inlay image at the far left depicts a schematic representation of the electrode grid placement with respect to S1 and M1, separated by a solid line representing the CS. This inlay serves as a reference for the exact electrode locations on the cortical surface. This caption holds all figures in this Appendix.*

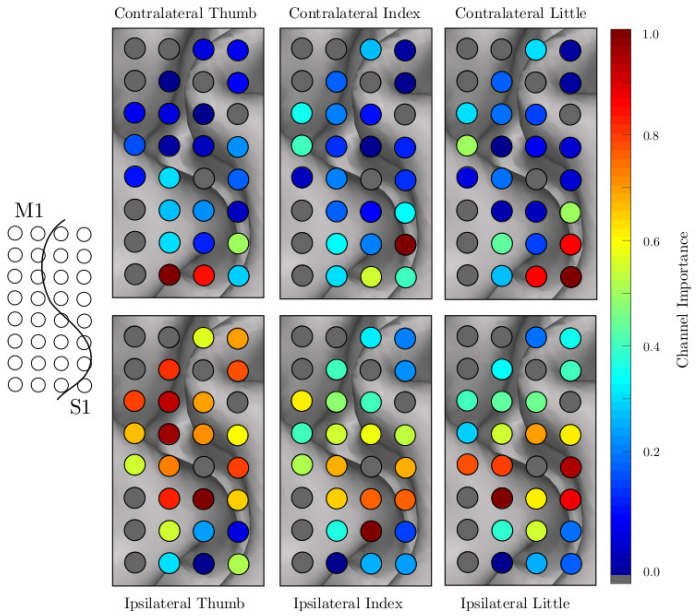

Figure T.2: *Relative channel importance for distinguishing between finger movement and rest for participant P4.*

U Spatial Analysis: Informative Areas for Distinguishing between Individual Finger Movement of the Same Laterality

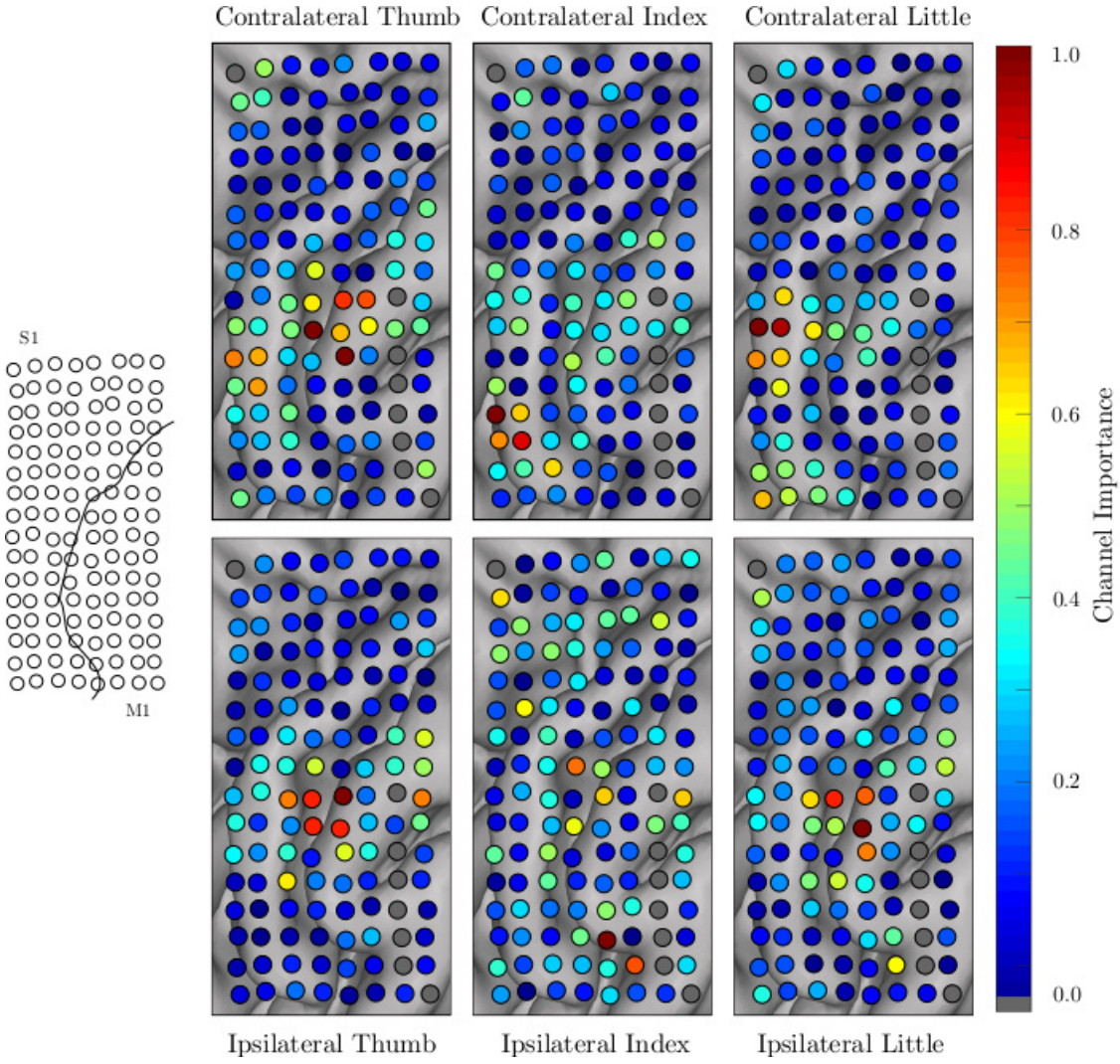

Figure U.1: *The relative importance of channels in distinguishing between movement of a specific finger against movement of fingers of the same laterality for participant P3. Faulty channels are denoted in gray. Channels in red denote a relatively high channel importance and channels in blue denote a relatively low channel importance as indicated by the color bar. The inlay image at the far left depicts a schematic representation of the electrode grid placement with respect to S1 and M1, separated by a solid line representing the CS. This inlay serves as a reference for the exact electrode locations on the cortical surface. This caption holds for the other figure in this Appendix.*

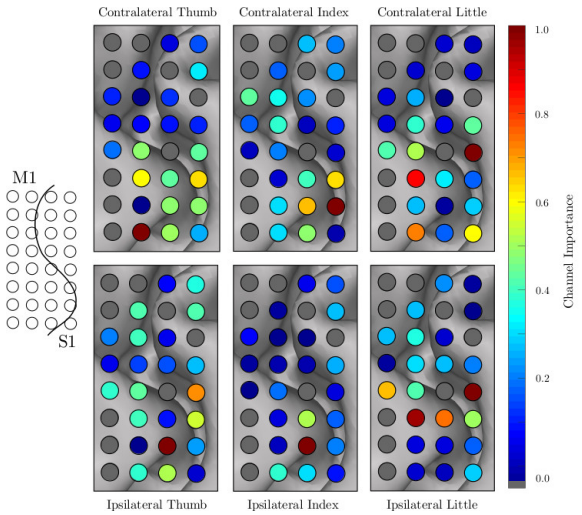

Figure U.2: *Relative channel importance in the classification between movement of a specific finger against movement of fingers of the same laterality for participant P4.*

V Spatial Analysis: Informative Areas for Distinguishing between Movement of Contralateral and Ipsilateral Finger Pairs

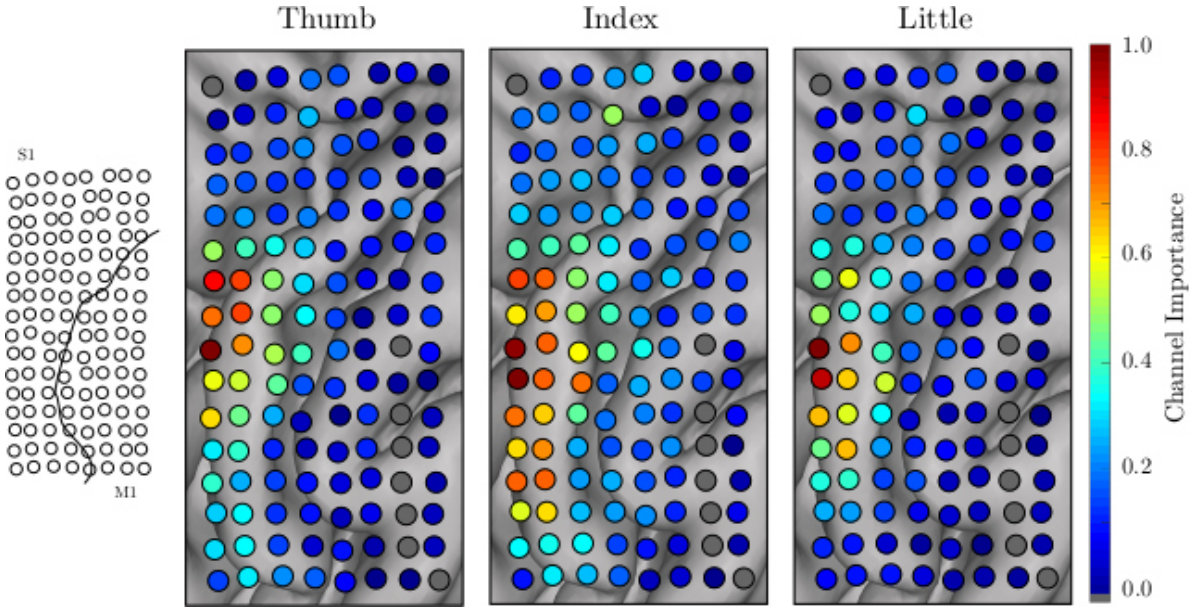

Figure V.1: *Relative channel importance in the classification between movements of contralateral and ipsilateral fingers separately for participant P3.*

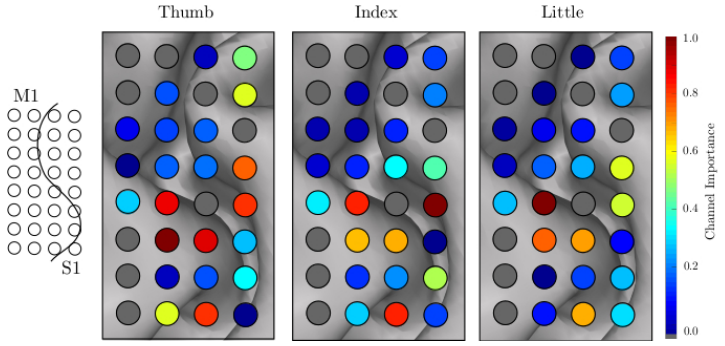

Figure V.2: *Relative channel importance in the classification between movements of contralateral and ipsilateral fingers separately for participant P4.*

W Spatial Analysis: Informative Areas for Distinguishing between Movement of all Contralateral and Ipsilateral Fingers.

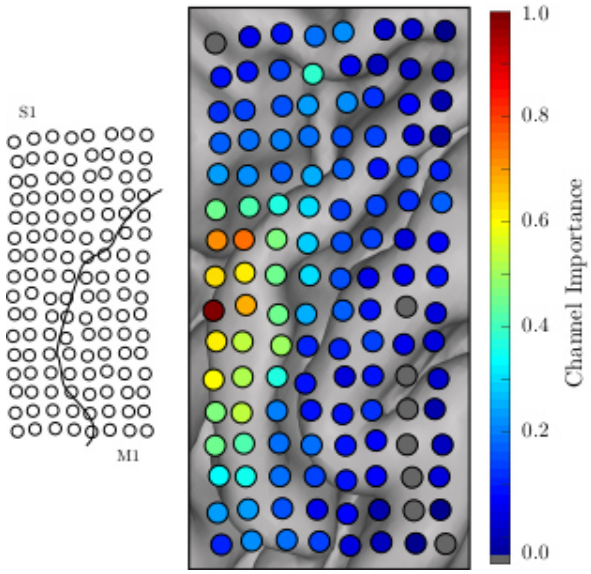

Figure W.1: *Relative channel importance in the classification between movement of all contralateral fingers versus movement of all ipsilateral fingers for participant P3.*

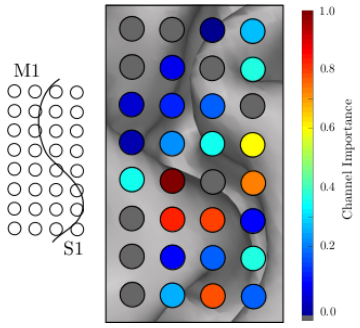

Figure W.2: *Relative channel importance in the classification between movements of all contralateral fingers versus movement of all ipsilateral fingers for participant P4.*